Department of Chemistry

Palaeoenvironmental reconstruction of the Induan/Olenekian event of the lower Triassic and to establish the source of gas in the Perth Basin, WA

Mojgan Ladjavardi

This thesis is presented for the Degree of
Doctor of Philosophy
of
Curtin University

August 2013

Declaration

To the best of my knowledge and belief this thesis contains no material previously published by any other person except where due acknowledgment has been made.

This thesis contains no material which has been accepted for the award of any other degree or diploma in any university.

Mojgan Ladjavardi

Perth, January 20, 2015

Abstract

Major catastrophic events happened at various times in Earth's history. The most profound mass extinction happened in the latest Permian. It saw the most acute mass extinction known in the latest Changhsingian which eliminated over 90 % of skeletonised marine species and around 70 % of species on land.

There was a period of continued global climatic and environmental change and stress during the early Triassic, following the late Changhsingian mass extinction that lasted some 5 million years and was characterised by a significant carbon isotope excursion in sedimentary organic matter (OM) and carbonates. This early Triassic period of environmental upheaval was also characterised by significant size reduction of many organisms and is referred to in the literature as the period of "delayed recovery" following the largest mass extinction event of the Phanerozoic. There are several important Earth processes for the late Permian–early Triassic mass extinction. These include, major climate perturbations, frequent shifts between oxic and anoxic/dysoxic conditions in the oceans and also climate warming.

The main aims of this PhD thesis were (i) to establish the paleoenvironmental changes that occurred around the early Triassic Induan–Olenekian Stage Boundary in the northern onshore Perth Basin using a combination of organic geochemical, bulk stable isotopic data and compound specific isotopic analysis (CSIA) and (ii) to develop a novel method of offline coupling of Micro Scale Sealed Vessel Pyrolysis (MSSV-Py) and Gas Chromatography-isotope ratio Mass Spectrometry (GC-irMS) in order to determine the $\delta^{13}C$ values of hydrocarbon gases generated by artificial maturation of sedimentary OM.

In **Chapter 2** of this thesis, for the first time the location of the early Triassic Induan–Olenekian Stage Boundary has been identified based on conodont faunas in the Senecio–1 well located in the northern Perth Basin, Western Australia (WA). $\delta^{13}C_{org}$ data from this boundary interval was obtained and correlated with the Global Stratotype Section Point (GSSP) in China spanning the Induan–Olenekian Boundary and provide age constraints on post-mass extinction anoxia/dysoxia in Western Australia. Recovery of biota following the end-Permian extinction was impeded by continued climate change and environmental perturbations that are recorded by $\delta^{13}C$ excursions.

Chapter 3 provides a comprehensive isotopic study including bulk stable isotopic data ($\delta^{13}C_{OM}$, $\delta^{13}C_{carbonate}$, $\delta^{34}S_{pyrite}$, $\delta^{2}H_{kerogen}$), compound specific stable carbon and hydrogen isotopic analysis of individual molecules from the early Triassic (Induan–Olenekian Stage Boundary), preserved in the Senecio–1 well. Compound specific isotope data combined with bulk isotopic data of OM and carbonate are concordant with destabilisation of gas clathrates and release of ^{13}C-depleted methane into the oceans leading to a shift in both ocean and atmospheric $^{12}CO_2$. This data extends previously reported data sets only reported for $\delta^{13}C_{carbonates}$ for this same time interval attributed to climate warming associated with volcanic activity in Siberia. The $\delta^{34}S$ values across the boundary are consistent with euxinic conditions existing in the ocean at the time. The distinct variations in isotope discrimination can be due to changes in the burial efficiency associated with changes in the availability of reactive OM, the organic substrate composition available for metabolism, or during times of euxinic conditions, changing contributions from processes at the chemocline. The shifts in $\delta^{2}H_{kerogen}$ mainly reflect changes in source and preservation of OM.

In **Chapter 4** the distributions of several polycyclic aromatic hydrocarbons (PAHs) across the Induan–Olenekian Boundary for the Senecio–1 core samples have been studied. The concentrations of combustion-derived PAHs, i.e. fluoranthene, pyrene, benzo(*a*)anthracene, benzo(*a*)pyrene, benzofluoranthene, benzo(*ghi*)perylene are abundant in the sample sets, suggesting a source from combustion. Volcanic activity or wildfires due to elevated global temperatures possibly account for high abundances of these components.

Chapter 5 reports the development of offline coupling of MSSV-Py and GC-irMS using a purpose built gas sampling device that enables multiple injections on GC and GC-irMS to measure the molecular composition and stable isotopic values of hydrocarbon gases (*n*-C_1 to *n*-C_5) generated by artificial maturation of sedimentary OM. The hydrocarbon gas yields using this technique have been calculated and compared with those obtained by online MSSV-Py for the same samples (Kockatea shale kerogen) under the same conditions. The major objective of this study was to investigate the potential isotopic fractionation of generated gaseous hydrocarbons within the gas sampling device as a function of time and temperature.

Acknowledgements

"We have come into this exquisite world to experience ever and ever more deeply our divine courage, freedom and light!"

Hafez (1325–1390)
Persian poet

Firstly, I would like to express my sincere appreciation to my supervisor Prof. Kliti Grice, for giving me this great opportunity to work on this PhD project, for her excellent scientific guidance and feedback during my entire PhD study and for providing excellent laboratory facilities. Thanks to Kliti, I was also able to present this research at many national and international conferences and travel to Indiana University to work in the laboratory of Assoc/Prof. Arndt Schimmelmann.

I acknowledge Curtin University, Geoscience Australia (GA) and Geo Forschungs Zentrum (GFZ) Germany for international Postgraduate Award scholarship and Australia-China LNG project for a PhD top-up scholarship.

I like to thank my Associate Supervisors Drs Chris J. Boreham and Lyndon J. Berwick for their time, supervision and advice on the development of the method of offline coupling of MSSV-Py and GC-irMS. I also wish to thank my other co-authors Assoc/Prof. Ian Metcalfe, Assoc/Prof. Michael E. Böttcher, Assoc/Prof. Arndt Schimmelmann, Dr Peter E. Sauer and Prof. Brian Horsfield for their contributions to different parts of this thesis. Furthermore, I would like to acknowledge Mr Geoff Chidlow, for providing excellent analytical support in GC-MS and Mr Stephen Clayton for his support with GC-irMS analyses. Mrs Tanya Chambers and Miss Alicia Harrison are thanked for all their support and organisation of travel.

I also like to thank all my PhD colleagues in the WA-Organic and Isotope Geochemistry Centre for creating a very nice environment to work and in particular Caroline Jaraula and Svenja Tulipani for their encouragements and scientific discussions during my PhD study. Finally but most importantly, all my special thanks go to my adoring family for their understanding, patience and support. I am particularly very thankful to my dear sister Dr Marjan Ladjavardi for her continued encouragement.

Primary and related Publications

This thesis is assembled by publications, either accepted, published, submitted and in preparation, which form the individual chapters and are listed below.

Chapter 2

Metcalfe, I., Nicoll, R.S, Willink, R., Ladjavardi, M., Grice, K. early Triassic (Induan–Olenekian) conodont biostratigraphy, global anoxia, carbon isotope excursions and environmental perturbations: New data from Western Australian Gondwana. *Gondwana Reasearch*, 23 (2013) 1136–1150. Excellence Research Australia (ERA) A* rated publication. Impact Factor: 8.122.

Chapter 3

Ladjavardi, M., Grice, K., Metcalfe, I., Boreham, C.J., Schimmelmann, A., Sauer, P.E., Böttcher, M.E., Melendez, I. Stable isotopic proxies (molecular fossils and bulk parameters) to establish the paleoenvironmental changes spanning the Induan–Olenekian Boundary in the northern onshore Perth Basin, Western Australia: Evidence for methane clathrate release in the early Triassic. *Gondwana Research*, in review (2013), Excellence Research Australia (ERA) A* rated publication. Impact Factor: 8.122.

Chapter 4

Ladjavardi, M., Grice, K., Metcalfe, I., Boreham, C.J. Significance of polycyclic aromatic hydrocarbons (PAHs) in Induan–Olenekian Boundary sections in the northern onshore Perth Basin, Western Australia. In preparation for submission to *Organic Geochemistry*, Excellence Research Australia (ERA) A rated publication. Impact Factor: 2.828.

Chapter 5

Ladjavardi, M., Berwick, L.J., Grice, K., Boreham, C.J., Horsfield, B. Rapid offline isotopic characterisation of hydrocarbon gases generated by micro scale sealed vessel pyrolysis. *Organic Geochemistry*, 58 (2013) 121-124. Excellence Research Australia (ERA) A rated publication. Impact Factor: 2.828.

Statement of Contributions of Others

The work presented in this thesis was primarily designed, experimentally executed, interpreted, and the individual manuscripts were prepared by the first author (Mojgan Ladjavardi). Contributions by co-authors are described below.

Chapter 2

Mojgan Ladjavardi performed all the experimental procedures to obtain bulk $\delta^{13}C$ analyses. Mojgan Ladjavardi and Kliti Grice interpreted the results and contributed to the writing of the paper.

Chapter 3

Mojgan Ladjavardi and Kliti Grice designed the organic geochemical experiments (except for the isolation of kerogens for $\delta^{2}H$ analysis which was designed by Arndt Schimmelmann). Mojgan Ladjavardi performed the experiments, interpreted the results and wrote the paper. All co-authors contributed to the interpretation and writing of the paper. Ian Metcalfe provided the samples and the stratigraphic log. Kliti Grice also provided analytical facilities. Total Organic Carbon (TOC %) contents and Rock-Eval analysis were performed by Chris J. Boreham at GA, Canberra, Australia. Michael E. Böttcher performed analyses of sulfur isotopes on pyrite at Leibniz-Institute for Baltic Sea Research, Warnemünde, Germany. Arndt Schimmelmann and Peter E. Sauer provided facilities for $\delta^{2}H$ measurements at the Department of Geological Sciences, Indiana University, USA. The project was funded by ARC for QEII Fellowship (Kliti Grice) and WA-Organic and Isotope Geochemistry Centre and the John de Laeter Centre for ARC Infrastructure support.

Chapter 4

The samples are the same as analysed in **Chapter 3**. Experiments were designed by Mojgan Ladjavardi and Kliti Grice. Mojgan Ladjavardi performed the experiments including identification and quantification of PAHs as well as all peak integrations and calculation of ratios and relative abundances, interpreted the results and wrote

the chapter. Kliti Grice provided analytical facilities. Kliti Grice, Ian Metcalfe and Chris J. Boreham provided intellectual input to the work. This research was funded by QEII and ARC Linkage grants (Kliti Grice).

Chapter 5

Mojgan Ladjavardi performed all the experiments, interpreted results and wrote the paper. Kliti Grice provided analytical facilities. Lyndon J. Berwick, Chris J. Boreham, and Geoff Chidlow contributed with the development of the method of offline coupling of MSSV-Py and GC-irMS. Brian Horsfield and Chris J. Boreham helped with the design of the gas sampling device. Geoff Chidlow helped with the GC-Flame Ionisation Detection (FID) and Stephen Clayton with the GC-irMS experiments. Lyndon J. Berwick also helped with the calculation and quantification of molecular compositions. The samples (used as test samples for development of the method) were provided by Chris J. Boreham at GA, Canberra, Australia. The artificial maturation experiments for the samples were also performed at GA by Mojgan Ladjavardi. All the co-authors contributed to the writing of the paper. This research was funded by GA, GFZ Potsdam and ARC Linkage grants (Kliti Grice).

Secondary Publications

Manuscripts and abstracts based on research that was conducted during the preparation of this thesis.

Peer reviewed journal articles not part of thesis research

Melendez, I., Grice, K., Trinajstic, K., **Ladjavardi, M**., Greenwood, P., Thompson, K., 2013. Biomarkers reveal the role of photic zone euxinia in exceptional fossil preservation: An organic geochemical perspective. *Geology* 41, 123-126. Excellence Research Australia (ERA) A* rated publication. Impact Factor: 4.638.

Conference abstracts

*****Directly related to PhD

Grice, K., Melendez, I., Jaraula, C., Tulipani, S., Twitchett, R., Böttcher, M., **Ladjavardi, M.,** Maslen, E., Nabbefeld, B., Summons, R.E., Trinajstic, K., Hays, L. Consistent changes in biomarkers (microbes and flora) and stable isotopes across several major extinction events of our planet. Gordon Research Conference. Organic Geochemistry. July 29–Aug 3, 2012, Holderness School, Holderness, New Hampshire, US.

Melendez, I., Grice, K., Trinajstic, K., Thompson, K., **Ladjavardi**, **M.,** Schimmelmann, A., Greenwood, P. Biomarkers and stable isotopes of euxinia and their role in fossil preservation. 18–23 September, 2011, Interlaken, Switzerland, oral presentation.

* **Ladjavardi**, **M.,** Grice, K., Boreham, C.J., Edwards, D., Metcalfe, I., Summons, R. The age and paleoenvironmental conditions spanning the Permian/Triassic Boundary in the northern onshore Perth Basin by using biomarker distributions and stable isotopes (C, H). 18–23 September, 2011, Interlaken, Switzerland, poster presentation.

Melendez, I., Grice, K., Trinajstic, K., **Ladjavardi**, **M.,** Thompson, K. Biomarkers and stable isotopes of euxinia and their role in fossil preservation. Australasian Environmental Isotope Conference and 3rd Australasian Hydrogeology Research Conference. 12–14 July, 2011, Cairns, Queensland, oral presentation.

Melendez, I., Grice, K., Trinajstic, K., **Ladjavardi**, **M.,** Greenwood, P.F., Thompson, K. Biomarkers and stable isotopes and their role in preservation, Western Australia. Australian New Zealand Mass Spectrometry Conference. February, 2011, Perth, Western Australia, oral presentation.

*** Ladjavardi, M.**, Grice, K., Edwards, D., Boreham, C.J., Metcalfe, I., Summons, R.E. Biomarker distributions and stable isotopes (C, H) establish the age and paleoenvironmental conditions spanning the Permian/Triassic in the northern onshore Perth Basin. Australian New Zealand Mass Spectrometry Conference. February, 2011, Perth, Western Australia, oral presentation.

Melendez, I., Grice, K., Trinajstic, K., **Ladjavardi**, **M.,** Greenwood, P.F., Thompson, K. Biomarkers and stable isotopes and their role in preservation, Western Australia, Australian Organic Geochemistry conference, Canberra, December 2010, oral presentation.

*** Ladjavardi, M.**, Grice, K., Edwards, D., Boreham, C.J., Metcalfe, I., Summons, R.E. Biomarker distributions and stable isotopes (C, H) establish the age and paleoenvironmental conditions spanning the Permian/Triassic in the northern onshore Perth Basin, Australian Organic Geochemistry conference, Canberra, December 2010, poster presentation.

*** Ladjavardi, M.**, Grice, K., Edwards, D., Boreham, C.J., Metcalfe, I., Summons, R.E., Volk, H., Horsfield, B. Exploration of oil and gas in northern Perth Basin using stable isotopes of gas inclusions and biomarkers from source rocks. The 5th International Symposium on Novel Carbon Resource Sciences, 22–23 April 2010, Curtin University, Perth, Australia, poster presentation.

*Metcalfe, I., Nicoll, R.S., Mundil, R., Amelin, Y., Schmitz, M., Renne, P., Denyszyn, S., Grice, K., **Ladjavardi, M**., Willink, R., Boreham, C.J., Foster,

C.B. International timescale calibration of the late Permian–early Triassic of Australia. Australian Earth Science Conference, June 2010.

*** Ladjavardi, M.**, Grice, K., Edwards, D., Boreham, C.,J., Metcalfe, I., Summons, R.E., Volk, H., Horsfield, B. Exploration of oil and gas in northern Perth Basin using stable isotopes of gas inclusions and biomarkers from source rocks. 10th Australasian Environmental Isotope Conference and 3rd Australasian Hydrogeology Research Conference, 1–3 December 2009, Curtin University, Perth, WA, poster presentation.

Table of Contents

List of Figures

Chapter 1

Chapter 2

Chapter 3

Chapter 4

Chapter 5

List of Tables

Chapter 2

Chapter 3

Chapter 4

Chapter 5

Chapter 1

Introduction

Biomarkers in organic geochemistry

Biological markers (biomarkers), also known as molecular fossils, are organic compounds that relate to natural product biological precursors (Peters et al., 2005), which have been shown to be strong recorders of past life (Eglinton et al., 1964). Biomarker distributions can therefore be used to extract paleoenvironmental information on deposition environment, photosynthesis, productivity (e.g. ecology, diversity of ancient communities) and are used in petroleum geochemistry for oil–oil and oil–source correlation studies.

In petroleum geochemistry, biomarkers and their stable isotopic compositions are useful to estimate the thermal maturity, transformation of OM into petroleum and to evaluate the geological age of reservoir oil (e.g. Philippi, 1965; Albrecht and Ourisson, 1969; Tissot and Welte, 1984; Peters and Moldowan, 1993). To reconstruct paleoenvironmental conditions during sediment deposition, biomarkers are used to evaluate the source inputs, degree of degradation and thermal maturity of sedimentary OM since the biomarker composition can reflect the ecological

communities and OM sources in the depositional environment (e.g. Philp, 1985; Pancost and Boot, 2004; Grice et al., 1998; Grice et al., 2007).

Biomarkers can be source specific or non-specific. For example, isorenieratane (**I**) is a specific biomarker derived from isorenieratene (**II**) that originated from the photosynthetic secondary carotenoid pigments of green/brown photosynthetic sulfur bacteria (e.g. *Chlorobiaceae*) (Summons and Powell, 1986, 1987; Kohnen et al., 1992; Grice et al., 1996a). Therefore, isorenieratane (**I**) demonstrates the presence of green sulfur bacteria (GSB) and thus photic zone euxinia (PZE), high concentrations of hydrogen sulfide (H_2S) in ocean are described as euxinic conditions and PZE develop when the H_2S reaches the zone of light penetration (Kump et al., 2005; Grice et al., 2005a; see also following sections for more explanations about euxinia). However, most biomarkers can have multiple biological precursors and are thus non-specific. Biomarker studies are often complemented with the analysis of bulk and compound specific stable isotopes, as described in the following section.

Stable isotopes in organic geochemistry

Stable isotope geochemistry is based on the relative and absolute concentrations of the elements and their isotopes on earth. For instance, carbon and hydrogen each have two stable isotopes; ^{12}C accounts for 98.899 weight % and ^{13}C only accounts for 1.111 weight % of the total C pool (Tissot and Welte, 1978; Hoefs, 1997) while ^{1}H accounts for 99.985 weight % and ^{2}H accounts for 0.0105 weight % of the total H pool. The stable isotope ratios of carbon ($^{13}C/^{12}C$) and hydrogen ($^{2}H/^{1}H$) provide insights into the processes (e.g. productivity and photosynthesis) in sedimentary OM as they are generally the most abundant elements and at the molecular level reveal more detailed information about the sources and biosynthesis of individual molecules than Gas Chromatography-Mass Spectrometry (GC-MS) techniques (Freeman et al., 1990; Hayes, 1993; Grice and Brocks, 2011).

The stable isotopic composition of a sample can give indicative information about its origin and environmental fate. Hence, stable isotope analysis has an extensive field of application in different subjects containing origin of biomarkers

and paleoenvironmental reconstruction (Summons and Powell, 1986), environmental sciences (Schmidt et al., 2004), and forensic sciences (Benson et al., 2006).

Stable isotope values

The stable isotope value is a ratio stated as the δ (delta) notation and expressed in per mil (‰):

$$\delta_{sample} = [(R_{sample} - R_{standard})/R_{standard}] \times 1000\ ‰$$

where R is the measured ratio of ^{13}C to ^{12}C for the sample and standard, respectively, relative to an international marine carbonate standard (i.e. Vienna Pee Dee Belemnite, VPDB) (Hoefs, 1987). Since PDB was exhausted several years ago, NBS–19 is used as carbonate reference material relative to PDB to define the VPDB scale (Coplen, 2011; Craig, 1957). For H, R is the measured ratio of ^{2}H to ^{1}H in a sample and standard, relative to the international Vienna Standard Mean Ocean Water (VSMOW) standard (Werner and Brand, 2001). Two methods of measuring stable isotope values of a sample are commonly employed today: bulk stable isotope analysis (BSIA) and compound specific isotope analysis (CSIA).

Bulk stable isotope analysis (BSIA)

BSIA is used to measure the stable isotopic values of all compounds (C, H, O, N and S) in the whole mixture and as a result only a single value representing the average stable isotopic value of all components in the analysed sample is obtained. BSIA is in general a strong technique used in geological studies (Joachimski et al., 2001; Dawson et al., 2007). For BSIA, The geochemical sediment samples are pre-treated to analyse specific fractions (e.g. removal of carbonates with hydrochloric acid for $\delta^{13}C$ analysis of kerogen).

Compound specific isotope analysis (CSIA)

CSIA measures single compounds in a complex mixture (e.g. sediments, soils, ground water, petroleum and natural gas) and results in more specific values. CSIA is conducted using a gas chromatograph - isotope ratio monitoring mass spectrometer, where GC is connected to ir-MS *via* a combustion interface which consists of a quartz tube containing CuO pellets (850 ^{o}C) and through a pyrolysis furnace to

determine $^{13}C/^{12}C$ and D/H of individual compounds in a complex mixture, respectively (Matthews and Hayes, 1978; Burgøyne and Hayes, 1998; Prosser and Scrimgeour, 1995). CSIA of stable carbon isotopic compositions is a complimentary tool to determine the biogeochemical changes and to confirm the evolutions in marine and atmospheric CO_2 (Grice et al., 2005a; Fenton et al., 2007). The D/H of biomarkers provides additional insights into their origin (Schimmelmann et al., 2006; Maslen et al., 2009; Dawson et al., 2005). It can also be used as a marker for changes in the ancient water cycle (e.g. paleosalinity and paleotemperature) (Sauer et al., 2001; Dawson et al., 2004). Therefore, a broad range of applications exists for CSIA methods in biogeochemistry (e.g. paleoreconstruction) (Hayes, 1993; Grice and Brocks, 2009).

$\delta^{13}C$ in OM and petroleum

Measured stable isotopic values of OM can provide valuable information about biochemical, ecological, environmental, and atmospheric changes as the principal components of OM (C and H) are important factors in biogeochemical processes associated with the carbon cycle in ancient depositional environments (Freeman et al., 1990). Distribution of stable carbon isotopes in plants and phytoplankton are controlled by many factors (Hayes, 1993), For instance the photosynthetic pathway involved in the uptake of CO_2 (Schouten et al., 1998), isotopic fractionations related with biosynthesis (e.g. lipids versus protein and carbohydrate biosynthesis) (Grice et al., 2005), growth rates of phytoplankton (Laws et al., 1995) and further physiological factors such as cell size and geometry (Popp et al., 1998). The process of photosynthesis results in the ^{13}C-depleted isotope in biolipids compared to the carbon source.

$\delta^{13}C$ values of petroleum components have been used widely in several areas of petroleum geochemistry such as oil-source rock correlation, oil-oil correlation (Dawson et al., 2007), gas-source correlation (Schoell, 1983) and also to determine age, origin and the nature of depositional environment of the source (Chung et al., 1992). $\delta^{13}C$ values of kerogen, source-rock extracts and

individual compounds (e.g. *n*-alkanes) shows an increase with thermal maturity that results preferential release of ^{12}C enriched products (Clayton, 1991).

Stable carbon isotope fractionation

The stable carbon isotope analysis of gases plays an important role for correlation of gases (e.g. methane, ethane, propane, and carbon dioxide) to their origin in petroleum reservoirs and presenting gas recharging history, maturity, predicting further gas reservoirs and to prevent other interpretations of the isotope anomalies such as mixing of gases from diverse sources (Whiticar, 1994; Boreham et al., 1998). Variations in stable isotopic composition or "isotopic fractionations" happen in nature due to chemical, physical and biological processes such as phase transfer, chemical reactions or steps in metabolic pathways depending on the strength of intramolecular bonds, which is caused by the difference in mass between isotopes of the same element (Hoefs, 1987; Sessions et al., 1999; Schouten et al., 2007). "Heavy" isotopes usually form stronger bonds compared to "light" isotopes (Bigeleisen and Mayer, 1947; Urey, 1947) and lighter elements usually display much more important isotope effects due to the bigger relative mass difference between isotopes. Isotopic fractionation is controlled by equilibrium and kinetic processes.

Equilibrium isotope effects

The effect that causes one isotope to become more concentrated in one component of a reversible system in equilibrium is called "equilibrium isotope effect" (Hoefs, 1987). Enriched or depleted components will be produced if the ^{13}C-enriched or ^{13}C-depleted isotope concentrates in the component of interest, respectively. As the components tend to form the stronger bond, it is mostly the ^{13}C-enriched isotope that concentrates in the component. In general, equilibrium isotope effects demonstrate differences in the bond strengths of the isotopes in the various components of the system. An equilibrium isotope effect for instance happens between the liquid and vapour phase of water in a closed system where deuterium becomes enriched in the liquid phase and depleted in the vapour (Urey, 1947).

Kinetic isotope effects

The effect that causes one isotope to react more rapidly in an irreversible system, in which the products are swept away from the reactants before coming to equilibrium, is called the "kinetic isotope effect" (Hoefs, 1987). As the ^{13}C -depleted isotope reacts more rapidly compared to the ^{13}C-enriched one, therefore the product will be lighter than the reactant, for example isotopic fraction in metabolic pathways or diffusion reaction (Bigeleisen and Wolfsberg, 1958). In gases the isotopic composition of ^{13}C-depleted hydrocarbon is controlled kinetically since ^{12}C-^{12}C bond strengths are slightly less stable than ^{12}C-^{13}C bonds (Tang et al., 2000).

Stable sulfur isotopes

The sulfur cycle has been studied thoroughly for many decades (Canfield, 2001). Most of the Earth's sulfur is locked up in rocks or is buried in oceanic sediments. Sulfur enters the atmosphere through both natural (e.g. volcanic eruptions, bacterial processes, evaporation from water or decaying organisms) and human sources (e.g. industrial processes). Once sulfur dioxide (SO_2) enters the atmosphere, it will react with other chemicals to produce sulfur salts or with water to produce sulfuric acid (H_2SO_4). All these particles will be consumed by plants and returned to the atmosphere; consequently the cycle will start this over again. Variations in the sulfur cycle have been related to the growth of earth surface chemistry, developing chemistry of the atmosphere and oceans, also to changes in ecology of sulfur-utilizing organisms (Farquhar, 2003).

There exist four stable isotopes in nature: ^{32}S (95.02 %), ^{33}S (0.75 %), ^{34}S (4.21 %), and ^{36}S (0.02 %) (Hoefs, 2008). The ratio of $^{34}S/^{32}S$ is usually measured since ^{34}S is the most abundant of the heavier isotopes and the relative mass difference to ^{32}S is enough to cause major isotope effects. The ratio is reported in the δ-notation versus Vienna-Canyon- Diablo-Troilite (V-CDT) standard (Mann et al., 2009) and used as traces in marine geochemistry, the composition of the atmosphere and investigation of secular changes of seawater chemistry.

The most important isotope fractionation in sulfur cycling occurs during dissimilatory reduction of dissolved sulfate in the bacterial cell (Rees, 1973), due to kinetic effects during bacterial sulfate and chemical exchange between sulfate

(SO_4^{2-}) and sulfide (S^{2-}) species (Canfield, 2004). The change in the valence state of sulfur by pure cultures produces H_2S that is enriched in the ^{32}S by about 50 ‰ compared with sulfate. The magnitude of isotope difference is determined by conditions such as substrate and sulfate concentrations, cellular sulfate reduction rate, and the organisms (Chambers and Trudinger, 1979; Canfield, 2001; Kaplan and Rittenberg, 1964; Amend et al., 2004; Bolliger et al., 2001). For source identification in aerobic surface environments, the sulfur isotopic composition of sulfate is used (e.g. anthropogenic versus geogenic sulfate in rain, river, and ground waters) (Clark and Fritz, 1997). $\delta^{34}S$ values of petroleum include limited evidence about paleoenvironmental conditions and OM sources as a result of significant isotopic fractionation during sulfur incorporation (Faure and Mensing, 2005), nevertheless the analysis of $\delta^{34}S$ of petroleum is quite beneficial in oil-oil correlations (Gaffney et al., 1980).

δ^2H in OM and petroleum

Hydrogen has the largest mass difference between its two stable isotopes (^1H and ^2H) and therefore shows the largest isotope effects. The measurement of δ^2H values is of great interest in organic geochemistry, as it is present in water and in all biomolecules. However, due to the very low abundance of δ^2H in nature, the hydrogen isotopic measurement is an analytical challenge. Ocean water as the world's largest natural reservoir of hydrogen and/or meteoric water produced by operation of the hydrological cycle are consumed by living organisms. Thus, the distribution of δ^2H is primarily controlled by the natural processes in the global hydrological cycle. Major isotopic fractionations in the hydrological cycle happen during phase transfer process causing δ^2H-depletion in meteoric waters and are effected by factors such as latitude or temperature (Craig, 1961; Gat, 1996; Kehew, 2001).

The isotopic composition in meteoric waters is reflected by δ^2H values of biolipids in primary producers, making the measurement of δ^2H values of biomarkers a strong tool for reconstruction of hydrological conditions and paleoclimates at the time of deposition (Sauer et al., 2001; Andersen et al., 2001; Dawson et al., 2004). The abundance of δ^2H in the water body is mirrored by δ^2H values of biolipids in

aquatic primary producers (e.g. aquatic plants or phytoplankton) and is chiefly controlled by the amount of fresh water input containing precipitation and evaporation (Gat, 1996; Ingram et al., 1996; Sachse et al., 2006). Information about thermal maturity, kerogen type, facies and paleoclimate can be obtained by using δ^2H on bulk kerogen ($\delta^2H_{kerogen}$; Schimmelmann et al., 2001).

However, there are limitations on $\delta^2H_{kerogen}$ as a paleoenvironmental indicator because an isotopically labile part of the bulk hydrogen (exchangeable H, H_{ex}) exchanges quickly and reversibly with water during thermal maturation (Nabbefeld et al., 2010c; Vandenbroucke and Largeau, 2007; Schimmelmann et al., 1999), subsequently resulting in a change in the hydrogen isotope composition of the kerogen. Hence, to reconstruct paleoenvironmental conditions, only δ^2H values of kerogens with low thermal maturity are assumed to be reliable (Lis et al., 2006; Hassan and Spalding, 2001).

OM deposition and preservation in sediments

Sediments contain OM derived from the remains of organisms that lived at the time of deposition (e.g. Prokaryotes, Eukaryotes and Archeae). Sedimentary OM can be autochthonous, i.e. produced in situ, similar to the environment of the precursor organism, or allochthonous deriving from the organisms that lived outside the place of deposition, for example, terrestrial OM transported into the lacustrine settings or oceans through surface runoff or rivers (Tissot and Welte, 1984). Allochthonous OM is rich in small lakes and streams while autochthonous is mostly deposited in large lakes and oceans. Conditions such as the energy situation in the water body and the supply of sedimentary particles must be suitable for considerable organic sedimentation, since too high or too low energy level of body water can cause erosion or insufficient sedimentation (Tissot and Welte, 1984).

Sediments can be deposited in various environments like lacustrine, fluvial, deltaic, tidal, lagoonal, shallow marine, deep water marine, reefal or glacial (Peters et al., 2005) which largely influence their composition and properties. Favourable conditions for the deposition of OM are along the continental margins (e.g. lakes, rivers, lagoons or swamps) due to high primary productivity of coastal waters and/or

high input of land-derived terrestrial plant material (Tissot and Welte, 1984). The sedimentary environments of lakes and oceans vary in some aspects, causing different types and quantities of OM. Lakes are smaller than the deep ocean basins, therefore can obtain more terrigenous clastic detritus compared with the deep oceans which increases primary productivity (Peters et al., 2005). In addition to the depositional conditions, other factors like high primary productivity (algae), controlled by elevated nutrient inputs (i.e. phosphate, nitrate) and oxygen-availability during photosynthesis are also of great importance and allow the primary producers to bloom (Suess, 1980; Betzer et al., 1984).

After the accumulation of OM in sediments, it starts degradation and remineralisation. The different stages that describe the alteration of OM and production of kerogen, bitumen and gas are described in the following sections. The preservation of OM during sedimentation and burial is determined by several causes like O_2 content of the water column, water circulation, organic productivity, sediment particle size and sedimentation rate (Demaison and Moore, 1980). Only 0.1 % of OM is preserved over geological time since the major part of the detrital OM gets recycled *via* pelagic organisms within the surface waters of the marine environment and the minor quantity of OM reaching the surface would get recycled by benthic organisms (e.g. Moodley et al., 2005; Killops and Killops, 2005). In order to achieve OM rich deposits, the remaining detrital OM should be incorporated into the sediments and altered under specific conditions (**Figure 1.1**).

Major amounts of OM are preserved in stagnant lakes and/or marine basins where restricted circulation exists and the access of oxygen to the sedimentation environment is restricted (Demaison and Moore, 1980; Waples, 1981). Where oxic conditions exist, the OM is mainly destroyed throughout sedimentation even when organic productivity is high (e.g. most polar regions in the modern oceans) (Demaison and Moore, 1980). OM quickly becomes oxidised under oxic water column aerobic bacteria and other organisms. The remaining OM after exhausting all available O_2 would then be oxidised by anaerobic organisms using other oxidants such as nitrate or sulfate (Peters et al., 2005).

Low oxygen/anoxic conditions (reducing conditions) are best to preserve OM (Demaison et al., 1984; Moodley et al., 2005) and approximately 10 % of OM is

preserved in reducing conditions, while < 0.1 % is preserved under oxygenated conditions (Demaison et al., 1984). The ideal anoxic conditions for OM preservation occur when the rate of oxidation of OM by bacteria is greater than the supply of oxygen; these conditions can be caused by certain factors such as stagnation periods, substantial inputs of OM and strong thermoclines (Moodley et al., 2005; Killops and Killops, 2005). Thermocline often happens in the bottom of stratified and stagnant water-columns where oxygen in the lower part gets utilised by aerobic decomposers and mixing with the oxygenated top water is prohibited, for instance through density stratification of warm layer water over cold bottom waters (Kling, 1988; Grice et al., 1998a). Enclosed area with restricted water exchange such as lagoons, lakes and coastal zones with upwelling carrying the nutrients to the surface are ideal environments for anoxic basins (Waples, 1981). Anoxia is the most important reason for high preservation of H and lipid-rich OM in petroleum source rocks (Demaison and Moore, 1980). Extracts from petroleum source rocks contain biomarkers and supporting parameters representing anoxic conditions (e.g. high Vanadium/Nickel porphyrin, low pristane/phytane) (Peters et al., 2005).

High concentrations of H_2S produced by sulfate-reducing bacteria in the ocean are defined as euxinic conditions (Killops and Killops, 2005). Sulfate-reducing bacteria utilise sulfate as an electron acceptor in their metabolism to produce H_2S (Trull et al., 2001). Euxinic conditions are usually limited to the bottom waters within a stratified ocean body, provoking some of the best quality source-rocks. In very exceptional cases, conditions of photic zone euxinia can arise if the H_2S progresses to the zone of light penetration (i.e. photic zone) (Grice et al., 2005). Only particular organisms such as purple sulfur bacteria (PSB), the brown sulfur bacteria (BSB) and the green sulfur bacteria (GSB) can endure under these conditions. This event happens constantly in only a few locations such as certain isolated deep Fjords and in the Black Sea (Anderson et al., 1988).

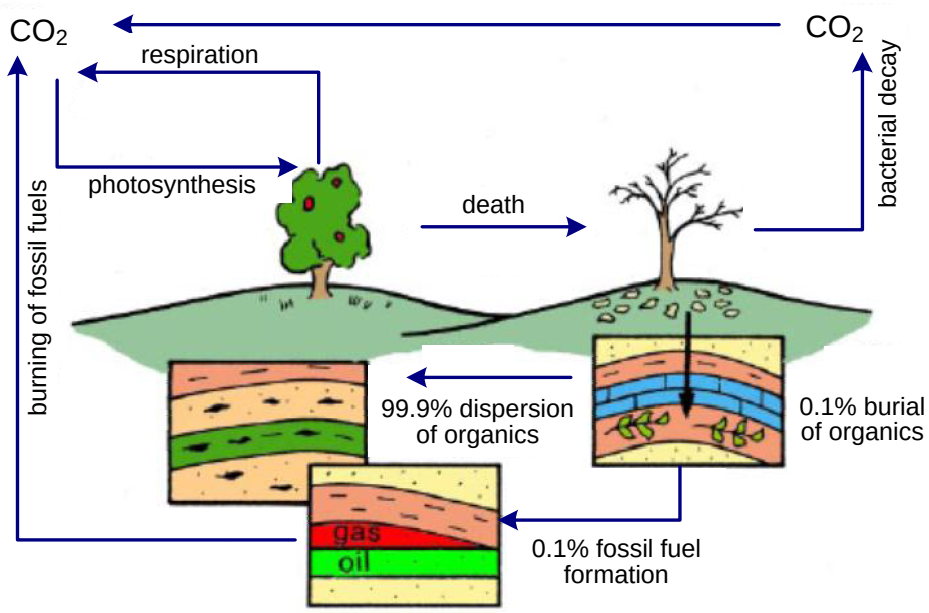

Figure 0.1: Preservation of OM in sediments (modified after Tissot and Welte, 1984).

Thermal maturity and generation of petroleum

OM in sediments is affected by gradual increases in temperature and pressure during burial resulting in degradation and chemical alteration (maturation) over geologic time (Peters et al., 2005). The degree of maturation can be determined using non-molecular parameters, for instance vitrinite reflectance (R_o %) and Rock-Eval pyrolysis (Peters, 1986) as well as molecular parameters (Peters et al., 2005). Vitrinite reflectance (R_o %) represents the reflection of a beam of normal incident white light from the surface of polished vitrinite as a function of maturity and is the typically measured thermal maturity parameter. With increasing maturity, coal rank and the chemical composition change and as a consequence the vitrinite macerals become progressively reflective (Killops and Killops, 2005). There are three OM maturation stages in sediments: diagenesis (R_o < 0.6 %), catagenesis (0.6 % < R_o <2.0 %) and metagenesis (2.0 % < R_o < 4.0 %) (**Figure 1.2**, See below for more details) (Peters and Moldowan, 1993).

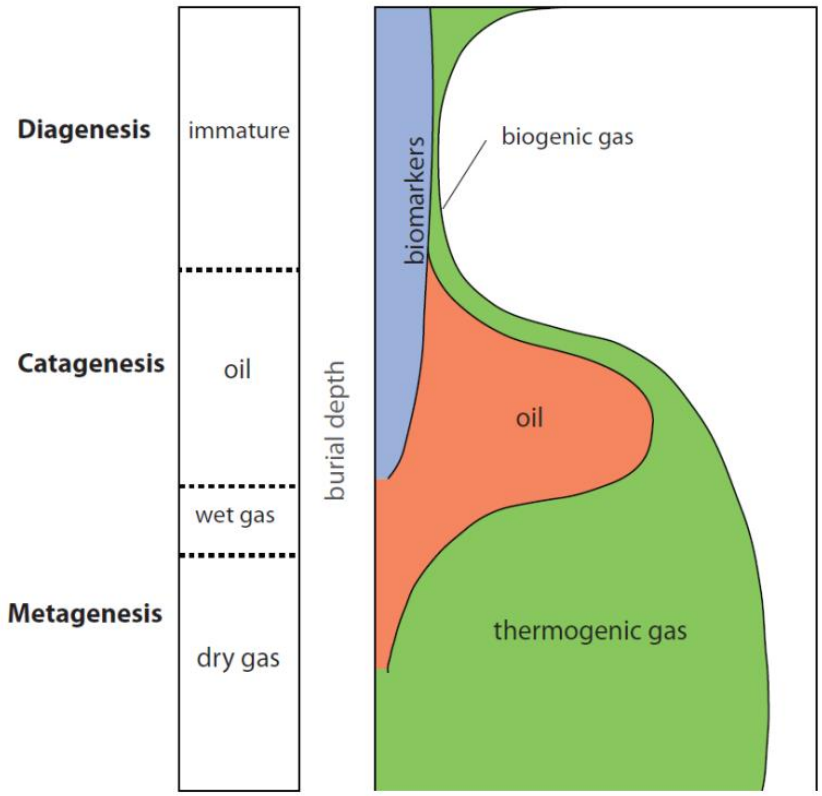

Figure 0.2: Simplified evolution of OM during and after sedimentation (modified after Peters et al. 2005).

Diagenesis

Diagenesis is the first stage in OM breakdown and alteration in soils and sediments (Tissot and Welte, 1984) and is mainly controlled by complex biological and chemical processes which transform biomolecules before major thermal alteration occur (Peters et al., 2005). These processes are strongly affected by conditions in the depositional environment such as O_2 or H_2S levels and many other biochemical parameters (Brocks and Grice, 2011). Under such conditions, bacterial activity is still considerable and causes the generation of biogenic methane (Rice and Claypool, 1981).

Biomarkers that form the hydrocarbon structural skeleton of the original molecule are developed during this stage by removal of functional groups from the natural biochemical (Huc, 1980). Diagenesis differs from the subsequent stages as it occurs in a limited depth range of subsidence and at low temperatures (below 60 °C).

Throughout diagenesis a highly complex macromolecular matrix (kerogen- see *kerogen* section for more details) is formed by enrichment of resistant biological macromolecules (e.g. algaenan, cellulose or diamondoids) as a result of selective degradation (Largeau and Derenne, 1993; Grice et al., 2003) also the incorporation of these macromolecules and other smaller compounds in sedimentary OM *via* condensation and cross-linking reactions (Tissot and Welte, 1984). During early diagenesis, the composition of the kerogen is dominated largely by the original input of OM as well as the nature and level of microbial activity in the upper sedimentary layers of sediment. With increasing depth and temperature, heteroatomic bonds are broken consecutively producing H_2O and CO_2 as volatile products (Tissot and Welte, 1984).

The first petroleum products released by this alteration generally consist of heteroatomic compounds of high molecular weight, mainly asphaltenes and resins during later stages of diagenesis (Tissot and Welte, 1984). Polycondensation reactions within OM result in the formation of fulvic and humic acids. Maturation has been indicated to affect the stable isotopic composition of petroleum in the subsurface (Clayton, 1991). It has been observed that $\delta^{13}C$ values of kerogen increase with thermal maturity as a result of thermal release of ^{13}C-depleted products (Clayton, 1991).

Catagenesis

The process of catagenesis follows diagenesis and is a process by which the OM in rocks is thermally altered within the deep-surface under increasing temperature (temperatures range between 60 and 150 °C) (Press and Siever, 2001). With increasing temperature in catagenesis, more bonds are broken such as esters and also some C-C bonds. The new produced fragments are smaller and devoid of O_2, therefore lower-molecular weight hydrocarbons are relatively enriched to form liquid bitumen (Peters et al., 2005, see *bitumen* section for more details). This corresponds to the major phase of oil formation (Tissot and Welte, 1984). The carbon of bitumen released by this process is more depleted in ^{13}C than carbon of the released kerogen. This isotope fractionation can be explained by the relationship between isotope distribution and chemical structure (Galimov, 1975). Bitumen is originated from chemical groups, initially depleted in ^{13}C, such as aliphatic chains or saturated

cycles; this isotopic character is conserved when hydrocarbon molecules are released from kerogen.

In the latter part of catagenesis, all potential source-rocks comprise great amounts of hydrocarbon gases (wet gas) (Hunt, 1996). The methane gas generated by cracking displays more negative $\delta^{13}C$ values compared to heavier hydrocarbons and kerogen due to higher probability for breaking ^{12}C-^{12}C bonds than ^{13}C-^{12}C (Stevenson et al., 1948).

Metagenesis

The second stage of thermal maturation is known as metagenesis and takes place at temperatures higher than 150°C (Hunt, 1996). During metagenesis, most labile functional groups and chains are eliminated and polycondensation and aromatisation of the residual kerogen increases. Such residual kerogen is unable to continue to generate hydrocarbons and the OM consists of methane and occasionally H_2S or N (Hunt, 1996). In the deepest part of the sedimentary basins, the remaining sulfur is mostly lost and H_2S generation increases. This is the major phase of "dry gas" formation (Tissot and Welte, 1984). Solid residues, at the end of metagenesis, are likely to have a structure that is similar to graphite. With increasing evolution of the sediments the amount of thermal methane increases and the $\delta^{13}C$ values become less negative. Early methane is depleted in ^{13}C as compared to the kerogen which is the source for it; however the difference is gradually reduced from diagenesis to catagenesis to metagenesis stages (Tissot and Welte, 1984).

Composition of OM

Source rocks are fine-grained organic rich rock that could produce (Potential source rock) or have already generated (effective source rock) important amount of petroleum (Peters et al., 2005). Immature rocks have endured diagenesis but have not yet been thermally transformed, while rocks in and after oil generative window are referred to as mature and post-mature, respectively.

In sedimentary rocks that have undergone strong thermal conditions during diagenesis and catagenesis, the OM consists of kerogen, bitumen and gas. **Figure 1.3**

shows the approximate percentage of the different fractions existing in sedimentary OM.

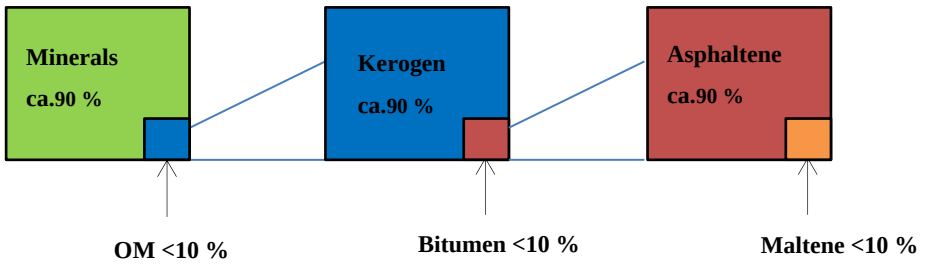

Figure 0.3: Approximate percentage of sedimentary OM during the maturation process (modified after Tissot and Welte, 1984).

Kerogen

Kerogen is a high molecular-weight of OM that is common in sedimentary rocks but not readily soluble in common organic solvents (Durand, 1980; Tissot and Welte, 1984). It is the most abundant form of OM on Earth.

Although the bulk OM undergoes chemical alteration through diagenetic processes, the resultant molecular products and their stable isotopic signatures can still provide information on past environmental processes and the production pathway of the OM, such as photosynthesis (Vandenbroucke and Largeau, 2007). Carbon isotope distributions in kerogen depend on the origin and chemical structure of OM (Hoefs, 1997). For instance, it has been observed that terrestrial OM is enriched in ^{13}C-depleted isotopes compared to marine planktons reflecting the isotopic composition of the carbon source for photosynthesis, since marine plants utilise carbonate complexes in seawater, while terrestrial plants use atmospheric CO_2 with a lower $\delta^{13}C$ (Tissot and Welte, 1984).

Kerogen can be classified into four types: I, II (II-S) and III according to the nature of their OM and the depositional environment (Durand and Espitalié, 1973; Tissot and Welte, 1984; Killops and Killops, 2005). Main chemical differences occur between organisms living in an aquatic and those living in subaerial environment (Tissot and Welte, 1984). These kerogen types have different oxygen/carbon (O/C)

and hydrogen/carbon (H/C) atomic ratios, which are commonly represented in the van Krevelen (1961) diagram, the plot shows different types of kerogen (**Figure 1.4**). Van Krevelen diagram provides an evaluation of hydrocarbon generative potential (Espitalié et al., 1997). Type I kerogen is comparatively rare and usually formed from algal OM deposited in a lacustrine or brackish water settings (e.g. *Botryococcus braunii*). It is highly oil-prone and includes a significant input from lipids, mainly long-chain *n*-alkanes from bacterially decayed algal material or bacterial remains, developing algal macerals or amorphous structures. Type I kerogen contain less aromatic and heteroatomic components, compared to other kerogen types. The H/C can reach up to 1.9. Type I kerogen typically develops in fine-grained, organic-rich sediments that are deposited under reducing conditions in oxygen depleted and shallow water bodies (Durand, 1980; Killops and Killops, 2005).

Type II kerogen primarily contains remains from mixed allochthonous phytoplankton, zooplankton, and bacterial OM, but also allochthonous OM, from lipid-rich remains of higher plants (e.g. spores, pollen, cuticles, resins and waxes) (Durand, 1980; Killops and Killops, 2005) and is commonly found in marine environments. This kerogen type contains more aromatic and ketone structures compared to Type I, but also shows the existence of aliphatic components and sulfur containing compounds (Durand, 1980; Killops and Killops, 2005). Type II kerogens that contain high sulfur contents (8 – 14 %) are sub-classified as Type II-S. The H/C ratio can be up to 1.4. Type-II and Type II-S kerogen are oil-prone (**Figure 1.4**).

Type III kerogen is formed from terrigenous/woody matter and usually deposited in a deltaic marine setting (Durand, 1980) (**Figure 1.4**). Microbial degradation in the basin of deposition is mostly limited as a result of significant sedimentation and rapid burial; since this type is quite frequent in thick detrital sedimentation along continental margins (Tissot and Welte, 1984).This kerogen type is gas-prone, containing mostly polyaromatic compounds (Tissot and Welte, 1984; Killops and Killops, 2005). The H/C ratio is 1 or less.

Type IV kerogen is controlled by inertinite macerals and contains mainly black opaque non-specific organic particles (Peters et al., 2005). There are several origins of this kind of nonreactive organic material such as reworked, oxidized OM (i.e. highly oxidised higher plant material) or inertinitic material developing due to

subaerial weathering or biological oxidation in swamps and soils (Tissot and Welte, 1984).

Type IV kerogens have no oil generative potential and little potential to generate gas (Durand, 1980; Tissot and Welte, 1984; Killops and Killops, 2005.).

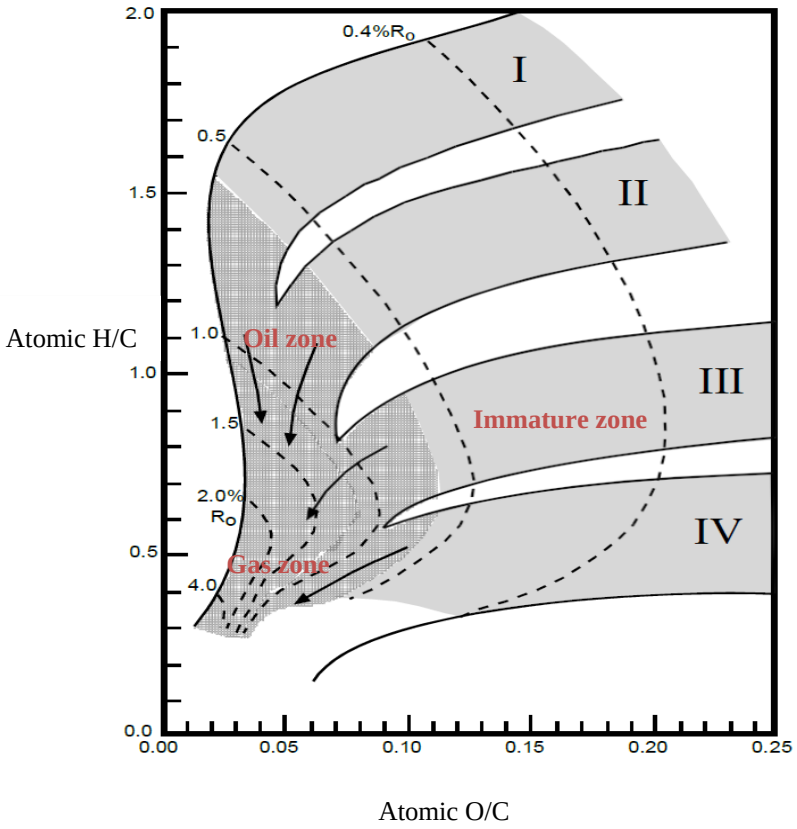

Figure 0.4: Different types of kerogen according to increased levels of burial and thermal maturity presented on van Krevelen diagram (the arrows point to increasing maturity) (modified after Tissot and Welte, 1978).

Bitumen

Bitumen (low-molecular weight compounds)) is referred to as *in situ* hydrocarbons that can be extracted using common organic solvents (e.g. dichloromethane and methanol) (Peters et al., 2005).

Bitumen is free OM dispersed within fine-grained sedimentary rocks which can be similar in composition to crude oil. It is primitive to the source rock unlike to

crude oil which has migrated away from the source rock and consists mostly of defunctionalised and isomerised saturated and aromatic hydrocarbons, containing many biomarkers, as well as hetero compounds (Tissot and Welte, 1978; Hunt, 1996., Brocks and Grice, 2011).

A second bitumen fraction (bitumen II) has been recently identified which is entrapped within the mineral matrix and can be released through heavy mineral separation. Bitumen II contains a different chemical composition than bitumen I and is becoming of great significance in investigating the role of OM related to mineral deposits (Nabbefeld et al., 2010a).

Offline coupling of MSSV-Py and GC-irMS

In order to establish the source of natural gas, it is essential to relate the gases with their sources, which is mainly based on the proportion or correlation of individual gas components and their carbon isotopic composition (Michels et al., 2002). The carbon isotopic compositions are used to identify the gas origin and evaluation of natural gases in petroleum reservoirs and to predict additional gas reserves (Boreham et al., 1998). During the geological history of a source rock, many physico-chemical parameters of natural samples can be changed by secondary phenomena such as, expulsion, oxidation and migration. In order to overcome these limitations, artificial maturation experiments using analytical pyrolysis techniques have been deployed (Michels et al., 2002; Dieckman et al., 2006).

Pyrolysis is used by geoscientists to thermally degrade and convert complex materials like: coals, kerogens and petroleum fraction to smaller molecular fragments. There exist two main categories for pyrolysis systems; in open system conditions, generated hydrocarbons are transported away from the heating device directly after their formation; however, in closed system condition the processes can happen throughout the progressive subsidence of sedimentary basins such as petroleum generation and migration (Horsfield et al., 1989; Dieckman et al., 2006). The characterisations of organic macromolecules have been performed using a range of analytical pyrolysis techniques coupled with online or offline GC-MS. In order to implicate less severe thermal conditions and to limit the fragmentation of organic

material, small quantities of sample (e.g. 0.1 – 10 mg) enclosed within glass tubes were heated under controlled temperature (e.g. 250 – 350 ºC) and time (e.g. hrs-days) conditions (Horsfield et al., 1989).

However, this technique only allows single analysis; the number of replicate analysis is not possible due to the online nature of this technique (Horsfield et al., 1989). In chapter 5, the method of offline coupling of MSSV-Py and GC-irMS has been established with the purpose of measuring molecular composition and stable isotopic values of hydrocarbon gases generated during the artificial maturation of sedimentary OM and to assess the source of gas. The importance of this study is to improve our knowledge of the processes that lead to the formation of natural gas and increases our ability to explore and assess natural gas resources (Boreham et al., 1998).

Permian/Triassic Mass Extinction Event

Major catastrophic events occurred at various times in Earth's history, causing the extinction of up to 90 % of the species that have populated the Earth. More than 70 % of species disappeared within a few hundred million years (e.g. Peters at al., 2005).

The most significant mass extinction events happened throughout the end–Ordovician, or are related to the Frasnian/ Famennian (F/F), The Permian/Triassic (P/Tr), the Triassic/Jurassic (Tr/J) and the Cretaceous/Tertiary (K/T) boundaries (**Figure 0.5**) also as many as 22 minor mass extinctions have been identified from the fossil record of the entire Phanerozoic (Sepkoski, 1986). Many of the minor mass extinctions led to 25 – 70 % of species loss.

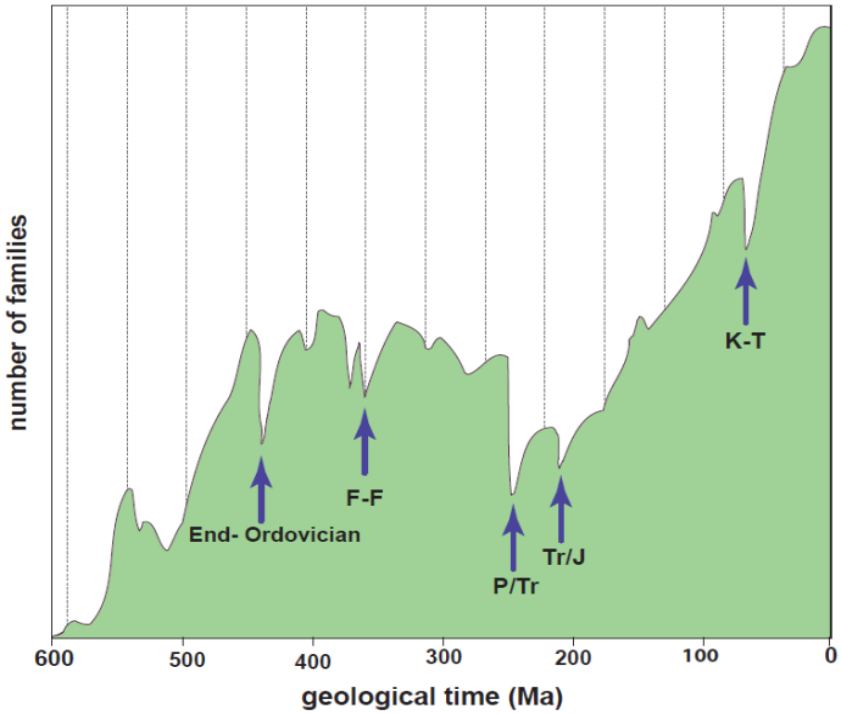

Figure 0.5: Mass extinction events identified throughout the history of Earth (modified after Sepkoski, 1993).

The end–Permian (ca.253 million years ago) extinction was the most intense extinction of the entire Phanerozoic. It is documented that both marine and terrestrial organisms are affected by mass extinctions, resulting in loss of species diversity (Sepkoski, 1986: Bowring et al., 1999; Bambach, 2006). The degree of these mass extinctions and their effects on different species are the subject of current research (Bambach, 2006). However, many theories have been suggested to explain the end–Permian mass extinction (Stanley, 1988; Erwin, 1994; Racki and Wignall, 2005). The least favoured theory is a bolide impact (Koeberl et al., 2004).

Kamo et al. (2006) discussed the coincidence in timing of the P/Tr extinction with the eruption of the Siberian flood basalts. During the eruptions, climate warming could have been developed due to the release of methane hydrates together with anoxic and sulfidic oceans releasing toxic gases such as H_2S into the atmosphere (Grice et al., 2005a; Racki and Wignall, 2005; Nabbefeld et al., 2010a; Sephton et al., 2005; Svensen et al., 2009). It has been widely reported that the oceans were anoxic (Wignall and Twitchett, 1996) and photic zone euxinic conditions developed globally (Grice et al., 2005a; Kump et al., 2005; Hays et al.,

2007; Nabbefeld et al., 2010a,b,c). Further, as described by Knoll et al. (1996) hypercapnia (high CO_2) can be considered as a kill mechanism for the selectivity of the extinction. Actually, a single mechanism may not be adequate, and the extinction may be the result of a combination of factors such as methane release, anoxia, euxinic conditions and hypercapnia (Erwin, 1994).

Early Triassic Induan–Olenekian Event

Following the late Changhsingian mass extinction, there was a period of continued global climatic and environmental upheaval and stress termed the early Triassic "cesspool" (Algeo, 2011). The recovery of the extinction was a “delay” in the Triassic (Metcalfe et al., 2013; Wignall and Twitchett, 2002). Throughout the early recovery phase, the variety of marine ecosystems was still low and only few marine clades recovered quite fast, for instance ammonoids and conodonts (Brayard et al., 2006; Orchard, 2007). Within the early Triassic, variations of ammonoid diversity in time and space have been deduced as fluctuations of the global temperature gradient (Brayard et al., 2006).

Sedimentary records of the basal Triassic indicate rare facies growth such as seafloor precipitated carbonate fans, microbialites, flat pebble conglomerates and wrinkle structures, as a result of infrequent ocean chemistry (Baud et al., 2007). Dysoxia/anoxia in the shallow-marine environment appeared in the latest Permian at the extinction level, later than in the deep-marine environment, and appears to be mainly restricted to the Induan (Griesbachian and Dienerian) and early Olenekian (Smithian) (Metcalfe et al., 2013). To better understand the paleoenvironmental changes that occurred around the early Triassic Induan–Olenekian (Dienerian–Smithian) Stage Boundary, a comprehensive study based on relatively abundant conodont faunas (Chapter 2), organic geochemical and compound specific stable carbon and hydrogen isotopic analysis of biomarkers (Chapter 3) and PAHs (Chapter 4) from the Senecio–1 core located in the northern Perth Basin, Western Australia has been carried out.

The Perth Basin, Western Australia

The Perth Basin formed during the continental development between the south-western continental border of Australia and greater India (Matte et al., 1997; Ali and Aitchison., 2005). The Perth Basin is located in southwest Western Australia (WA) (**Figure 1.6**) (Thomas and Barber, 2004). It is a deep, north to south trending and extends over 1,000 km from Geraldton to the north of WA. In the northern Perth Basin, the offshore and onshore are detached by an intra-basin high including the Dongara Terrace and Beagle Ridge. The Beagle Ridge forms an intra-basin high between the Abrolhos sub-basin to the west and Dandaragan to the east (Playford and Willmott., 1958; Dickins et al., 1961; McTavish., 1965). The Perth Basin sediments comprise of rocks of Permian−Early Cretaceous age (Thomas and Barber, 2004).

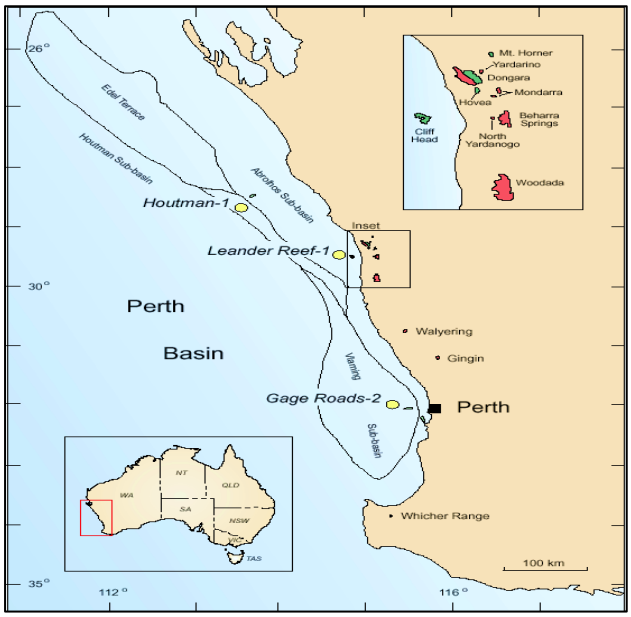

Figure 0.6: A map of the Perth Basin (modified after Metcalfe et al., 2013).

The Perth Basin petroleum system has been explored for the last few decades, resulting in gas and oil production from several onshore fields (e.g. Summons et al., 1995). From the beginning of petroleum evaluation in the Perth Basin, the Lower Triassic Kockatea Shale has been identified as the main source for the oils from the

Dongara Terrace and near surroundings (e.g. Dongara, Mondarra, North Erregula and Woodada fields) (Powell and McKirdy, 1973).

The Dongara gas field in the onshore Perth Basin holds more than half the oil and gas reserves (Thomas et al., 2004). More discoveries of Kockatea shale-sourced oils have spread further than the Dongara Terrace to the accumulations at Eremia, Hovea and Jingemia and offshore at Cliff Head (Thomas and Barber, 2004; Jones and Hall., 2002). Thomas and Barber (2004) limited the effective source rock to early Triassic, middle Sapropelic interval in the Hovea Member of the Kockatea Shale. As well as being central to the petroleum prospectivity of the Perth Basin, deposition of the Kockatea Shale has also been closely related to events across the Permian−Triassic mass extinction (Grice et al., 2005a; 2005b). This thesis study continues our focused research into better defining the age, organic facies and deposition conditions associated with this World class source rock. The Perth Basin sediments used in this study are from the Senecio–1 drill core, which is located approximately 15.5 km to the north of Dongara.

Aims of the thesis

The main objectives of this thesis were to better understand the paleoenvironmental changes that occurred around the Induan–Olenekian Stage Boundary using sediments from Senecio–1 core in the northern onshore Perth Basin and to provide an increased spatial understanding of the mass extinction event around the boundary by looking at carbon cycling and variations in OM composition within the context of redox and global environmental change. For this Purpose, a comprehensive study, comprising of the analyses of several bulk stable isotopes (δ^{13}Corg, δ^{13}Ccarbonate, δ^{34}Spyrite), biomarker abundances, δ^{13}C and δ^{2}H CSIA of selected biomarkers have been carried out. Another aim was to develop an offline sampling technique coupled to GC and GC-irMS in order to establish the source of gas by determining the gas yields and δ^{13}C values of gas hydrocarbons generated from MSSV-Py artificial maturation of kerogen.

In **Chapter 2** the aim was to establish the early Triassic Induan – Olenekian Stage Boundary in the Perth Basin based on conodont faunas and to place the

recorded anoxia in the Perth Basin Hovea Member into a wider context by studying geographic and temporal variation of dysoxia and anoxia in both deep and shallow-marine environments globally.

The objective of **Chapter 3** was to establish paleoenvironmental conditions spanning the early Triassic (Induan–Olenekian) Boundary in the northern onshore Perth Basin using a complete organic geochemical, biomarker and CSIA of biomarkers for the Senecio–1 core. Despite the extensive amount of research on the Permian–Triassic mass extinction, post Permian–Triassic crisis recovery (e.g. Induan and Olenekian) remains controversial and has been rarely studied with such resolution. Therefore, the present dataset has high interest for the characterisation of events that follows the Permian–Triassic crisis.

In **Chapter 4** the main intention was to determine the distribution, potential sources (e.g. wild fires) and significance of selected PAHs in samples spanning the early Triassic Induan–Olenekian Boundary from the Senecio–1 core and to better understand the paleoenvironmental changes that occurred around this early Triassic boundary.

In order to establish the source of natural gas, it is essential to relate the gases with their sources, which is mainly based on the proportion or correlation of individual gas components and their carbon isotopic composition. Therefore, **Chapter 5** presents a modification of the MSSV-Py system for the compositional and isotopic analysis of artificially matured kerogens. This method offers several advantages over the online MSSV sampling system. The foremost is that replicate $\delta^{13}C$ analyses can be conducted on the same sample. This offline sampling technique is also rapid and inexpensive. The approach has great scope for characterising gas formation in sedimentary systems.

References

Albrecht, P., Ourisson, G., 1969. Triterpene alcohol isolation from oil shale. *Science* 163, 1192–1193.

Algeo, T.J., 2011. The early Triassic cesspool: Marine conditions following the end-Permian mass extinction. In: Håkansson, E., Trotter, J. (Eds), Programme and Abstracts, The XVII International Congress on the Carboniferous and Permian, Perth 3–8 July 2011: *Geological Survey of Western Australia*, Record 2011/20, 38.

Ali, J.R., Aitchison, J.C., 2005. Greater India. *Earth-Science Reviews* 72, 169–188.

Amend, J.P., Edwards, K.J., Lyons, T.W. (Eds.), 2004. Sulfur Biogeochemistry-Past and Present. Boulder: *Geological Society of America*.

Andersen, N., Paul, H.A., Bernasconi, S.M., McKenzie, J.A., Behrens, A., Schaeffer, P., Albrecht, P., 2001. Large and rapid climate variability during the Messinian salinity crisis: Evidence from deuterium concentrations of individual biomarkers. *Geology* 29, 799–802.

Anderson, L.G., Dyrssen, D., Hall, P.O.J., 1988. On the sulfur chemistry of a super-anoxic fjord, Framvaren, South Norway. *Marine Chemistry* 23, 283–293.

Bambach, R.K., 2006. Phanerozoic biodiversity mass extinctions. *Annual Review of Earth and Planetary Sciences* 34, 127–155.

Baud, A., Richoz, S., Pruss, S., 2007. The Lower Triassic anachronistic carbonate facies in space and time. *Global and Planetary Change* 55, 81–89.

Benson, S., Lennard, C., Maynard, P., Roux, C., 2006. Forensic applications of isotope ratio mass spectrometry–A review. *Forensic Science International* 157, 1–22.

Benton, M.J., Twitchett, R.J., 2003. How to kill (almost) all life: the end-Permian extinction event. *Trends Ecology and Evolution* 18, 358–365.

Betzer, P.R., Byrne, R.H., Acker, J.G., Lewis, C.S., Jolley, R.R., Feely, R.A., 1984. The oceanic carbonate system: A reassessment of biogenic controls. *Science* 226, 1074–1077.

Bigeleisen, J., Mayer, M.G., 1947. Calculation of equilibrium constants for isotopic exchange reactions. *Journal of Chemical Physics* 15, 261–267.

Bigeleisen, J., Wolfsberg, M., 1958. Theoretical and experimental aspects of isotope effects in chemical kinetics. *Advances in Chemical Physics* 1, 15–76.

Bolliger, C., Schroth, M.H., Bernasconi, S.M., Kleikemper, J., Zeyer, J., 2001. Sulfur isotope fractionation during microbial sulfate reduction by toluene-degrading bacteria. *Geochimica et Cosmochimica Acta* 65, 3289–3298.

Boreham, C.J., Golding, S.D., Glikson, M., 1998. Factors controlling the origin of gas in Australia Bowen Basin coals. *Organic Geochemistry* 29, 347–362.

Bowring, S.A., Erwin, D.H., Isozaki, Y., 1999. The tempo of mass extinction and recovery: The end-Permian example. *Proceedings of the National Academy of Sciences of the United States of America* 96, 8827–8828.

Brayard, A., Bucher, H., Escarguel, G., Fluteau, F., Bourquin, S., Galfetti, T., 2006. The early Triassic ammonoid recovery: Paleoclimatic significance of diversity gradients. *Paleogeography, Paleoclimatology, Paleoecology* 239, 374–395.

Brocks, J., Grice, K., 2011. Biomarker (Organic, Coumpound–Specific Isotopes) in: Reitner, J., Thiel, V. (Eds.), *Encyclopedia of Geobiology*. Springer, Dordrecht Netherlands.

Burgoyne, T.W., Hayes, J.M., 1998. Quantitative production of H_2 by pyrolysis of gas chromatographic effluents. *Analytical Chemistry* 70, 5136–5141.

Canfield, D.E., 2001. Biogeochemistry of sulfur isotopes. In Valley, J. W., and Cole, D. R. (Eds.), Reviews in Mineralogy and Geochemistry, *The Mineralogical Society of America* 607.

Canfield, D.E., 2004. The evolution of the Earth surface sulfur reservoir. *American Journal of Science* 304, 839–861.

Chambers, L.A., Trudinger, P.A., 1979. Microbiological fractionation of stable sulfur isotopes: a review and critique. *Geomicrobiology Journal* 1, 249–293.

Chung, H.M., Rooney, M.A., Toon, M.B., Claypool, G.E., 1992. Carbon isotope composition of marine crude oils. *The American Association of Petroleum Geologists Bulletin* 76, 1000–1007.

Clark, I.D., Fritz, P., 1997. Environmental Isotopes in Hydrogeology.Boca Raton: Lewis Publishers.

Clayton, C., 1991. Effect of maturity on carbon isotope ratios of oils and condensates. *Organic Geochemistry* 17, 887–899.

Coplen, T.B., 2011. Guidelines and recommended terms for expression of stable-isotope-ratio and gas-ratio measurement results. *Rapid Communications in Mass Spectrometry* 25, 2538–2560.

Craig, H., 1957. Isotopic standards for carbon and oxygen and correction factors for mass-spectrometric analysis of carbon dioxide. *Geochimica et Cosmochimica Acta* 12, 133–149.

Craig, H., 1961. Isotopic variations in meteoric waters. *Science* 133, 1702–1703.

Dawson, D., Grice, K., Wang, S.X., Alexander, R., Radke, J., 2004. Stable hydrogen isotopic composition of hydrocarbons in torbanites (late Carboniferous to late Permian) deposited under various climatic conditions. *Organic Geochemistry* 35, 189–197.

Dawson, D., Grice, K., Alexander, R., 2005. Effect of maturation on the indigenous δD signatures of individual hydrocarbons in sediments and crude oils from the Perth Basin (Western Australia). *Organic Geochemistry* 36, 95–104.

Dawson, D., Grice, K., Alexander, R., Edwards, D., 2007. The effect of source and maturity on the stable isotopic compositions of individual hydrocarbons in sediments and crude oils from the Vulcan Sub–basin, Timor Sea, Northern Australia. *Organic Geochemistry* 38, 1015–1038.

Demaison, G.J., Moore, G.T., 1980. Anoxic environments and oil source bed genesis. *Organic Geochemistry* 2, 9–31.

Demaison, G.J., Holck, A.J.J., Jones, R.W., Moore, G.T., 1984. Predictive source bed stratigraphy: A guide to regional petroleum occurrence - North Sea Basin and eastern North American continental margin: *Proceedings of the Eleventh World Petroleum Congress*, London, 1983. New York, John Wiley and Sons, 17–29.

Dickins, J.M., McTavish, R.A., Balme, B.E., 1961. The Beagle Ridge bore: *Australian Oil and Gas Journal* 1960, 20–21.

Dieckmann, V., Ondrak, R., Cramer, B., Horsfield, B., 2006. Deep basin gas; New insights from kinetic modelling and isotopic fraction in deep-formed gas precursors. *Marine and Petroleum Geology* 23, 183–199.

Durand, B., Espitalié, J., 1973. Evolution de la matiere organique au cours de l'enfouissement des sediments. *Compte Rendu de l'Academie des Sciences* 276, 2253–2256.

Durand, B., 1980. Sedimentary organic matter and kerogen. Definition and quantitative importance of kerogen: insoluble organic matter from sedimentary rocks. Editions Technip, Paris, 13–33.

Eglinton, G., Scott, P.M., Besky, T., Burlingame, A.L., Calvin, M., 1964. Hydrocarbons from a one-billion-year-old sediment. *Science* 145, 263–264.

Erwin, D.H., 1994. The Permo–Triassic Extinction. *Nature* 367, 231–236.

Espitalié, J., Laporte, J.L., Madec, M., Marquis, F., Leplat, P., Paulet, J., Boutfeu, A., 1977. Méthode rapide de charactérisation des roches méres, de leur potential pétrolier et de leur degré d'évolution. *Revue de l'Institut Français du Pétrole* 32, 23–42.

Farquhar, J., Johnston, D.T.,Wing, B.A., Habicht, K.S., Canfield, D.E., Airieau, S.,Thiemens, M.H., 2003. Multiple sulfur isotopic interpretations of biosynthetic pathways: implications for biological signatures in the sulfur isotope record. *Geobiology* 1, 27–36.

Faure, G., Mensing, T.M., 2005. Isotopes, Principles and Applications, Third Edition. John Wiley & Sons, Inc., Hoboken, New Jersey.

Fenton, S., Grice, K., Twitchett, R.J., Böttcher, M.E., Looy, C.V., Nabbefeld, B., 2007. Changes in biomarker abundances and sulfur isotopes of pyrite across the Permian–Triassic (P/Tr) Schuchert Dal section (East Greenland). *Earth and Planetary Science Letters* 262, 230–239.

Freeman, K.H., Hayes, J.M., Trendel, J.M., Albrecht, P., 1990. Evidence from Carbon Isotope Measurements for Diverse Origins of Sedimentary Hydrocarbons. *Nature* 343, 254–256.

Gaffney, J.S., Premuzic, E.T., Manowitz, B., 1980. On the usefulness of sulfur isotope ratios in crude oil correlations. *Geochimica et Cosmochimica Acta* 44, 135–139.

Galimov, E.M., 1975. Carbon isotopes in oil-gas geology. NASA Technical Translation. NASA TT F–682, Washington DC, 395.

Gat, J.R., 1996. Oxygen and hydrogen isotopes in the hydrologic cycle. *Annual Review of Earth and Planetary Sciences* 24, 225–262.

Gelin, F., Damsté, J.S.S., Harrison, W.N., Reiss, C., Maxwell, J.R., De Leeuw, J.W., 1996. Variations in origin and composition of kerogen constituents as revealed by analytical pyrolysis of immature kerogens before and after desulfurization. *Organic Geochemistry* 24, 705–714.

Grice, K., Gibbison, R., Atkinson, J.E., Schwark, L., Eckardt, C.B., Maxwell, J.R., 1996. Maleimides (1H-pyrrole-2,5-diones) as molecular indicators of anoxygenic photosynthesis in ancient water columns. *Geochimica et Cosmochimica Acta* 60, 3913–3924.

Grice, K., Schouten, S., Nissenbaum, A., Charrach, J., Sinninghe Damsté, J.S., 1998. A remarkable paradox: Sulfurised freshwater algal (*Botryococcus braunii*) lipids in an ancient hypersaline euxinic ecosystem. *Organic Geochemistry* 28, 195–216.

Grice, K., Schouten, S., Blokker, P., Derenne, S., Largeau, C., Nissenbaum, A., Damsté, J.S.S., 2003. Structural and isotopic analysis of kerogens in sediments rich in free sulfurised Botryococcus braunii biomarkers. *Organic Geochemistry* 34, 471–482.

Grice, K., Cao, C., Love, G.D., Böttcher, M.E., Twitchett, R.J., Grosjean, E., Summons, R.E., Turgeon, S.C., Dunning, W., Jin, Y., 2005a. Photic Zone Euxinia During the Permian–Triassic Superanoxic Event. *Science* 307, 706–709.

Grice, K., Backhouse, J., Alexander, R., Marshall, N., Logan, G.A., 2005b. Correlating terrestrial signatures from biomarker distributions, $\delta^{13}C$, and palynology in fluvio-deltaic deposits from NW Australia (Triassic–Jurassic). *Organic Geochemistry* 36, 1347–1358.

Grice, K., Nabbefeld, B., Maslen, E., 2007. Source and significance of selected polycyclic aromatic hydrocarbons in sediments (Hovea–3 well, Perth Basin, Western Australia) spanning the Permian–Triassic boundary. *Organic Geochemistry* 38, 1795–1803.

Grice, K., Brocks, J.J., 2009. Biomarkers (organic, compound specific isotopes) In: J. Reitner, V. Thiel (Eds.), *Encyclopedia of Geobiology in review*. Springer.

Grice, K., Brocks, J., 2011. Biomarkers (Molecular fossils), in: Reitner, J., Thiel, V. (Eds.), *Encyclopedia of Geobiology*. Springer, Dordrecht Netherlands, 147–167.

Hassan, K.M., Spalding, R.F., 2001. Hydrogen isotope values in lacustrine kerogen. *Chemical Geology* 175, 713–721.

Hayes, J.M., 1993. Factors controlling ^{13}C contents of sedimentary organic compounds: Principles and evidence. *Marine Geology* 113, 111–125.

Hays, L.E., Beatty, T., Henderson, C.M., Love, G.D., Summons, R.E., 2007. Evidence for photic zone euxinia through the end-Permian mass extinction in the Panthalassic Ocean (Peace River Basin, Western Canada). *Paleoworld* 16, 39–50

Hoefs J., 1987. Stable isotope geochemistry. Springer-Verlag, Berlin.

Hoefs, J., 1997. Stable Isotope Geochemistry. Springer Verlag, New York.

Hoefs, J., 2008. Stable Isotope Geochemistry, 6th edn. Berlin, Springer.

Horsfield, B., Disko, U., Leistner, F., 1989. The micro-scale simulation of maturation: Outline of a new technique and its potential application. *Geologische Rundschau* 78, 361–374.

Huc, A.Y., 1980. Origin and formation of organic matter in recent sediments and its relation to kerogen. In Kerogen insoluble organic matter from sedimentary rocks (ed. B. Durand). Editions Technip, Paris, 475-484.

Hunt, J.M., 1996. Petroleum geochemistry and geology. 2nd Editon. Freeman. 743.

Ingram, B.L., Conrad, M.E., Ingle, J.C., 1996. Stable isotope and salinity systematics in estuarine waters and carbonates: San Francisco Bay. *Geochimica Cosmochimica Acta* 60, 455–467.

Joachimski, M.M., Ostertag-Henning, C., Pancost, R.D., Strauss, H., Freeman, K.H., Littke, R., Sinninghe Damsté, J.S., Racki, G., 2001. Water column anoxia, enhanced productivity and concomitant changes in $\delta^{13}C$ and $\delta^{34}S$ across the Frasnian–Famennian boundary (Kowala–Holy Cross Mountains/Poland). *Chemical Geology* 175, 109–131.

Jones, N.T., Hall, A.D., 2002. The Cliff Head oil discovery offshore Perth Basin.In: Keep, M. and Moss, S.J. (Eds.), 2002, The sedimentary basins of Western Australia 3: Proceedings of the petroleum exploration society of Australia Symposium, perth, 901–909.

Kamo, S.L., Crowley, J., Bowring, S.A., 2006. The Permian–Triassic Boundary event and eruption of the Siberian flood basalts: An inter-laboratory U-Pb dating study. *Geochimica et Cosmochimica Acta* 70, 303–405.

Kaplan, I.R., Rittenberg, S.C., 1964. Microbiological fractionation of sulfur isotopes. *Journal of General Microbiology* 34, 195–212.

Kehew, A.E., 2001. Applied Chemical Hydrogeology. Prentice Hall, New Jersey.

Killops, S., Killops, V., 2005. Introduction to Organic Geochemistry. *Blackwell publishing*.

Kling, G.W., 1988. Comparative Transparency, Depth of Mixing, and Stability of Stratification in Lakes of Cameroon, West Africa. *Limnology and Oceanography* 33, 27–40.

Knoll, A.H., Bambach, R.K., Canfield, D.E., Grotzinger, J.P., 1996. Comparative Earth History and late Permian Mass Extinction. *Science* 273, 452–457.

Koeberl, C., Farley, K.A., Peucker-Ehrenbrink, B., Sephton, M.A., 2004. Geochemistry of the end-Permian extinction event in Austria and Italy: no evidence for an extraterrestrial component. *Geology* 32, 1053–1056.

Kohnen, M.E.L., Schouten, S., Sinninghe Damsté, J.S., De Leeuw, J.W., Merrit, D.A., Hayes, J.M., 1992. Recognition of paleobiochemicals by a combined molecular sulfur and isotope geochemical approach. *Science* 256, 358–362.

Kump, L.R., Pavlov, A., Arthur, M.A., 2005. Massive release of hydrogen sulfide to the surface ocean and atmosphere during intervals of oceanic anoxia. *Geology* 33, 397–400.

Largeau, C., Derenne, S., 1993. Relative efficiency of the Selective Preservation and Degradation Recondensation pathways in kerogen formation. Source and environment influence on their contributions to type I and II kerogens. *Organic Geochemistry* 20, 611–615.

Laws, E.A., Popp, B.N., Bidigare, R.R., Kennicutt, M.C., Macko, S.A., 1995. Dependence of phytoplankton isotopic composition on growth rate and [CO_2]aq: Theoretical considerations and experimental results. *Geochimica et Cosmochimica Acta* 59, 1131–1138.

Lis, G.P., Schimmelmann, A., Mastalerz, M., 2006. D/H ratios and hydrogen exchangeability of type-II kerogens with increasing thermal maturity. *Organic Geochemistry* 37, 342–353.

Mann, J.L., Vocke, R.D., Kelly, W.R., 2009. Revised $\delta^{34}S$ reference values for IAEA sulfur isotope reference materials S-2 and S-3. *Rapid Communications in Mass Spectrometry* 23, 1116–1124.

Maslen, E., Grice, K., Gale, J.D., Hallmann, C., Horsfield, B., 2009. Crocetane: A potential marker of photic zone euxinia in thermally mature sediments and crude oils of Devonian age. *Organic Geochemistry* 40, 1–11.

Matte, P., Mattauer, M., Olivet, J.M., Griot, D.A., 1997. Continental subductions beneath Tibet and the Himalayan orogeny: a review. *Terra Nova* 9, 264–270.

Matthews, D.E., Hayes, J.M., 1978. Isotope-ratio-monitoring gas chromatography-mass spectrometry. *Analytical Chemistry* 50, 1465–1473.

McTavish, R.A., 1965. Completion Report, BMR 10 and 10A, Beagle Ridge, Western Australia: Australia Bureau of Mineral Resources, *Geology and Geophysics*, Report 80.

Metcalfe, I., Nicoll, R.S., Willink, R., Ladjavadi, M., Grice, K., 2013. early Triassic (Induan–Olenekian) conodont biostratigraphy, global anoxia, carbon isotope excursions and environmental perturbations: New data from Western Australian Gondwana. *Gondwana Research* 23, 1136–1150.

Michels, R., Raoult, N.E., Elie, M., Mansuay, L., Faure, P., Oudin, J.L., 2002. Understanding of reservoir gas compositions in a natural case using stepwise semi-open artificial maturation. *Marine and Petroleum Geology* 19, 589–599.

Moodley, L., Middelburg, J.J., Herman, P.M.J., Soetaert, K., de Lange, G.J., 2005. Oxygenation and organic-matter preservation in marine sediments: Direct experimental evidence from ancient organic carbon–rich deposits. *Geology* 33, 889–892.

Nabbefeld, B., Grice, K., Twitchett, R.J., Summons, R.E., Hays, L., Böttcher, M.E., Asif, M., 2010a. An integrated biomarker, isotopic and paleoenvironmental study through the late Permian event at Lusitaniadalen, Spitsbergen. *Earth and Planetary Science Letters* 291, 84–96.

Nabbefeld, B., Grice, K., Schimmelmann, A., Summons, R.E., Troitzsch, U., Twitchett, R.J., 2010b. A comparison of thermal maturity parameters between freely extracted hydrocarbons (Bitumen I) and a second extract (Bitumen II) from within the kerogen matrix of Permian and Triassic sedimentary rocks. *Organic Geochemistry* 41, 78–87.

Nabbefeld, B., Grice, K., Schimmelmann, A., Sauer, P.E., Böttcher, M.E., Twitchett, R., 2010c. Significance of $\delta D_{kerogen}$, $\delta^{13}C_{kerogen}$ and $\delta^{34}S_{pyrite}$ from several Permian/Triassic (P/Tr) sections. *Earth and Planetary Science Letters* 295, 21–29.

Orchard, M.J., 2007. Conodont diversity and evolution through the latest Permian and early Triassic upheavals. *Paleogeography, Paleoclimatology, Paleoecology* 252, 93–117.

Pancost, R.D., Boot, C.S., 2004. The paleoclimatic utility of terrestrial biomarkers in marine sediments. *Marine Chemistry* 92**,** 239–261.

Peters, K.E., 1986. Guidelines of evaluating petroleum source rock using programmed pyrolysis. *Association of Petroleum Geologists Bulletin* 70, 318–329.

Peters, K.E., Moldowan J.M., 1993. The Biomarker Guide. Interpreting Molecular Fossils in Petroleum and Ancient Sediments. Prentice Hall, New Jersey.

Peters, K.E., Walters, C.C., Moldowan, J.M., 2005. The biomarker guide: Interpreting molecular fossils in petroleum and ancient sediments. Prentice-Hall, New Jersey.

Philippi G.T., 1965. On the depth, time and mechanism of petroleum generation. *Geochimica et Cosmochimica Acta* 29, 1021–1049.

Philp, R., 1985. Fossil fuel biomarkers: *Methods in geochemistry and geophysics* 23, Elsevier, New York.

Playford, P. E., Willmott, S.P., 1958. Stratigraphy and structure of the Perth Basin: West Australian Petroleum Pty Ltd, Report (unpublished), *Western Australia Geological Survey*, S-series report S103.

Popp, B.N., Laws, E.A., Bidigare, R.R., Dore, J.E., Hanson, K.L., Wakeham, S.G., 1998. Effect of phytoplankton cell geometry on carbon isotopic fractionation. *Geochimica et Cosmochimica Acta* 62, 69–79.

Powell, T.G., McKirdy, D.M., 1973. Crude oil correlations in the Perth and Carnarvon Basins. *Australian Petroleum and Production Association Journal* 13, 81–85.

Press, F., Siever, R., 2001. Understanding Earth, 3rd Edition. W.H. Freeman and Company, New York.

Prosser, S.J., Scrimgeour, C.M., 1995. High-precision determination of D/H in H2 and H2O by continuous-flow isotope ratio mass spectrometry. *Analytical Chemistry* 67, 992–1997.

Racki, G., Wignall, P.B., 2005. late Permian double-phased mass extinction and volcanism: an oceanographic perspective, in: D.J. Over, J.R.M., Wignall, P.B. (Eds.), *Developments in Paleontology and Stratigraphy* 263–297.

Rees, C.E., 1973. A steady-state model for sulfur isotope fractionation in bacterial reduction processes. *Geochimica et Cosmochimica Acta* 37, 1141–1162.

Rice, D.D., Claypool, G.E., 1981. Generation, accumulation, and resource potential of biogenic gas. *The American Association of Petroleum Geologists Bulletin* 65, 5–25.

Sachse, D., Radke, J., Gleixner, G., 2006. δD values of individual *n*-alkanes from terrestrial plants along a climatic gradient – Implications for the sedimentary biomarker record. *Organic Geochemistry* 37, 469–483.

Sauer, P.E., Eglinton, T.I., Hayes, J.M., Schimmelmann, A., Sessions, A.L., 2001. Compound specific D/H ratios of lipid biomarkers from sediments as a proxy for environmental and climatic conditions. *Geochimica et Cosmochimica Acta* 65, 213–222.

Schimmelmann, A., Lewan, M.D., Wintsch, R.P., 1999. D/H isotope ratios of kerogen, bitumen, oil, and water in hydrous pyrolysis of source rocks containing kerogen types I, II, IIS, and III. *Geochimica et Cosmochimica Acta* 63, 3751–3766.

Schimmelmann, A., Boudou, J.P., Lewan, M.D., Wintsch, R.P., 2001. Experimental controls on D/H and $^{13}C/^{12}C$ ratios of kerogen, bitumen and oil during hydrous pyrolysis. *Organic Geochemistry* 32, 1009–1018.

Schimmelmann, A., Sessions, A.L., Mastalerz, M., 2006. Hydrogen isotopic (D/H) composition of organic matter during diagenesis and thermal maturation. *Annual Review of Earth and Planetary Science* 34, 501–533.

Schmidt, T., Zwank, L., Elsner, M., Berg, M., Meckenstock, R., Haderlein, S., 2004. Compound-specific stable isotope analysis of organic contaminants in natural environments: a critical review of the state of the art, prospects, and future challenges. *Analytical and Bioanalytical Chemistry* 378, 283–300.

Schoell, M., 1988. Multiple origin of methane in the Earth. *Chemical Geology* 71, 1–10.

Schouten, S., Klein Breteler, W.C.M., Blokker, P., Schogt, N., Rijpstra, W.I.C., Grice, K., Baas, M., Sinninghe Damsté, J.S., 1998. Biosynthetic effects on the stable carbon isotopic compositions of algal lipids: implications for deciphering the carbon isotopic biomarker record. *Geochimica et Cosmochimica Acta* 62, 1397–1406.

Schouten, S., Woltering, M., Rijpstra, W.I.C., Sluijs, A., Brinkhuis, H., Sinninghe Damste, J.S., 2007. The Paleocene-Eocene carbon isotope excursion in higher plant organic matter: Differential fractionation of angiosperms and conifers in the Arctic. *Earth and Planetary Science Letters* 258**,** 581–92.

Schwartzkopf, T. A., 1990. Relationship between petroleum generation, migration and sandstone diagenesis, Middle Jurassic, Gifhorn Trough, N Germany. *Marine Petroleum Geology* 7, 153–170.

Sephton, M.A., Looy, C.V., Brinkhuis, H., Wignall, P.B., de Leeuw, J.W., Visscher, H., 2005. Catastrophic soil erosion during the end- Permian biotic crisis. *Geology* 33, 941–944.

Sepkoski, J.J., 1986. Phanerozoic overview of mass extinction, in: Raup, D.M., Jablonski, D. (Eds.), Patterns and Processes in the History of Life. Springer Verlag, Berlin, 277–295

Sepkoski, J.J., Jr., 1993. Ten Years in the Library: New Data Confirm Paleontological Patterns. *Paleobiology* 19, 43–51.

Sessions, A.L., Burgoyne, T.W., Schimmelmann, A., Hayes, J.M., 1999. Fractionation of hydrogen isotopes in lipid biosynthesis. *Organic Geochemistry* 30, 1193–1200.

Stanley, S.M., 1988. Paleozoic mass extinctions: shared patterns suggest global cooling as a common cause. *American Journal of Science* 288, 334–352.

Stevenson, D.P., Wagner, C.D., Beeck, O., Otvos, J.W., 1948. Isotope Effect in the Thermal Cracking of Propane-1-C^{13}. *Journal of Chemical Physics* 16, 993–994.

Suess, E., 1980. Particulate organic carbon flux in the oceans: surface productivity and oxygen utilization. *Nature* 288, 260–263.

Summons, R.E., Powell, T.G., 1986. *Chlorobiaceae* in Paleozoic seas revealed by biological markers, isotopes and geology. *Nature* 319, 763–765.

Summons, R.E., Powell, T.G., 1987. Identification of aryl isoprenoids in source rocks and crude oils: Biological markers for the green sulfur bacteria. *Geochimica et Cosmochimica Acta* 51, 557–566.

Summons, R.E., Boreham, C.J., Foster, C.B., Murray, A.P., Gorter J.D., 1995. Chemostratigraphy and the composition of oils in the Perth Basin, Western Australia. *Australian Petroleum and Production Association Journal* 35, 613–631.

Svensen, H., Planke, S., Polozov, A.G., Schmidbauer, N., Corfu, F., Podladchikov, Y.Y., Jamtveit, B., 2009. Siberian gas venting and the end-Permian environmental crisis. *Earth and Planetary Science Letters* 277, 490–500.

Tang, Y., Perry, J.K., Jenden, P.D., Schoell, M., 2000. Mathematical modeling of stable carbon isotope ratios in natural gases. *Geochimica et Cosmochimica Acta* 64, 2673–2687.

Tegelaar, E.W., de Leeuw, J.W., Derenne, S., Largeau, C., 1989. A reappraisal of kerogen formation. *Geochimica et Cosmochimica Acta* 53, 3103–3106.

Thomas, B.M., Barber, C.J., 2004. A re-evaluation of the hydrocarbon habitat of the northern Perth Basin. *Australian Petroleum Production and Exploration Association Journal* 44, 59–92.

Thomas, B.M., Willink, R.J., Grice, K., Twitchett, R.J., Purcell, R.R., Archbold, N.W., George, A.D., Tye, S., Alexander, R., Foster, C.B., Barber, C.J., 2004. Unique marine Permian–Triassic Boundary section from Western Australia. *Australian Journal of Earth Sciences* 51, 423–430.

Tissot, B.P., Welte, D.H., 1978. Petroleum formation and occurrence: a new approach to oil and gas exploration. Springer-Verlag, New York.

Tissot, B., Welte, D.H., 1984. Petroleum Formation and Occurrence, in: Tissot, B., Welte, D.H. (Eds.). Springer, Berlin, 699.

Trull, T., Gibson, J.E., Beaumont, K.L., Bowman, J., Burton, H.R., Davidson, A.T., Summons, R.E., Swadling, K.M., Volkman, J.K., 2001. Site Holds Promise for

Ecosystem and Biogeochemical Investigations. Eos Transactions, *American Geophysical Union* 82, 306–311.

Urey, H.C., 1947. The thermodynamic properties of isotopic substances. *Journal of the Chemical Society (Resumed)* 562–581.

Vandenbroucke, M., Largeau, C., 2007. Kerogen origin, evolution and structure. *Organic Geochemistry* 38, 719–833.

Van Krevelen, D.W., 1961. Coal. Elsevier Editions, Amsterdam.

Waples, D., 1981. Organic geochemistry for exploration geologists. Burgess Pub.Co., Minneapolis, US, 151.

Werner, R.A., Brand, W.A., 2001. Referencing strategies and techniques in stable isotope ratio analysis. *Rapid Communications in Mass Spectrometry* 15, 501–519.

Whiticar, M.J., 1994. Correlation of natural gases with their sources. In: The Petroleum system – from source to trap, Magoon, L.B., Dow, W.G. (Eds.). *American Association of Petroleum Geologists Memoir* 60, 261–283.

Wignall, P.B., 2001. Large igneous provinces and mass extinctions. *Earth-Science Reviews* 53, 1–33.

Wignall, P.B., Twitchett, R.J., 1996. Oceanic anoxia and the end-Permian mass extinction. *Science* 272, 1155–1158.

Wignall, P.B., Twitchett, R.J., 2002. Extent, duration and nature of the Permian–Triassic superanoxic event. In: Koeberl, C., MacLeod, K.C. (Eds.), Catastrophic events and mass extinctions: impacts and beyond: Boulder, Colorado. *Geological Society of America Special Paper* 356, 395–413.

Appendix

I
Isorenieratane

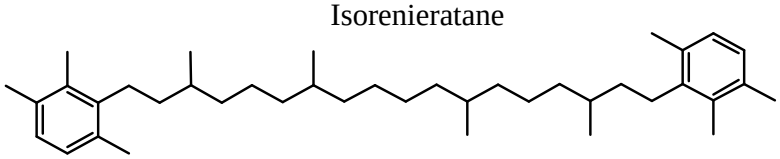

II
Isorenieratene

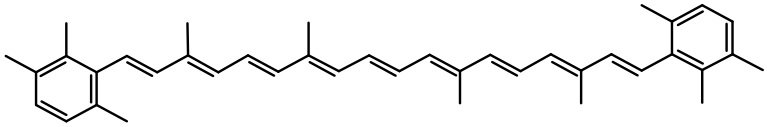

Chapter 2

Early Triassic (Induan–Olenekian) conodont biostratigraphy, global anoxia, carbon isotope excursions and environmental perturbations: New data from Western Australian Gondwana

Ian Metcalfe, Robert. S. Nicoll, Rob Willink, Mojgan Ladjavardi, Kliti Grice

***Gondwana Reasearch*, 23 (2013) 1136–1150**

Abstract

The early Triassic Induan–Olenekian Stage Boundary (Dienerian–Smithian Sub–Stage Boundary) has been identified at a depth of 2719.25 m in the petroleum exploration well Senecio–1 located in the northern Perth Basin, Western Australia. Conodont faunas represent three conodont zones in ascending order, the *Neospathodus dieneri* Zone, the *Neospathodus waageni eowaageni* Zone and the *Neospathodus waageni waageni* Zone. The Induan–Olenekian (Dienerian–Smithian) Boundary is placed at the base of *the Neospathodus waageni eowaageni* Zone equivalent to the first appearance of *Neospathodus* ex. gr. *waageni* utilised elsewhere and adopted by the IUGS ICS Triassic Subcommission to define the base of the Olenekian. Bulk $\delta^{13}C$ carbon isotopes define a positive peak of c. 4 per mille that essentially coincides with the Induan–Olenekian Boundary as seen in proposed Global Stratotype Sections and Points (GSSPs) in South China and Spiti, India demonstrating the global utility of this level for correlation. An anoxic zone is recognised in the lower part of the Senecio–1 core and the upper limit of this zone dated as late Induan (late Dienerian). Temporal and spatial mapping of marine anoxia and dysoxia globally demonstrates that pulses of dysoxia/anoxia affected shallow-marine zones at different times in different locations. Dysoxia/anoxia in the shallow-marine environment appeared in the latest Permian at the extinction level, later than in the deep-marine environment, and appears to be largely restricted to the Induan (Griesbachian and Dienerian) and early Olenekian (Smithian). Temporally and geographically restricted upwelling of an oxygen minimum zone into the ocean surface layer due to environmental perturbations including extreme climate warming, increased terrestrial chemical weathering intensity and continental erosion, sea level rise, and changes in marine nutrient inventories and productivity rates, is interpreted as a likely cause of observed variation in shallow-marine dysoxia/anoxia in the early Triassic.

Keywords

early Triassic, Induan–Olenekian Boundary, conodonts, carbon isotopes, anoxia, environmental perturbations

Introduction

The latest Permian – early Triassic transitional period is globally important in Earth history. It saw the most profound mass extinction known to science in the latest Changhsingian with approximately 90+ % of skeletonized marine species (Erwin, 1993; Alroy et al., 2008) and approximately 70 % of species on land wiped out (Maxwell, 1992) within a short period of time, estimated at several hundred thousands of years or less (Mundil et al., 2004; Huang et al., 2011). Following the late Changhsingian mass extinction, there was a period of continued global climatic and environmental upheaval and stress termed the early Triassic "cesspool" (e.g. Algeo, 2011a) that lasted 5 million years and which was characterised by significant carbon isotope excursions, the global "coal gap", "reef gap", "radiolarian gap" and a range of unusual facies and biota including microbialites, and flat pebble conglomerates. This early Triassic period of environmental upheaval was also characterised by significant size reduction of many organisms and is referred to in the literature as the period of "delayed recovery" following the mass extinction. The early Triassic was also marked by significant variation in redox conditions both in time and space (Kato et al., 2002; Wignall and Twitchett, 2002; Kidder and Worsley 2004; Wignall et al., 2010) and by marked increase in chemical weathering intensity (Retallack and Krull, 1999; Michaelson, 2002; Sheldon, 2006; Algeo and Twitchett, 2010; Algeo, 2011b; Algeo et al., 2011).

In shallow-marine environments there were frequent shifts between oxic and anoxic/dysoxic conditions, particularly in the Induan Stage (Bond and Wignall, 2010). These fluctuations of redox conditions have been interpreted to result from expansion of a shallow oxygen minimum zone into the ocean surface layer due to environmental perturbations (Algeo et al., 2011). The spatial and temporal mapping of these fluctuating redox conditions will greatly enhance our understanding of the causative environmental perturbations. We review the geographic and temporal variation of dysoxia and anoxia in both deep and shallow-marine environments globally, placing the recorded anoxia in the Perth Basin Hovea Member in wider context. The latest Permian–early Triassic in Western Australia includes economically important carbon-rich shallow-marine shales (Hovea Member, basal Kockatea Shale of the Perth Basin) that record dysoxic/anoxic conditions in the early

Triassic and have acted as significant source rocks for hydrocarbons. The Late Changhsingian mass extinction and Permian–Triassic Boundary levels also occur within the lower Hovea Member (Thomas and Barber, 2004; Thomas et al., 2004; Metcalfe et al., 2008; Gorter et al., 2009). The precise age of the Hovea Member has to date been poorly controlled and based mainly on endemic palynology and macro-fossils and limited conodont and ammonoid data. The specific placement of Permian –Triassic stage boundaries in Australia has until now been elusive or at best very poorly constrained. The early Triassic Induan–Olenekian Stage Boundary (Dienerian–Smithian Sub–Stage Boundary) is yet to be formally ratified in a GSSP section by the Subcommission on Triassic Stratigraphy (STS). However, the STS has decided that the first appearance of the conodont *Neospathodus waageni* ex. gr. should be used for boundary definition and recognition in the GSSP (Tong et al., 2004; Krystyn et al., 2007; Tong and Zhao, 2011).

The occurrence of Lower Triassic conodonts in Western Australia was first reported by McTavish (1973) in cores taken in petroleum exploration wells drilled in the Carnarvon and Perth basins. Smithian conodont faunas with *Neospathodus waageni* were recovered in the Carnarvon Basin and possible Dienerian strata in the Perth Basin based on a few *Neospathodus dieneri.* Additional limited conodont material from the Perth Basin (Metcalfe et al., 2008) failed to provide sufficient control to firmly place any stage boundary although the occurrence of *Clarkina jolfensis* Kozur in the basal Sapropelic Interval suggests that the biostratigraphic GSSP Permian–Triassic Boundary level is within the lower part of the Sapropelic Interval of the Hovea Member (**Figure 2.1**). We here provide unequivocal placement of the proposed Induan–Olenekian Boundary in the Perth Basin, Western Australia (Senecio–1 Core) based on relatively abundant conodont faunas. We also report $\delta^{13}C_{org}$ data from this boundary interval and correlate the studied sequence with proposed Induan–Olenekian GSSP sections in China and India and provide age constraints on post-mass extinction anoxia/dysoxia in Western Australia.

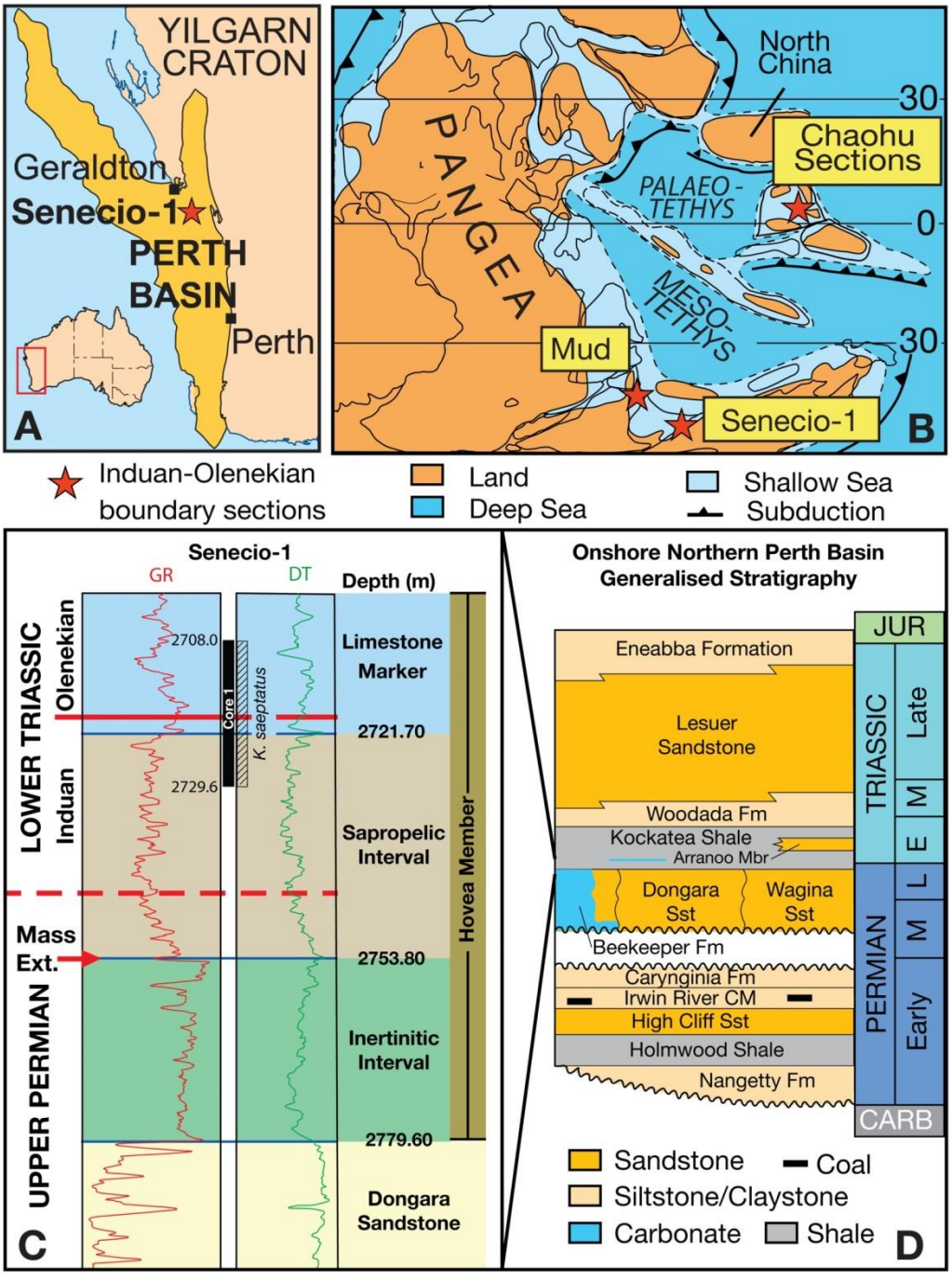

Figure 0.1: **A**. Location of Perth Basin and Senecio–1. **B**. End–Permian (253 Ma) paleogeography showing locations of Senecio–1 and proposed GGSP sections at Chaohu and Mud. **C**. Upper Permian–Lower Triassic stratigraphy of the northern Perth Basin penetrated by Senecio–1, stratigraphic coverage of the cored interval shown in black. **D**. Generalised Permian–Triassic stratigraphy of the onshore Northern Perth Basin (after Mory et al., 2005).

Stratigraphy and geological setting of the studied sequence

Permian–Triassic transitional sequences of Western Australia occur in the Perth, Carnarvon, Canning and Bonaparte continental margin basins. The Permian–Triassic transitional strata of these basins include thick marine shales that range from the latest Permian or earliest Triassic to as high as the early Anisian of the Middle Triassic (McTavish, 1973; McTavish and Dickins, 1974). In the Perth Basin the Kockatea Shale may be up to 1000 m thick, is usually black in colour and becomes progressively less marine in its upper part (Mory and Iasky, 1996). The basal part of the Kockatea Shale in the Perth Basin has been named the Hovea Member (Thomas and Barber, 2004; Thomas et al., 2004) and consists of a basal Inertinitic Interval, a middle Sapropelic Interval and an upper Limestone Marker unit (**Figure 2.1**). The Hovea Member is c. 30–70 m thick and contains high total organic carbon (TOC) content up to 5 % (Thomas and Barber, 2004; Thomas et al., 2004; Metcalfe et al., 2008). The bulk of the Kockatea Shale, above the Hovea Member, has a much lower average TOC of 0.8 % (Mory and Iasky, 1996) perhaps reflecting high sedimentation rate.

The studied Induan–Olenekian Boundary sequence is recorded in a core taken in the onshore petroleum exploration well Senecio–1 drilled by Arc Energy Ltd in 2005 and located in the northern Perth Basin, east of Dongara at GPS coordinates Latitude 29 14 25.94 S, Longitude 115 05 29.28 E (see **Figure 2.1** for stratigraphic position and location). The Permian–Triassic transition in the Perth Basin (**Figure 2.1**) occurs in the lower part of the Kockatea Shale (Hovea Member). The Hovea Member comprises a lower Inertinitic Interval (named for the high level of inert kerogen); a Sapropelic Interval (organic-rich mud with phytoplankton-derived kerogen) and an upper calcareous horizon termed the ‘Limestone Marker’ (Thomas et al., 2004). The Senecio–1 well penetrated the lower Hovea Member of the Kockatea Shale and bottomed in the Dongara Sandstone reservoir. The 21.6 m cored sequence (2708.00–2729.60 m depth) here studied straddles the upper Sapropelic Interval lower ‘Limestone Marker’ section of the Hovea Member (**Figure 2.1**). Carbon and sulfur isotopes and biomarker studies from the nearby Hovea–3 well (Thomas et al., 2004; Grice et al., 2005a; 2005b; Nabbefeld et al., 2010) indicate that the late Changhsingian mass extinction level corresponds to the Inertinitic Interval-

Sapropelic Interval boundary and based on very limited conodont material and palynology, the biostratigraphic GSSP-defined Permian–Triassic Boundary is placed in the lower part of the Sapropelic Interval (Metcalfe et al., 2008; **Figure 2.1**). Isotope studies and biomarker data indicate periodic PZE (sulfidic conditions) at the time of deposition of the Sapropelic Interval in the Perth Basin and during the late Permian–early Triassic mass extinction and recovery interval globally (Grice et al., 2005a). Limited palynological studies (Purcell, 2006) indicate that the entire core falls within the Lower Triassic *Kraeuselisporites saeptatus* Zone. The Sapropelic Interval in the core (2721.70–2729.60 m) comprises organic C-rich (up to 2.5 % TOC) finely laminated mudstones with rare thin generally sharp-based siltstones that represent an anoxic high-stand systems tract deposited on the distal shelf below storm wave base (Thomas et al., 2004).

The mudstones and siltstones of the Sapropelic Interval show a high degree of pyritization and contain pyrite nodules, pyrite spheres and framboids and pyritised microfossils (in particular common pyritised micro-bivalves and micro gastropods at some levels) are devoid of bioturbation (bioturbation index of 0) and contain no apparent infauna. Analysis of pyrite framboid size in the Hovea Member of the Kockatea Shale in Hovea–3 suggests anoxic conditions prevailed throughout the late Permian and early Triassic (Bond and Wignall, 2010). The smallest mean diameter pyrite framboids (4.5–5.1 µm) indicates that anoxia was most intense in the lower part of the Sapropelic Interval. This interval is interpreted to have been deposited under anoxic conditions. The upper part of the core (2708.00–2721.70 m) represents the upper Hovea Member "Limestone Marker" unit and comprises laminated mudstones with siltstones.

Carbonate cemented intervals and concretions are common. The base of the unit is marked by a 40 cm thick sharp-based, fining-upwards, glauconitic siltstone that contains abundant largely broken and in some cases abraded *Clarkina* conodont Pa elements interpreted as transported. This and other siltstones in this unit are regarded as distal turbidites or tempestites (with mud rip-up clasts in places) deposited on the continental shelf below storm wave base but more shore proximal than the underlying Sapropelic Interval. Bioturbation is common, suddenly increasing to a Bioturbation Index (Bann and Fielding, 2004) of 4–5 (compared with 0 in underlying Sapropelic Interval) then gradually reducing with an upward

deepening trend. Both horizontal and vertical burrows are present and the upper "Limestone marker" is considered to have been deposited in oxygenated conditions. The relatively rare and poorly preserved macro-fossils in the core are dominated by epifaunal pelagic thin-shelled bivalves and ammonites. Other epifauna commonly found in the cores include rare to abundant fish teeth and scales, small foraminifera, conodonts and ostracods.

Conodont faunas and the Induan–Olenekian Boundary in Western Australia

Conodont samples and processing

Eighty seven samples, from top to bottom, C1 to C87 (each 25 cm in length and c. 1 kg in weight) of a one–third slab of the Senecio–1 core were processed to extract conodonts. Samples were broken down by a variety of methods including treatment with hexane, dilute acetic/formic acid, sodium hypochlorite and sodium hydroxide. Residues were sieved and dried and then conodonts concentrated by heavy liquid (sodium polytungstate) and magnetic separation and picked under an optical binocular microscope. Imaging of conodonts was undertaken using a JEOL JSM– 6480 LA Scanning Electron Microscope at Macquarie University, Sydney.

Conodont fauna and maturity

The Senecio–1 conodont samples produced 1000+ conodont elements. Conodont yields varied from 0 to 200+ elements per sample. The conodont fauna is of relative low diversity with 10 species/subspecies of *Neospathodus* and two (possibly three) species of *Clarkina*. Taxonomic notes and comments on stratigraphically important conodonts are given below. The conodont Colour Alteration Indicex (CAI) of Senecio–1 elements is 2 to 2.5 and is consistent with spore colour which gives a Staplin Thermal Alteration Index (TAI) averaging 3 but with a range 2+ to 4 (Purcell, 2006). This indicates that the Senecio–1 core sedimentary rocks are mature to over-mature but probably in the upper liquid window (**Figure 2.2**)

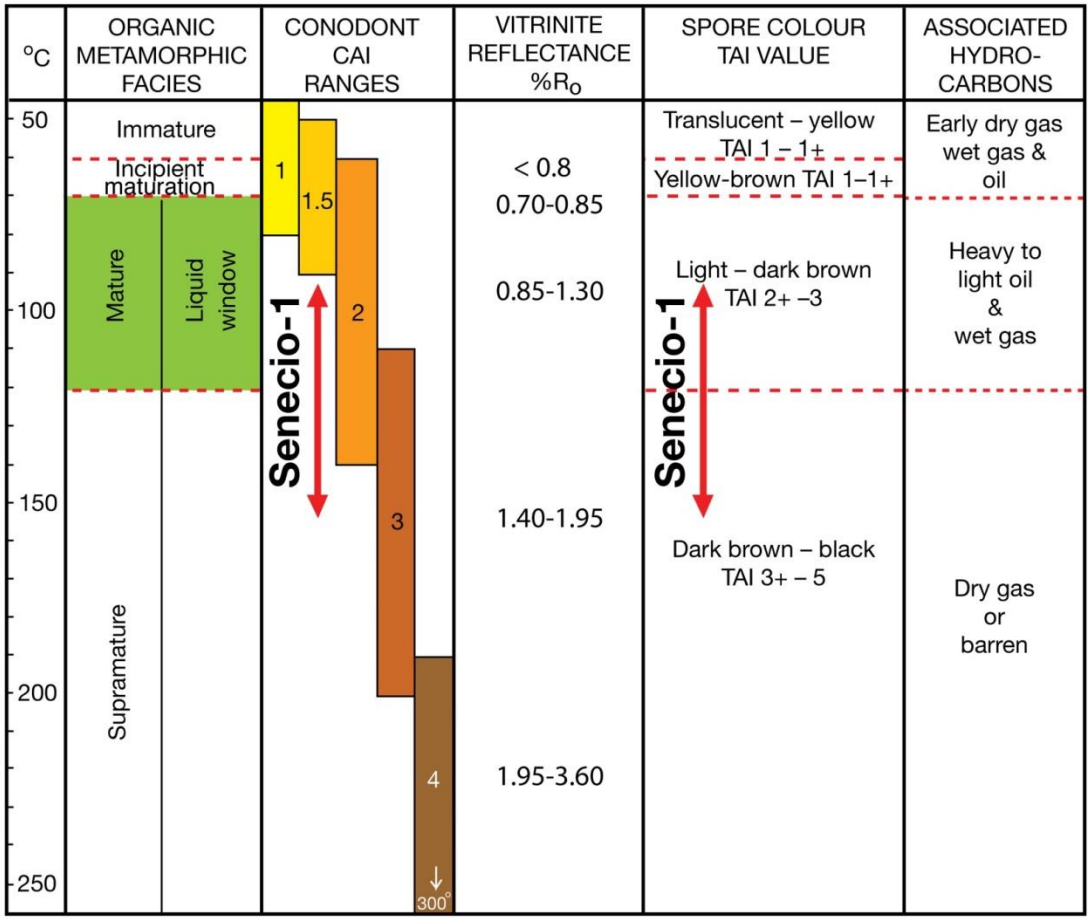

Figure 0.2: Organic metamorphic facies and maturity indices showing the maturity level indicated for the Senecio–1 sediments based on conodont and spore colour. Partly after Metcalfe and Riley (2010), Nowlan and Barnes (1987) and Epstein, Epstein and Harris (1977).

Taxonomic notes and comments

Only the Pa elements of selected taxa have been illustrated in this study. Material illustrated is currently riposted at the University of New England, Armidale, Australia. We recognise several species of *Clarkina* in the Senecio–1 core material but have so far failed to classify these into known species. There may be up to three new species in our material and specific designation/description awaits further taxonomic work. We illustrate some typical Pa elements of this genus in **Figure 2.3**

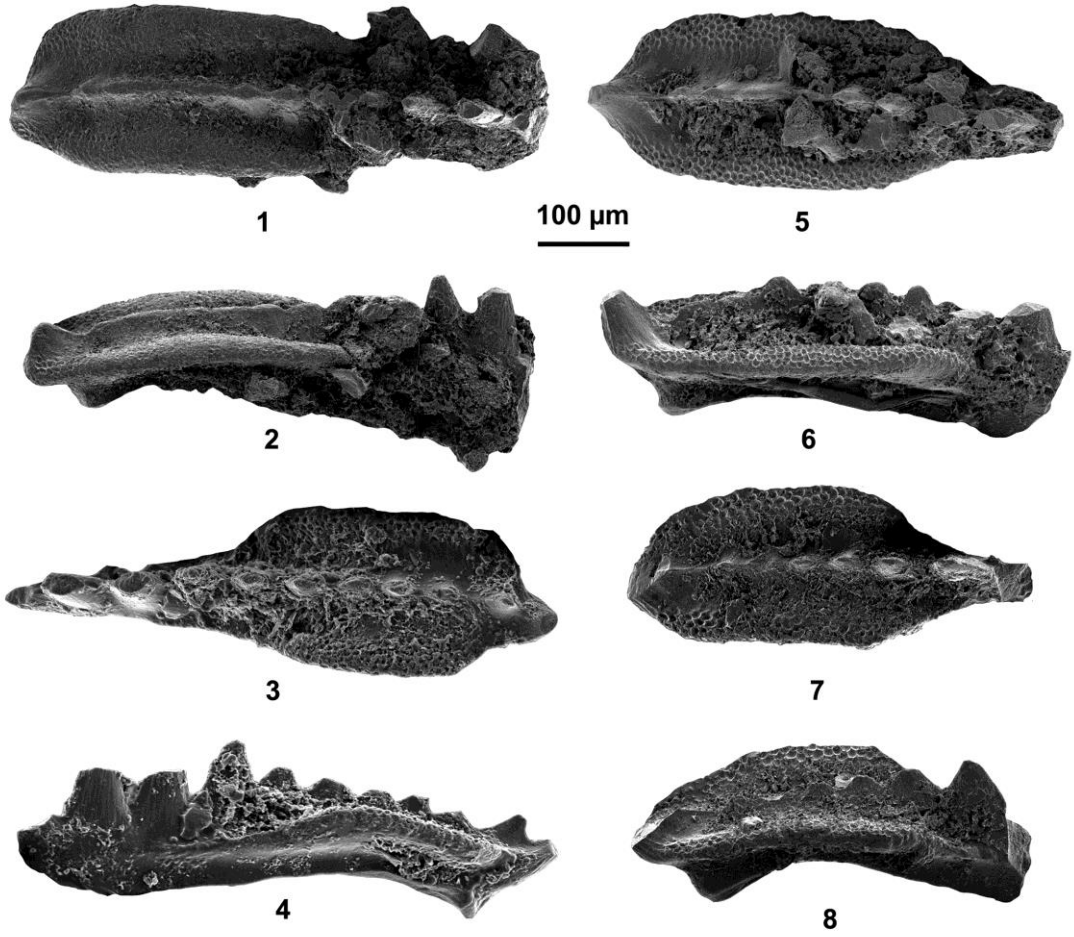

Figure 0.3: Clarkina spp. Pa elements, all samples C36 (2716.75–2717.00 m depth), Senecio–1 core. **1, 2.** Oral and inner lateral views of specimen C36/1. **3, 4.** Oral and inner lateral views of specimen C36/2. **5, 6.** Oral and inner lateral views of specimen C36/3. **7, 8.** Oral and inner lateral views of specimen C36/4.

Neospathodus dieneri Sweet, 1970 (**Figure 2.4**) is a well-known early Triassic conodont species. Three morphotypes are recognised by some authors and used to designate sub-zones (e.g. Zhao et al., 2007). See Shigeta et al. (2009, p.186) for recent synonymy. The species ranges from the early Dienerian to the middle Smithian but is most commonly found in the Dienerian where it is used to designate a *Neospathodus dieneri* Zone (e.g. Orchard and Tozer, 1997, Tong et al., 2004).

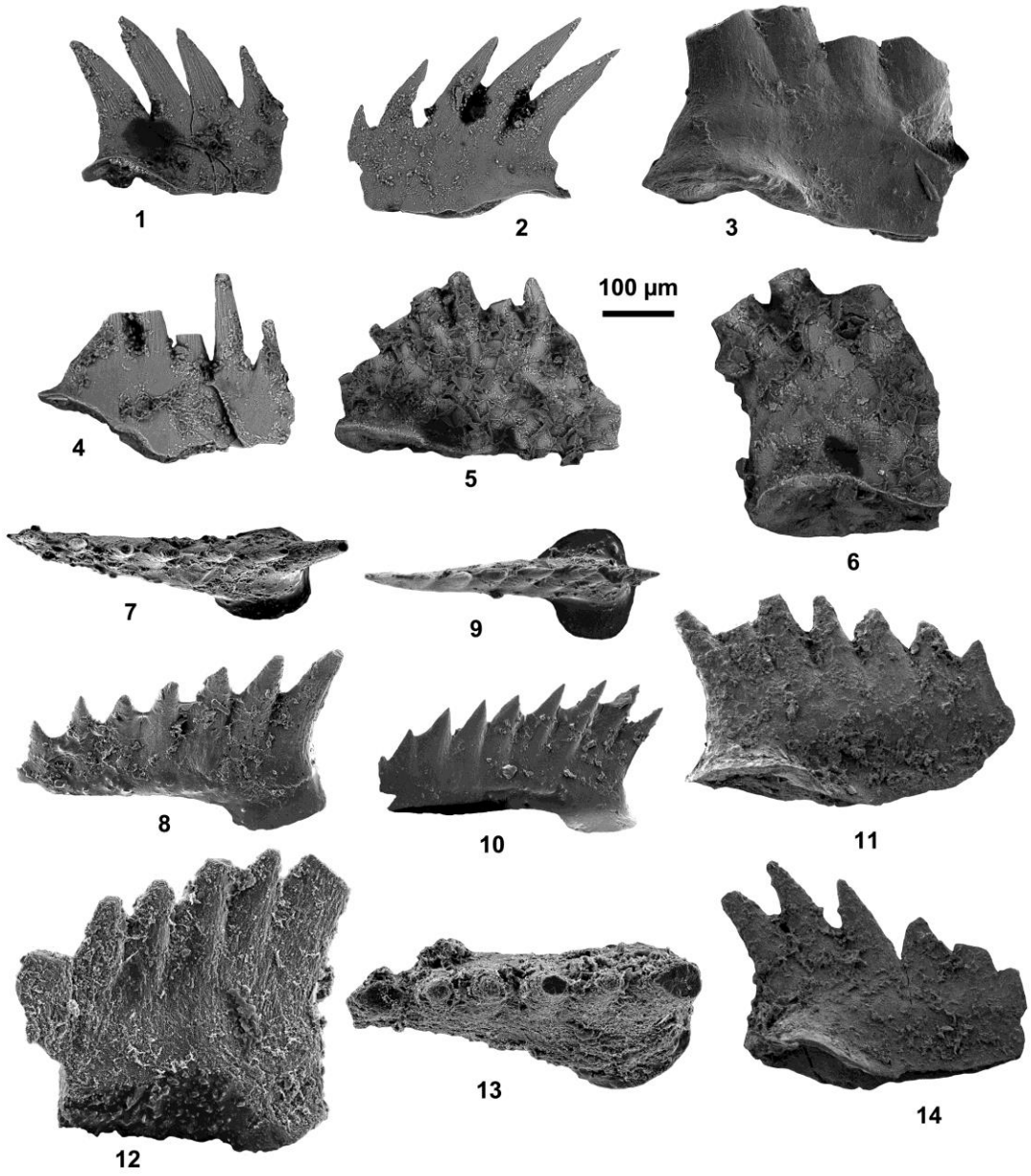

Figure 0.4: Neospathodus dieneri Sweet Pa elements, Senecio–1 core. **1.** Specimen C29/5, lateral view, sample C29 (2715.00–2715.25 m depth). **2.** Specimen C29/8, lateral view, sample C29 (2715.00–2715.25 m depth). **3.** Specimen C49/3, lateral view, sample C49 (2720.00–2720.25 m depth). **4.** Specimen C53/16, lateral view, sample C53 (2721.00–2721.25 m depth). **5.** Specimen C76/1, lateral view, sampleC76 (2726.75–2727.00 m depth). 6–14 all from sample C77 (2727.00–2727.25 m depth): **6.** Specimen C77/23, lateral view; **7,8.** Oral and outer lateral views of specimen C77/1; **9, 10.** Oral and inner lateral views of specimen C77/2; **11.** Lateral view of specimen C77f; **12, 13.** Lateral and oral views of specimen C77/11; **14.** Lateral view of specimen C77d.

Neospathodus novaehollandiae McTavish, 1973 (**Figure 2.5**) was first described from the Carnarvon Basin of Western Australia by McTavish (1973).

Some workers (e.g. Orchard, 2010) have placed this species in synonymy with *Neospathodus pakistanensis* but we here regard it as a separate species characterised by development of robust lateral flanges, developing into node like features in the posterior part of the element. None of the original McTavish material was illustrated by SEM. We here provide an SEM image of the Holotype Pa element (**Figures 2.5: 2.6)** for comparison and it is identical to Pa elements recovered from the Senecio–1 Well. The species appears to be restricted to the Lower Olenekian (Smithian) and was used, together with *Neospathodus waageni* to define a basal Olenekian *Neospathodus* ex gr. *waageni-Neospathodus novaehollandiae* Zone in South Primorye, Russia (Shigeta et al., 2009).

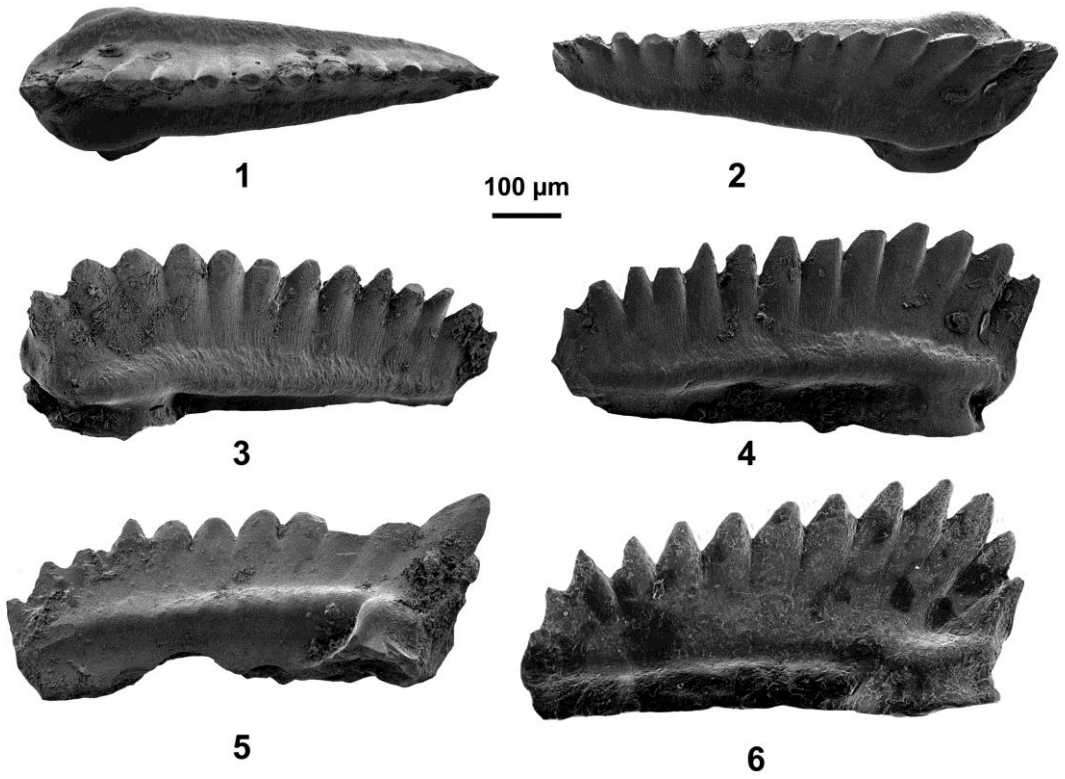

Figure 0.5: Neospathodus novaehollandiae McTavish Pa elements, Senecio–1 core. **1,2,3,4.** Oral, oblique oral, inner lateral and outer lateral views of specimen C29/3, sample C29 (2715.00–2715.25 m depth). **5.** Inner lateral view of specimen C25/7. Sample C25 (2714.00–2714.25 m depth). **6.** Inner lateral view of Holotype specimen number UWA69120B of McTavish (1973) reimaged using the SEM for comparison with Senecio–1 material.

Neospathodus pakistanensis Sweet, 1970 (**Figure 2.6**) is a long-established early Triassic conodont species first described from West Pakistan where it defines a *Neospathodus pakistanensis* Zone that is succeeded by the *Neospathodus waageni*

Zone. This species ranges from the late Dienerian (late Induan) to the middle Smithian (early Olenekian).

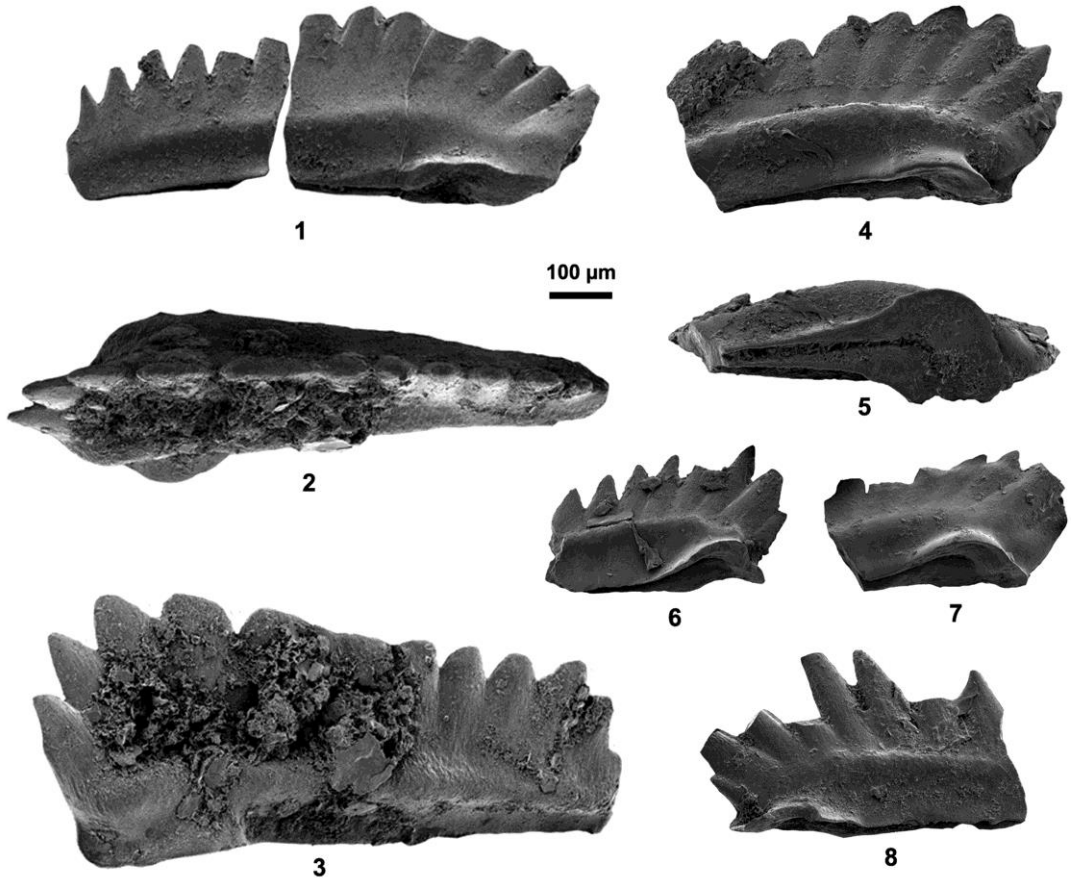

Figure 0.6: Neospathodus pakistanensis Sweet Pa elements, Senecio–1 core. **1.** Lateral view of specimen C10/1, sample C10 (2710.25–2710.50 m depth). **2, 3.** Oral and inner lateral views of specimen C25/3, sample C25 (2714.00–2714.25 m depth). **4, 5.** Lateral and basal views of specimen C25/2, sample C25 (2714.00–2714.25 m depth). **6.** Lateral view of specimen C25/8, sample C25 (2714.00–2714.25 m depth). **7.** Lateral view of specimen C29/4, sample C29 (2715.00–2715.25 m depth). **8.** Lateral view of specimen C10/16, C10 (2710.25–2710.50 m depth).

Neospathodus ex gr. *waageni* Sweet 1970 *sensu lato* is a long-established Smithian species, the first appearance of which has been chosen to define the base of the Olenekian Stage by the IUGS, ICS Subcommission on Triassic Stratigraphy. The species gives rise to several new *Neospathodus* species and species of *Novispathodus* in the early Spathian *via* the basal Spathian species *Neospathodus pingdingshanensis* (Orchard, 2007). Morphological variability in the species has led some authors to recognise up to six morphotypes (Orchard and Krystyn, 2007). Two subspecies, *Neospathodus waageni eowaageni* and *Neospathodus waageni waageni* were

recognised by Zhao et al. (2008). We here recognise a third subspecies, *Neospathodus waageni* subsp. Nov. A is similar to, and possibly the ancestor of *Neospathodus pingdingshanensis.*

Neospathodus waageni eowaageni Zhao et al., 2008 (**Figure 2.7**) is the oldest subspecies and is characterised by a shorter element and upright denticles. The subspecies is rare compared to *Neospathodus waageni waageni* and has its first occurrence before *Neospathodus waageni waageni* in all proposed Induan–Olenekian GSSP sections studied in China, India and Russia and in the Senecio–1 Well, Australia. The sub-species has a very short range at the base of the Olenekian and defines a short-duration *Neospathodus waageni eowaageni* Zone which is succeeded upwards by the first appearance of *Neospathodus waageni waageni* defining the base of the *Neospathodus waageni waageni* Zone.

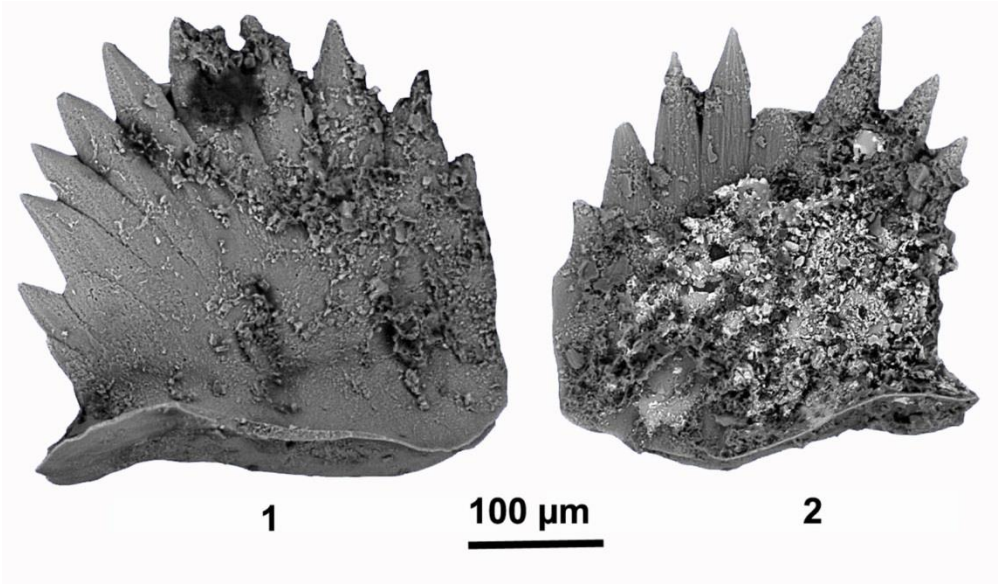

Figure 0.7: Neospathodus waageni eowaageni Zhao & Orchard Pa elements, Senecio–1 core. **1.** Lateral view of specimen C25/26, sample C25 (2714.00–2714.25 m depth). **2.** Lateral view of specimen C35/7, sample C35 (2716.50–2716.75 m depth).

Neospathodus waageni waageni Sweet 1970 (**Figure 2.8**) is the commonest subspecies, characterised by its typical reclined denticles. We do not here recognise any morphotypes. The subspecies ranges from just above the base of the Olenekian to the top of the Smithian Sub-Stage.

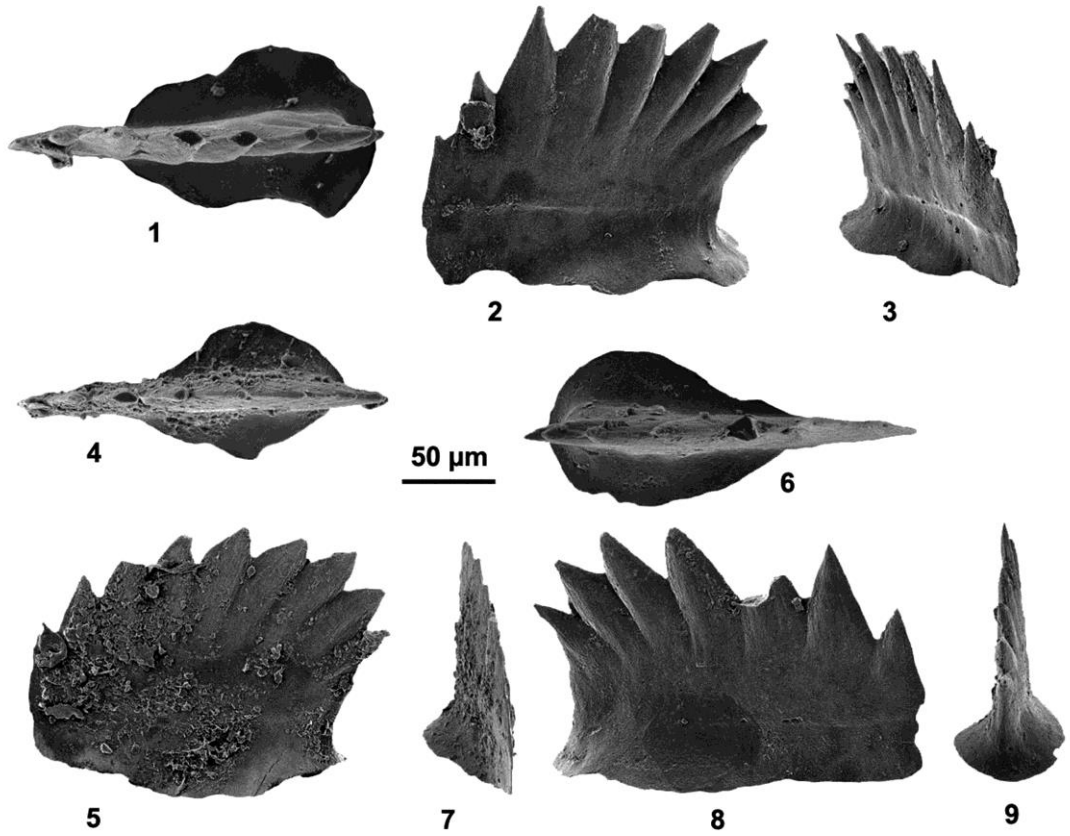

Figure 0.8: Neospathodus waageni waageni Sweet Pa elements, Senecio–1 core, from sample C28 (2714.75–2715.00 m depth). **1, 2, 3.** Oral, outer lateral and anterior views of specimen C28/2. **4, 5.** Oral and inner lateral views of specimen C28/3. **6–9.** Oral, anterior, outer lateral and posterior views of specimen C28/4.

Neospathodus waageni subsp. nov. A (**Figure 2.9**) appears some distance above the base of the *Neospathodus waageni waageni* Zone and is relatively common. It is characterised by denticles that are curved towards the posterior similar to those in *Neospathodus pingdingshanensis*. The sub-species also exhibits wider and broader striations on the denticles compared to other sub-species. We here utilise this subspecies to define a *Neospathodus waageni* subsp. nov. A sub-zone in the Senecio–1 succession.

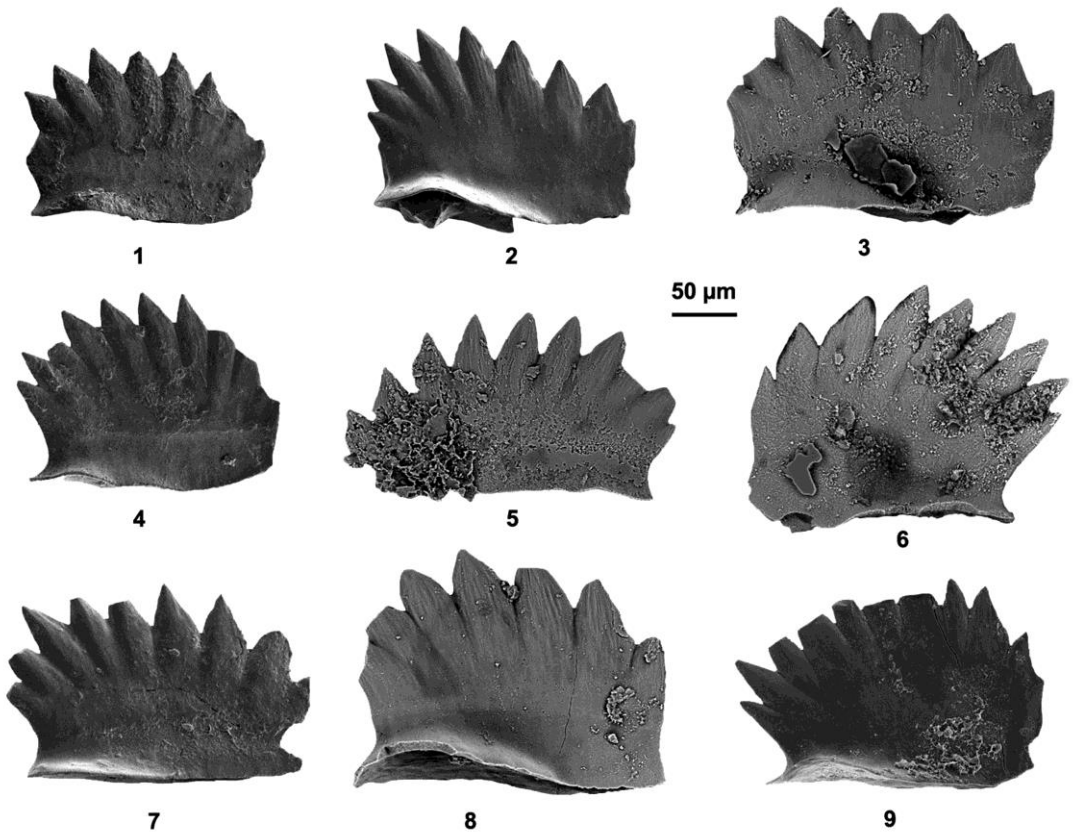

Figure 0.9: Neospathodus waageni subsp. nov. A Pa elements, Senecio–1 core. **1.** Lateral view of specimen C20/1, sample C20 (2712.75–2713.00 m depth). **2.** Lateral view of specimen C20/5, sample C20 (2712.75–2713.00 m depth). **3.** Lateral view of specimen C23/8, sample C23 (2713.50–2713.75 m depth). **4.** Lateral view of specimen C20/2, sample C20 (2712.75–2713.00 m depth). **5.** Lateral view of specimen C23/4, sample C23 (2713.50–2713.75 m depth). **6.** Lateral view of specimen C25/1, sample C25 (2714.00–2714.25 m depth). **7.** Lateral view of specimen C20/3, sample C20 (2712.75–2713.00 m depth). **8.** Lateral view of specimen C23/6, sample C23 (2713.50–2713.75 m depth). **9.** Lateral view of specimen C28/5, sample C28 (2714.75–2715.00 m depth).

Conodont zonation and the Induan–Olenekian Boundary

The critical age and zonal-indicative species and sub-species discussed above allow the unequivocal placement of the proposed Induan–Olenekian Boundary at 2719.25 m depth in the core (in the lower part of the "Limestone marker" unit). The ranges and relative abundance of important conodont taxa and conodont zonation are given in **Figure 2.10** three Zones and one Sub-Zone are recognised in the core in ascending order: *Neospathodus dieneri* Zone (2719.25–2729.60 m) characterised by the co-ocurrence of *Neospathodus pakistanensis* and *Clarkina* spp.

Neospathodus waageni eowaageni Zone (2717.25–2719.25 m) Characterised by the co-occurrence of *Neospathodus waageni eowaageni* and *Clarkina* spp. and the base defined by the first occurrence of *Neospathodus waageni eowaageni.*

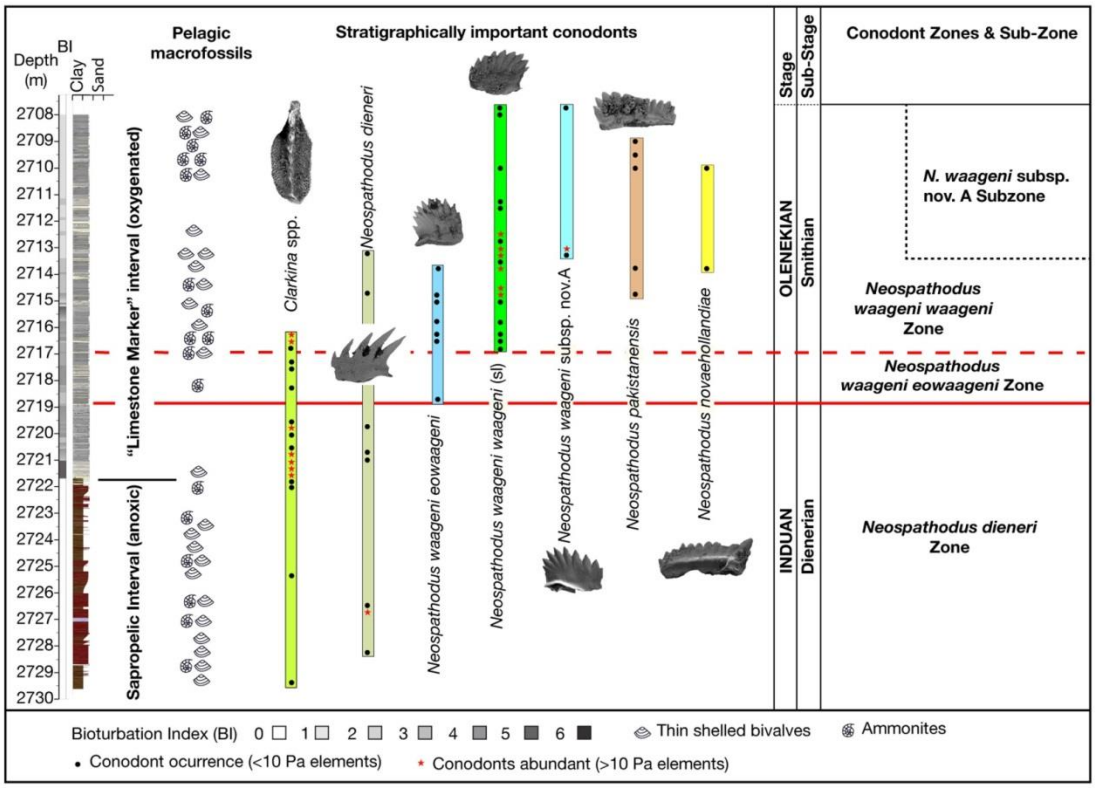

Figure 0.10: Ranges of important conodont taxa and conodont zones, occurrence of pelagic macro-fossils and bioturbation index values in the Senecio–1 core and placement of the Induan–Olenekian Boundary.

Neospathodus waageni waageni Zone (2708.00–2717.25 m) characterised by the zonal name species together with *Neospathodus dieneri*, *Neospathodus novaehollandiae*, and *Neospathodus pakistanensis*. Base defined by first appearance of *Neospathodus waageni waageni.*

Neospathodus waageni subsp. nov. A Sub-Zone (2708.00–2715.00 m) corresponds to the upper part of the *Neospathodus waageni waageni* Zone and characterised by the occurrence of *Neospathodus waageni* subsp. nov. A.

The first appearance of *Neospathodus waageni* ex. gr. (*sensu lato*) is used to define the base of the proposed Olenekian Stage of the Lower Triassic (Tong et al.,

2004; Krystyn et al., 2007; Tong and Zhao, 2011). This corresponds to the first appearance of *Neospathodus waageni eowaageni* in proposed GSSP sections at Chaohu, China (Zhao et al., 2007; Zhao et al., 2008; Tong and Zhao, 2011) and Mud, Spiti, India (Krystyn et al., 2007; Orchard and Krystyn, 2007; Tong et al., 2011) and to the first appearance of *Neospathodus waageni* ex. gr. (*sensu lato*) in other Induan–Olenekian Boundary sections globally, e.g. Abrek Bay, South Primorye (Shigeta et al., 2009), The first appearance of *Neospathodus waageni eowaageni* occurs slightly before the appearance of *Neospathodus waageni waageni* in the proposed GSSP sections and this is also the case in the Senecio–1 core in the Perth Basin. We here place the Induan–Olenekian Stage (Dienerian–Smithian Sub–Stage) Boundary at this first appearance in the core at a depth of 2719.25 m. This is the first unequivocally established international stage boundary in the Permian and Triassic of Australia.

Carbon isotopes

Analytical methodology

Sample preparation

The samples were surface washed with a mixture of dichloromethane (DCM) and methanol (CH_3OH) [9:1, vol %: vol %] in an ultrasonic bath (20 min) to remove surface contamination. The air-dried samples were then ground to a particle size of approximately 150 µm using a ring mill.

Elemental analysis-isotope ratio mass spectrometry (EA-irMS)

To remove inorganic carbon from the ground samples for $\delta^{13}C$ of bulk OM analysis, the ground samples were acidified with Hydrochloric acid (HCl, 1M) and then oven-dried at approximately 40 ^{o}C [48h] in an oven. Then the samples were washed at least three times with double-distilled water to remove any remaining HCl. These decarbonised samples were measured for $\delta^{13}C$ of bulk OM analysis using a Micromass IsoPrime isotope ratio mass spectrometer interfaced to a EuroVector EuroEA3000 elemental analyser.

The samples were combusted (1025 ^{o}C) under an oxygen-enriched atmosphere. Subsequently, the composition products were transported *via* a constant helium flow through an oxidation catalyst (chromium oxide) into a reduction reactor (650 ^{o}C) containing copper granules to reduce nitrogen oxides (NO, N_2O and N_2O_2) to N_2. Excess oxygen and water were removed. Remaining CO_2 and N_2 were separated on a 3 m chromatographic column (Poropak Q) before the gas was transported through a thermal conductivity detector (TCD) and into the isotope ratio mass spectrometer. For more detail of the procedure see Grice et al. (2007). Isotopic compositions are given in the δ–notation relative to the Vienna Pee Dee Belemnite (VDPB) standard (**Table 2.1**).

Sample no.	Depth (m)	C [wt %]	δ^{13}C [‰ VPDB]
1	2708.10 – 2708.14	0.4	–32.88
4	2708.85 – 2708.87	0.5	–32.91
8	2709.83 – 2709.86	0.3	–31.8
12	2710.84 – 2710.87	0.2	–31.82
16	2711.92 – 2711.95	0.4	–32.3
20	2712.88 – 2712.91	0.4	–31.79
24	2713.82 – 2713.83	0.3	–31.69
28	2714.88 – 2714.90	0.4	–31.54
32	2715.85 – 2715.87	0.6	–28.98
36	2716.81 – 2716.84	0.4	–30.18
40	2717.90 – 2717.92	0.7	–29.44
44	2718.92 – 2718.95	0.4	–28.61
48b	2719.85 – 2719.88	0.3	–27.52
52	2720.87 – 2720.89	0.5	–28.03
56	2721.94 – 2721.96	1.4	–27.9
60	2722.91 – 2722.93	1.2	–28.5
64	2723.85 – 2723.87	0.9	–28.79
68	2724.88 – 2724.90	1.7	–28.95
72	2725.88 – 2725.90	1	–29.31
76	2726.88 – 2726.91	1.5	–29.66
80	2727.85 – 2727.88	2	–29.37
84	2728.85 – 2728.88	1.4	–29.89

Table 0.1: Senecio–1 Carbon isotope samples, total organic carbon (wt %) and δ^{13}C values.

Isotope values and interpretation

$\delta^{13}C_{org}$ values vary from –27.5 to –32.9 ‰ VPDB (**Table 2.1**) and define a broad positive excursion of approximately 4 ‰ (**Figure 2.11**). The peak of this

excursion essentially coincides with the base of the *Neospathodus waageni eowaageni* Zone and hence the biostratigraphically defined Induan–Olenekian Boundary in the core. Similar positive $\delta^{13}C_{carb}$ excursions have been reported globally (Corsetti et al., 2005) and from proposed marine GSSP sections at West and North Pingdingshan, Chaohu, China, and at Mud, Spiti, India (Tong and Yin, 2002; Horacek et al., 2007; see **Figure 2.11**). In addition, positive excursions are also known at other Induan–Olenekian Boundary sections including Jinya/Waili, northwestern Guangxi, South China (Galfetti et al., 2007a), Daxiakou Section, Hubei, China (Tong and Yin, 2002), Guandao section, Guizhou, China (Tong et al., 2002), Zuodeng Section, Tiandong, Guangxi Province, China (Tong and Yin, 2002), Bulla section, Southern Alps, Italy (Posenato, 2008), L´Om Picol/Uomo section, northern Italy (Horacek et al., 2007), Losar, North India (Galfetti et al., 2007b) and Kamura, Japan (Horacek et al., 2009).

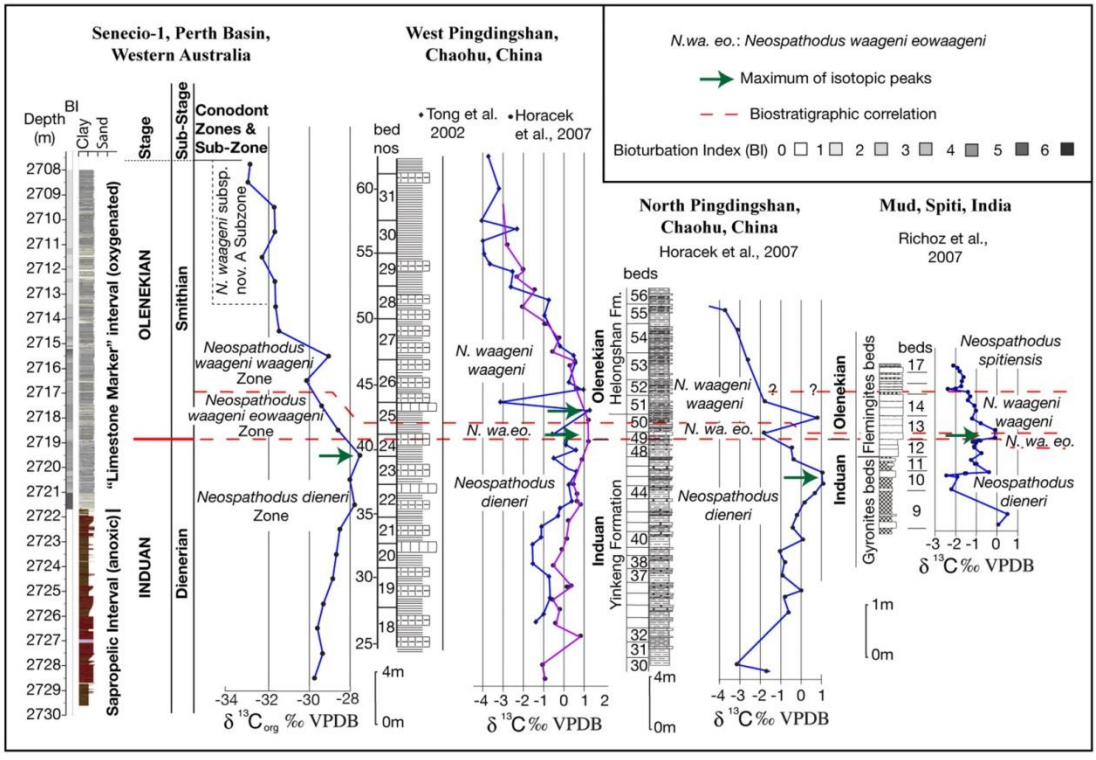

Figure 0.11: Correlation of the $\delta^{13}C$ curve and conodont zones for Senecio–1 core with those of proposed Induan–Olenekian GSSP sections at Chaohu, China and Mud, India.

Global anoxia/dysoxia in the late Permian–early Triassic

The late Permian–early Triassic is characterised by significant global development of marine dysoxia (low oxygen concentration), anoxia (water and sediments lacking oxygen) and euxinia (sulfidic anaerobic conditions with sulfate-reducing bacteria leading to accumulation of organic-rich black shales).

Evidence that indicates dysoxia/anoxia in the Permian–Triassic transitional interval includes lithostratigraphy (Wignall and Twitchett, 1996, 2002; Isozaki, 1997), sulfur isotopes (Newton et al., 2004; Nielsen and Shen, 2004), occurrence and size distribution of framboidal pyrite (Nielsen and Shen, 2004; Wignall et al., 2005; Gorjan et al., 2007; Bond and Wignall, 2010), trace metal distributions (Kakuwa and Matsumoto, 2006; Kakuwa, 2008), type or total lack of biotubation (Twitchett and Wignall, 1996; Kakuwa, 2008), low-diversity, thin-shelled benthic faunas (Wignall and Twitchett, 2002), S/C ratio distributions (Gorjan et al., 2007), high levels of Total Organic Carbon (Takahashi et al., 2009).

Western Tethys

Wignall and Twitchett (2002) indicate anoxic conditions for the Griesbachian in deep-water, deep basin sequences of Sicily, Italy. In shallow marine environments, Newton et al. (2004) based on $\delta^{34}S$ and $\delta^{18}O$ studies of sediments in the Permian–Triassic of Siusi, in the dolomites of northern Italy indicate anoxia in the latest Permian and Griesbachian. Dysoxic conditions in the post extinction latest Permian and Griesbachian are indicated by trace fossil, geochemical and sedimentological data (Wignall and Hallam, 1992; Twitchett and Wignall, 1996; Twitchett, 1999). Dolenec et al. (2001) using redox sensitive elements, S, C, REE distributions and Ce anomaly data in Permian–Triassic shallow-marine sediments in western Slovenia interpret anoxic conditions in the latest Permian and oxic/dysoxic conditions in the Griesbachian. Gorjan et al. (2007) discuss paleoredox conditions in the Bulla section, northern Italy and again interpret anoxia in the latest Permian and Griesbachian.

Eastern Tethys

Deep-marine basin sequences in N. Sichuan, China record anoxia from the latest Changhsingian (extinction level) to the early Dienerian (Wignall and Twitchett,

2002). In the shallow-marine low-latitude environment in South China (Meishan) anoxia commenced at the extinction horizon (top of Bed 24) but then fluctuated between oxic, dysoxic and anoxic in the basal Induan (Bond and Wignall, 2010). Biomarker studies indicate periodic PZE in the latest Permian and Griesbachian at Meishan (Grice et al., 2005a). Kershaw et al (1999) indicate probable onset of anoxic/dysoxic conditions at the extinction level based on a sudden increase in pyrite, appearance of pyrite framboids, micro-gastropods and microsperes in the Baizhuyuan section, Sichuan Province, South China. Galfetti et al. (2007b) interpret two periods of dysoxia-anoxia in the Jinya/Waili sections of SW South China, one in the Griesbachian–Dienerian and one in the Smithian.

Panthalassa

Data from deep ocean floor sediments of Panthalassa now incorporated into accretionary complexes in Japan led Kajiwara et al. (1993a, 1993b, 1994) based on $\delta^{34}S$ data and Kato et al. (2002) using lithostratigraphic and geochemical data (major trace and rare earth elements, including Ce anomaly) to interpret the onset of dysoxic conditions in the Wuchiapingian and anoxic conditions from the late Changhsingian (mass extinction level) into the lower Induan (Griesbachian). Wignall et al. (2010) also proposed dysoxic conditions in late Permian deep-marine Panthalassic sediments of accreted terranes in Japan and appearance of distinct anoxia at the late Changhsingian extinction horizon that extends through the Griesbachian. A further pulse of anoxia is recorded in the late Spathian.

In the shallow-water central Panthalassa (sea mounts incorporated into accretionary complexes in Japan), geochemical signatures in dark-grey to black Griesbachian micritic limestones indicate dysoxic conditions at this time on shallow-marine intra-Panthalassic sea mounts (Musashi et al., 2001). Shallow marine higher-latitude eastern Panthalassa continental margin sequences in Idaho, W. North America record anoxia from the extinction level up into the Griesbachian (Wignall and Hallam, 1992; Bond and Wignall, 2010). Dysoxia in the Griesbachian of Utah and Idaho is indicated by abundant *Lingula* and *Claraia* (Schubert and Bottjer, 1995). PZE is documented in the latest Permian, Griesbachian and Smithian in the Peace River Basin, Western Canada (Hays et al., 2007).

Peri-Gondwana

Brookfield et al. (2003) suggest there is little evidence for dysaerobic conditions in the deep-water P–T transition in the Guryul Ravine and Pahlgam sections in Indian Kashmir. However, the lower Khunamuh Formation (upper Permian–basal Triassic) lacks bioturbation and Wignall et al. (2005), based on pyrite framboid evidence, have interpreted this to have been deposited under oxygen poor conditions.

In shallow-marine Peri-Gondwana P–T sequences at Julfa, Iran, dysoxic conditions in the Griesbachian are indicated by Ce anomaly studies (Kakuwa and Matsumoto, 2006). In the Salt Range, Pakistan, Wignall and Hallam (1993) indicate early Griesbachian normal marine conditions but dysoxic conditions in the late Griesbachian. Hermann et al. (2011) assessed the paleoredox data for the Salt Range and Surghar Range sections in Pakistan and interpret, based on composition of particulate OM that oxygenated conditions existed in the early Triassic except in the Dienerian–earliest Smithian and challenge the interpretation of an anoxic event in the late Griesbachian. They indicate dysoxic conditions throughout the Dienerian and in the late Smithian (Hermann et al., 2011, **Figure 2.12**). The Triassic sequence at Losar, India records two episodes of anoxia, one in the late Dienerian and one in the late Smithian separated by dysoxic conditions (Galfetti et al., 2007a).

At Selong, Southern Tibet, Wignall and Newton (2003) demonstrate that the basal Triassic is oxygenated and dysoxic conditions only appear in the late Griesbachian and anoxic conditions in the Dienerian.

Peri-Gondwanan shallow-marine P–T sequences are present in the Perth, Carnarvon and Bonaparte basins of Western Australia. Biostratigraphic control is mainly based on endemic palynomorphs, brachiopods and bivalves and on limited more globally relevant conodonts and ammonoids. Metcalfe et al. (2008) and Gorter et al. (2009) discussed the placement of the P–T Boundary in the Perth and Bonaparte basins. The Griesbachian is yet to be unequivocally proved present in any of these sequences based on international robust biostratigraphy but is generally regarded as probably present in the Perth Basin (Thomas et al., 2004, Metcalfe et al., 2008) but with the possibility of a stratigraphic break at the extinction level (Inertinitic Interval–Sapropelic Interval Boundary). The presence of the Griesbachian

in the Carnarvon and Bonaparte basins is also equivocal and as yet unproven. The latest Permian and basal Triassic appear missing in the Carnarvon Basin where there is an unconformity (Felton et al., 1993). The Lower Triassic in the Carnarvon Basin is represented by the Locker Shale but there is no indication of oxygen deficient conditions at that time or in the underlying Permian Kennedy Group. There is also an unconformity present in the latest Permian in the Bonaparte Basin (Gorter et al., 2009) but this occurs below the *Protohaploxypinus microcorpus* palynofloral Zone interpreted as of late but not latest Changhsingian age (Metcalfe et al., 2008). The Griesbachian may be represented within the Mairmull Formation in the Bonaparte Basin. There is no indication of dysoxia or anoxia in the Permian–Triassic transitional interval in the Bonaparte Basin and the organic-rich source rocks of the Lower Triassic seen in the Perth Basin are not present there.

Anoxic conditions are interpreted for the Sapropelic Interval of the Hovea Member of the Kockatea Shale in the Perth Basin (Thomas et al., 2004, Metcalfe et al., 2008, and discussions in this paper) commencing at the late Changhsingian extinction level and terminating in the late Dienerian. In addition, biomarker studies indicate PZE during deposition of the Sapropelic Interval of the Kockatea Shale (Grice et al., 2005a).

Discussion

The development of global anoxia has been suggested to be a primary cause of the late Changhsingian marine mass extinction (Wignall and Hallam, 1992; Isozaki, 1997; Wignall and Twitchett 2002). The development of dysoxia and anoxia in the Permian–Triassic transition exhibits both depth-related and geographic variations (**Figure 2.12**).

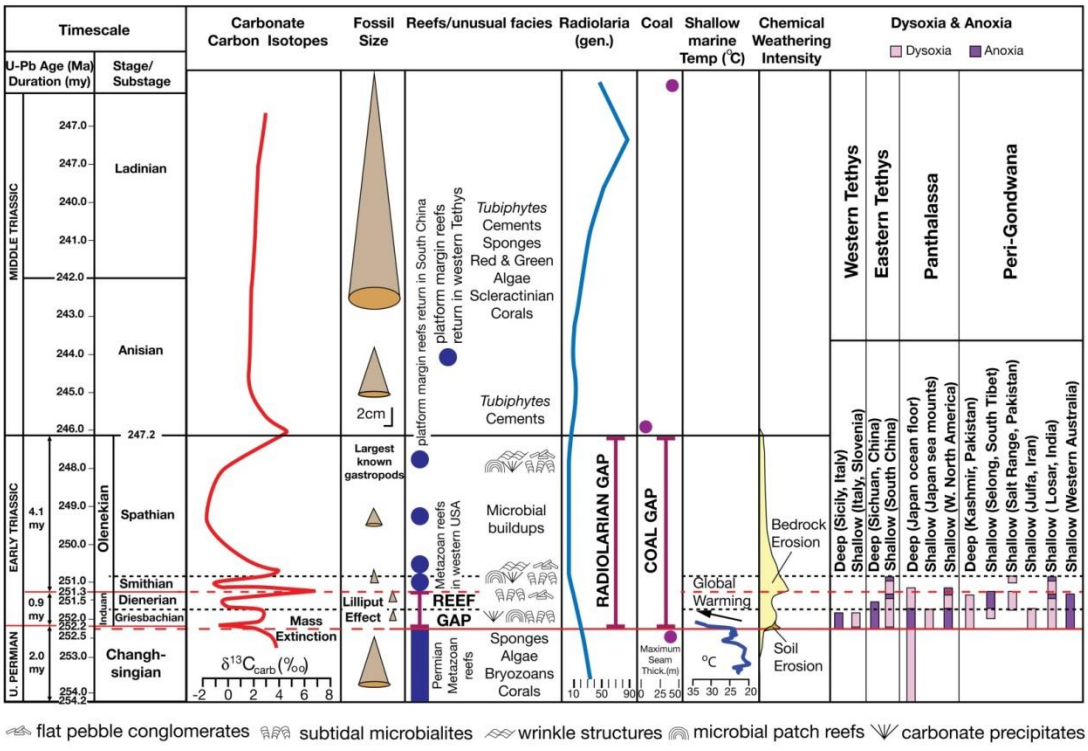

Figure 0.12: Temporal and geographic distribution of deep and shallow-marine dysoxia and anoxia in the late Permian and early Triassic plotted against physical, biotic and chemostratigraphic events that relate to the late Changhsingian mass extinction and 5 million year along early Triassic cesspool. Permian–Triassic numerical timescale is compiled from Mundil et al. (2004), Ovtcharova et al. (2006), Lehrmann et al. (2006), Galfetti et al. (2007b), Mundil et al. (2010), Shen et al. (2010) and Shen et al. (2011). Carbon isotope curve (adjusted to the latest numerical timescale) and gastropod size data are from Payne et al. (2004). Shallow-marine temperature curve from Joachimski et al. (2012). Chemical weathering intensity from Algeo et al. (2011). Reef frameworks, unusual facies and radiolarian data from Knoll et al. (2007), Pruss and Böttcher (2005) and Brayard et al., (2011). Coal seam thickness data from Retallack et al. (1996). Sources of temporal distribution of dysoxia and anoxia are discussed in the text.

It has previously been suggested that dysoxia and anoxia in the deep-marine environment commences in the late Middle Permian (late Capitanian) and extends to the early Middle Triassic (early Anisian) and has been referred to as a long-lasting "superanoxic event" (Kajiwara et al., 1994; Isozaki, 1997; Kato et al., 2002; Isozaki, 2009). Oceanic stagnation during this "superanoxic event" has been shown, based on modeling, to be unlikely (Hotinski et al., 2001; Winguth and Maier-Reimer, 2005). Biomarker and C and S isotope studies in China, Australia, Greenland and Western Canada (Grice et al., 2005a; Hays et al., 2006, 2007) have indicated that widespread periodic photic-zone sulfidic conditions (PZE) existed during this "superanoxic

event" and that sulfide toxicity was a contributory factor to the extinction and a factor in delayed recovery in the early Triassic. Earth system modeling (Meyer et al., 2008) suggests that H_2S toxicity and hypercapnia may have provided the kill mechanism for the P–T extinction. Photic-zone sulfidic conditions as a principal cause for the late Changhsingian ecosystem collapse and mass extinction is more problematic and has been recently challenged by Nielsen et al. (2010).

Anoxia in the pre-extinction late Permian has been interpreted, based on modeling, to not have been globally widespread but confined to an oxygen minimum zone and the deep eastern Panthalassa (Winguth and Winguth, 2012). Anoxia in the shallow-marine environment appeared in the latest Permian at the extinction level (**Figure 2.12**), later than in the deep-marine environment, and appears to be largely restricted to the Induan (Griesbachian and Dienerian) and early Olenekian (Smithian). Extreme climate warming occurred in the latest Permian–early Triassic, immediately post-mass extinction (Joachimski et al., 2012), with major changes in the Earth's ocean and atmosphere heat transfer systems (Kidder and Worsley, 2004). Pulses of shallow-marine anoxia during the Induan–Early Olenekian correspond to major global positive $\delta^{13}C$ isotopic excursions (**Figure 2.12**) and are suggested to be caused by repeated expansion of the oxygen minimum zone into the ocean surface layer due to environmental perturbations (Algeo, 2011a; 2011b) including extreme climate warming, increased chemical weathering intensity and continental erosion, sea level rise, and changes in marine nutrient inventories and productivity rates (Algeo et al., 2011).

Wignall and Twitchett (2002) discussed the temporal and spatial distribution of both deep and shallow-marine anoxia globally and indicated that oxygen-poor shallow-marine conditions widely developed in the latest Changhsingian and was at its maximum in the mid–Griesbachian and had waned by the mid–Dienerian to low-latitude areas of Panthalassa and a region of peri-Gondwana in a shallow-marine embayment in the India Madagascar region. Better constraints on the spatial distribution and upper limit of shallow-marine anoxia in the early Triassic are now available and our new data from the Perth Basin in Western Australia expands the known region of Induan shallow-marine anoxia in the peri-Gondwanan Meso-Tethys and dates its termination as late Dienerian. A compilation of currently available data on shallow-marine anoxia/dysoxia (**Figure 2.12**) demonstrates synchronous

establishment of dysoxia/anoxia at the Late Changhsingian mass extinction level but different timings of the cessation of anoxia in different paleogeographical regions and settings. It is not yet clear if different temporal pulses of anoxia in the shallow-marine environment are global or regional in nature. Thomas et al. (2004) suggested that upwelling on the west Australian Gondwana margin resulted in abnormally high productivity that produced the unique Lower Triassic organic-rich source rocks of the Sapropelic Interval of the Hovea Member of the Kockatea Shale.

This upwelling may also explain the relatively late cessation (late Dienerian) of anoxia along this part of the peri-Gondwana margin. Another possible explanation for the anoxia and organic-rich source rocks of the Sapropelic Interval of the Hovea Member is increased surface ocean productivity due to restricted water circulation and PZE (Grice et al., 2005b). Further detailed temporal and spatial mapping of anoxia in the late Permian–early Triassic will lead to further understanding of the driving forces for anoxia and how environmental perturbations both on-land and in the seas underpinned these forces.

Conclusions

Conodont biostratigraphy has unequivocally established the Induan–Olenekian Stage (Dienerian–Smithian Sub–Stage) Boundary in the Permo–Triassic succession of the onshore northern Perth Basin, Australia, specifically in the lower part of the "Limestone Marker" of the Hovea Member of the Kockatea Shale cored in the petroleum exploration well Senecio–1. This is the first unequivocally established stage boundary for either the Permian or Triassic of Australia utilising internationally robust biostratigraphy.

$\delta^{13}C_{org}$ values from the Induan–Olenekian transition in the Perth Basin vary from –27.5 to –32.9 ‰ VPDB and define a broad positive excursion of approximately 4 ‰. This correlates with a globally recognised positive excursion at this level and enhances correlation of the Senecio–1 section conodont zonation with proposed Induan–Olenekian GSSP sections in China and India and demonstrates the utility of this conodont defined level for stage boundary definition and global correlation.

The upper limit of anoxic conditions recognised in the Sapropelic Interval of the Hovea Member of the Kockatea Shale, Perth Basin is dated as late Induan (late Dienerian). Temporal and spatial mapping of marine anoxia and dysoxia globally demonstrates that pulses of anoxia affected shallow-marine zones at different times in different locations. This was probably caused by repeated expansion and/or geographically restricted upwelling of an oxygen minimum zone into the ocean surface layer due to environmental perturbations including extreme climate warming, increased terrestrial chemical weathering intensity and continental erosion, sea level rise, and changes in marine nutrient inventories and productivity rates.

Acknowledgments

IM and RSN were supported by Australian Research Council Discovery Grant DP109288. KG and ML were supported by ARC QEII Discovery grant to KG. ML was supported by Geoscience Australia, GFZ Potsdam and Curtin University for a Curtin International Tuition Scholarship. The Institute for Geoscience Australia and John de Le State Centre provided support. The authors wish to extend their thanks to Arc Energy Ltd, now AWE Ltd and its joint venture partner Origin Energy Ltd for permission to access its Senecio–1 core for research. Paul Wignall and Charles Henderson are thanked for their helpful reviews of the paper.

References

Algeo, T.J., 2011a. The early Triassic cesspool: Marine conditions following the end–Permian mass extinction. In: Håkansson, E., Trotter, J. (Eds), Programme and Abstracts, the XVII International Congress on the Carboniferous and Permian, Perth 3–8 July 2011: *Geological Survey of Western Australia*, Record 2011/20, 38.

Algeo, T.J., 2011b. Enhanced continental weathering in the latest Permian to early Triassic: Effects on shallow marine biotas. In: Håkansson, E., Trotter, J. (Eds), Programme and Abstracts, the XVII International Congress on the Carboniferous and Permian, Perth 3–8 July 2011: *Geological Survey of Western Australia*, Record 2011/20, 38.

Algeo, T.J., Twitchett, R.J., 2010. Anomalous early Triassic sediment fluxes due to elevated weathering rates and their biological consequences. *Geology* 38, 1023–1026.

Algeo, T., Chen, Z.Q., Fraiser, M.L., Twitchett, R.J., 2011. Terrestrial–marine teleconnections in the collapse and rebuilding of early Triassic marine ecosystems. *Paleogeography, Paleoclimatology, Paleoecology* 308, 1–11.

Alroy, J., Aberhan, M., Bottjer, D.J., Foote, M., Fürsich, F.T., Harries, P.J., Hendy, A.J.W., Holland, S.M., Ivany, L.C., Kiessling, W., Kosnik, M.A., Marshall, C.R., McGowan, A.J., Miller, A.I., Olszewski, T.D., Patzkowsky, M.E., Peters, S.E., Villier, L., Wagner, P.J., Bonuso, N., Borkow, P.S., Brenneis, B., Clapham, M.E., Fall, L.M., Ferguson, C.A., Hanson, V.L., Krug, A.Z., Layou, K.M., Leckey, E.H., Nürnberg, S., Powers, C.M., Sessa, J.A., Simpson, C., Tomašových, A., Visaggi, C.C., 2008. Phanerozoic trends in the global diversity of marine invertebrates. *Science* 321, 97–100.

Bann, K.L., Fielding, C.R., 2004. An integrated ichnological and sedimentological comparison of non-deltaic shoreface and subaqueous delta deposits in Permian reservoir units of Australia. In McIlroy, D. (Ed), the Application of Ichnology to Paleoenvironmental and Stratigraphic Analysis. *Geological Society of London*, Special Publication 228, 273–310.

Bond, D.P.G., Wignall, P.B., 2010. Pyrite framboid study of marine Permian–Triassic Boundary sections: A complex anoxic event and its relationship to contemporaneous mass extinction. *Geological Society of America Bulletin* 122, 1265–1279.

Brayard, A., Vennin, E., Olivier, N., Bylund, K.G., Jenks, J., Stephen, D.A., Bucher, H., Hofmann, R., Goudemand, N., Escarguel, G., 2011. Transient metazoan reefs in the aftermath of the end–Permian mass extinction. *Nature Geoscience* 4, 693–697.

Brookfield, M.E., Twitchett, R.J., Goodings, C., 2003. Paleoenvironments of the Permian–Triassic transition sections in Kashmir, India. *Paleogeography, Paleoclimatology, Paleoecology* 198, 353–371.

Corsetti, F.A., Baud, A., Marenco, P.J., Richoz, S., 2005. Summary of early Triassic carbon isotope records. *Comptes Rendus Palevol* 4, 473–486.

Dolenec, T., Lojen, S., Ramovs, A., 2001. The Permian–Triassic Boundary in Western Slovenia (Idrijca Valley section): magnetostratigraphy, stable isotopes, and elemental variations. *Chemical Geology* 175, 175–190.

Epstein, A.G., Epstein, J.B., Harris, L.D., 1977. Conodont colour alteration; an index to organic metamorphism. U.S. *Geological Survey Professional Paper* 995, 27.

Erwin, D.H., 1993. The Great Paleozoic Crisis. Columbia Univ. Press, New York.

Felton, E.A., Miyazaki, S., Dowling, L. Pain, L., Vuckovic V., le Poidevin, S.R., 1993. Carnarvon Basin, W.A., Bureau of Resource Sciences, *Australian Petroleum Accumulations* Report 8.

Galfetti, T., Bucher, H., Brayard, A., Hochuli, P.A., Weissert, H., Guodun, K., Atudorei, V., Guex, J., 2007a. Late Early Triassic climate change: insights from carbonate carbon isotopes, sedimentary evolution and ammonoid paleobiogeography. *Paleogeography, Paleoclimatology, Paleoecology* 243, 394–411.

Galfetti, T., Bucher, H., Ovtcharova, M., Schaltegger, U., Brayard, A., Bruhwiler, T., Goudemand, N., Weissert, H., Hochuli, P.A., Cordey, F., Guodun, K., 2007b. Timing of the early Triassic carbon cycle perturbations inferred from new U–Pb ages and ammonoid biochronozones. *Earth and Planetary Science Letters* 258, 593–604.

Gorjan, P., Kaiho, K., Kakegawa, T., Niitsuma, S., Chen, Z.Q., Kajiwara, y., Nicora, A., 2007. Paleoredox, biotic and sulfur-isotopic changes associated with the end–Permian mass extinction in the western Tethys. *Chemical Geology* 244, 483–492.

Gorter, J.D., Nicoll, R.S., Metcalfe, I., Willink, R.J. and Ferdinando, D. 2009. The Permian–Triassic Boundary in Western Australia: evidence from the Bonaparte and Northern Perth basins: exploration implications. *Australian Petroleum Production and Exploration Association Journal* 2009, 311–336.

Grice, K., Cao, C., Love, G.D., Bottcher M.E., Twitchett, R.J., Grosjean E., Summons R.E., Turgeon S. C., Dunning W., Jin Y., 2005a. Photic zone euxinia during the Permian – Triassic Superanoxic Event. *Science* 307, 706–709.

Grice, K., Summons, R.E., Grosjean, E., Twitchett, R.J., Dunning, W., Wang, S.X., Böttcher, M.E., 2005b. Depositional conditions of the northern onshore Perth Basin (basal Triassic). *Australian Petroleum Production and Exploration Association Journal* 45, 263–273.

Grice, K., Nabbefeld, B., Maslen, E., 2007. Source and significance of selected polycyclic aromatic hydrocarbons in sediments (Hovea–3 well, Perth Basin, Western Australia) spanning the Permian–Triassic Boundary. *Organic Geochemistry* 38, 1795–1803.

Hays, L., Love, G.D., Foster, C.B., Grice, K., Summons, R.E., 2006. Lipid biomarker records across the Permian–Triassic Boundary from Kap Stosch, Greenland: Eos (Transactions, *American Geophysical Union*) 87, no. 52, PP41B–1203.

Hays, L.E., Beatty, T., Henderson, C.M., Love, G.D., Summons, R.E., 2007. Evidence for photic zone euxinia through the end–Permian mass extinction in the Panthalassic Ocean (Peace River Basin, Western Canada): *Paleoworld* 16,

39–50.

Hermann, E., Hochuli, P.A., Méhay, S., Bucher, H., Brühwiler, T., Ware, D., Hautmann, M., Roohi, G., ur-Rehman, K., Yaseen, A., 2011. Organic matter and paleoenvironmental signals during the early Triassic biotic recovery: The Salt Range and Surghar Range records. *Sedimentary Geology* 234, 19–41.

Horacek, M., Brandner, R., Abart, R., 2007. Carbon isotope record of the P/T Boundary and the Lower Triassic in the Southern Alps: evidence for rapid changes in storage of organic carbon. *Paleogeography, Paleoclimatology, Paleoecology* 252, 347–354.

Horacek, M., Koike, T., Richoz, S., 2009. Lower Triassic $\delta^{13}C$ isotope curve from shallow-marine carbonates in Japan, Panthalassa realm: Confirmation of the Tethys $\delta^{13}C$ curve. *Journal of Asian Earth Sciences* 36, 481–490.

Hotinski, R.M., Bice, K.L., Kump, L.R., Najjar, R.G., Arthur, M.A., 2001. Ocean stagnation and end–Permian anoxia. *Geology* 29, 7–10.

Huang, C., Tong, J., Hinnov, L., Chen, Z.Q., 2011. Did the great dying of life take 700 k.y.? Evidence from global astronomical correlation of the Permian–Triassic Boundary interval. *Geology* 39, 779–782.

Isozaki, Y., 1997. Permo–Triassic Boundary superanoxia and stratified superocean: Records from lost deep sea. *Science* 276, 235–238.

Isozaki, Y. 2009. Integrated ‘‘plume winter” scenario for the double-phased extinction during the Paleozoic–Mesozoic transition: The G-LB and P-TB events from a Panthalassan perspective. *Journal of Asian Earth Sciences* 36, 459–480.

Joachimski, M.M., Lai, X., Shen, S., Jiang, H., Luo, G., Chen, J., Sun, Y., 2012. Climate warming in the latest Permian and the Permian–Triassic mass extinction. *Geology* 40, 195–198.

Kajiwara, Y., Ishida, K., Tanikura, Y., Ishiga, H., 1993a. Sulfur isotope data from the Permian–Triassic Boundary at Sasayama in the Tanba Terrane in southwestern Honshu, Japan. *Annual Report of Institut Geoscience.,* University of Tsukuba 19, 67–72.

Kajiwara, Y., Yamakita, S., Kobayashi, D., Imai, A., 1993b. Sulfur isotope data from the Permian–Triassic Boundary at Tenjinmaru in the Chichibu Terrane in eastern Shikoku, Japan. *Annual Report of Institut Geoscience.,* University of Tsukuba 19, 59–66.

Kajiwara, Y., Yamakita, S., Ishida, K., Ishida, H., Imai, A., 1994. Development of a largely anoxic stratified ocean and its temporary massive mixing at the Permian/Triassic Boundary supported by the sulfur isotopic record. *Paleogeography, Paleoclimatology, Paleoecology* 111, 367–379.

Kakuwa, Y., 2008. Evaluation of paleo-oxygenation of the ocean bottom across the Permian–Triassic Boundary. *Global and Planetary Change* 63, 40–56.

Kakuwa, Y., Matsumoto, R., 2006. Cerium negative anomaly just before the Permian and Triassic Boundary event — The upward expansion of anoxia in the water column. *Paleogeography, Paleoclimatology, Paleoecology* 229, 335– 344.

Kato, Y., Nakao, K., Isozaki, Y., 2002. Geochemistry of late Permian to early Triassic pelagic cherts from southwest Japan: implications for an oceanic redox change. *Chemical Geology* 182, 15–34.

Kershaw, S., Zhang, T., Lan, G., 1999. A microbialite carbonate crust at the Permian–Triassic Boundary in South China, and its paleoenvironmental significance. *Paleogeography, Paleoclimatology, Paleoecology* 146, 1–18.

Kidder, D.L., Worsley, T.R., 2004. Causes and consequences of extreme Permo–Triassic warming to globally equable climate and relation to the Permo–Triassic extinction and recovery. *Paleogeography, Paleoclimatology, Paleoecology* 203, 207–237.

Knoll, A.H., Bambach, R.K., Payne, J.L., Pruss, S., Fischer, W.W., 2007. Paleophysiology and end–Permian mass extinction. *Earth and Planetary Science Letters* 256, 295–313.

Kozur, H., 1990. The taxonomy of the gondolellid conodonts in the Permian and Triassic. *Courier Forschungs Institut Senckenberg* 117, 409–469.

Krystyn, L., Bhargava, O. N., Richoz, S., 2007. A candidate GSSP for the base of the Olenekian Stage: Mud at Pin Valley; district Lahul and Spiti, Himachal Pradesh (Western Himalaya), India. *Albertiana* 35, 5–29.

Lehrmann, D.J., Ramezani, J., Bowring, S.A., Martin, M.W., Montgomery, P., Enos, P., Payne, J.L., Orchard, M.J., Wang, H., Wei, J.Y., 2006. Timing of recovery from the end–Permian extinction: geochronologic and biostratigraphic constraints from South China. *Geology* 34, 1053–1056.

Maxwell, W.D. 1992. Permian and early Triassic extinction of non-marine tetrapods. *Paleontology* 35, 571–583.

McTavish, R. A., 1973. Triassic conodont faunas from Western Australia. *Neues Jahrbuch fur Geologie und Palaontologie Abhandlungen* 143, 275–303.

McTavish, R. A., Dickins, J.M., 1974. The age of the Kockatea Shale (Lower Triassic), Perth Basin—a reassessment. *Journal of the Geological Society of Australia* 21, 195–201.

Metcalfe, I., Nicoll, R.S., Willink, R.J., 2008. Conodonts from the Permian Triassic transition in Australia and position of the Permian–Triassic Boundary. *Australian Journal of Earth Sciences* 55, 349–361.

Metcalfe, I., Riley, N.J., 2010. Conodont Colour Alteration pattern in the Carboniferous of the Craven Basin and adjacent areas, northern England. *Proceedings of the Yorkshire Geological Society* 58, 1–9.

Meyer, K.M., Kump, L.R., Ridgwell, A., 2008. Biogeochemical controls on photic-zone euxinia during the end–Permian mass extinction. *Geology* 36, 747–750.

Michaelson, P., 2002. Mass-extinction of peat-forming plants and the effect on flu vial styles across the Permian–Triassic Boundary, northern Bowen Basin, Australia. *Paleogeography, Paleoclimatology, Paleoecology* 179, 173–188.

Mory, A.J., Haig, D.W., McLoughlin, S., Hocking, R., 2005. Geology of the northern Perth Basin, Western Australia — a field guide. *Western Australia Geological Survey*, Record 2005/9, 71.

Mory, A. J., Iasky, R. P., 1996. Stratigraphy and structure of the onshore northern Perth Basin, Western Australia. *Western Australia Geological Survey*, Report 46, 101.

Mundil, R., Ludwig, K.R., Metcalfe, I., Renne, P.R., 2004. Age and Timing of the Permian Mass Extinctions: U/Pb Geochronology on Closed-System Zircons. *Science* 305, 1760–1763.

Mundil, R., Palfy, J., Renne, P.R., Brack, P., 2010. The Triassic time scale: new constraints and a review of geochronological data. In: Lucas, S.G. (Ed.), the Triassic Timescale. *Geological Society of London Special Publication* 334, 41–60.

Musashi, M., Isozaki, Y., Koike, T., Kreulen, R., 2001. Stable carbon isotope signature in mid–Panthalassa shallow-water carbonates across the Permo–Triassic Boundary: evidence for ^{13}C-depleted super Ocean. *Earth and Planetary Science Letters* 191, 9–20.

Nabbefeld, B., Grice, K., Schimmelmann, A., Sauer, P.E., Böttcher, M.E., Twitchett, R., 2010. Significance of $\delta D_{kerogen}$, $\delta^{13}C_{kerogen}$ and $\delta^{34}S_{pyrite}$ from several Permian/Triassic (P/Tr) sections. *Earth and Planetary Science Letters* 295, 21–29.

Newton, R., Pevitt, E.L., Wignall, P.B., Bottrell, S.H., 2004. Large shifts in the isotopic composition of seawater sulfate across the Permo–Triassic Boundary in northern Italy. *Earth and Planetary Science Letters* 218, 331–345.

Nielsen, J. K., Shen, Y., 2004. Evidence for sulfidic deep water during the late Permian in the East Greenland Basin. *Geology* 32, 1037–1040.

Nielsen, J.K., Shen, Y., Piasecki, S., Stemmerik, L., 2010. No abrupt change in redox condition caused the end–Permian marine ecosystem collapse in the East Greenland Basin. *Earth and Planetary Science Letters* 291, 32–38.

Nowlan, G.S., Barnes, C.R., 1987. Application of conodont colour alteration indices to regional and economic geology. In: Austin, R.L. (Ed.) Conodonts: Investigative Techniques and Applications. *British Micropaleontological Society Series*, Ellis Horwood Limited, Chichester, 188–202.

Orchard, M.J., 2007. Conodont diversity and evolution through the latest Permian and early Triassic upheavals. *Paleogeography, Paleoclimatology, Paleoecology* 252, 93–117.

Orchard, M.J., 2010. Triassic conodonts and their role in stage boundary definition. In: Lucas, S. G. (Ed.). The Triassic Timescale. *Geological Society of London Special Publication* 334, 139–161.

Orchard, M.J., Krystyn, L., 2007. Conodonts from the Induan–Olenekian Boundary interval at Mud, Spiti. *Albertiana* 35, 30–34.

Orchard, M.J., Tozer, E.T., 1997. Triassic conodont biochronology and intercalibration with the Canadian ammonoid sequence. *Albertiana* 20, 33–44.

Ovtcharova, M., Bucher, H., Schaltegger, U., Galfetti, T., Brayard, A., Guex, J., 2006. New Early to Middle Triassic U–Pb ages from South China: calibration with ammonoid biochronozones and implications for the timing of the Triassic biotic recovery. *Earth and Planetary Science Letters* 243, 463–475.

Payne, J.L., Lehrmann, D.J., Wei, J., Orchard, M.J., Schrag, D.P., Knoll, A.H., 2004. Large perturbations of the carbon cycle during recovery from the end–Permian extinction. *Science* 305, 506–509.

Posenato, R., 2008. Global correlations of mid early Triassic events: The Induan/Olenekian Boundary in the Dolomites (Italy). *Earth-Science Reviews* 91, 93–105.

Purcell, R., 2006. Palynology Report Senecio–1, L1, North Perth Basin, Western Australia. Report to Arc Energy NL, 7.

Pruss, S.B., Böttcher, D.J., 2005. The reorganization of reef communities following the end–Permian mass extinction. *Comptes Rendus Palevol* 4, 553–568.

Retallack, G.J., Krull, E.S., 1999. Landscape ecological shift at the Permian–Triassic Boundary in Antarctica. *Australian Journal of Earth Sciences* 46, 785–812.

Retallack, G.J., Veevers, J.J., Morante, R., 1996. Global coal gap between Permian–Triassic extinction and Middle Triassic recovery of peat-forming plants, *Geological Society for American Bulletin* 108, 195–207.

Richoz, S. Krystyn, L., Horacek, M., Spötl, C., 2007. Carbon isotope record of the Induan–Olenekian candididate GSSP Mud and comparison with other sections. *Albertiana* 35, 35–39.

Schubert, J.K., Bottjer, D.J., 1995. Aftermath of the Permian–Triassic mass extinction event: Paleoecology of Lower Triassic carbonates in the western USA. *Paleogeography, Paleoclimatology, Paleoecology* 116, 1–39.

Sheldon, N.D., 2006. Abrupt chemical weathering increase across the Permian–Triassic boundary. *Paleogeography, Paleoclimatology, Paleoecology* 231, 315– 321.

Shen, S.Z., Henderson, C.M., Bowring, S.A., Cao, C.Q., Wang, Y., Wang, W., Zhang, H., Zhang, Y.C., Mu, L., 2010. High-resolution Lopingian (late Permian) timescale of South China. *Geological Journal* 45, 122–134.

Shen, S. Z., Crowley, J.L., Wang, Y., Bowring, S.A., Erwin, D.H., Sadler, P.M., Cao, C.Q., Rothman, D.H., Henderson, C.M., Ramezani, J., Zhang, H., Shen, Y., Wang, X.d., Wang, W., Mu, L., Li, W.z., Tang, Y.g., Liu, X.l., Liu, L.j., Jiang, Y.f., Jin, Y.g., 2011. Calibrating the end-Permian mass extinction. *Science* 334, 1367–1372.

Shigeta, Y., Zakharov, Y.D., Maeda, H., Popov, A.M., (Eds) 2009. The Lower Triassic System in the Abrek Bay area, South Primorye, Russia. Tokyo, *National Museum of Nature and Science Monographs* 38, 218.

Takahashi, S., Yamakita, S., Suzuki, N., Kaiho, K., Ehiro, M., 2009. High organic carbon content and a decrease in radiolarians at the end of the Permian in a newly discovered continuous pelagic section: A coincidence?, *Paleogeography, Paleoclimatology, Paleoecology* 271, 1–12.

Thomas, B. M., Barber, C.J., 2004. A re-evaluation of the hydrocarbon habitat of the northern Perth Basin. *Australian Petroleum Production and Exploration Association Journal* 44, 59 – 92.

Thomas, B.M., Willink, R.J., Grice, K., Twitchett, R.J., Purcell, R.R., Archbold, N.

W., George, A.D., Tye, S., Alexander, R., Foster, C.B., Barber, C.J., 2004. Unique marine Permian – Triassic Boundary section from Western Australia. *Australian Journal of Earth Sciences* 51, 423 – 430.

Tong, J., Yin, Y., 2002. The Lower Triassic of South China. *Journal of Asian Earth Sciences* 20, 803–815.

Tong, J., Zhao, L., 2011. Lower Triassic and Induan–Olenekian Boundary in Chaohu, Anhui Province, South China. *Acta Geologica Sinica* 85, 399–407.

Tong, J., Zakharov, Y.D., Orchard, M.J., Yin, H., Hansen, H.J., 2004. Proposal of Chaohu section as the GSSP candidate of the Induan/Olenekian Boundary. *Albertiana* 29, 13–28.

Twitchett, R.J., 1999. Paleoenvironments and faunal recovery after the end-Permian mass extinction. *Paleogeography, Paleoclimatology, Paleoecology* 154, 27–37.

Twitchett, R.J., Wignall, P.B., 1996. Trace fossils and the aftermath of the Permo–Triassic mass extinction: evidence from northern Italy. *Paleogeography, Paleoclimatology, Paleoecology* 124, 137–151.

Wignall, P.B., Hallam, A., 1992. Anoxia as a cause of the Permian/Triassic extinction: Facies evidence from northern Italy and the western United States. *Paleogeography, Paleoclimatology, Paleoecology* 93, 21–46.

Wignall, P.B., Hallam, A., 1993. Griesbachian (Earliest Triassic) paleoenvironmental changes in the Salt Range, Pakistan and southeast China and their bearing on the Permo–Triassic mass extinction. *Paleogeography, Paleoclimatology, Paleoecology* 102, 215–237.

Wignall, P.B., Twitchett, R.J., 1996. Oceanic anoxia and the end-Permian mass extinction. *Science* 272, 1155–1158.

Wignall, P.B., Twitchett, R.J., 2002. Extent, duration and nature of the Permian–Triassic superanoxic event. In: Koeberl, C., MacLeod, K.C. (Eds) Catastrophic Events and Mass Extinctions: Impacts and Beyond. Boulder, Colorado. *Geological Society of America Special Paper* 356, 395–413.

Wignall, P.B., Newton, R., 2003. Contrasting Deep-water Records from the upper Permian and Lower Triassic of South Tibet and British Columbia: Evidence for a Diachronous Mass Extinction. *Palaios* 18, 153–167.

Wignall, P.B., Newton, R., Brookfield, M.E., 2005. Pyrite framboid evidence for oxygen-poor deposition during the Permian–Triassic crisis in Kashmir. *Paleogeography, Paleoclimatology, Paleoecology* 216, 183–188.

Wignall, P.B., Bond, D.P.G., Kuwahara, K., Kakuwa, Y., Newton, R.J., Poulton, S.W., 2010. An 80 million year oceanic redox history from Permian to Jurassic pelagic sediments of the Mino-Tamba terrane, SW Japan, and the origin of four mass extinctions. *Global and Planetary Change* 71, 109–123.

Winguth, A.M.E, Maier-Reimer, E., 2005. Causes of the marine productivity and oxygen changes associated with the Permian–Triassic Boundary: A reevaluation with ocean general circulation models. *Marine Geology* 217, 283–304.

Wignuth, C., Winguth, A.M.E, 2012. Simulating Permian–Triassic oceanic anoxia

distribution: Implications for species extinction and recovery. *Geology* 40, 127–130.

Zhao, L., Orchard, M.J., Tong, J., Sun, Z., Zuo, J., Zhang, S., Yun, A., 2007. Lower Triassic conodont sequence in Chaohu, Anhui Province, China and its global correlation. *Paleogeography, Paleoclimatology, Paleoecology* 252, 24–38.

Zhao, L., Tong, J., Sun, Z., Orchard, M.J., 2008. A detailed Lower Triassic conodont biostratigraphy and its implications for the GSSP candidate of the Induan–Olenekian Boundary in Chaohu, Anhui Province. *Progress in Natural Science* 18, 79–90.

Chapter 3

Stable isotopic proxies (molecular fossils and bulk parameters) to establish the paleoenvironmental changes spanning the Induan–Olenekian Boundary in the northern onshore Perth Basin, Western Australia: Evidence for methane clathrate release in the early Triassic

Mojgan Ladjavardi, Kliti Grice, Ian Metcalfe, Chris J. Boreham, Arndt Schimmelmann, Peter E. Sauer, Michael E. Böttcher, Ines Melendez

***Gondwana Research*, in revision**

Abstract

The early Triassic Induan–Olenekian Stage Boundary has been established by conodont biostratigraphy at a depth of 2719.25 m in the Senecio–1 well in the northern onshore Perth Basin, Western Australia. A comprehensive study using organic geochemical and compound specific stable carbon and hydrogen isotopic analysis is used to further establish the paleoenvironmental conditions spanning the Induan–Olenekian Stage Boundary in the Senecio–1 well. Rock-Eval pyrolysis and TOC analyses suggest that the Senecio–1 sequence is within the oil window. Based on Rock-Eval pyrolysis data, the Induan section of the core (2729.60–2721.70 m) consists mostly of kerogen Type II-III, followed by an inertinitic section across the boundary (2720.88– 2718.94 m) representing Type III kerogen with the Olenekian part of the core (2719.37–2708.12 m) also Type III kerogen. The results of $\delta^{13}C_{OM}$ show a gradual positive excursion in the upper Induan which is followed by a more pronounced negative excursion in the early Olenekian. $\delta^{13}C_{carbonate}$ values show a similar trend to the $\delta^{13}C_{OM}$ for the studied section (2721.95–2710.86). Similarly the $\delta^{13}C$ values for individual *n*-alkanes and regular isoprenoids (largely derived from eukaryotes) show a general positive excursion in the Induan section close to the boundary and becoming significantly more ^{13}C-depleted in the early Olenekian. Individual aromatic compounds also show a similar isotopic trend shifting to more ^{13}C-depleted values in the Olenekian. The negative isotopic trend in the Olenekian is attributed to and consistent with a ^{13}C-depleted carbon source from the melting of methane clathrates as a result of climate warming and from massive volcanic activity in Siberia. The values of $\delta^{34}S_{pyrite}$ show a shift in $\delta^{34}S$ values across the boundary consistent with euxinic conditions existing in the ocean at the time.

Keywords

Triassic, Induan–Olenekian, isoprenoids, methane clathrates

Introduction

The most profound mass extinction in Earth's history occurred in the latest Permian (Raup and Sepkoski, 1982; Erwin, 1993; Alroy et al., 2008). Substantial evidence exists for late Permian–early Triassic major climate perturbations (Korte et al., 2004, 2010; Benton and Newell, 2013), frequent shifts between oxic and anoxic/dysoxic conditions in the oceans (Kato et al., 2002; Wignall and Twitchett, 2002; Kidder and Worsley, 2004; Grice et al., 2005a; Fenton et al., 2007; Nabbefeld et al., 2010a; Wignall et al., 2010; Metcalfe et al., 2013) and also climate warming or hothouse conditions have been suggested (Joachimski et al., 2012). Recovery of biota following the end-Permian extinction was impeded by continued climate change and environmental perturbations that are recorded by $\delta^{13}C$ excursions, variations in ocean redox conditions, global hiatuses in the accumulation of coal, carbonate reefs and a range of unusual facies and biota including microbialites, and flat pebble conglomerates (Wignall et al., 2010; Algeo, 2011; Metcalfe et al., 2013).

Frequent shifts between oxic and anoxic/dysoxic conditions, particularly in the Induan Stage (Bond and Wignall, 2010; Metcalfe et al., 2013), have been understood as the consequence of the expansion of a shallow oxygen minimum zone into the ocean surface layer due to a combination of environmental perturbations (Algeo, 2011). Here we present a comprehensive isotopic study from the early Triassic spanning the Induan–Olenekian Stage Boundary, preserved in Senecio–1, a petroleum exploration drill core recovered from the northern onshore Perth Basin, Western Australia. Our aim is to better understand the paleoenvironmental changes that occurred around the Induan–Olenekian Boundary.

Further, compound specific isotope data combined with bulk isotopic data of OM and carbonate are concordant with destabilisation of gas clathrates and release of ^{13}C-depleted methane into the oceans leading to a shift in both ocean and atmospheric $^{12}CO_2$. Our data extends previously reported data sets only reported for $\delta^{13}C_{carbonates}$ for this same time interval attributed to climate warming associated with volcanic activity in Siberia that happened around the same time (Clarkson et al., 2013; Korte and Kozur, 2010). The large negative excursion has also been suggested to be associated with the oceanic anoxia and collapse of the biological productivity (Nabbefeld et al., 2010a). Similarly, reduction of the organic carbon burial and

increase in microbial respiration rates are believed to be probable explanations for the carbon isotope excursions during the early Triassic (Stanley, 2010). Greenhouse warming conditions have also been suggested as a contributing cause of the mass extinction during the early Triassic evolving high primary productivity (Morante, 1995; 1996; Grice et el., 2005a).

Geological Settings

The Perth Basin in southwest Western Australia extends from near Geraldton in the north to the south of Perth (**Figure 3.1.**A and B). The sediments of the Perth Basin include rocks of Permian to Early Cretaceous age. The Perth Basin sediments analysed in this study chapter are from Senecio–1 drill core (Latitude 29°14'25.94"S, Longitude 115°05'29.28"E) located in the northern Perth Basin, approximately 15.5 km to the east of Dongara (**Figure 3.1.** B).

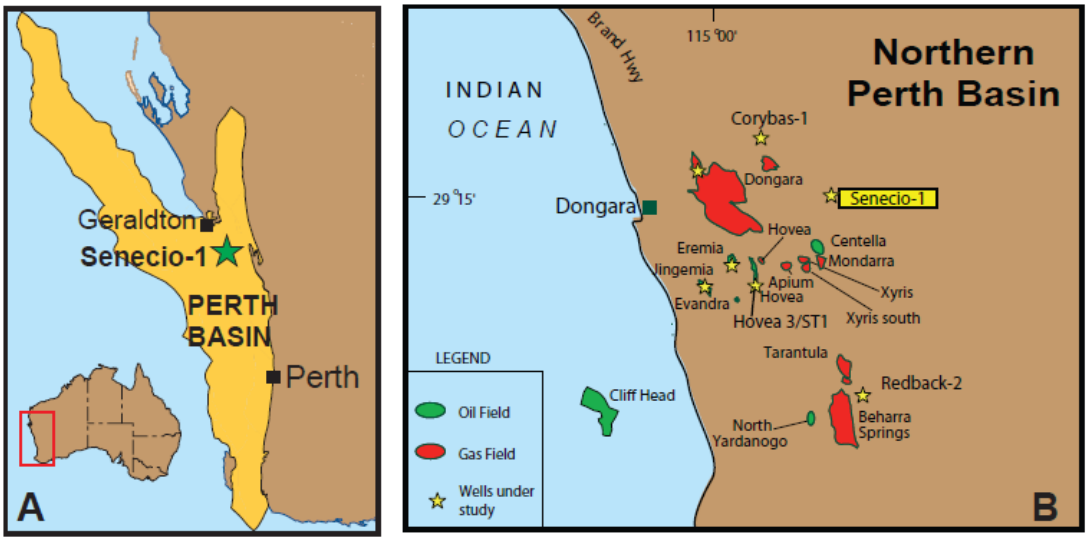

Figure 0.1: **A**. The location of the Perth Basin, Western Australia and **B**. Senecio–1 well in the northern onshore Perth Basin (modified after Metcalfe et al., 2013).

Exploration in the Perth Basin petroleum system for the last few decades has led to the production of gas and oil from a number of onshore fields (e.g. Summons et al., 1995; Thomas and Barber, 2004). The offshore area has shown to be gas prone but with important oil reserves, e.g. the near-shore Cliff Head oil field (Thomas and

Barber, 2004). The marine Kockatea Shale, now referred as Hovea Member (**Figure 3.2**), is recognised as the chief source rock for petroleum in the Perth Basin (e.g. Thomas et al., 2004; Grice et al., 2005b). The Hovea Member at the basal part of the Kockatea Shale includes a basal inertinitic interval, a middle sapropelic interval (being the H-richest interval), and an upper limestone marker unit (Thomas et al., 2004) (**Figure 3.2**). The Hovea Member is 30 to 70 m thick with TOC ca. 5 wt. % (Thomas and Barber, 2004; Thomas et al., 2004; Grice et al., 2005a; Metcalfe et al., 2013). However the average TOC values in the Kockatea Shale, above the Hovea Member, is ca. 0.8 wt. % (Mory and Iasky, 1996) possibly revealing high sedimentation rates and thus dilution of the OM. The Permian–Triassic transition in the Perth Basin is situated in the lower part of the Kockatea Shale (Hovea Member), based on limited palynology, conodont biostratigraphy and carbon isotope stratigraphy (Metcalfe et al., 2008; 2013).

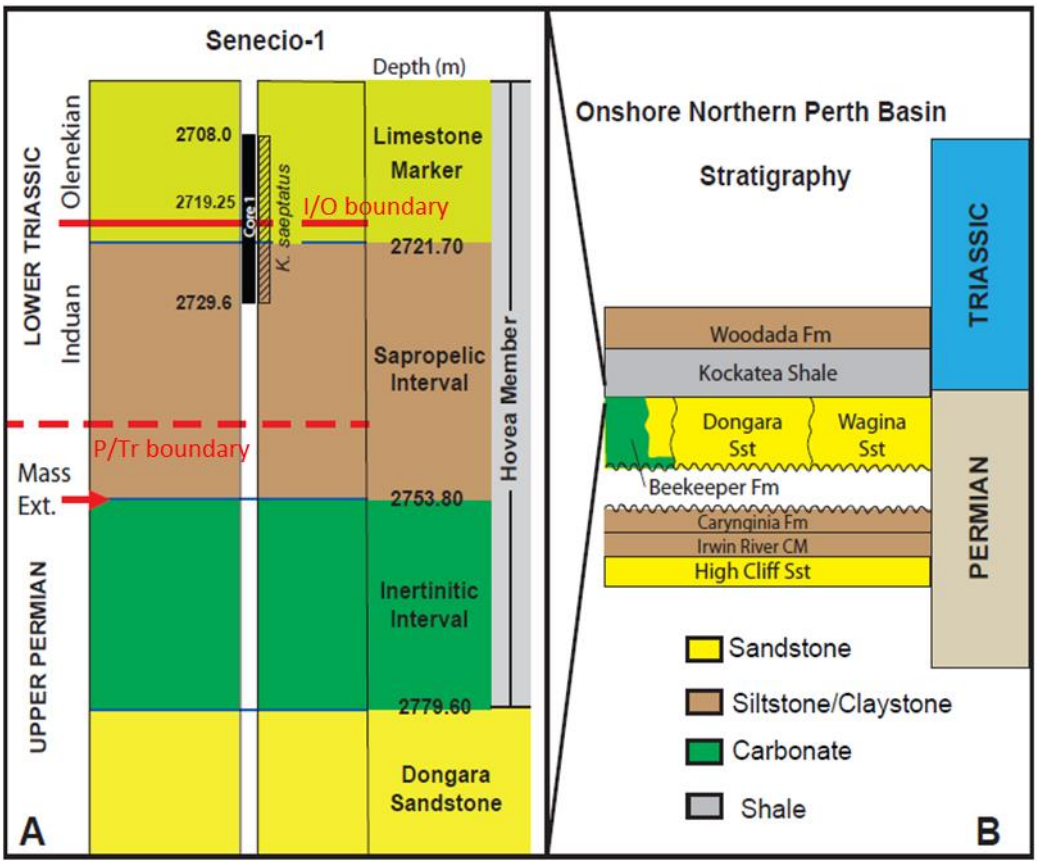

Figure 0.2: **A**. Lower Triassic Hovea Member stratigraphy covered by the Senecio–1 well and the sampled cored interval and **B**. Permian–Triassic stratigraphy of the northern Perth Basin placing the Kockatea Shale in context (modified after Metcalfe et al., 2013).

The Senecio–1 core covers part of the lower Hovea Member of the Kockatea Shale, spanning the Induan–Olenekian Stage Boundary in the central part of the Lower Triassic (**Figure 3.2.** A). The early Triassic Induan–Olenekian Stage Boundary (Dienerian–Smithian Sub-Stage Boundary) has been recognized at a depth of 2719.25 m in the Senecio–1, using conodont biostratigraphy (Metcalfe et al., 2013). Purcell (2006) has demonstrated that the whole core is within the Lower Triassic *Kraeuselisporites saeptatus* Zone, based on palynology. The sedimentary log of the Senecio–1 well is shown in **Figure 3.3.** (Metcalfe et al., 2013).

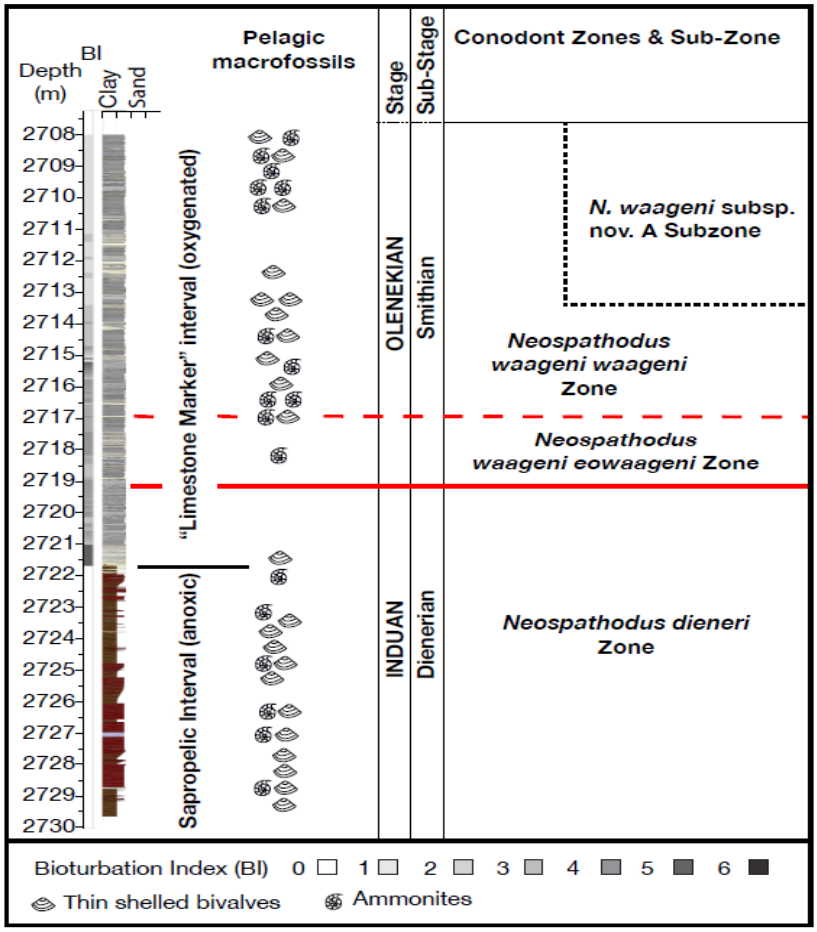

Figure 0.3: Sedimentary log of the Senecio–1 well in the northern Perth Basin, WA. The position of the Induan–Olenekian Boundary has been unequivocally determined by conodont biostratigraphy (after Metcalfe et al., 2013).

The lower section of the core in the so called sapropelic interval is typified as an anoxic high-stand, based on organic carbon-rich finely laminated mudstones and siltstones with TOC values of ca. 2.5 wt. % (Thomas et al., 2004). The Limestone

Marker unit in the upper Hovea Member covers the upper section of the core and includes laminated mudstones with siltstones. The base of the unit is characterised by a 40 cm thick sharp-based, glauconitic siltstone comprising a large amount of mostly damaged *Clarkina* conodont elements (inferred as transported). This *Clarkina* conodont-bearing siltstone, together with other siltstones in this unit, are considered as distal turbidites or tempestites and located on the continental shelf below storm wave. The macrofossils in the core (poorly preserved and comparatively rare) are dominated by ammonites and epifaunal pelagic thin-shelled bivalves. Fish teeth and scales, tiny foraminifera, conodonts and ostracods are commonly observed in the core. The upper part of the unit was deposited under oxygenated conditions (Metcalfe et al., 2013). The maturity of the Senecio–1 core samples has also been identified by using conodont Colour Alteration Index (CAI) by Metcalfe et al., 2013. CAI of Senecio–1 elements are 2 to 2.5 indicating that the sedimentary rocks are mature to over-mature but probably in the upper part of the oil window.

Analytical methods

Sample preparation and extraction

Eighty seven samples (each 25 cm in length and ca. 1 kg in weight) from Senecio–1 well were collected from 2708.10 to 2729.64 m depths. Thirty one of these span the Induan–Olenekian interval and were selected at 1 m spacing. To remove external contamination, the samples were surface-washed with a mixture of DCM and CH_3OH (9:1, v: v) in an ultrasonic bath for 20 mins. Each sample was ground to a fine powder and extracted by an automated Accelerated Solvent Extractor (ASE) using a Dionex ASE 200 (Dionex, Sunnyvale, CA, USA). Following the methodology of Grice et al. (2005b), the ground sediments were weighed into pre-extracted stainless steel extraction cells containing pre-rinsed glass fibre filters and loaded into the turret of the ASE. After being preheated at 100 °C for 2 mins, a mixture of DCM and CH_3OH (9:1, v: v) was pumped into the cells using a pressure of 6.89 M Pascals [1000 psi] for 5 mins. The whole procedure was repeated until the extracted solvent became colourless, which we assume to indicate full

extraction of target compounds without resultant isotopic fractionation. The extracts were then combined and the solvent was removed under a N_2 purge.

TOCand Rock-Eval pyrolysis parameters

Rock-Eval parameters and TOC (wt. %) values have been determined using a Rock Eval 6 instrument as described by Lafargue et al. (1998).

Column Chromatography

The extracts were separated into 6 fractions by column chromatography on activated silica gel (120 °C, 8 hr) following the methodology by Grice et al. (2005b); 6 fractions (saturated hydrocarbons, aromatic hydrocarbons, equivalent to nickel porphyrins, equivalent to vanadyl porphyrins, a fifth fraction equivalent to maleimides and NSO polar lipids in the final fraction) were eluted using solvent mixtures of increasing polarity containing *n*-hexane, DCM/*n*-hexane (1:4, v:v), DCM/*n*-hexane (1:1, v:v), DCM, acetone/DCM (1:20, v:v) and DCM/CH_3OH (1:1, v:v), respectively.

Gas Chromatography – Mass Spectrometry (GC-MS) analysis

The saturated and aromatic hydrocarbon fractions were characterised by GC-MS. GC-MS analyses were performed using a Hewlett Packard (HP) 5973 mass-spectrometer combined with a HP 6890 gas chromatograph instrument (GC), fitted with a split/splitless injector and using a DB-5 fused silica capillary column (60 m x 0.25 mm i.d. x 0.25 μm film thickness). Helium was used as carrier gas at flow rate of 1 mL/min.

The GC oven temperature was programmed from 40 °C to 325 °C with a heating rate of 3 °C per minute and was held isothermally for 30 mins. The mass spectrometer was operated in full scan (50–550 amu) with ionisation energy of 70 *eV*, an electron multiplier voltage of 1800 V and a source temperature of 180 °C. The identification of aromatic hydrocarbons was performed by comparison of mass spectra and corresponding retention times with those of reference compounds previously reported (e.g. Grice et al., 2007).

5A molecular sieving of the saturated hydrocarbon fraction

Straight-chain components of the saturated fraction were separated from the branched and cyclic components using 5A molecular sieves following the procedure of Dawson et al. (2005). A portion of the saturated fraction in cyclohexane was added to a 2 mL vial ¾ full of activated 5A molecular sieves. The vial was then capped and placed into a pre-heated aluminium block at 85 ^{o}C overnight. The resulting solution was cooled and filtered through a small column of silica (pre-rinsed with cyclohexane); the sieves were then rinsed thoroughly with cyclohexane and the branched/cyclic fractions were obtained (5A excluded). The branched/cyclic fractions were analysed by GC-MS and GC-irMS.

Gas chromatography - isotope ratio mass spectrometry (GC-irMS)

The δ^{13}C of biomarkers in the saturated and aromatic fractions was measured using CSIA on a Micromass IsoPrime isotope ratio monitoring - mass spectrometer connected to a Hewlett Packard HP6890 gas chromatograph. The column was the same as used for GC-MS analysis. As described by Grice et al. (2008), the fractions were injected in pulsed splitless mode with 30 seconds hold time at 103.4 K Pascals [15 psi] above the head pressure of the column and 35 seconds for purge. The flow rate was 1 mL/min. The GC oven was programmed from an initial temperature of 40 °C for 1 min over a temperature ramp of 3 °C/min to 300 °C and was held for 30 min. The δ^{13}C values of the analysed compounds are reported relative to reference gas pulses of CO_2 of known δ^{13}C composition. An average value of at least two analytical runs with a standard deviation of less than 0.4 ‰ for each compound is reported. An in-house calibration mixture of *n*-alkanes with known isotopic compositions were regularly (after every 2 samples) analysed to confirm accuracy of measured isotopic ratios. The δ^{13}C values are reported in the δ-notation relative to Vienna Pee dee belemnite (VPDB) scale.

δ^{2}H of biomarkers

Stable hydrogen isotope ratios (expressed as δ^{2}H values) of saturated hydrocarbons were analysed using a Micromass IsoPrime isotope ratio mass spectrometer coupled to an Agilent Technologies 6890N gas chromatograph,

utilizing the same GC column as used for $\delta^{13}C$. As described by Nabbefeld et al. (2010a), the GC oven was heated from 50 to 310 °C at 10 °C/min with initial and final hold times of 1 and 10 min, respectively. The $\delta^{2}H$ of samples was measured by integration of the *m/z* 2 and 3 ion currents of the H_2 peaks produced by pyrolysis of the GC-separated compounds using chromium powder catalyst heated at 1050 °C. An interfering species, H^{3+} is formed in the ion source of the mass spectrometer as a result of H^{2+} and H_2 molecule collisions. This creates an isobaric interference with DH, therefore the H^{3+} has to be determined for correction of the measured isotope ratios. The correction on the contributions from H^{3+} produced in the ion source by ion-molecule collisions can be performed by measuring *m/z* 3 of the H_2 reference gas and incorporation of the calculated H^{3+} factor (Dawson et al., 2004). The values of individual compounds are presented relative to that of reference gas pulses obtained from the calculation of H_2. Presented values are the average of three replicate measurements of each sample with a standard deviation of less than 5 ‰ for each compound. An in-house calibration mixture of *n*-alkanes with known isotopic compositions were regularly (after ~8 analyses) analysed to monitor the instrument's performance, precision and accuracy. $\delta^{2}H$ values are given in the δ-notation in per mil (‰) relative to Vienna Standard Mean Ocean Water (VSMOW).

$\delta^{2}H$ of kerogens

The separation of kerogen has been previously described by Holman et al. (2012). In brief, pre-extracted ground samples were decarbonated with HCl (1 M). The calcium ions were washed away with a rinse of deionised water; the decarbonated samples were then placed inside polyethylene centrifuge vials and digested using an ice-cold mixture of concentrated hydrofluoric acid (HF) (48 %) and an equal volume of Milli-Q purified water. To minimize the pressure caused by the exothermic reaction, the vials were placed inside an ice bath and regularly shaken for 2 hrs. The samples were then washed 3 times with Milli-Q water and freeze-dried. Dry samples were first extracted with DCM using an ultrasonication bath for 1 hour, followed by centrifugation and decanting of the supernatant organic phase. This procedure was repeated 3 times, yielding a combined solution of Bitumen II in DCM and a lipid-free kerogen concentrate. The kerogen was air-dried overnight at room temperature. Next, a few drops of purified water were added to the kerogen to

make it moist. Heavy liquid separation was performed using pre-extracted DCM aqueous zinc bromide ($ZnBr_2$) solution to separate the light kerogen from the residual acid-resistant, heavy minerals. After centrifugation, the floating kerogen was separated, washed extensively with slightly acidified water to remove zinc bromide, and freeze dried. **Figure 3.4** shows the experimental procedure that leads to the measurement of δ^2H values of kerogen.

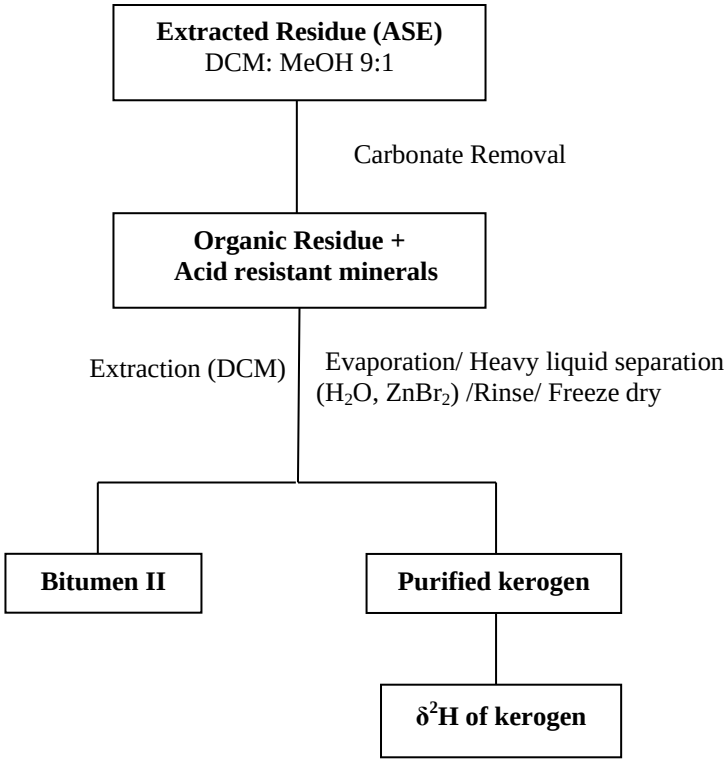

Figure 0.4: Experimental procedure to obtain δ^2H values of kerogen.

Equilibration and measurement of $\delta^2H_{kerogen}$

The quantification of the amount of labile organic hydrogen (i.e. isotopically exchangeable with hydrigen in water) and a correction for its contribution to the δ^2H of kerogen has been performed by hydrogen-isotopic equilibration of kerogen, which aids in controlling the isotopic composition of the exchangeable hydrogen component in kerogen (Schimmelmann et al., 2006).

δ^2H values of kerogens were measured following the technique used by Sauer et al. (2009). According to this method, two aliquots (0.4–0.5 mg) of each sample were weighed into silver capsules. To allow the exchange of water vapour, the silver capsules were perforated at the bottom with pin-holes that were small enough to prevent sample spillage. The prepared capsules were placed in an air-tight aluminium equilibration chamber which contained a carousel for a ZeroBlank Autosampler (Costech Analytical, Valencia, California, USA). After purging the chamber with dry N_2 for several hrs, water vapour of known isotopic composition was passed through the chamber at 115 ^oC at a flow rate of 4 mL/h. All water entering the chamber was immediately vapourised. The samples equilibrated with steam for at least 6 hrs and were then dried in a flow of dry N_2. After cooling the carousel by turning off the oven and flushing with dry N_2, the autosampler carousel was quickly transferred to a He-purged auto sampler that was attached to a pyrolysis elemental analyser (EA) interfaced with a Delta Plus XP isotope ratio mass spectrometer.

The EA operated at 1410 ^oC with a helium flow of 90 mL/min. The pyrolysis products were separated from H_2 (measured through the pyrolysis technique) using a Thermo Finnigan 5A molecular sieve GC column at 70 ^oC. According to Sauer et al. (2009), δ^2H values of samples were calculated by direct comparison with data from isotopically diverse organic reference materials (e.g. polyethylene foil IAEA-CH-7; hexatriacontane and coumarin; http://mypage.iu.edu/~aschimme/hc.html) in the same carousel, thus effectively applying a multi-point isotopic calibration along the VSMOW-SLAP scale. In this method, two aliquots of each kerogen were equilibrated by using two isotopically contrasting water vapours, i.e. hydrogen-depleted water from Saskatoon, Canada (δ^2H_w = − 136 ‰), and hydrogen-enriched water (δ^2H_w = +1173 ‰), which enabled us to use isotopic mass-balances to determine the δ^2H value of non-exchangeable hydrogen and also the fraction of hydrogen in kerogen that is exchangeable (H_{ex}).

Elemental Analysis-isotope ratio Mass Spectrometry (EA-irMS)

$\delta^{13}C_{carbonate}$

$\delta^{13}C_{carbonate}$ values of samples were obtained following the procedure by Nabbefeld et al. (2010b). Carbonate was digested by adding anhydrous phosphoric

acid (H_3PO_4) (100 %) onto the ground sample. The CO_2 produced was separated from water and purified by trapping in two Kiel III Carbonate device cold traps linked to a Finnigan Delta Plus mass spectrometer. To measure the masses of 44, 45 and 46, the second cold trap was warmed up to allow CO_2 to enter the dual-inlet of isotope ratio mass spectrometer. NBS 19 and L-SVEC as carbonate reference materials were run alongside unknown samples to allow 2–point calibration and normalisation to the VPDB scale.

$\delta^{34}S_{pyrite}$

Total reducible inorganic sulfur (TRIS; essentially pyrite) was extracted from the ground sediments using hot acidic chromium (II) chloride solution ($CrCl_2$) as described by Fossing and Jørgensen (1989). The evolved sulfide was quantitatively trapped in Zn acetate solution as ZnS and the concentration was measured spectrophotometrically (Sepcord 40 photometer, Analytic Jena). ZnS was then filtered and converted to Ag_2S through reaction with $AgNO_3$ solution.

The dried Ag_2S was weighed into Sn cups with V_2O_5 (p.a. grade) as a catalyst for stable sulfur isotope analysis (Nabbefeld et al., 2010b). The $^{34}S/^{32}S$ ratios were measured by means of Combustion-isotope ratio mass spectrometry (C-irMS) *via* a Thermo Finnigan MAT 253 mass spectrometer which was coupled to an elemental analyser (Thermo Flash 2000) using a split interface (Thermo Finnigan Conflo IV). International reference materials (IAEA-S–1, –2, –3) and in-house calibration materials were used to relate the measured isotope ratios versus the V-CDT (Vienna Canon Diablo Troilite) scale (Mann et al., 2009). The values are reported in the standard δ-notation.

Results and Discussion

Thermal maturity and kerogen type

Thirty one samples from Senecio–1 well, including the Induan–Olenekian Stage Boundary interval have been analysed in this chapter (2708.12– 2729.37 m). The studied sequence comprises the so-called sapropelic interval and the ‘Limestone Marker’ part of the Hovea Member. **Table 3.1** shows the depth of the samples, Rock-

Eval pyrolysis data and pristane/phytane (Pr/Ph) ratios. The samples have TOC values ranging from 0.13 to 2.48 wt. %, hydrogen indices (HI) ranging from 25 to 254 mg HC/g TOC, Production Index (PI) from 0.06 to 0.39, and T_{max} values varying between 417 and 442 °C (average 436 ± 5 ^{o}C).

Depth (ave.) (m)	TOC (wt. %)	T_{max} (^{o}C)	HI (mg/g)	OI (mg/g)	PI	Pr/Ph
2708.12	0.32	436	78	41	0.07	1.26
2708.42	0.35	442	172	10	0.07	1.57
2708.86	0.62	438	143	11	0.09	1.77
2709.85	0.24	435	61	34	0.08	0.34
2710.86	0.13	440	151	97	0.18	0.94
2711.94	0.32	440	130	47	0.06	1.11
2712.90	0.28	437	116	53	0.08	0.95
2713.40	0.26	441	149	17	0.08	0.42
2713.83	0.33	417	145	17	0.07	0.91
2714.89	0.31	436	68	96	0.09	0.89
2715.36	0.28	442	96	25	0.12	1.53
2715.86	0.47	441	82	51	0.11	0.42
2716.83	0.39	435	60	30	0.12	0.25
2717.61	0.23	440	104	28	0.09	0.74
2717.91	0.69	440	91	13	0.10	0.96
2718.94	0.40	438	52	33	0.12	0.55
2719.15	0.25	440	60	21	0.10	0.71
2719.37	0.17	440	63	26	0.11	0.54
2719.87	0.13	437	25	112	0.12	0.57
2720.88	0.37	434	47	28	0.14	1.63
2721.95	1.42	436	164	8	0.18	2.03
2722.92	1.02	434	149	13	0.21	1.58
2723.86	0.90	435	176	12	0.17	1.26
2724.89	1.57	428	94	8	0.33	1.21
2725.89	0.91	434	146	8	0.18	1.14
2726.90	1.62	434	101	8	0.23	1.15
2727.35	0.87	441	181	8	0.39	1.05
2727.87	2.24	430	121	13	0.26	1.02
2728.87	1.34	431	109	11	0.25	1.06
2729.14	2.48	429	132	13	0.21	1.01
2729.37	2.10	440	254	3	0.16	1.03

Table 0.1: Rock-Eval, TOC and Pr/Ph values for the Senecio-1 well samples for the stratigraphic depth (m).

Rock- Eval pyrolysis and TOC analysis suggest that the Senecio–1 sequence is within the early oil window (average calculated vitrinite reflectance 0.69 % using the T_{max}-R_o correlation of Jarvie et al., 2001). Rock-Eval pyrolysis data indicate that the samples contain two slightly different organo-facies types, mainly Type III kerogen

with some contribution from Type II kerogen. **Figure 3.5** shows the trends of TOC, HI and the Pr/Ph values over the stratigraphic depth.

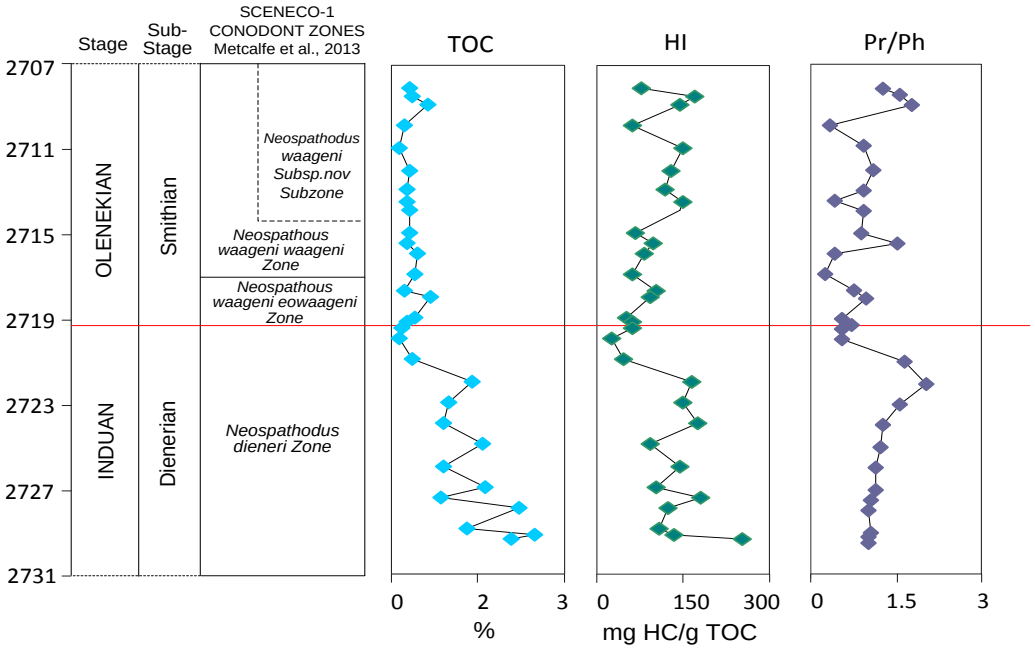

Figure 0.5: Stratigraphic trends of total organic carbon (TOC), hydrogen index (HI) and pristane/phytane ratios (Pr/Ph) for the Induan–Olenekian Boundary from Senecio–1 core, Perth Basin, Western Australia.

The Limestone Marker (**Figure 3.2 A**) shows very low TOC % and based on previous work of Metcalfe et al. (2013) supports highly oxygenated and (likely) reworked OM, the values of HI also support highly degraded OM. The equivalent sapropelic interval to the Hovea member has TOC % ranging from 0.9 to 2.48 and is a Type II-III kerogen likely deposited under relatively more reducing conditions. The HI values are consistent with TOC results, presenting a decrease from 254 mg HC/g TOC at 2729.37 m to a minimum of 94 mg HC/g TOC at 2724.89 m. As shown in **Figure 3.5**, the equivalent sapropelic interval of the core to the Hovea Member (below 2721.70 m) consists mostly of kerogen type III with the deepest sample the more hydrogen-rich type II-III, following is an inertinitic interval across the Induan–Olenekian Boundary (2720.88– 2718.94 m) containing type IV kerogen, then a gradual improvement in kerogen quality up the core to type III kerogen. The isoprenoids, Pr (**I**) and Ph (**II**) are mainly resulted from chlorophyll *a* (**III**) in phototrophic organisms (Peters et al., 2005).

The Pr/Ph ratio is a paleoredox indicator (Koopmans et al., 1999; Rontani and Bonin, 2011) by oxidation or reduction of the phytol side chain of chlorophyll *a* depending on the paleoredox and salinity conditions (Rontani and Bonin, 2011). Anoxic conditions are usually indicated by low values of Pr/Ph ratio. However, the Pr and Ph can be derived from different sources including archaea (Nabbefeld et al., 2010a) and Pr may be produced through thermal maturation from chromans or tocopherols (Peters et al., 2005), therefore difference in the sources and thermal maturity of OM can influence the paleoredox proxy (Peters et al., 2005). The Pr/Ph ratio decreases from 2.03 at 2721.95 m below the boundary to a minimum value of around 0.54 at 2719.37 m close to the boundary, followed by an increase to 1.53 at 2715.36 m above the boundary in the Olenekian section, indicating a change from sub-oxic to anoxic conditions near the end of Induan and a return to more sub-oxic conditions in the upper part of the Olenekian.

Significance of stable isotopic data across the Induan–Olenekian Stage Boundary

Bulk $\delta^{13}C_{OM}$ and $\delta^{13}C_{carbonate}$

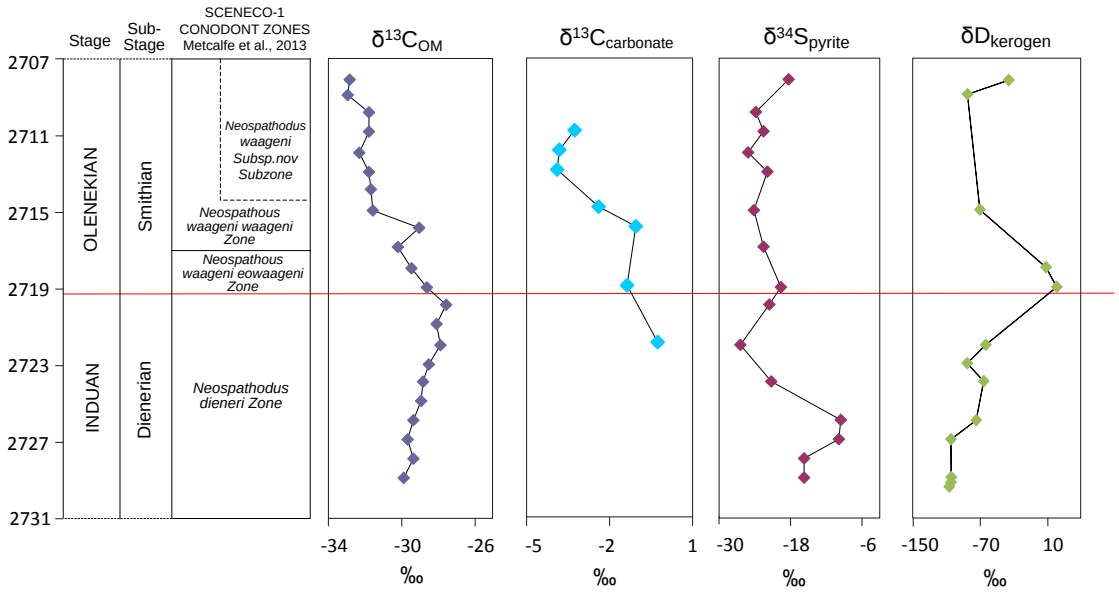

Figure 0.6: Stable isotope values (‰) for $\delta^{13}C_{OM}$, $\delta^{13}C_{carbonate}$, $\delta^{34}S_{pyrite}$ and $\delta^{2}H_{kerogen}$ for the Induan–Olenekian Boundary in Senecio–1 core, Perth Basin, Western Australia.

As shown in **Figure 3.6**, values of $\delta^{13}C_{OM}$ steadily rise from –30 to –27 ‰ in the upper Induan, but the trend abruptly reverses in the early Olenekian, where

values decrease from –27.5 to –32.9 ‰. The positive excursion of ca. 4 ‰ compares globally with the Induan–Olenekian Stage Boundary sections recorded in archives in India, China and Spiti (Galfetti et al., 2007; Metcalfe et al., 2013). $\delta^{13}C_{carbonate}$ values show a similar trend to the $\delta^{13}C_{OM}$ for the Senecio–1 core studied section (2710.86–2721.95 m). The values of $\delta^{13}C_{carbonate}$ for a few limited samples vary between –0.3 and –1.3 ‰ below the boundary (i.e. a –1 ‰ shift). A negative spike of 2.9 ‰ from –1.0 ‰ to –3.9 ‰ occurs above the Induan–Olenekian Boundary coinciding with the negative shift of $\delta^{13}C_{OM}$ in the early Olenekian. **Figure 3.7** shows an excellent correlation ($R^2 = 0.93$) for $\delta^{13}C_{OM}$ plotted against $\delta^{13}C_{carbonate}$ (corresponding to deep to shallower depths), suggesting the same source for negative shifts in isotopic values of OM and carbonate. The analytical experiments have been performed once on the samples to obtain $\delta^{13}C$ values of carbonate and OM, therefore no error bars have been produced on data points in **Figure 3.7**.

The change to more negative values of $\delta^{13}C_{OM}$ (up to 5.4 ‰) and $\delta^{13}C_{carbonate}$ (up to 3.6 ‰) in the Olenekian section of the core can be explained by the decomposition of methane hydrates that released ^{13}C-depleted carbon into the atmosphere (Chen and Benton, 2012; Xie et al., 2007). Other factors including diagenesis and changes in OM source as a result of biotic crisis, sea level rise or a combination of both can also affect the isotopic shift in $\delta^{13}C_{OM}$ (Foster et al., 1997).

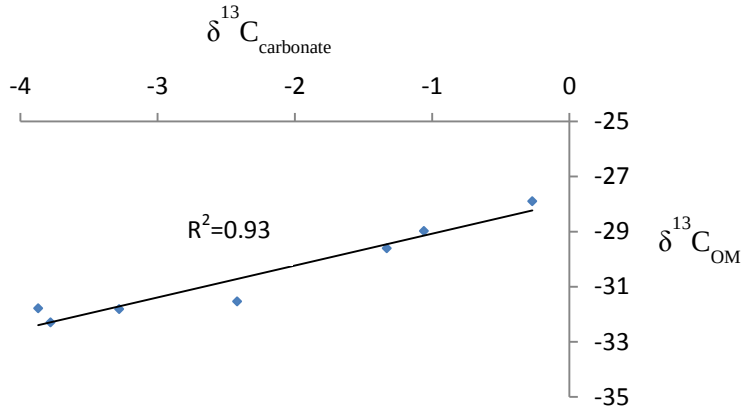

Figure 0.7: Isotopic results of $\delta^{13}C_{OM}$ ‰ versus $\delta^{13}C_{carbonate}$ ‰.

Bulk $\delta^{34}S_{pyrite}$

The transition of the upper Permian to the early Triassic was globally characterised by a shift in the isotopic composition of seawater sulfate increasing gradually from relatively light towards much heavier sulfur isotope data (e.g. Claypool et al., 1980; Korte et al., 2004; Newton et al., 2004; Fenton et al., 2007; Nabbefeld et al., 2010a; Nabbefeld et al., 2010b; Takahashi et al., 2013). Compared to the sulfur isotope composition of sulfate, the buried pyrite is typically depleted in the heavier isotopes. The strong ^{34}S depletion suggests that isotope fractionation accompanying elemental sulfur disproportionation causes the ^{34}S depletion of sedimentary sulphides (e.g., Habitch and Canfield, 1997).

In the investigated samples, the $\delta^{34}S$ values of pyrite vary between –9.3 and –26.4 ‰ below the boundary in the Late Induan following enrichment up to –19.6 ‰ at 2718.94 m across the Induan–Olenekian Stage Boundary showing a positive shift of about 7 ‰ (**Figure 3.6**). There is a gradual negative excursion of about 4 ‰ above the boundary in the early Olenekian, from –19.6 to –23.8 ‰, coinciding with shifts in $\delta^{13}C_{OM}$ and $\delta^{13}C_{carbonate}$. The light sulfur isotopic composition of pyrite may indicate pyrite formation without pronounced impact by sulfate limitation. The observed results are comparable to those in sediments of modern brackish euxinic basins of the Baltic Sea (Böttcher and Lepland, 2000) but less enriched in the light isotope when compared, for instance, to the Holocene Black Sea (e.g. Fry et al., 1991; Neretin et al., 2001). However, these light sulfur isotope values do not indicate that the water column was euxinic (Raiswell, 1997).

Considering an isotopic range for early Triassic seawater sulfate between about +20 and +30 ‰ vs. Vienna Canon Diablo Troilite (VCDT) and assuming sulfate reduction to occur under essentially open system conditions (Hartmann and Nielsen, 2012), the overall isotope enrichment factors between ca. –29 and –56 ‰ are estimated from the data in **Figure 3.6**, in the upper range of or even exceeding the experimental results obtained with pure cultures metabolizing more simple organic substrates at relatively low cellular rates (Sim et al., 2011). Assuming a constant seawater composition during the investigated time interval, the overall magnitude of sulfur isotope discrimination increased from the Induan to the Olenekian (**Figure 3.6**). The distinct variations in isotope discrimination can be due to changes in the

burial efficiency associated with changes in the availability of reactive OM , the organic substrate composition available for metabolism (Sim et al., 2011), or during times of euxinic conditions, changing contributions from processes at the chemocline (Canfield and Thamdrup, 1994). The rapid decrease of sulfur isotope values at the end of the sapropelic interval may reflect increase in sulfate availability due to more oxygenated conditions.

The possibly enhanced impact of methane as deduced from shifts in the carbon isotope signatures (see **Figure 3.7**) may also have had an influence on the sulfur cycle. However, since sulfur isotope fractionation during anaerobic oxidation of methane on a cellular base does not differ from OM oxidation (Böttcher et al., 2006), we do not expect methane to significantly change the development of sulfur isotope signatures. Other factors that may have led to changes in the emergent sulfur isotope signals were quality of OM which can affect sulphur isotope discrimination (Grice et al., 2005a), the overturn of stagnant euxinic deep oceans (Kajiwara et al., 1994; Knoll et al., 1996) or H_2S outgassing from the deep ocean produced by climate warming (Maruoka et al., 2003; Kidder and Worsley, 2004).

δ^2H of kerogen

δ^2H of kerogen can provide information about ancient precursor biomass and the paleoenvironment of biosynthesis, as well as influences during diagenesis (Krishnamurthy et al., 1995; Hassan and Spalding, 2001; Schimmelmann et al., 2004, 2006; Lis et al., 2006). $\delta^2H_{kerogen}$ values vary from –105 ‰ at 2729.3 m to –58 ‰ at 2721.95 m in the so-called sapropelic interval of the core (i.e. a positive shift of 47 ‰), following positive value of +31 and +18 ‰ at 2718.94 and 2717.91 m respectively in the Hovea member equivalent inertinitic section of the core coinciding with shift in $\delta^{13}C_{carbonate}$ and $\delta^{13}C_{OM}$. The high δ^2H values for kerogen can be related to the high sulfur contents in this part of the core (Sauer, personal communication). $\delta^2H_{kerogen}$ returns to more negative values in the upper part of the section **(Figure 3.6)**.

The changes in $\delta^2H_{kerogen}$ values can be explained by various possibilities, including the biochemical character of the original biomass, preservation characteristics of biomass, kerogen type (changing maceral composition), and the influence of thermal maturity and associated transfer of hydrogen between water and

OM (Nabbefeld et al., 2010b). The transfer of hydrogen from water to OM throughout the breaking of carbon-carbon bonds is the main mechanism that causes an increase in the δ^2H of organic hydrogen (Schimmelmann et al., 2006).

Thermal maturity and kerogen type are thought to be the most likely reasons for the observed changes, since thermal maturation progressively changes the bulk isotopic composition of non-exchangeable hydrogen in kerogen as a result of methane release, cracking reactions and aromatisation effects (Hassan and Spalding, 2001; Schimmelmann et al., 2006; Nabbefeld et al., 2010b). Differences in kerogen types can also affect the $\delta^2H_{kerogen}$ values due to significant variation of fractionation between water and biomass (Schimmelmann et al., 2006; Nabbefeld et al., 2010). However, in this study the Senecio–1 core samples above and below the boundary have essentially the same thermal maturity, so the argument of maturity-related changes cannot be used to interpret changes across the boundary. Maturation can only produce an overall background shift, whereas the isotopic perturbations over short depth intervals must be due to original differences in sedimentary OM.

The degree of fractionation between water and biomass can vary significantly as a result of different environmental conditions and biochemical pathways of the original precursor material of the kerogens which causes different values for $\delta^2H_{kerogen}$ (Schimmelmann et al., 2006). Therefore, differences in kerogen types as observed for Senecio-1 well samples can influence the $\delta^2H_{kerogen}$. The $\delta^2H_{kerogen}$ excursions in the Senecio–1 core coincide with facies changes from Type II-III in the late Induan to inertinitic kerogen across the Induan–Olenekian Boundary and a return to Type III in the upper Olenekian, above the boundary (**Figure 3.6**). The samples containing Type II-III kerogen show relatively depleted $\delta^2H_{kerogen}$ values compared to Type III kerogens. Type III kerogens originate mainly from lignin and cellulose-rich biomass of terrestrial plants, where the carbon-bound hydrogen is relatively hydrogen-enriched, however lipidic OM which partly builds up the marine kerogen Type II-III, is relatively hydrogen-depleted (Schimmelmann et al., 2006). The shifts in $\delta^2H_{kerogen}$ mainly reflect changes in source and preservation of OM. Variations in the isotopic signature of the original precursor biomass for kerogen were caused by general biological responses to changing paleoecological conditions (Nabbefeld et al., 2010b).

$\delta^{13}C$ and $\delta^{2}H$ of selected biomarkers

As displayed in **Figure 3.8**, the $\delta^{13}C$ and $\delta^{2}H$ of selected *n*-alkanes (C_{17}, C_{19}, C_{27} and C_{29}) throughout the studied section were measured. $\delta^{13}C$ values of Pr and Ph were determined for a few samples, due to the relative low abundances of these compounds. As the interpretation of bulk analyses is restricted to a single value representing the average isotopic composition of the whole sample, therefore CSIA of biomarkers is employed in combination with $\delta^{13}C_{OM}$ and $\delta^{13}C_{carbonate}$ for a better understanding of the probable causes of isotope shifts and to examine the isotopic composition of paleoatmospheric and paleooceanic CO_2. (Nabbefeld et al., 2010a; Grice et al., 2005b; Fenton et al., 2007). These *n*-alkanes originate from different biological sources, e.g. *n*-C_{17} - *n*-C_{19} from algae (Gelpi et al., 1970) and *n*-C_{27} - *n*-C_{29} alkanes derived from plant waxes (Eglinton and Hamilton, 1967). $\delta^{13}C$ values of the *n*-alkanes displays the same shift for the leaf wax-derived *n*-alkanes (C_{27} and C_{29}) as for the algal-derived *n*-alkanes (C_{17} and C_{19}), therefore proposing a source-independent signal and synchronous changes in both atmospheric and oceanic CO_2.

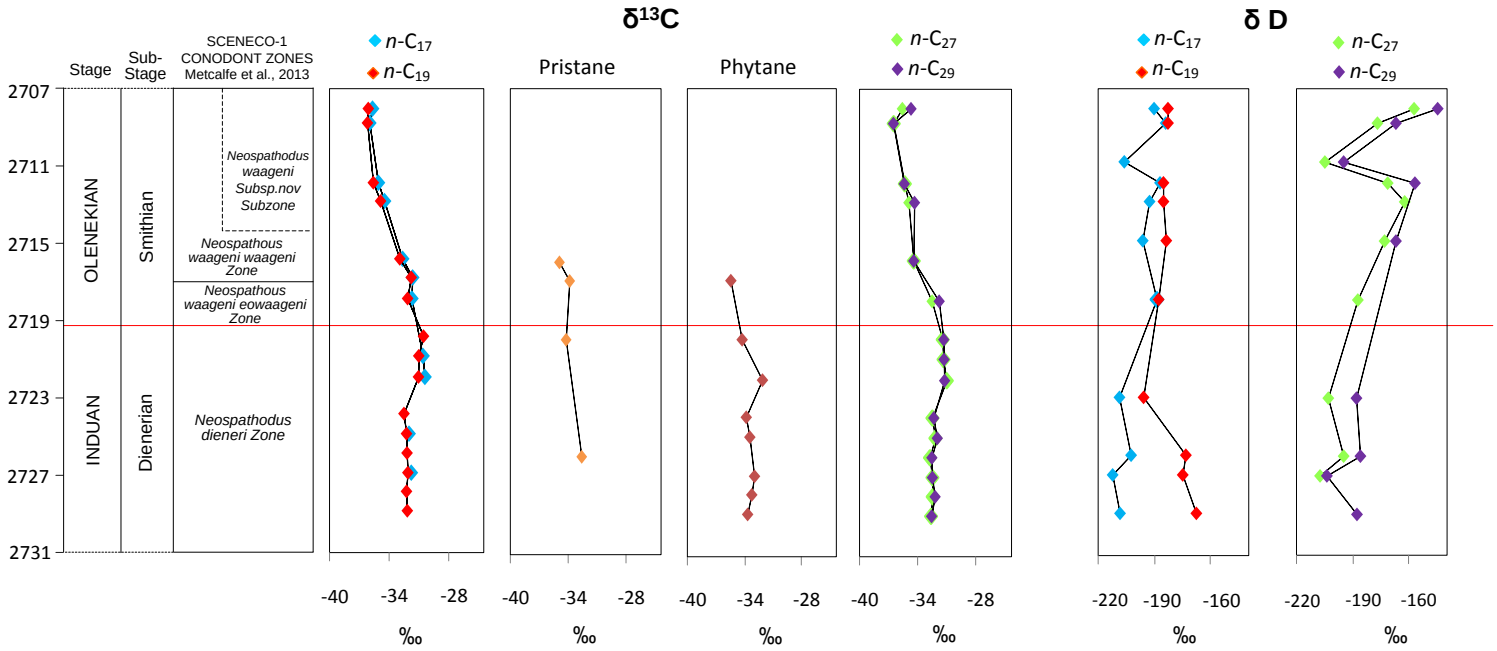

Figure 0.8: $\delta^{13}C$ and $\delta^{2}H$ in ‰ of selected biomarkers (Pr, Ph, C_{17}-C_{29} *n*-alkanes) against depth (m).

$\delta^{13}C$ of *n*-alkanes follow a similar trend to the measured isoprenoids. Overall the $\delta^{13}C$ values for the *n*-alkanes show a general trend towards a positive excursion in the Induan section from –32.0 ‰ at 2728.87 m to –30.4 ‰ at 2719.87 m near to the boundary, then become more ^{13}C-depleted (–36.2 ‰ at 2708.86 m) in the Olenekian section. The negative isotopic trend in the Olenekian is also consistent with the shifts observed for $\delta^{13}C_{OM}$ and $\delta^{13}C_{carbonate}$ with a ^{13}C-depleted carbon source from the melting of methane clathrates.

$\delta^{2}H$ of biomarkers gives information for changes occurring in the ancient water cycle, including paleosalinity and paleotemperature (Anderson et al., 2001; Sauer et al., 2001). Variations in $\delta^{2}H$ of biomarkers could signify a change in the source of OM, microbial diversification, thermal maturity and sea level rise reflecting less saline conditions during the Triassic (Dawson et al., 2004). The average $\delta^{2}H$ of the leaf wax-derived *n*-alkanes (C_{27} and C_{29}) is less negative than the algal-derived *n*-alkanes (C_{17} and C_{19}), indicating the plants are probably taking in heavy water (D_2O) due to evapotranspiration effect which is the evaporative loss of the light isotopic species of water on leaf surfaces, causing an enrichment of $\delta^{2}H$ values and the heat stress imposed; however, this is different for the algal markers that have lipid $\delta^{2}H$ values which are related to the $\delta^{2}H$ of their growth water (Anderson et al., 2001). As suggested by Zhang et al. (2009) significant changes in $\delta^{2}H$ of biomarkers can be explained by the fractionation of hydrogen within organisms which is controlled by the biosynthesis of NADPH. The $\delta^{2}H$ profiles of *n*-alkanes (C_{17}, C_{19}, C_{27} and C_{29}) throughout the studied section show a general trend towards more enriched values of $\delta^{2}H$ after the Induan–Olenekian Boundary, which is consistent with the hothouse conditions existing for this part of the section.

$\delta^{13}C$ of aromatic isomers: OM provenance

Alkylated aromatic hydrocarbons are regular constituents of sedimentary OM and their variations in the molecular distributions are of great interest in the field of organic geochemistry as indicators of source, thermal history, facies type and paleoenvironments of source rocks (Alexander et al., 1985; Maslen et al., 2011). Aromatic compounds are primarily formed by geosynthetic processes which result in a host of isomerised, alkylated and dealkylated components (Alexander et al., 1985).

$\delta^{13}C$ values of the individual aromatic compounds are possibly controlled by their source, relative thermal maturity and age of their source rock (Maslen et al., 2011). In this study $\delta^{13}C$ values for various sub-classes of aromatic fractions such as Naphthalene (N), Methyl-naphthalenes (MNs), Dimethyl-naphthalenes (DMNs), Trimethyl-naphthalenes (TMNs), Phenanthrene (P), Methyl-phenanthrenes (MPs), Dimethyl-phenanthrenes (DMPs) and for several isomers of the aromatic fraction such as 2-MN (**IV**) 1,6-DMN (**V**), 1,2,5-TMN (**VI**), 1-MP (**VII**), 1,9-DMP(**VIII**), benzo(*e*)pyrene (**IX**) and benzo(*a*)anthracene (**X**) were determined (**Figure 3.9)**.

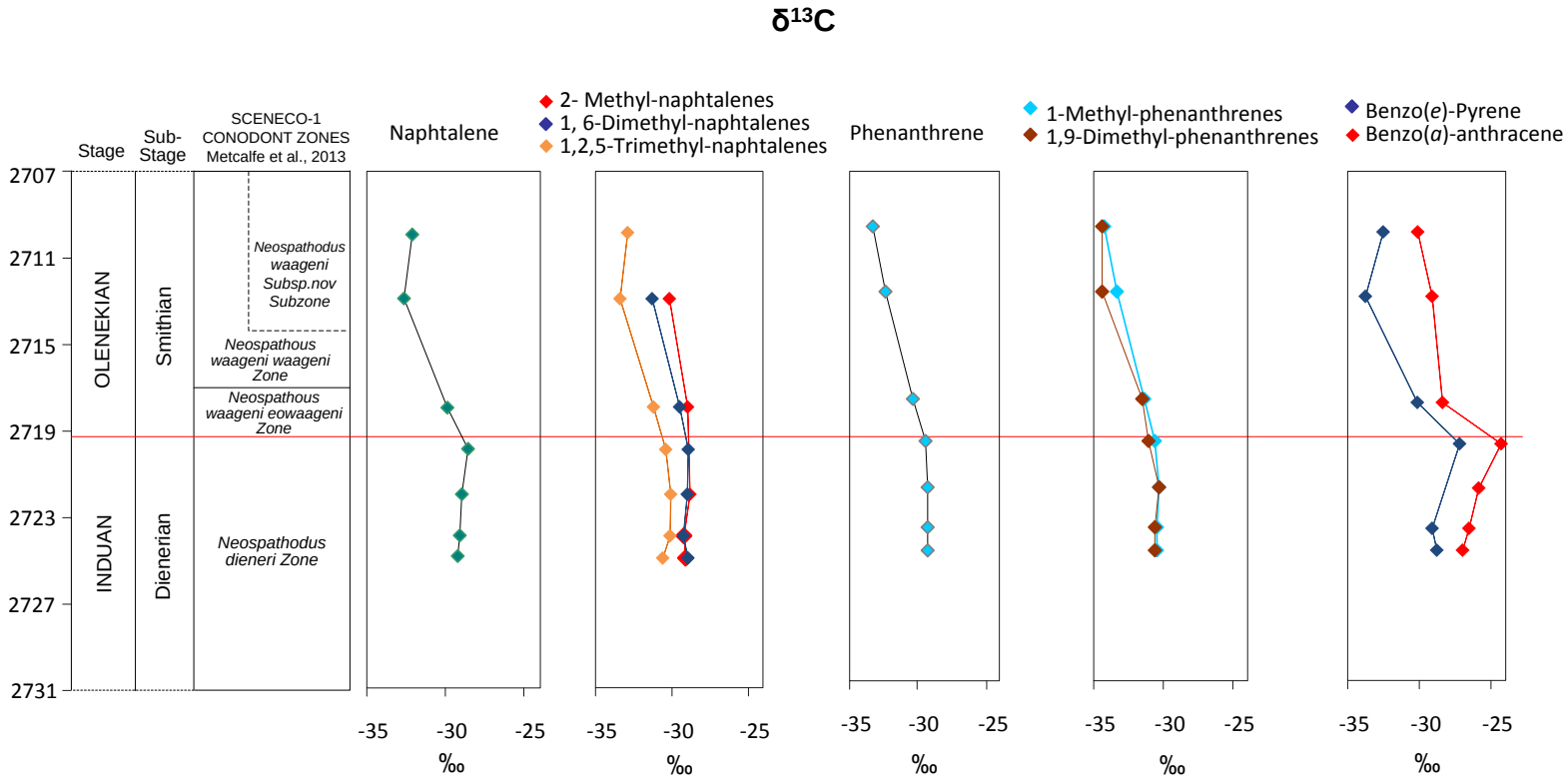

Figure 0.9: $\delta^{13}C$ in ‰ of selected aromatic fractions (N, MN, DMN, TMN, P, MP, DMP, benzo*(e)*pyrene and benzo*(a)*anthracene) against depth (m).

$\delta^{13}C$ values of the individual aromatic compounds in the Senecio–1 core show a similar trend with less negative isotopic values in the lower part of the section (Induan) shifting to more negative values above the boundary in the Olenekian section of the core. $\delta^{13}C$ values range from around –29 ‰ in the Induan section to –34 ‰ in the Olenekian section (**Figure 3.9**). There is also an overall depletion in $\delta^{13}C$ of the aromatic compounds with the degree of methylation and also rising numbers of aromatic rings (Maslen et al., 2011). The $\delta^{13}C$ depletion of Alkyl-phenanthrenes (APs) within their sub-groups are evaluated to Alkyl-naphthalenes (ANs) which show a more obvious depletion with increasing methylation and rising number of rings compared to ANs (**Figure 3.9**). The 1,6-DMN is an aromatization product of a number of natural product precursors (Maslen et al., 2011; Alexander et al., 1992; Püttmann and Villar, 1987) and is thought to be from OM of higher plants (Alexander et al., 1992). In general, less negative $\delta^{13}C$ values of OM suggest a greater contribution of terrestrial plant material to the marine biomass as a result of the pre-Miocene having ^{13}C-enriched terrestrial OM relative to marine OM (Popp et al., 1998).

1,2,5-TMN is assumed to be derived from the degradation of D-ring monoaromatic 8,14-secohopanoids (XI) (Puttmann and Villar, 1987), suggesting a microbial origin (Maslen et al., 2011; Puttmann and Villar, 1987). As suggested by Radke et al. (1998) $\delta^{13}C$ of P and MPs reflects OM type (Maslen et al., 2011). In **Figure 3.9**, $\delta^{13}C$ values of 1-MP and 1, 9-DMP in the studied section of the Senecio–1 core vary from –29 ‰ to –33 ‰ and –30 ‰ to –34 ‰, respectively. $\delta^{13}C$ values of 1-MP and 1,9-DMP are less negative in the Induan section of the core, possibly revealing the varying inputs of terrigenous OM to the sediments. Marine derived OM sediments are more depleted in ^{13}C compared with terrigenous derived OM (Radke et al., 1998), therefore more negative $\delta^{13}C$ values above the boundary in the Olenekian section reflect a marine source.

Conclusions

The Senecio–1 core is located in the northern onshore Perth Basin and spans the Induan–Olenekian Stage Boundary in the central part of the Lower Triassic (Metcalfe et al., 2013). Pr/Ph ratio indicate a change from sub-oxic to anoxic conditions near the end of Induan and a return to more sub-oxic conditions in the upper part of the Olenekian. Coincident negative shifts of $\delta^{13}C_{OM}$ and $\delta^{13}C_{Carbonate}$ in the Olenekian section of the core is consistent with a ^{13}C-depleted carbon source from the melting of methane clathrates due to hothouse conditions related to volcanic activity in Siberia that happened around the same time. A shift in $\delta^{34}S$ values across the boundary, coincide with the shifts in $\delta^{13}C_{OM}$ and $\delta^{13}C_{carbonate}$. The differences in $\delta^{34}S$ values can also be due to the effect of methane as reasoned for the shifts in the carbon isotope signatures and influence the sulfur cycle. The negative isotopic trend recorded in the $\delta^{13}C$ values of the *n*-alkanes in the Olenekian is also consistent with the shifts observed for $\delta^{13}C_{OM}$ and $\delta^{13}C_{carbonate}$ with a ^{13}C-depleted carbon source from the melting of methane clathrates. Selected aromatic compounds in the studied core show a similar trend to $\delta^{13}C$ values for the *n*-alkanes with less negative isotopic values in the Induan shifting to more negative values above the boundary, in the Olenekian section of the core. The $\delta^{2}H_{kerogen}$ coincides with a change from Type II-III kerogen in the late Induan to Type III kerogen at the Olenekian, above the boundary. The shifts in $\delta^{2}H_{kerogen}$ mainly reflect changes in source and preservation of OM.

Acknowledgements

The authors thank Geoff Chidlow and Stephen Clayton for providing GC-MS and GC-irMS technical support. Mojgan Ladjavardi thanks Curtin University, Geoscience Australia and GFZ Potsdam for international Postgraduate Award scholarship and Australia-China LNG project for a PhD top-up scholarship. Kliti Grice acknowledges ARC for QEII Fellowship and John de Laeter Centre for ARC LIEFP support. Ian Metcalfe acknowledges the ARC for Discovery Grant number DP109288. Michael E. Böttcher wishes to thank P. Escher and I. Scherff, for analytical support.

References

Alexander, R., Kagi, R.I., Rowland, S.J., Sheppard, P.N., Chirila, T.V., 1985. The effects of thermal maturity on distributions of dimethylnaphtalenes and trimethylnaphtalenes in some ancient sediments and petroleums. *Geochimica et Cosmochimica Acta*, 49, 385–395.

Alexander, R., Larcher, A.V., Kagi, R.I., 1992. An oil-source correlation study using age specific plant-derived aromatic biomarkers. In Biological Markers in Sediments and Petroleum (Eds. J.M.P. Moldowan, P. Albrecht and R.P. Philps). Prentice Hall, Englewood Cliffs 201−221.

Algeo, T.J., 2011. The early Triassic cesspool: Marine conditions following the end-Permian mass extinction. In: Håkansson, E., Trotter, J. (Eds), Programme and Abstracts, the XVII International Congress on the Carboniferous and Permian, Perth 3–8 July 2011: *Geological Survey of Western Australia*, Record 2011/20, 38.

Alroy, J., Aberhan, M., Bottjer, D.J., Foote, M., Fürsich, F.T., Harries, P.J., Hendy, A.J.W., Holland, S.M., Ivany, L.C., Kiessling, W., Kosnik, M.A., Marshall, C.R., McGowan, A.J., Miller, A.I., Olszewski, T.D., Patzkowsky, M.E., Peters, S.E., Villier, L., Wagner, P.J., Bonuso, N., Borkow, P.S., Brenneis, B., Clapham, M.E., Fall, L.M., Ferguson, C.A., Hanson, V.L., Krug, A.Z., Layou, K.M., Leckey, E.H., Nürnberg, S., Powers, C.M., Sessa, J.A., Simpson, C., Tomašových, A., Visaggi, C.C., 2008. Phanerozoic trends in the global diversity of marine invertebrates. *Science* 321, 97–100.

Andersen, N., Paul, H.A., Bernasconi, S.M., McKenzie, J.A., Behrens, A., Schaeffer, P., Albrecht, P., 2001. Large and rapid climate variability during the Messinian salinity crisis: Evidence from deuterium concentrations of individual biomarkers. *Geology* 29, 799–802.

Benton, M.J., Twitchett, R.J., 2003. How to kill (almost) all life: the end-Permian extinction event. *Trends Ecology and Evolution* 18, 358–365.

Benton, M.J., Newell, A. J., 2013. Impacts of global warming on Permo–Triassic terrestrial ecosystems, *Gondwana Research* 25, 1308–1337.

Bond, D.P.G., Wignall, P.B., 2010. Pyrite framboid study of marine Permian–Triassic Boundary sections: A complex anoxic event and its relationship to contemporaneous mass extinction. *Geological Society of America Bulletin* 122, 1265–1279.

Boreham, C.J., Hope, J.M., Hartung-Kagi, B., 2001. Understanding source, distribution and preservation of Australian natural gas: a geochemical perspective. *Australian Petroleum production and Exploration Association Journal* 41, 523–547.

Böttcher, M.E., Lepland, A., 2000. Biogeochemistry of sulfur in a sediment core from the west-central Baltic Sea: Evidence from stable isotopes and pyrite textures. *Journal of Marine Systems* 25, 299–312.

Böttcher, M.E., Boetius, A., Rickert, D., 2006. Sulfur isotope fractionation during microbial sulfate reduction associated with anaerobic methane oxidation. *Geophysical Research Abstracts* 8, 10040.

Canfield, D. E., Thamdrup, B., 1994. The production of ^{34}S-depleted sulfide during bacterial disproportionation of elemental sulfur. *Science* 266, 1973–1975.

Chen, Z.Q., Benton, M. J., 2012. The timing and pattern of biotic recovery following the end-Permian mass extinction. *Nature Geoscience* 5, 375–383.

Clarkson, M.O., Richoz, S., Wood, R.A., Maurer, F., Krystyn, L., McGurty, D.J., Astratti, D., 2013. A new high-resolution δ^{13}C record for the Early Triassic: Insights from the Arabian Platform. *Gondwana Research* 24, 233–242.

Claypool, G.E., Hosler, W.T., Kaplan, I.R., Sakai, H., Zak, I., 1980. The age curves of sulfur and oxygen isotopes in marine sulfate and their mutual interpretation. *Chemical Geology* 28, 199–260.

Coplen, T.B., 2011. Guidelines and recommended terms for expression of stable-isotope-ratio and gas-ratio measurement results. *Rapid Communications in Mass Spectrometry* 25, 2538–2560.

Dawson, D., Grice, K., Wang, S.X., Alexander, R., Radke, J., 2004. Stable hydrogen isotopic composition of hydrocarbons in torbanites (Late Carboniferous to late Permian) deposited under various climatic conditions. *Organic Geochemistry* 35, 189–197.

Dawson, D., Grice, K., Alexander, R., 2005. Effect of maturation on the indigenous delta D signatures of individual hydrocarbons in sediments and crude oils from the Perth Basin (Western Australia). *Organic Geochemistry* 36, 95–104.

Eglinton, G., Hamilton, R.J., 1967. Leaf Epicuticular Waxes. *Science* 156, 1322–1334.

Erwin, D.H., 1993. The Great Paleozoic Crisis. Columbia Univ. Press, New York.

Fenton, S., Grice, K., Twitchett, R.J., Böttcher, M.E., Looy, C.V., Nabbefeld, B., 2007. Changes in biomarker abundances and sulfur isotopes of pyrite across the Permian–Triassic (P/Tr) Schuchert Dal section (East Greenland). *Earth and Planetary Science Letters* 262, 230–239.

Fossing, H., Jørgensen, B.B., 1989. Measurement of bacterial sulfate reduction in sediments: evaluation of a single-step chromium reduction method. *Biogeochemistry* 8, 205–222

Foster, C.B, Logan, A., Summons, R.E, Gorter, J.D., Edwards, D.S., 1997. Carbon isotopes, kerogen types and the Permian–Triassic Boundary in Australia: implications for exploration. *Australian Petroleum Production and Exploration Association* 37, 472–789.

Fry, B., Jannasch, H.W., Molyneaux, S.J., Wirsen, C.O., Muramoto, J.A., King, S., 1991. Stable isotope studies of the carbon, nitrogen and sulfur cycles in the Black Sea and the Cariaco Trench. *Deep Sea Research* 38, 1003–1019.

Galfetti, T., Bucher, H., Brayard, A., Hochuli, P.A., Weissert, H., Guodun, K., Atudorei, V., Guex, J., 2007. Late Early Triassic climate change: insights from carbonate carbon isotopes, sedimentary evolution and ammonoid

paleobiogeography. *Paleogeography, Paleoclimatology, Paleoecology* 243, 394–411.

Gelpi, V., Schneider, H., Mann, J., Oro, J., 1970. Hydrocarbons of geochemical significance in microscopic algae. *Phytochemistry* 9, 603–612.

Grice, K., Cao, C.Q., Love, G.D., Böttcher, M.E., Twitchett, R.J., Grosjean, E., Summons, R.E., Turgeon, S.C., Dunning, W., Jin, Y.G., 2005a. Photic zone euxinia during the Permian–Triassic superanoxic event. *Science* 307, 706–709.

Grice, K., Summons, R.E., Grosjean, E., Twitchett, R.J., Dunning, W., Wang, S.X., Böttcher, M.E., 2005b. Depositional conditions of the northern onshore Perth Basin (Basal Triassic). *Australian Petroleum Production Exploration Journal* 45, 263–274.

Grice, K., Nabbefeld, B., Maslen, E., 2007. Source and significance of selected polycyclic aromatic hydrocarbons in sediments (Hovea–3 well, Perth Basin, Western Australia) spanning the Permian–Triassic Boundary. *Organic Geochemistry* 38, 1795–1803.

Grice, K., de Mesmay, R., Glucina, A., Wang, S., 2008. An improved and rapid 5A molecular sieve method for gas chromatography isotope ratio mass spectrometry of *n*-alkanes (C8-C30+). *Organic Geochemistry* 39, 284–288.

Habitch, K.S., Canfield, D.E., 1997. Sulfur isotope fractionation during bacterial sulfate reduction in organic-rich sediments. *Geochimica et Cosmochimica Acta* 61, 5351–5361.

Hartmann, M., Nielsen, H., 2012. $\delta^{34}S$ values in recent sea sediments and their significance using several sediment profiles from the western Baltic Sea. *Isotopes in Environmental and Health Studies* 48, 7–32.

Hassan, K.M., Spalding, R.F., 2001. Hydrogen isotope values in lacustrine kerogen. *Chemical Geology* 175, 713–721.

Holman, A.I., Grice, K., Jaraula, C.M.B., Schimmelmann, A., Brocks, J.J., 2012. Efficiency of extraction of polycyclic aromatic hydrocarbons from the Paleoproterozoic Here's Your Chance Pb/Zn/Ag ore deposit and implications for a study of Bitumen II. *Organic Geochemistry* 52, 81–87.

Jarvie, D.M., Claxton, B.L., Henk, F., Breyer, J.T., 2001. Oil and shale gas from the Barnett Shale, Fort Worth basin, Texas. *American Association of Petroleum Geologists*, Annual Meeting Program 10, 100.

Joachimski, M.M., Lai, X., Shen, S., Jiang, H., Luo, G., Chen, J., Sun, Y., 2012. Climate warming in the latest Permian and the Permian–Triassic mass extinction. *Geology* 40, 195–198.

Kajiwara, Y., Yamakita, S., Ishida, K., Ishiga, H., Imai, A., 1994. Development of a largely anoxic stratified ocean and its temporary massive mixing at the Permian Triassic Boundary supported by the sulfur isotopic record. *Paleogeography, Paleoclimatology, Paleoecology* 111, 367–379.

Kato, Y., Nakao, K., Isozaki, Y., 2002. Geochemistry of late Permian to early Triassic pelagic cherts from southwest Japan: implications for an oceanic redox change. *Chemical Geology* 182, 15–34.

Kidder, D.L., Worsley, T.R., 2004. Causes and consequences of extreme Permo–Triassic warming to globally equable climate and relation to Permo–Triassic extinction and recovery. *Paleogeography, Paleoclimatology, Paleoecology* 203, 207–237.

Knoll, A.H., Bambach, R.K., Canfield, D.E., Grotzinger, J.P., 1996. Comparative Earth History and late Permian Mass Extinction. *Science* 273, 452–457.

Koopmans, M.P., Rijpstra, W.I.C., Klapwijk, M.M., de Leeuw, J.W., Lewan, M.D., Sinninghe Damsté, J.S.,1999. A thermal and chemical degradation approach to decipher pristane and phytane precursors in sedimentary organic matter. *Organic Geochemistry* 30, 1089–1104.

Korte, C., Kozur, H.W., Joachimski, M.M., Strauss, H., Veizer, J., Schwark, L., 2004. Carbon, sulfur, oxygen and strontium isotope records, organic geochemistry and biostratigraphy across the Permian/Triassic Boundary in Abadeh, Iran. *International Journal of Earth Sciences* 93, 565–581.

Korte, C., Kozur, H.W., 2010. Carbon-isotope stratigraphy across the Permian – Triassic Boundary: A review. *Journal of Asian Earth sciences* 39, 215–235.

Korte, C., Pnade, P., Kalle, P., Kozur, H.W., Joachimski, M.M., Oberhänsli, H., 2010. Massive volcanism at the Permian–Triassic Boundary and its impact on the isotopic composition of the ocean and atmosphere. *Asian Journal of Earth Sciences* 37, 293–311.

Krishnamurthy, R.V., Syrup, K.A., Baskaran, M., Long, A., 1995. Late glacial climate record of midwestern United States from the hydrogen isotope ratio of lake organic matter. *Science* 269, 1565–1567.

Lafargue, E., Marquis, F., Pillot, D., 1998. Rock-Eval 6 Applications in Hydrocarbon Exploration, Production, and Soil Contamination Studies. *Revue de l'institut Francais du Petrole* 53, 421–437.

Lis, G.P., Schimmelmann, A., Mastalerz, M., 2006. D/H ratios and hydrogen exchangeability of type-II kerogens with increasing thermal maturity. *Organic Geochemistry* 37, 342–353.

Mann, J.L., Vocke, R.D., Kelly, W.R., 2009. Revised delta ^{34}Sreference values for IAEA sulfur isotope reference materials S-2 and S-3. *Rapid Communications in Mass Spectrometry* 23, 1116–1121.

Maruoka, T., Koeberl, C., Hancox, P.J., Reimold, W.U., 2003. Sulfur geochemistry across a terrestrial Permian–Triassic Boundary section in the Karoo Basin, South Africa. *Earth and Planetary Science Letters* 206, 101–117.

Maslen, E., Grice, K., Métayer, P.L., Dawson, D., Edwards, D., 2011. Stable carbon isotopic compositions of individual aromatic hydrocarbons as source and age indicators in oils from western Australian basins. *Organic Geochemistry* 42, 387–398.

Metcalfe, I., Nicoll, R.S., Willink, R.J., 2008. Conodonts from the Permian Triassic transition in Australia and position of the Permian–Triassic Boundary. *Australian Journal of Earth Science* 55, 349 – 361.

Metcalfe, I., Nicoll, R.S., Willink, R., Ladjavadi, M., Grice, K., 2013. early Triassic (Induan–Olenekian) conodont biostratigraphy, global anoxia, carbon isotope

excursions and environmental perturbations: New data from Western Australian Gondwana. *Gondwana Research* 23, 1136–1150.

Morante, R., 1995. Permian–Triassic stable isotope stratigraphy of Australia. PhD thesis, Macquarie University, Sydney.

Morante, R., 1996. Permian and early Triassic isotopic records of carbon and strontium in Australia and a scenario of events about the Permian-Triassic boundary. *Historical Biology* 11, 289–310.

Mory, A. J., Iasky, R. P., 1996. Stratigraphy and structure of the onshore northern Perth Basin, Western Australia. *Western Australia Geological Survey,* Report 46, 101.

Nabbefeld, B., Grice, K., Twitchett, R., Summons, R., Hays, L., Böttcher, M., Asif, M., 2010a. An integrated biomarker, isotopic and paleoenvironmental study through the late Permian event at Lusitaniadalen, Spitsbergen. *Earth and Planetary Science Letters* 291, 84–96.

Nabbefeld, B., Grice, K., Schimmelmann, A., Sauer, P., Böttcher, M., Twitchett, R., 2010b. Significance of $\delta D_{kerogen}$, $\delta^{13}C_{kerogen}$ and $\delta^{34}S_{pyrite}$ from several Permian/Triassic (P/Tr) sections. *Earth and Planetary Science Letters* 295, 21–29.

Neretin, L., Volkov, I., Böttcher, M.E., Grinenko, V.A., 2001. A sulfur budget for the Black Sea anoxic zone. Deep-Sea Research I 48, 2569–2593.

Newton, R.J., Pevitt, E.L., Wignall, P., Bottrell, S.H., 2004. Large shifts in the isotopic composition of seawater sulfate across the Permo–Triassic Boundary in northern Italy. *Earth and Planetary Science Letters* 218, 1–15.

Peters, K.E., Walters, C.C., Moldowan, J.M., 2005. The biomarker guide: Interpreting molecular fossils in petroleum and ancient sediments. Prentice-Hall, New Jersey.

Popp, B.N., Laws, E.A., Bidigare, R.R., Dore, J.E., Hanson, K.L., Wakeham, S.G., 1998. Effect of phytoplankton cell geometry on carbon isotopic fractionation. *Geochimica et Cosmochimica Acta* 62, 69–79.

Purcell, R., 2006. Palynology Report Senecio–1, L1, North Perth Basin, Western Australia. Report to Arc Energy NL, 7.

Puttmann, W., Villar, H., 1987. Occurrence and geochemical significance of 1,2,5,6-tetramethylnaphthalene. *Geochimica et Cosmochimica Acta* 51, 3023–3029.

Radke, M., Hilkert, A., Rullkötter, J., 1998. Molecular stable carbon isotope compositions of alkylphenanthrenes in coals and marine shales related to source and maturity. *Organic Geochemistry* 28, 785–795.

Raiswell, R., 1997. A geochemical framework for the application of stable sulfur isotopes to fossil pyritization. *Journal of the Geological Society* 154, 343–356.

Raup, D.M., Sepkoski, J.J. Jr., 1982. Mass extinctions in the marine fossil record. *Science* 215, 1501–1503.

Rontani, J.F., Bonin, P., 2011. Production of pristane and phytane in the marine environment: role of prokaryotes. *Research in Microbiology* 162, 923–933.

Sauer, P.E., Eglinton, T.I., Hayes, J.M., Schimmelmann, A., Sessions, A.L., 2001. Compound specific D/H ratios of lipid biomarkers from sediments as a proxy for environmental and climatic conditions. *Geochimica et Cosmochimica Acta* 65, 213–222.

Sauer, P.E., Schimmelmann, A., Sessions, A.L., Topalov, K., 2009. Simplified batch equilibration for D/H determination of non-exchangeable hydrogen in solid organic material. *Rapid Communications in Mass Spectrometry* 23, 949–956.

Schimmelmann, A., Sessions, A.L., Boreham, C.J., Edwards, D.S., Logan, G.A., Summons, R.E., 2004. D/H ratios in terrestrially sourced petroleum systems. *Organic Geochemistry* 35, 1169–1195.

Schimmelmann, A., Sessions, A.L., Mastalerz, M., 2006. Hydrogen isotopic (D/H) composition of organic matter during diagenesis and thermal maturation. Annual Reviews *Earth and Planetary Science* 34, 501–533.

Sim, M.S., Bosak, T., Ono, S., 2011. Large Sulfur Isotope Fractionation Does Not Require Disproportionation. *Science* 333, 74–77.

Stanley, S.M., 2010. Relation of Phanerozoic stable isotope excursions to climate, bacterial metabolism, and major extinctions. *Geology, Evolution* 107, 19185–19189.

Summons, R. E., Boreham, C. J., Foster, C. B., Murray, A. P., Gorter, J. D., 1995. Chemostratigraphy and the composition of oils in the Perth Basin, Western Australia. *Australian Petroleum Production Exploration Journal* 35, 613–631.

Takahashi, S., Kaiho, K., Hori, R.S., Gorjan, P., Watanabe, T., Yamakita, S., Aita, Y., Takemura, A., Spörli, K.B., Kakegawa, T., Oba, M., 2013. Sulfur isotope profiles in the pelagic Panthalassic deep sea during the Permian–Triassic transition. *Global and Planetary Change* 105, 68–78.

Thomas, B.M., Barber, C.J., 2004. A re-evaluation of the hydrocarbon habitat of the northern Perth Basin. *Australian Petroleum Production Exploration Journal* 44, 59–92.

Thomas, B.M., Willink, R.J., Grice, K., Twitchett, R.J., Purcell, R.R., Archbold, N.W., George, A.D., Tye, S., Alexander, R., Foster, C.B., Barber, C.J., 2004. Unique marine Permian–Triassic Boundary section from Western Australia. *Australian Journal of Earth Sciences* 51, 423–430.

Twitchett, R.J., 2007.The Lilliput effect in the aftermath of the end-Permian extinction event. *Paleogeography, Paleoclimatology, Paleoecology* 252, 132–144.

Wignall, P.B., Twitchett, R.J., 2002. Extent, duration and nature of the Permian–Triassic superanoxic event. In: Koeberl, C., MacLeod, K.C. (Eds.), Catastrophic events and mass extinctions: impacts and beyond: Boulder, Colorado. *Geological Society of America Special Paper* 356, 395–413.

Wignall, P.B., Bond, D.P.G., Kuwahara, K., Kakuwa, Y., Newton, R.J., Poulton, S.W., 2010. An 80 million year oceanic redox history from Permian to Jurassic pelagic sediments of the Mino-Tamba terrane, SW Japan, and the origin of four mass extinctions. *Global and Planetary Change* 71, 109–123.

Xie, S., Pancost, R.D., Huang, X., Jiao, D., Lu, L., Huang, J., Yang, F., Evershed, R.P., 2007. Molecular and isotopic evidence for episodic environmental change across the Permo/Triassic Boundary at Meishan in South China. *Global and Planetary Change* 55, 56–65.

Zhang, X., Gillespie, A.L., Sessions, A.L., 2009. LargeD/H variations in bacterial lipids reflect central metabolic pathways. *Proceedings of the National Academy of Sciences* 106, 12580–12586.

Appendix

I
Pristane

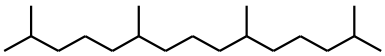

II
Phytane

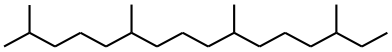

III
Chlorophyll *a*

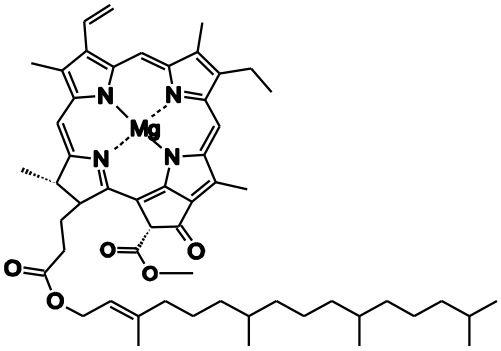

IV
2-Methylnaphthalene

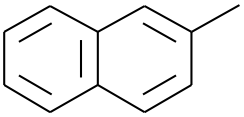

V
1,6-Dimethylnaphthalene

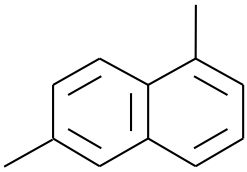

VI
1,2,5-Trimethylnaphthalene

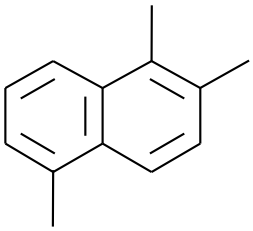

VII
1-Methylphenanthrene

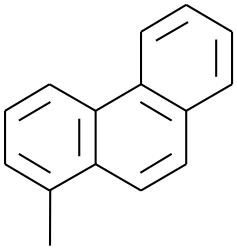

VIII
1,9-Dimethylphenanthrene

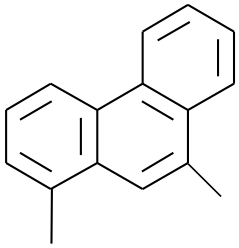

IX
Benzo[*e*]pyrene

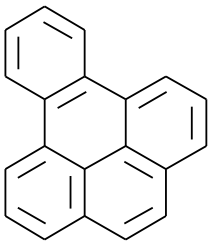

X
Benzo[*a*]anthracene

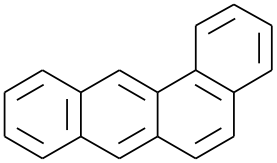

XI
D-ring aromatic 8,14-secohopanoids

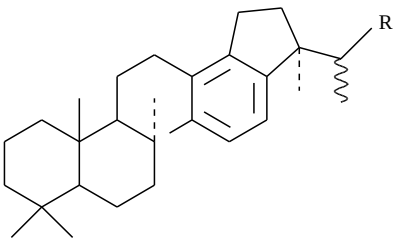

Supplementary Online Material (SOM)

Table A0.1: Isotopic results (‰) of $\delta^{13}C_{OM}$, $\delta^{13}C_{carbonate}$, $\delta^{34}S_{pyrite}$ and $\delta^{2}H_{kerogen}$. Data included in **Figure 3.6**. N.D. not determined.

Depth (ave.) (m)	$\delta^{13}C_{OM}$ (‰)	$\delta^{13}C_{carbonate}$ (‰)	$\delta^{34}S_{pyrite}$ (‰)	$\delta^{2}H_{kerogen}$ (‰)
2708.12	–32.9	N.D.	–18.2	–29.8
2708.42	N.D.	N.D.	N.D.	N.D.
2708.86	–32.9	N.D.	N.D.	–81.7
2709.85	–31.8	N.D.	–23.8	N.D.
2710.86	–31.8	–3.3	–22.4	N.D.
2711.94	–32.3	–3.8	–25.0	N.D.
2712.9	–31.8	–3.9	–21.9	N.D.
2713.4	N.D.	N.D.	N.D.	N.D.
2713.83	–31.7	N.D.	N.D.	N.D.
2714.89	–31.5	–2.4	–24.0	–65.7
2715.36	N.D.	N.D.	N.D.	N.D.
2715.86	–29.0	–1.1	N.D.	N.D.
2716.83	–30.2	N.D.	–22.6	N.D.
2717.61	N.D.	N.D.	N.D.	N.D.
2717.91	–29.4	N.D.	N.D.	17.5
2718.94	–28.6	–1.3	–19.6	31.1
2719.15	N.D.	N.D.	N.D.	N.D.
2719.37	N.D.	N.D.	N.D.	N.D.
2719.87	–27.5	N.D.	–21.5	N.D.
2720.88	–28.0	N.D.	N.D.	N.D.
2721.95	–27.9	–0.3	–26.4	–58.4
2722.92	–28.5	N.D.	N.D.	–81.9
2723.86	–28.8	N.D.	–21.3	–61.2
2724.89	–29.0	N.D.	N.D.	N.D.
2725.89	–29.3	N.D.	–9.3	–70.5
2726.9	–29.7	N.D.	–9.8	–102.3
2727.35	N.D.	N.D.	N.D.	N.D.
2727.87	–29.4	N.D.	–15.6	N.D.
2728.87	–29.9	N.D.	–15.7	–101.9
2729.14	N.D.	N.D.	N.D.	–102.4
2729.37	N.D.	N.D.	N.D.	–104.7

Table A0.2: Stable ^{13}C and ^{2}H isotopic values (‰) of *n*-alkanes against depth (m) for the Senecio–1 samples. Data included in **Figure 3.8**. N.D. not determined.

	δ^{13}C [‰ VPDB] ±standard deviation				δD [‰ VSMOW] ±standard deviation					
Depth (ave.) (m)	***n*-C$_{17}$**	***n*-C$_{19}$**	**Pr**	**Ph**	***n*-C$_{27}$**	***n*-C$_{29}$**	***n*-C$_{17}$**	***n*-C$_{19}$**	***n*-C$_{27}$**	***n*-C$_{29}$**
2708.12	–35.7± 0.0	–36.1± 0.1	N.D.	N.D.	–35.5± 0.1	–34.5± 0.0	–190± 3	–183± 3	–157± 2	–144± 2
2708.42	N.D.	N.D.	N.D.	N.D.	N.D.	N.D.	N.D.	N.D.	N.D.	N.D.
2708.86	–36.0± 0.1	–36.2± 0.1	N.D.	N.D.	–36.4± 0.2	–36.4± 0.2	–184± 1	–183± 0	–176± 2	–166± 0
2709.85	N.D.	N.D.	N.D.	N.D.	N.D.	N.D.	N.D.	N.D.	N.D.	n N.D.
2710.86	N.D.	N.D.	N.D.	N.D.	N.D.	N.D.	–206± 1	N.D.	–204± 1	–194± 2
2711.94	–35.1± 0.0	–35.6± 0.1	N.D.	N.D.	–35.2± 0.0	–35.3± 0.1	–187± 0	–185± 0	–171± 1	–156± 1
2712.90	–34.4± 0.4	–34.8± 0.4	N.D.	N.D.	–34.8± 0.3	–34.2± 0.4	–193± 1	–185± 3	–162± 2	N.D.
2713.40	N.D.	N.D.	N.D.	N.D.	N.D.	N.D.	N.D.	N.D.	N.D.	N.D.
2713.83	N.D.	N.D.	N.D.	N.D.	N.D.	N.D.	N.D.	N.D.	N.D.	N.D.
2714.89	N.D.	N.D.	N.D.	N.D.	N.D.	N.D.	–196± 0	–184± 2	–172± 3	–166± 1
2715.36	N.D.	N.D.	N.D.	N.D.	N.D.	N.D.	N.D.	N.D.	N.D.	N.D.
2715.86	–32.5± 0.0	–32.8± 0.0	–34.7± 0.3	N.D.	–34.3± 0.1	–34.3±0.1	N.D.	N.D.	N.D.	N.D.
2716.83	–31.5± 0.2	–31.6± 0.4	–33.6± 0.2	–35.2± 0.1	N.D.	N.D.	N.D.	N.D.	N.D.	N.D.
2717.61	N.D.	N.D.	N.D.	N.D.	N.D.	N.D.	N.D.	N.D.	N.D.	N.D.

Table A3.2 (continued): Stable ^{13}C and ^{2}H isotopic values (‰) of *n*-alkanes against depth (m) for the Senecio–1 samples. Data included in **Figure 3.8**. N.D. not determined.

	δ^{13}C [‰ VPDB] ±standard deviation				δD [‰ VSMOW] ±standard deviation					
Depth (ave.) (m)	***n*-C$_{17}$**	***n*-C$_{19}$**	**Pr**	**Ph**	***n*-C$_{27}$**	***n*-C$_{29}$**	***n*-C$_{17}$**	***n*-C$_{19}$**	***n*-C$_{27}$**	***n*-C$_{29}$**
2717.91	–31.6± 0.1	–32.0± 0.0	N.D.	N.D.	–32.3± 0.2	–31.6± 0.1	–189± 0	–188± 1	–186± 1	N.D.
2718.94	N.D.	N.D.	N.D.	N.D.	N.D.	N.D.	N.D.	N.D.	N.D.	N.D.
2719.15	N.D.	N.D.	N.D.	N.D.	N.D.	N.D.	N.D.	N.D.	N.D.	N.D.
2719.37	N.D.	N.D.	N.D.	N.D.	N.D.	N.D.	N.D.	N.D.	N.D.	N.D.
2719.87	N.D.	–30.4± 0.4	–34.0± 0.3	–34.1± 0.2	–31.2± 0.3	–31.1± 0.3	N.D.	N.D.	N.D.	N.D.
2720.88	–30.4± 0.3	–30.8± 0.0	N.D.	N.D.	–31.1± 0.2	–31.1± 0.2	N.D.	N.D.	N.D.	N.D.
2721.95	–30.2± 0.0	–30.9± 0.0	N.D.	–31.8± 0.1	–30.8± 0.1	–31.0± 0.0	N.D.	N.D.	N.D.	N.D.
2722.92	N.D.	N.D.	N.D.	N.D.	N.D.	N.D.	–209± 2	–196± 4	–202± 2	–187± 3
2723.86	N.D.	–32.4± 0.0	N.D.	–33.6± 0.1	–32.3± 0.1	–32.2± 0.1	N.D.	N.D.	N.D.	N.D.
2724.89	–31.8± 0.0	–32.1± 0.1	N.D.	–33.2± 0.3	–32.0± 0.1	–31.8± 0.0	N.D.	N.D.	N.D.	N.D.
2725.89	N.D.	–32.1± 0.0	–32.4± 0.1	N.D.	–32.5± 0.0	–32.4± 0.2	–202± 2	–174± 2	–194± 4	–185± 3
2726.90	–31.6± 0.3	–32.0± 0.0	N.D.	–32.7± 0.2	–32.3± 0.0	–32.3± 0.0	-212± 1	–175± 4	–206± 2	–203± 1
2727.35	N.D.	N.D.	N.D.	N.D.	N.D.	N.D.	N.D.	N.D.	N.D.	N.D.
2727.87	N.D.	–32.1± 0.2	N.D.	–33.0± 0.1	–32.3± 0.2	–32.0± 0.3	N.D.	N.D.	N.D.	N.D.
2728.87	N.D.	–32.0± 0.2	N.D.	–33.4± 0.0	–32.5± 0.1	–32.4± 0.0	–208± 3	–168± 5	N.D.	N.D.
2729.14	N.D.	N.D.	N.D.	N.D.	N.D.	N.D.	N.D.	N.D.	N.D.	N.D.
2729.37	N.D.	N.D.	N.D.	N.D.	N.D.	N.D.	N.D.	N.D.	N.D.	N.D.

Table A0.3: Stable ^{13}C isotopic values (‰) of selected aromatic fractions. Data included in **Figure 3.9** N.D. not determined.

$\delta^{13}C$ of selected aromatic fractions [‰ VPDB] ±standard deviation

Depth (ave.) (m)	N	2-MN	1,6- DMN	1,2,5- TMN	P	1-MP	1,9- DMP	Benzo (*e*)-Pyrene	Benzo (*a*)-anthracene
2708.12	N.D.	N.D.	N.D.	N.D.	N.D.	N.D.	N.D.	N.D.	N.D.
2708.42	N.D.	N.D.	N.D.	N.D.	N.D.	N.D.	N.D.	N.D.	N.D.
2708.86	N.D.	N.D.	N.D.	N.D.	N.D.	N.D.	N.D.	N.D.	N.D.
2709.85	–32.2± 0.0	N.D.	N.D.	–32.8± 0.4	–33.3± 0.0	–34.3± 0.0	–34.2± 0.1	–32.5± 0.2	–30.1± 0.3
2710.86	N.D.	N.D.	N.D.	N.D.	N.D.	N.D.	N.D.	N.D.	N.D.
2711.94	N.D.	N.D.	N.D.	N.D.	N.D.	N.D.	N.D.	N.D.	N.D.
2712.90	–32.6± 0.0	–30.1± 0.0	–31.3± 0.0	–33.3± 0.1	–32.4± 0.4	–33.4± 0.3	–35.0± 0.4	–33.8± 0.0	–29.1± 0.2
2713.40	N.D.	N.D.	N.D.	N.D.	N.D.	N.D.	N.D.	N.D.	N.D.
2713.83	N.D.	N.D.	N.D.	N.D.	N.D.	N.D.	N.D.	N.D.	N.D.
2714.89	N.D.	N.D.	N.D.	N.D.	N.D.	N.D.	N.D.	N.D.	N.D.
2715.36	N.D.	N.D.	N.D.	N.D.	N.D.	N.D.	N.D.	N.D.	N.D.
2715.86	N.D.	N.D.	N.D.	N.D.	N.D.	N.D.	N.D.	N.D.	N.D.
2716.83	N.D.	N.D.	N.D.	N.D.	N.D.	N.D.	N.D.	N.D.	N.D.
2717.61	N.D.	N.D.	N.D.	N.D.	N.D.	N.D.	N.D.	N.D.	N.D.
2717.91	–29.9± 0.1	–29.0± 0.3	–29.5± 0.4	–31.2± 0.2	–30.3± 0.3	–31.3± 0.4	–31.3± 0.0	–30.1± 0.2	–28.4± 0.3
2718.94	N.D.	N.D.	N.D.	N.D.	N.D.	N.D.	N.D.	N.D.	N.D.
2719.15	N.D.	N.D.	N.D.	N.D.	N.D.	N.D.	N.D.	N.D.	N.D.

Table A3.3 (continued): Stable ^{13}C isotopic values (‰) of selected aromatic fractions. Data included in **Figure 3.9** N.D. not determined.

$\delta^{13}C$ of selected aromatic fractions [‰ VPDB] ±standard deviation

Depth (ave.) (m)	N	2-MN	1,6- DMN	1,2,5- TMN	P	1-MP	1,9- DMP	Benzo (*e*)-Pyrene	Benzo (*a*)-anthracene
2719.37	N.D.	N.D.	N.D.	N.D.	N.D.	N.D.	N.D.	N.D.	N.D.
2719.87	–28.6± 0.0	N.D.	–28.9± 0.1	–30.4± 0.2	–29.5± 0.2	–30.6± 0.1	–30.6± 0.2	–27.2± 0.3	–24.3± 0.3
2720.88	N.D.	N.D.	N.D.	N.D.	N.D.	N.D.	N.D.	N.D.	N.D.
2721.95	–28.9± 0.3	–28.8± 0.0	–29.0± 0.0	–30.0± 0.1	–29.2± 0.1	–30.3± 0.1	–29.7± 0.2	N.D.	–25.9± 0.2
2722.92	N.D.	N.D.	N.D.	N.D.	N.D.	N.D.	N.D.	N.D.	N.D.
2723.86	–29.1± 0.3	–29.2± 0.1	–29.2± 0.0	–30.1± 0.4	–29.2± 0.1	–30.4± 0.1	–30.2±0.3	–29.1± 0.4	–26.5± 0.0
2724.89	–29.3± 0.0	–29.1± 0.0	–29.0± 0.1	–30.6± 0.1	–29.2± 0.1	–30.4± 0.1	–30.3± 0.3	–28.8± 0.1	–27.0± 0.3
2725.89	N.D.	N.D.	N.D.	N.D.	N.D.	N.D.	N.D.	N.D.	N.D.
2726.90	N.D.	N.D.	N.D.	N.D.	N.D.	N.D.	N.D.	N.D.	N.D.
2727.35	N.D.	N.D.	N.D.	N.D.	N.D.	N.D.	N.D.	N.D.	N.D.
2727.87	N.D.	N.D.	N.D.	N.D.	N.D.	N.D.	N.D.	N.D.	N.D.
2728.87	N.D.	N.D.	N.D.	N.D.	N.D.	N.D.	N.D.	N.D.	N.D.
2729.14	N.D.	N.D.	N.D.	N.D.	N.D.	N.D.	N.D.	N.D.	N.D.
2729.37	N.D.	N.D.	N.D.	N.D.	N.D.	N.D.	N.D.	N.D.	N.D.

Chapter 4

Significance of polycyclic aromatic hydrocarbons (PAHs) in the early Triassic (Induan–Olenekian) Boundary section

Mojgan Ladjavardi, Kliti Grice, Ian Metcalfe, Chris J. Boreham.

(In preparation for *Organic Geochemistry)*

Abstract

In this study, the abundances of several PAHs have been measured throughout the early Triassic Induan-Olenekian Stage Boundary from the Senecio–1 core in the northern onshore Perth Basin, Western Australia. Biphenyl and 3-methylbiphenyl were found to decrease in abundance shortly before the boundary and can be explained as a result of an increase in distance from the paleo-shore of the paleodepositional environment, due to changes in paleosea-level.

Similar distribution patterns of combustion-derived PAHs such as fluoranthene, pyrene, benzo(*a*)anthracene, benzo-fluoranthene, benzo(*e*)pyrene and benzo(*ghi*)perylene with highest concentrations before the Induan–Olenekian Boundary indicate a predominant origin from combustion sources. The combustion-derived PAHs also increase slightly later within the Olenekian section. Benzo(*e*)pyrene as the most representative combustion product displays high abundances slightly later within the Olenekian section, coinciding with other combustion-derived PAHs and can be related to volcanic activity and/or other sources of OM. Maximum concentrations of chrysene and triphenylene also accord with other combustion-derived PAHs suggesting similar source. Wild fires and volcanic activity caused by elevated global temperatures possibly explain the high abundances of these components indicating that forest fires events happened within the early Triassic Induan–Olenekian Stage Boundary in the Senecio–1 core.

Keywords

Senecio–1core, Induan–Olenekian, early Triassic, Western Australia, polycyclic aromatic hydrocarbons, paleo-shore, forest fires

Introduction

PAHs with two or more rings are common compounds found in recent and ancient sediment, which have been generally used as biological markers for incomplete combustion of vegetation and/or fossil fuels or by derivation from biological precursors that were altered through sedimentary diagenesis and catagenesis (Grice et al., 2007; Nabbefeld et al., 2010). The major source for unsubstituted PAHs, such as fluoranthene, pyrene, coronene, benzo(*a*)anthracene, benzo(*b*)fluoranthene, benzo(*k*)fluoranthene, benzo(*e*)pyrene, benzo(*a*)pyrene and benzo(*ghi*)perylene in recent sediments is incomplete combustion of OM as a result of forest fires and residential or industrial heating (Laflamme and Hites, 1978; Lichtfouse et al., 1997; Youngblood and Blumer, 1975; Lima et al., 2005; Wakeham et al., 1980). These PAHs are usually sorbed onto combustion-generated airborne particulate matter and ultimately deposited into sediments (Laflamme and Hites, 1978).

Phenanthrene and chrysene were found in recent sediments through combustion of OM together with inputs as a result of sedimentary diagenetic processes (Wakeham et al., 1980; Laflamme and Hites, 1978). Although some PAHs are formed in hydrothermal mineral deposits (e.g. Williford et al., 2011), impact crater events (Hallmann et al., 2010), perylene is associated with fungal pigments (Grice et al., 2009) and benzo(*e*)pyrene has been attributed to algal sourced OM in Permian/Triassic sediments from Hovea–3 drill well, Perth Basin, W.A. (Grice et al., 2007). Moreover, it has been demonstrated that contact of OM with the products of intrusive and extrusive volcanism can cause production of unsubstituted PAHs that later found their way into sediments (Murchison and Raymond, 1989).

Global fire is thought as a major biological crisis that caused the extinction of many marine and terrigenous organisms at the end of the Permian and the beginning of Triassic (Ward et al., 2005) and possibly was the result of a series of environmental changes (Erwin, 1994; Grice et al., 2007; Knoll et al., 2007). In this study, our aim was to determine the abundances, distributions, potential sources and significance of selected PAHs in samples spanning the early Triassic Induan–Olenekian Boundary from the Senecio–1 core and to better understand the paleoenvironmental changes that occurred around this early Triassic boundary.

Materials and Methods

Sample preparation and extraction

The samples used in this study are the same as analysed in Chapter 3, from Senecio–1 core (2708.10 to 2729.64 m depths) in the northern onshore Perth Basin, Western Australia. To summarize, each sample was surface washed with a mixture of DCM and CH_3OH (9:1, v:v), ground to a fine powder and extracted using an ASE, as previously described in detail by Grice et al. (2005).

Column Chromatography

Following the extraction, the extracts of all samples were then separated *via* column chromatography on silica gel (20 cm x 0.9 cm I.D.) using solvent mixtures with increasing polarity, as described by Grice et al. (2005). The hydrocarbon fractions relevant for this study were eluted in DCM/*n*-hexane (1:4, v: v).

Gas Chromatography – Mass Spectrometry (GC-MS) analysis

GC-MS analysis was performed on an Agilent 5973 GC-MS equipped with a HP 6890 auto-sampler and a DB-5MS capillary column (60 m x 0.25 mm i.d. x 0.25 μm film thickness). The GC oven was heated from 40 ^{o}C to 325 ^{o}C with a heating rate of 3 °C per minute with initial and final hold times of 1 and 30 min, respectively. Samples were injected into a split/splitless injector in a pulsed-splitless mode. He was used as the carrier gas at a constant flow rate of 1 mL/min. Selected ion monitoring (SIM) was used to achieve a better resolution for quantification of aromatic compounds.

Quantification of aromatic hydrocarbon fraction

A known amount of D14 *p*-terphenyl standard was added to the aromatic fractions to allow semi-quantitative measurements of individual compounds. The quantity of each compound was determined by calculating the proportion of the compound peak area to the standard peak area, factoring the amount of extract and the TOC content of each sample. In this study, values are shown in ng/g TOC.

Results and Discussion

The distributions of several PAHs (**Table 4.1**) across the Induan–Olenekian Boundary for the Senecio–1 core samples have been studied and shown in **Figure 4.1**.

PAH	***Abbreviation***	***m/z***	***Structure (Appendix)***
Naphthalene	N	128	I
2-Methylnaphthalene	2-MN	142	II
Biphenyl	BP	154	III
3-Methylbiphenyl	3-MBP	168	IV
Phenanthrene	P	178	V
9-Methylphenanthrene	9-MP	192	VI
Pyrene	Pyr	202	VII
Fluoranthene	Fla	201	VIII
Benzo(*a*)anthracene	BaAn	228	IX
Chrysene	Chry	228	X
Triphenylene	Tpn	228	XI
Benzo-fluoranthene	Bfla	252	XII
Benzo(*e*)pyrene	BePy	252	XIII
Perylene	Pery	252	XIV
Benzo(*ghi*)perylene	Bpery	276	XV

Table 0.1: Names, abbreviations and *m/z* of PAHs determined in this study, their chemical structures are presented in the Appendix.

Benzofluoranthenes are integrated as the sum of benzo(*b*)fluoranthene, benzo(*j*)fluoranthene and benzo(*k*)fluoranthene. Triphenylene and chrysene could not be separated and thus were determined as a composite.

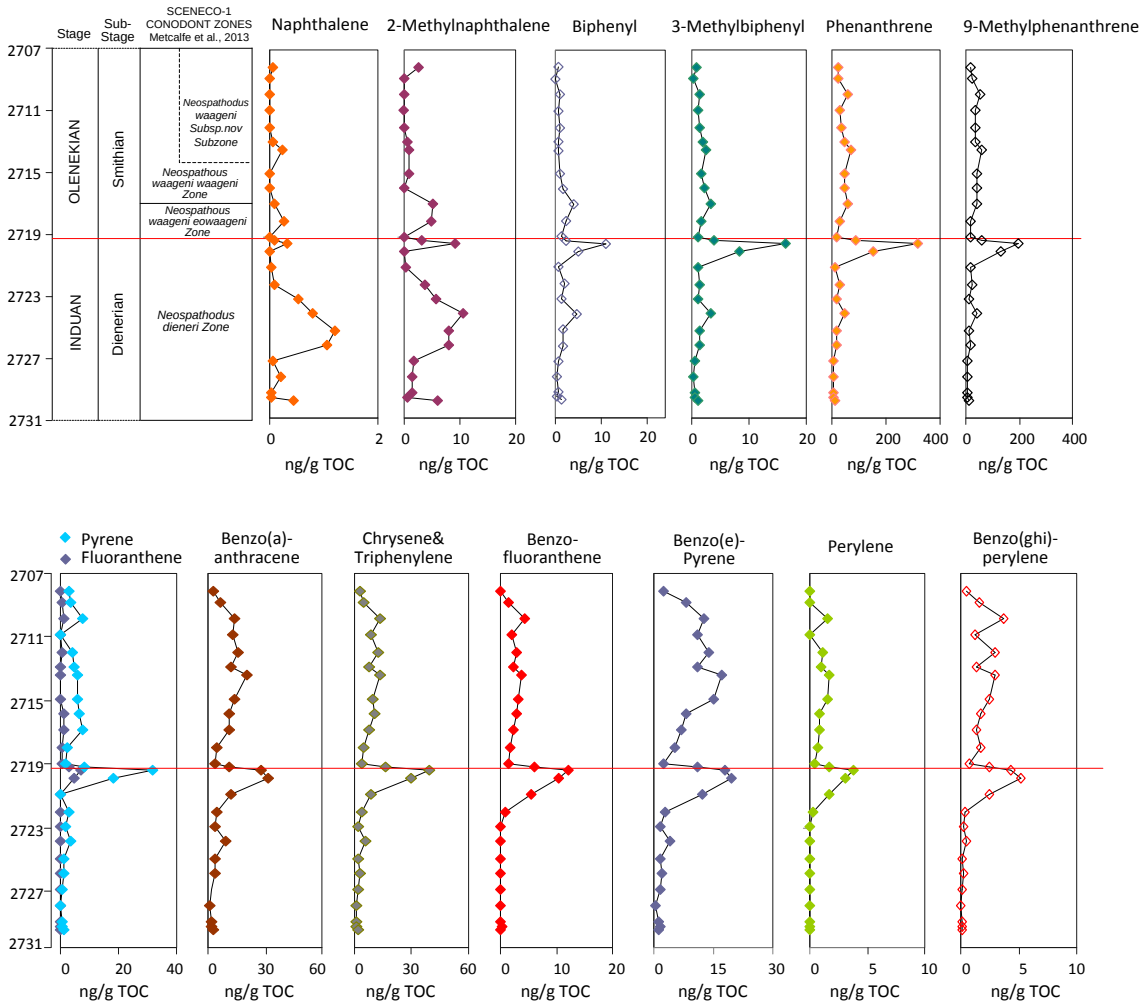

Figure 0.1: PAH concentrations versus depth (m) for the Induan–Olenekian Boundary from Senecio–1 core, Perth Basin, Western Australia.

Of the 15 distinct PAHs measured in this study, 13 compounds show their greatest concentrations shortly before the Induan–Olenekian transition. The two exceptions are naphthalene and 2-methylnaphthalene, with a maximum value of 1.19 ng/g TOC at 2724.89 m and 10.46 ng/g TOC at 2723.86 m, respectively in the 'equivalent sapropelic' interval of the core. The changes in PAH abundances are possibly because of different types of combustion material, combustion temperature and/or post depositional processes (Jiang et al., 1998).

Biphenyl and 3-methylbiphenyl occur with a maximum value of 10.98 ng/g TOC and 16.53 ng/g TOC, respectively at 2719.37 m near to the established Induan–Olenekian Boundary. A decrease of biphenyl and 3-methylbiphenyl shortly before the boundary in the Senecio–1 core could be caused by an increase in distance from the paleo-shore of the paleodepositional environment, consequent of changes in paleosea-level. Combustion-derived PAHs, i.e. fluoranthene, pyrene, benzo(*a*)anthracene, benzo(*e*)pyrene, benzofluoranthene, benzo(*ghi*)perylene are abundant in our samples and show similar distribution patterns. The combustion-derived PAHs show high concentrations before the Induan–Olenekian Boundary in Senecio–1 core and increase slightly later within the section. Wild fires caused by elevated global temperatures as a result of intensive activity in Siberia (Wignall, 2001; Sephton et al., 2005) possibly explain the high abundances of these components.

The most typical combustion product among the combustion-derived PAHs is benzo(*e*)pyrene, which has been suggested as the most stable among the 5-ring PAHs (Stein and Fahr, 1985; Stein, 1978; Nabbefeld et al., 2010), and may be associated with volcanic activity and/or other sources of OM (Grice et al., 2007). Benzo(*e*)pyrene shows its maximum value at 2719.37 m (19.67 ng/g TOC) and also displays high abundances (17.24 ng/g TOC) slightly later within the Olenekian section, coinciding with other combustion-derived PAHs. The differences in abundances of combustion-derived compounds can be related to changes in the type of combusted material, post-depositional processes and combustion temperature (Jiang et al., 1998). In addition, the original distribution of combustion-derived PAHs could be altered by alkylation reactions through sedimentation and diagenesis (Smit

et al., 1995; Alexander et al., 1995); however some PAHs might have a higher tendency to post-depositional alterations compared to others.

Perylene was detected in the Senecio–1 core and can be attributed to quinone pigments in wood degrading fungi and is generally developed in anoxic conditions (Grice et al., 2009; Suzuki et al., 2010). In this study benzo(*ghi*)perylene follows the distribution over depth of perylene, suggesting that it may have more than one source (Jiang et al., 1998) also likely to be formed by diagenetic transformation of marine precursors (Readman et al., 2002). Chrysene and triphenylene show a maximum concentration of 39.83 ng/g TOC at 2719.37 m with some variations from 4.39 to 13.81 (ng/g TOC) after the boundary in the early Olenekian. Concentrations of chrysene and triphenylene have been shown to be combustion-derived (Laflamme and Hites, 1978), but may also be formed through diagenesis from natural biological precursors (e.g. natural biolipids) (Killops and Massoud, 1992; Tan et al., 1996).

The similarity between phenanthrene and the 9-methylphenanthrenes (i.e. **VI,** maximum: 196 ng/g TOC at 2719.37 m) points towards a similar origin for all these compounds. 9-Methyl-phenanthrene results from phenanthrene as a function of maturity. A ratio resulting from the abundance of these compounds has been used as a marker to evaluate the maturity of OM (Radke et al., 1982).

Conclusions

Combustion derived PAHs (fluoranthene, pyrene, benzo(*a*)anthracene, benzo-fluoranthene, benzo(*e*)pyrene and benzo(*ghi*)perylene) are present throughout the Senecio–1 core samples in the northern onshore, Western Australia. The concentration profiles of most detected PAHs, with the exception of naphthalene and 2-methylnaphthalene, are similar with highest concentrations before the Induan–Olenekian Boundary at 2719.37 m and increase to some extent later in the section, indicating a predominant origin from combustion sources. The abundance of combustion derived PAHs can be indicative of wildfires and volcanic activity as shown by previous studies (e.g. Murchison and Raymond, 1989).

Benzo(*ghi*)perylene is usually attributed to a pyrogenic origin (Killops and Massoud, 1992). In this study benzo(*ghi*)perylene follows the distribution of

perylene and thus suggests additional sources of this PAH. However, its depth profile in the analysed section is similar to those of combustion markers. A decrease of biphenyl and 3-methylbiphenyl shortly before the Induan–Olenekian Boundary in the Senecio–1 core could be caused by an increase in distance from the paleo-shore of the paleodepositional environment as a result of changes in paleosea-level. The other PAHs that are not clearly related to volcanism display changes in PAH abundances likely due to different types of combustion materials, combustion temperature and/or post-depositional processes (Jiang et al., 1998).

The present study increases our knowledge about paleoenvironmental changes spanning the Induan–Olenekian Boundary in senecio–1 core and if correlated with other datasets, might be helpful to reconstruct global events. Results from this work indicate that wildfires and volcanism were major factors in early Triassic Induan–Olenekian Boundary from Senecio–1 core in the northern onshore Perth basin, WA.

Acknowledgements

The authors thank Geoff Chidlow for providing GC-MS technical support. Mojgan Ladjavardi thanks Curtin University, Geoscience Australia and GFZ Potsdam for international Postgraduate Award scholarship and Australia-China LNG project for a PhD top-up scholarship. Kliti Grice acknowledges ARC for QEII Fellowship and John de Laeter Centre for ARC LIEFP support. Ian Metcalfe acknowledges the ARC for Discovery Grant number DP109288.

References

Alexander, R., Bastow, T.P., Fisher, S., Kagi, R., 1995. Geosynthesis of organic compounds: II. Methylation of phenanthrene and alkylphenanthrenes. *Geochimica et Cosmochimica Acta* 59, 4259–4266.

Erwin, D.H., 1994. The Permo–Triassic Extinction. *Nature* 367, 231–236.

Grice, K., Summons, R.E., Grosjean, E., Twitchett, R.J., Dunning, W., Wang, S.X., Böttcher, M.E., 2005. Depositional conditions of the northern onshore Perth Basin (basal Triassic). *Australian Petroleum Production and Exploration Association Journal* 45, 263–273

Grice, K., Nabbefeld, B., Maslen, E., 2007. Source and significance of selected polycyclic aromatic hydrocarbons in sediments (Hovea–3 well, Perth Basin, Western Australia) spanning the Permian–Triassic Boundary. *Organic Geochemistry* 38, 1795–1803.

Grice, K., Lu, H., Atahan, P., Asif, M., Hallmann, C., Greenwood, P., Maslen, E., Tulipani, S., Williford, K., Dodson, J., 2009. New insights into the origin of perylene in geological samples. *Geochimica et Cosmochimica Acta* 73, 6531–6543.

Hallmann, C., Grey, K., Webster, L., McKirdy, D., Grice, K., 2010. Molecular signature of the Neoproterozoic Acraman impact event. *Organic Geochemistry* 41, 111–5.

Jiang, C., Alexander, R., Kagi, R.I., Murray, A.P., 1998. Polycyclic aromatic hydrocarbons in ancient sediments and their relationships to paleoclimate. *Organic Geochemistry* 29, 1721–1735.

Killops, S.D., Massoud, M.S., 1992. Polycyclic aromatic hydrocarbons of pyrolytic origin in ancient sediments: evidence for Jurassic vegetation fires. *Organic Geochemistry* 18, 1–7.

Knoll, A.H., Bambach, R.K., Payne, J.L., Pruss, S., Fischer, W.W., 2007. Paleophysiology and endPermian mass extinction. *Earth and Planetary Science Letters* 256, 295–313.

Laflamme, R.E., Hites, R.A., 1978. The global distribution of polycyclic aromatic hydrocarbons in recent sediments. *Geochimica et Cosmochimica Acta* 42, 289–303.

Lichtfouse, É., Budzinski, H., Garrigues, P., Eglinton, T.I., 1997. Ancient polycyclic aromatic hydrocarbons in modern soils: ^{13}C, ^{14}C and biomarker evidence. *Organic Geochemistry* 26, 353–359.

Lima, A.L., Farrington, J.W., Reddy, C.M., 2005. Combustion-derived polycyclic aromatic hydrocarbons in the environment. *Environmental Forensics* 6, 109–131.

Murchison, D.G., Raymond, A.C., 1989. Igneous activity and organic maturation in the Midland Valley of Scotland. *International Journal of Coal Geology* 14, 47–82.

Nabbefeld, B., Grice, K., Summons, R.E., Hays, L.E., Cao, C., 2010. Significance of polycyclic aromatic hydrocarbons (PAHs) in Permian/Triassic Boundary sections. *Applied Geochemistry* 25, 1374–1382.

Radke, M., Welte, D.H., Willsch, H., 1982. Geochemical study on a well in the Western Canada Basin: relation of the aromatic distribution pattern to maturity of organic matter. *Geochimica et Cosmochimica Acta* 46, 1–10.

Readman, J.W., Fillmann, G., Tolosa, I., Bartocci, J., Villeneuve, P., Catinni, C., Mee, L.D., 2002. Petroleum and PAH contamination of Black Sea. *Marine Pollution Bulletin* 44, 48–62.

Sephton, M.A., Looy, C.V., Brinkhuis, H., Wignall, P.B., de Leeuw, J.W., Visscher, H., 2005. Catastrophic soil erosion during the end- Permian biotic crisis. *Geology* 33, 941–944.

Smith, J.W., George, S.C., Batts, B.D., 1995. The geosynthesis of alkylaromatics. *Organic Geochemistry* 23, 71–80.

Stein, S.E., 1978. High temperature chemical equilibria of polycyclic aromatic hydrocarbons. *Journal of Physical Chemistry* 82, 566–571.

Stein, S.E., Fahr, A., 1985. High temperature stability of hydrocarbons. *Journal of Physical Chemistry* 89, 3714–3725.

Suzuki, N., Yessalina, S., Kikuchi, T., 2010. Probable fungal origin of perylene in Late Cretaceous to Paleogene terrestrial sedimentary rocks of northeastern Japan as indicated from stable carbon isotopes. *Organic Geochemistry* 41, 234–241.

Tan, Y.L., Kong, A., Monetti, M., 1996. Biogenic polycyclic aromatic hydrocarbons in an Alaskan arctic lake sediment. *Polycyclic Aromatic Compounds* 9, 185–192.

Ward, P.D., Garrison, G., Botha, J., Buick, R., Erwin, D.H., Kirschvink, J.L., De Kock, M.O., Smith, R., 2005. Abrupt and gradual extinction among land vertebrates in the Karoo Basin, South Africa. *Science* 307, 709–714.

Wakeham, S.G., Schaffner, C., Giger, W., 1980. Polycyclic aromatic hydrocarbons in Recent lake sediments-II. Compounds derived from biogenic precursors during early diagenesis. *Geochimica Cosmochimica Acta* 44, 415–429.

Wignall, P.B., 2001. Large igneous provinces and mass extinctions. *Earth-Science Reviews* 53, 1–33.

Williford, K.H., Grice, K., Logan, G.A., Chen, J., Huston, D., 2011. New insights into the hydrothermal alteration of organic matter from the Paleoproterozoic McArthur River Pb/Zn/Ag ore deposit of northern Australia based on compound specific hydrogen and carbon isotopes. *Earth and Planetary Science Letters* 301, 382–392.

Youngblood, W.W., Blumer, M., 1975. Polycyclic aromatic hydrocarbons in the environment: Homologous series in soils and recent sediments. *Geochimica et Cosmochimica Acta* 39, 1303−1314.

Appendix

I
Naphthalene

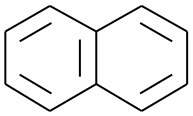

II
2-Methylnaphthalene

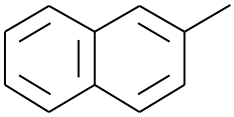

III
Biphenyl

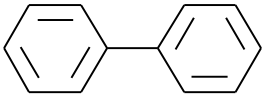

IV
3-Methylbiphenyl

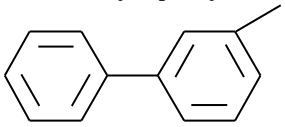

V
Phenanthrene

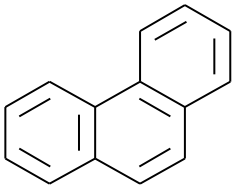

VI
9-Methylphenanthrene

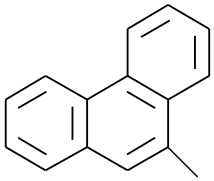

VII
Pyrene

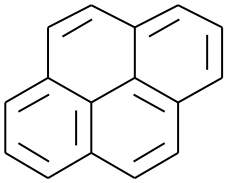

VIII
Fluoranthene

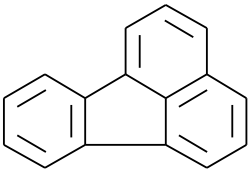

IX
Benzo[*a*]anthracene

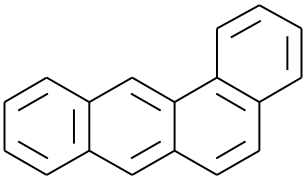

X
Chrysene

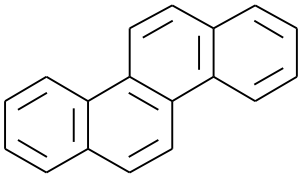

XI
Triphenylene

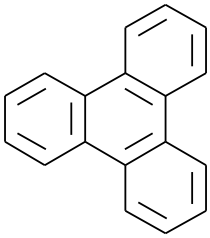

XII
Benzofluoranthene

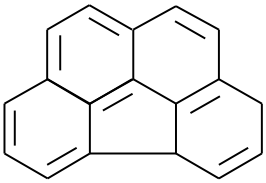

XIII
Benzo[*e*]pyrene

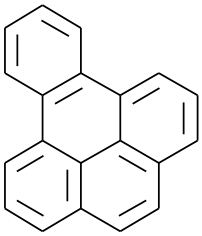

XIV
Perylene

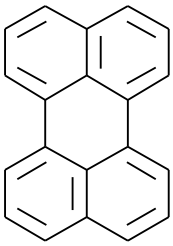

XV
Benzo[*ghi*]perylene

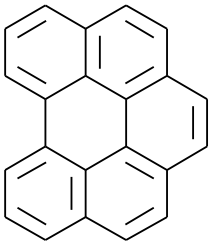

Chapter 5

Rapid offline isotopic characterisation of hydrocarbon gases generated by micro-scale sealed vessel pyrolysis

Mojgan Ladjavardi, Lyndon J. Berwick, Kliti Grice, Chris J. Boreham, Brian Horsfield

***Organic Geochemistry*, 58 (2013) 121–124**

Abstract

The method of offline coupling of MSSV-Py and GC-irMS was developed using a purpose built gas sampling device. The sampling device allows multiple GC and GC-irMS injections to quantify the molecular composition and isotopic evolution of hydrocarbon gases (*n*-C_1 to *n*-C_5) generated by artificial maturation of sedimentary OM. Individual MSSV tubes were introduced into the gas sampling device, which was then evacuated to remove air and filled with helium at atmospheric pressure. The tube was crushed using a plunger after which the device was heated at 120 ^{o}C for 1 min to thermally mobilize and equilibrate the generated gas products. Aliquots of the gas phase were sampled using a gas tight syringe and analysed *via* GC-FID and GC-irMS.

Hydrocarbon gas yields using this technique have been calculated and compared with those obtained previously by online MSSV-Py of the same samples under the same conditions. The major objective of this study was to investigate the potential isotopic fractionation of generated gaseous hydrocarbons within the gas sampling device as a function of time and temperature. For this purpose several tests using a standard gas mixture have been performed on the GC-irMS. The analyses showed no isotopic fractionation of $C_{1–5}$ hydrocarbons within 1 hour, minor $\delta^{13}C$ enrichment after 5 hrs, and significant enrichment after 22 hrs for all the compounds at a temperature of 120 ˚C.

Keywords

Micro scale sealed vessel pyrolysis, artificial maturation, stable isotopes, $\delta^{13}C$, methane, hydrocarbon gas, isotopic fractionation

Introduction

The formation of petroleum (oil and gas) cannot be extrapolated from geochemical data derived from naturally occurring basins (Michels et al., 2002). In order to overcome the limitations of natural samples, artificial maturation experiments using analytical pyrolysis techniques have been employed to simulate the formation of gases (Dieckman et al., 2006; Michels et al., 2002).

The study of $\delta^{13}C$ of the hydrocarbon gases, particularly when combined with compositional data, is of great importance to evaluate natural gas resources (Boreham et al., 1998). A range of analytical pyrolysis techniques, coupled with online or offline GC-MS, have been used to characterise organic macromolecules and simulate geochemical reactions over laboratory timescales. MSSV-Py involves heating small quantities of sample (typically 0.1–10 mg) enclosed within glass tubes under controlled temperature (e.g. 250–350 ºC) and time (e.g. hours-days) conditions (Horsfield et al., 1989).

However, this approach does not allow replicate analyses from a single run of a sample required to obtain reliable quantitative and stable isotopic compositions. Here we report the development of offline MSSV-Py that enables multiple injections on GC and GC-irMS in order to measure the molecular composition and stable isotopic values of HC gases (C_1–C_5) generated by artificial maturation of sedimentary OM.

Experimental

Kerogen sample

Kerogen was isolated from Hovea–3 well core from the basal Kockatea Shale, Perth Basin Western Australia at 978.3–978.4 m, which is a representative of the Sapropelic Interval, Hovea Member. The uppermost Permian interval of the Hovea Member consists of inertinitic kerogen (Intertinitic Interval) whereas the Lower Triassic Sapropelic Interval contains Type II algal-rich kerogen (Thomas and Barber, 2004; Thomas et al., 2004; Grice et al., 2005, 2007). The sampled kerogen contained

61 % TOC and yielded Rock-Eval HI (624 mg/g TOC), OI (22 mg/g TOC) and a T_{max} at 428 ºC.

MSSV-Py

Artificial maturation experiments were performed using the principles of MSSV-Py (Horsfield et al., 1989). Aliquots of kerogen (0.87 and 2.75 mg) were loaded into MSSV glass capillary tubes (5 cm x 5 mm i.d.), the void volume was filled with thermally pre-cleaned (400 ºC overnight) glass beads (60–80 mesh) and the tubes were flame sealed. The MSSV tubes were heated in an Al block at 300 ºC. The temperature was increased at 0.7 ºC/min and the tubes were removed from the heating block at 389 ºC and 415 ºC, representing kerogen transformation ratios (TR) of 0.3 and 0.7, respectively (Horsfield and di Primio, 2010). The method developed (see below) was then applied to determine the gas yields of the artificially matured Kockatea shale samples for comparison with previously published results from the same samples and under the same conditions using online MSSV-Py (Horsfield and di Primio, 2010).

Offline gas sampling

The apparatus and procedure for offline sampling of the generated hydrocarbon gases is shown in **Figure 5.1**. The individual MSSV tubes were placed between the side port and main chamber of the gas sampler. The device was evacuated for 5 mins by connecting the side port of the sampler to a vacuum line using a custom Swagelok fitting. The device was then filled with helium at atmospheric pressure after which the MSSV tube was crushed by winding down the threaded glass stopcock. The main chamber of the sampling device containing the crushed sample was heated to 120 ºC by inserting through a vacant injector port of a Hewlett Packard 5890 GC oven. After cooling to ambient temperature the gaseous products released were sampled using a gas-tight syringe and analysed by GC and GC-irMS.

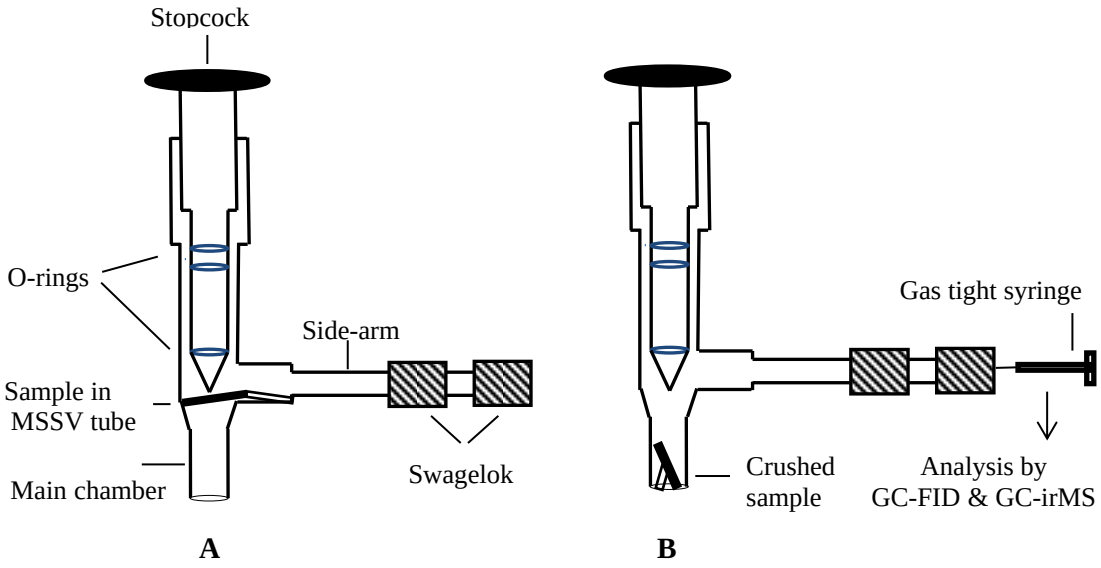

Figure 0.1: Schematic representation of gas sampling device; **A**. Sample loading and evacuation **B**. Sample crushing and gas analysis.

GC and GC-irMS analysis

GC analysis of *n*-C_1 to *n*-C_5 hydrocarbon gases was performed using a Hewlett Packard 5890 gas chromatograph equipped with a HP-PlotQ column (30 m x 0.32 mm i.d.; film thickness 20 µm). Helium carrier gas was used at a constant pressure of 16 psi and a split ratio of 20:1. The GC oven temperature was held isothermal at 200 ºC to achieve optimum separation of gases and the flame ionisation detector at 250 ºC. A gas standard consisting of $C_{1–5}$ hydrocarbons (**Table 5.1**) was used to confirm baseline resolution of the individual components and to check linearity, analytical reproducibility and detection limits for GC analysis.

Calibration curves for quantitation of individual compounds were developed by performing multiple injections of different volumes of the gas standard from gas sampling bags filled at known pressure (1 atm). Peak areas were plotted as a function of the number of moles of each component, calculated from the ideal gas law ($PV = nRT$); where P is the partial pressure of the gas, V is the volume of gas injected, and T is the laboratory temperature (22 ºC). The calibration was repeated every 3 days to ensure stability and reproducibility. The yields (µg/g sample) of generated hydrocarbon gases from the Kockatea shale kerogen were calculated by injecting a 200 µl aliquot from the gas sampling device (total volume 1.6 mL) at known internal

pressure (1 atm). The carbon isotope analysis of the generated gases was performed using a Micromass IsoPrime isotope ratio monitoring-mass spectrometer interfaced to a Hewlett Packard HP 6890 gas chromatograph (GC) with a GS-Carbon plot column (30 m x 0.32 mm i.d x 3 µm film thickness). The GC oven was initially held at 70 ºC for 1 min, heated at rate of 20 ºC/min to 250 ºC, and held for 5 min. Helium was used as carrier gas. Analyses were performed using two different sized gas loops (250 µl and 500 µl) with a split ratio of 20:1. Stable carbon isotopic compositions are expressed in ‰ relative to the international carbon isotope reference material Vienna Pee Dee Belemnite (VPDB).

Component	Mole Fraction (%)	$\delta^{13}C$ (‰)	22 ˚C	120 ˚C
Methane	75.9	–46	–45.6 [0.11]^2	–45.6 [0.08]^2
Ethane	9.14	–31.3	–30.9 [0.07]^2	–30.9 [0.09]^2
Propane	5.87	–35.1	–35.2 [0.16]^2	–35.2 [0.18]^2
iso-Butane	2.97	–29.3	–30.0 [0.21]^2	–30.0 [0.15]^2
n-Butane	3.01	–25.2	–25.3 [0.19]^2	–25.3 [0.22]^2
iso-Pentane	1.07	–27.1	–23.6 [0.31]^2	–23.7 [0.26]^2
n-Pentane	1.05	–23.8		
CO_2	0.989	–8.2		

Table 0.1: Composition and carbon isotopic values of the standard gas mixture and stable carbon isotope measurements of the gases within the sampling device at ambient temperature (22 ºC) and after heating to 120 ºC. Numbers in parentheses are standard deviations; superscript indicates the number of replicate analyses.

Results and discussion

Gas composition and yield

The procedure was applied to Kockatea shale kerogen samples, artificially matured to transformation ratios (TR) of 0.3 and 0.7, to confirm reproducibility and compare the hydrocarbon gas yields using the offline technique with those obtained previously by online MSSV-Py (Horsfield and di Primio, 2010). Excellent reproducibility was observed for duplicate offline pyrolysis experiments (**Table 5.2**).

Hydrocarbon gas yield increased with temperature due to increased conversion of kerogen to volatile products. However, it is evident that the gas yields from the offline injection method are between 1.6–4.8 times lower than those obtained by online MSSV-Py. This is most likely related to the different injection conditions employed for each method. Online MSSV-Py involves crushing the sample tube directly inside a heated injector system (typically 300 ºC) under a constant flow of helium.

In contrast, the offline approach involves heating the crushed sample to 120 ºC to mobilise and equilibrate the gaseous components within the sampling device prior to GC analysis. Adsorption of gas products to the exposed pyrolysed kerogen residue may explain the lower yields. However, no significant differences in gas yields were observed by adding a known amount of the standard gas mixture to the device with and without kerogen residue. In addition, heating the main chamber of the sampling device to higher temperatures (350 ºC) after crushing duplicate MSSV pyrolysed kerogen samples also showed no significant difference in gas distribution and yields at the higher temperature, indicating minimal, if any, adsorption to the kerogen residue. We therefore attribute the lower gas yields compared with the previous online study not to thermal transfer effects but to the absence of helium carrier gas flushing within the offline system.

	TR 0.3		*TR 0.7*	
Component	**Offline**	**Online**	**Offline**	**Online**
Methane	1471, 1423	2569	3868, 3978	6334
Ethane	850, 818	1968	2422, 2462	5881
Propane	916, 908	2123	2750, 2806	5837
iso-Butane	242, 220	617	718, 786	1432
n-Butane	424, 406	1462	1862, 1896	4222
iso-Pentane	174, 160	797	616, 644	1777
n-Pentane	244, 214	915	1743, 1761	2977

Table 0.2: Comparison of gas yields (µg/g) from Kockatea shale kerogen at two different transformation ratios (0.3 and 0.7) using offline (this study) and online (Horsfield and di Primio, 2010) GC analysis. Duplicate values for the new offline technique are provided.

$\delta^{13}C$ of gaseous hydrocarbons

The gas sampling device was filled with the standard gas mixture at atmospheric pressure to investigate the potential for isotopic fractionation due to temperature and time. **Table 5.1** shows that no significant isotopic fractionation was observed for any $C_{1–5}$ hydrocarbons as a result of the mild heating (120 ºC) used to mobilise/equilibrate the gaseous products within the device. **Figure 5.2** shows changes in $\delta^{13}C$ values for $C_{1–4}$ hydrocarbons over a 23 h period using 250 µl and 500 µl gas loops. $\delta^{13}C$ values showed no isotopic fractionation within 1 hour and only minor fractionation to more enriched values within 5 hrs.

However, significant fractionation was observed after 22 hrs. The $\delta^{13}C$ values for all the compounds become heavier over time, most likely due to preferential loss of the isotopically lighter components from the system through the punctured septa of the gas sampling device. It is recommended that the generated gas hydrocarbons should be sampled within 1 hour to avoid isotopic alteration.

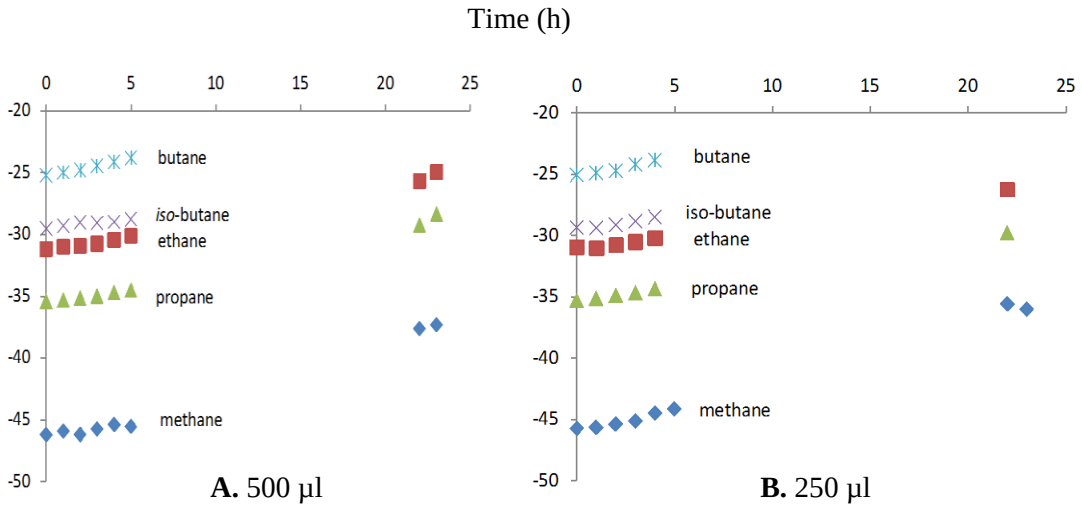

Figure 0.2: Stable carbon isotope measurement of hydrocarbon gases over time using **A.** 500 µl and **B.** 250 µl gas loop.

Conclusions

An offline sampling technique coupled to GC and GC-irMS was developed in order to determine the gas yields and $\delta^{13}C$ values of hydrocarbons ($C_{1–5}$) generated from MSSV-Py artificial maturation of kerogen from the Kockatea Shale (Perth Basin, WA). The hydrocarbon gas yields using this offline approach were slightly lower than previous results for the same sample using online MSSV-Py, most likely due to the absence of helium carrier gas flushing within the offline system. GC-irMS results showed no significant isotopic fractionation of hydrocarbon gases within 1 hr of crushing the MSSV sample, nor due to the mild heating used to mobilise the gaseous components within the sampling device. This offline sampling technique is rapid and inexpensive, enabling multiple isotopic analyses of gases generated by laboratory maturation. The approach has great scope for characterising gas formation in sedimentary systems.

Acknowledgments

The authors thank Geoff Chidlow and Stephen Clayton for GC-FID and GC-irMS technical support. Mojgan Ladjavardi thanks Curtin University, Geoscience Australia and GFZ Potsdam for an International Postgraduate Award scholarship and Australia-China LNG project for a PhD top-up scholarship. KG acknowledges ARC for QEII Fellowship and John de Laeter Centre for ARC LIEFP support.

References

Boreham, C.J., Golding, S.D., Glikson, M., 1998. Factors controlling the origin of gas in Australia Bowen Basin coals. *Organic Geochemistry* 29, 347–362.

Dieckmann, V., Ondrak, R., Cramer, B., Horsfield, B., 2006. Deep basin gas; New insights from kinetic modelling and isotopic fraction in deep-formed gas precursors. *Marine and Petroleum Geology* 23, 183–199.

Grice, K., Cao, C., Love, G.D., Böttcher, M.E., Twitchett, R.J., Grosjean, E., Summons, R.E., Turgeon, S., Dunning, W.J., Jin, Y., 2005. Photic zone euxinia during the Permian–Triassic superanoxic event. *Science* 307, 706–709.

Grice, K., Nabbefeld, B., Maslen, E., 2007. Source and significance of selected polycyclic aromatic hydrocarbons in sediments (Hovea–3 well, Perth Basin, Western Australia) spanning the Permian–Triassic Boundary. *Organic Geochemistry* 38, 1795–1803.

Horsfield, B., Disko, U., Leistner, F., 1989. The micro-scale simulation of maturation: Outline of a new technique and its potential application. *Geologische Rund*schau 78, 361–374.

Horsfield, B., di Primio, R., 2010. Oil and gas generation characteristics of a kerogen concentrate and an oil asphaltene as inferred from Phase Kinetic analysis. GeoS4 Report 20100703.

Michels, R., Raoult, N.E., Elie, M., Mansuay, L., Faure, P., Oudin, J.L., 2002. Understanding of reservoir gas compositions in a natural case using stepwise semi-open artificial maturation. *Marine and Petroleum Geology* 19, 589–599.

Thomas, B.M., Barber, C.J., 2004. A re-evaluation of the hydrocarbon habitat of the northern Perth basin. *Australian Petroleum Production and Exploration Association Journal* 44, 59–92.

Thomas, B.M., Willink, R.J., Grice, K., Twitchett, R.J., Purcell, R.R., Archbold, N.W., George, A.D., Tye, S., Alexander, R., Foster, C.B., Barber, C.J. 2004. Unique marine Permian/Triassic Boundary section from Western Australia. *Australian Journal of Earth Sciences* 51, 423–430.

Chapter 6

Conclusions and outlook

General

The latest Permian–early Triassic transitional period is globally important in Earth's history as the most profound mass extinction. However, despite the vast amount of research that has been carried on the Permian–Triassic mass extinction, post Permian–Triassic crisis recovery has been rarely studied with such resolution. The results presented in this thesis increase our knowledge about the paleoenvironmental conditions that occurred in the early Triassic (Induan–Olenekian) Stage Boundary and provide an increased spatial understanding of the mass extinction event around the boundary by looking at carbon cycling and variations in OM composition within the context of redox and global environmental change. For this purpose, a comprehensive multi-proxy dataset including a combination of bulk stable isotopic data ($\delta^{13}C_{OM}$, $\delta^{13}C_{carbonate}$, $\delta^{34}S_{pyrite}$, $\delta^{2}H_{kerogen}$), compound specific stable carbon and hydrogen isotopic analysis of individual compounds as well as distributions of selected PAHs have been performed for the Senecio–1 core samples spanning the early Triassic Induan–Olenekian Boundary.

The placement of the Induan–Olenekian Boundary is also established for the first time based on conodont faunas.

Furthermore, a new method of offline coupling of MSSV-Py and GC-irMS was developed which enables multiple injections on GC and GC-irMS to obtain reliable stable isotopic compositions of a sample and therefore increases our ability to explore and establish natural gas resources. This approach has great scope for characterising gas formation in sedimentary systems.

Conodont biostratigraphy, global anoxia, carbon isotope excursions and environmental perturbations in the Induan–Olenekian Stage Boundary

The objectives were to determine the early Triassic Induan–Olenekian Stage Boundary in the Perth Basin based on conodont faunas and to place the recorded anoxia in the Perth Basin Hovea Member into a wider context by studying geographic and temporal variation of dysoxia and anoxia in both deep and shallow-marine environments globally. **Chapter 2** provides unequivocal placement of the proposed Induan–Olenekian Boundary at a depth of 2719.25 m in the petroleum exploration well Senecio–1 located in the northern Perth Basin (WA) based on relatively abundant conodont faunas. This is the first unequivocally recognised stage boundary for either the Permian or Triassic in Australia utilising internationally robust biostratigraphy.

Also $\delta^{13}C_{org}$ data is reported from this boundary interval. The isotopic data show a broad positive excursion of approximately 4 ‰ which correlates with a globally recognised positive excursion at this level and associates the Senecio–1 section conodont zonation with proposed Induan–Olenekian GSSP sections in China and India and demonstrates the utility of this conodont defined level for stage boundary definition and global correlation. Temporal and spatial mapping of marine anoxia and dysoxia globally demonstrates that pulses of anoxia affected shallow-marine zones at different times in different locations.

Paleoenvironmental reconstruction spanning the early Triassic (Induan–Olenekian) Boundary in the northern onshore Perth Basin WA, using stable isotopic proxies

Chapter 3 presents multi-proxy organic geochemical records, including bulk stable isotopic data ($\delta^{13}C_{OM}$, $\delta^{13}C_{carbonate}$, $\delta^{34}S_{pyrite}$, $\delta^{2}H_{kerogen}$) and compound specific stable carbon and hydrogen isotopic analysis to establish the paleoenvironmental conditions spanning the early Triassic (Induan–Olenekian) Stage Boundary in the Perth Basin (WA). Although an extensive amount of research has been carried on the Permian–Triassic mass extinction; post Permian–Triassic crisis recovery (e.g. Induan and Olenekian) remains undiscussed. Therefore, the present dataset has high interest for the characterisation of events that follow the Permian–Triassic crisis.

Coincident negative shifts of $\delta^{13}C_{OM}$ and $\delta^{13}C_{carbonate}$ in the Olenekian section of the core is consistent with a ^{13}C-depleted carbon source from the melting of methane clathrates as a result of hothouse conditions and associated massive volcanic activity in Siberia. $\delta^{34}S$ values of pyrite across the boundary are consistent with euxinic conditions existing in the ocean at the time. The distinct variations in isotope discrimination can be due to changes in the burial efficiency associated with changes in the availability of reactive OM, the organic substrate composition available for metabolism, or during times of euxinic conditions, changing contributions from processes at the chemocline. Further, compound specific isotope data combined with bulk isotopic data of OM and carbonate are concordant with destabilisation of gas clathrates and release of ^{13}C-depleted methane into the oceans leading to a shift in both ocean and atmospheric $^{12}CO_2$. Our data extends previously reported data sets only reported for $\delta^{13}C_{carbonates}$ for this same time interval attributed to climate warming associated with volcanic activity in Siberia (Chen and Benton, 2012; Benton and Twitchett, 2003; Twitchett, 2007). The results also provide evidence for major climate changes in the early Triassic, including frequent shifts between oxic and anoxic/dysoxic conditions in the oceans and climate warming and/or hothouse conditions which have been understood as the consequence of the expansion of a shallow oxygen minimum zone into the ocean surface layer due to environmental perturbations (Algeo et al., 2011).

Polycyclic aromatic hydrocarbon distributions of Senecio–1 core in the Induan–Olenekian Boundary

The main intentions were to determine the potential sources and importance of selected PAHs in samples spanning the early Triassic Induan–Olenekian Boundary from the Senecio–1 core and understand the main causes for the paleoenvironmental changes (e.g. wild fires caused by elevated global temperatures) that occurred around this early Triassic boundary.

Chapter 4 presents the distributions of selected PAHs across the Induan–Olenekian Boundary for the Senecio–1 core samples. Combustion-derived PAHs, i.e. fluoranthene, pyrene, benzo(*a*)anthracene, benzo(*a*)pyrene, benzofluoranthene, benzo(*ghi*)perylene are abundant in the sample sets and display similar concentration patterns. The concentrations of these compounds show sharp peaks before the main boundary in Senecio–1 core and an increase slightly later within the Olenekian section, suggesting a source from combustion. Wild fires and volcanic activity caused by elevated global temperatures possibly explain the high abundances of these components indicating that forest fires events happened within the early Triassic Induan–Olenekian Stage Boundary in the Senecio–1 core.

A decrease of these compounds shortly before the boundary in the Senecio–1 core sediments could also be caused by the demise of land plants or by an increase in distance from the paleoshore for the paleodepositional environment, due to changes in paleosea-level. The differences within these combustion-derived compounds can be attributed to variations in the type of combusted material, combustion temperature and post-depositional processes. Benzo(*e*)pyrene as the most representative combustion product displays high abundances slightly later within the Olenekian section, coinciding with other combustion-derived PAHs and can be related to volcanic activity and/or other sources of OM. Maximum Concentrations of chrysene and triphenylene also accord with other combustion-derived PAHs suggesting a similar source. Results from this work indicate that wildfires and volcanism were major factors for the paleoenvironmental changes in the early Triassic Induan–Olenekian Boundary from Senecio–1 core in the northern onshore Perth basin, WA.

Offline coupling of MSSV-Py and GC-irMS: a novel method for rapid isotopic characterisation of hydrocarbon gases generated by artificial maturation

The objective of this study was to increase our ability to explore and establish natural gas resources by developing an offline pyrolysis method to obtain reliable stable isotopic compositions of a sample and to investigate the potential isotopic fractionation of generated gaseous hydrocarbons within the gas sampling device as a function of time and temperature.

Chapter 5 reports the development of offline coupling of MSSV-Py and GC-irMS using a purpose built gas sampling device. The method offers several advantages over the online MSSV sampling system. The foremost is that the sampling device allows multiple GC and GC-irMS injections to obtain reliable stable isotopic values of hydrocarbon gases (C_1–C_5) generated by artificial maturation of sedimentary OM. This offline sampling technique is also rapid, inexpensive and has great scope for characterising gas formation in sedimentary systems.

The hydrocarbon gas yields using this technique have been calculated and compared with those obtained previously by online MSSV-Py for the same samples (Kockatea shale kerogen) under the same conditions. The hydrocarbon gas yields using this offline approach were slightly lower compared to online method, most likely due to the absence of helium carrier gas flushing within the offline system.

Several tests were also performed to investigate the potential isotopic fractionation of generated gaseous hydrocarbons within the sampling device as a function of time and temperature. The GC-irMS results showed no significant isotopic fractionation of $C_{1–5}$ hydrocarbons within 1 hr, minor $\delta^{13}C$ enrichment after 5 hrs, and significant enrichment after 22 hrs for all the compounds. The $\delta^{13}C$ values for $C_{1–5}$ hydrocarbons showed no isotopic fractionation with increasing the temperature from ambient temperature (22 ºC) to 120 ºC.

Future Work

The $\delta^{13}C$ and $\delta^{2}H$ values of individual hydrocarbons in combination with other organic geochemical parameters have useful applications in understanding the paleoenvironmental conditions. However, similar studies to those presented in **Chapter 3** and **Chapter 4** could be performed to a wider range of sediments deposited in other localities spanning the early Triassic (Induan–Olenekian) Stage Boundary to validate these studies and provide an increased spatial understanding of the mass extinction event around the boundary by looking at variations in OM composition within the context of redox and global environmental change. The spatial and temporal mapping of these fluctuating redox conditions will greatly improve our understanding of the causative environmental perturbations. Although the findings for the Senecio–1 core in the northern Perth Basin (WA) provide a very comprehensive insight into a short period of time around the Induan–Olenekian transition; however, a longer period well into the Lower Triassic would be desirable to obtain a more complete dataset of the paleoenvironmental changes occurring in this section.

In **Chapter 3**, the hydrogen exchange is suggested as a main process in altering the $\delta^{2}H$ values of hydrocarbons during maturation; however $\delta^{2}H$ analysis of a different range of carbon-skeletons will help to better understand the mechanisms that cause the changes. The potential of $\delta^{2}H$ values of individual hydrocarbons to evaluate the thermal maturity of sedimentary OM also needs further investigation and may prove useful in cases where traditional biomarker maturity parameters are ineffective (i.e. high maturity levels).

Furthermore, the offline MSSV-Py method developed in **Chapter 5** presents several advantages over the online MSSV sampling system. This offline sampling technique is a reliable way of conducting simulation experiments and is also rapid and inexpensive. For future work, this method can be extended and applied to tight gas shales to obtain reliable stable isotopic compositions of samples and therefore increase our ability to explore and establish natural gas resources. This method has great scope for characterising gas formation in sedimentary systems.

Bibliography

"Every reasonable effort has been made to acknowledge the owners of copyright material. I would be pleased to hear from any copyright owner who has been omitted or incorrectly acknowledged"

A

Albrecht, P., Ourisson, G., 1969. Triterpene alcohol isolation from oil shale. *Science* 163, 1192–1193.

Alexander, R., Kagi, R.I., Rowland, S.J., Sheppard, P.N., Chirila, T.V., 1985. The effects of thermal maturity on distributions of dimethylnaphtalenes and trimethylnaphtalenes in some ancient sediments and petroleums. *Geochimica et Cosmochimica Acta*, 49, 385–395.

Alexander, R., Larcher, A.V., Kagi, R.I., 1992. An oil-source correlation study using age specific plant-derived aromatic biomarkers. In Biological Markers in Sediments and Petroleum (Eds. J.M.P. Moldowan, P. Albrecht and R.P. Philps). Prentice Hall, Englewood Cliffs 201–221.

Alexander, R., Bastow, T.P., Fisher, S., Kagi, R., 1995. Geosynthesis of organic compounds: II. Methylation of phenanthrene and alkylphenanthrenes. *Geochimica et Cosmochimica Acta*, 59, 4259–4266.

Ali, J.R., Aitchison, J.C., 2005. Greater India. *Earth Science Reviews* 72, 169–188.

Algeo, T.J., 2011a. The early Triassic cesspool: Marine conditions following the end-Permian mass extinction. In: Håkansson, E., Trotter, J. (Eds), Programme and Abstracts, The XVII International Congress on the Carboniferous and Permian, Perth 3–8 July 2011: *Geological Survey of Western Australia*, Record 2011/20, 38.

Algeo, T.J., 2011b. Enhanced continental weathering in the latest Permian to early Triassic: Effects on shallow marine biotas. In: Håkansson, E., Trotter, J. (Eds), Programme and Abstracts, The XVII International Congress on the Carboniferous and Permian, Perth 3–8 July 2011: *Geological Survey of Western Australia*, Record 2011/20, 38.

Algeo, T.J., Twitchett, R.J., 2010. Anomalous early Triassic sediment fluxes due to elevated weathering rates and their biological consequences. *Geology* 38, 1023–1026.

Algeo, T., Chen, Z.Q., Fraiser, M.L., Twitchett, R.J., 2011. Terrestrial–marine teleconnections in the collapse and rebuilding of early Triassic marine ecosystems. *Paleogeography, Paleoclimatology, Paleoecology* 308, 1–11.

Alroy, J., Aberhan, M., Bottjer, D.J., Foote, M., Fürsich, F.T., Harries, P.J., Hendy,

A.J.W., Holland, S.M., Ivany, L.C., Kiessling, W., Kosnik, M.A., Marshall, C.R., McGowan, A.J., Miller, A.I., Olszewski, T.D., Patzkowsky, M.E., Peters, S.E., Villier, L., Wagner, P.J., Bonuso, N., Borkow, P.S., Brenneis, B., Clapham, M.E., Fall, L.M., Ferguson, C.A., Hanson, V.L., Krug, A.Z., Layou, K.M., Leckey, E.H., Nürnberg, S., Powers, C.M., Sessa, J.A., Simpson, C., Tomašových, A., Visaggi, C.C., 2008. Phanerozoic trends in the global diversity of marine invertebrates. *Science* 321, 97–100.

Amend, J.P., Edwards, K.J., Lyons, T. W. (Eds.), 2004. Sulfur Biogeochemistry - Past and Present. Boulder: *Geological Society of America*.

Andersen, N., Paul, H.A., Bernasconi, S.M., McKenzie, J.A., Behrens, A., Schaeffer, P., Albrecht, P., 2001. Large and rapid climate variability during the Messinian salinity crisis: Evidence from deuterium concentrations of individual biomarkers. *Geology* 29, 799–802.

Anderson, L.G., Dyrssen, D., Hall, P.O.J., 1988. On the sulfur chemistry of a super-anoxic fjord, Framvaren, South Norway. *Marine Chemistry* 23, 283–293.

B

Bambach, R.K., 2006. Phanerozoic biodiversity mass extinctions. *Annual Review of Earth and Planetary Sciences* 34, 127–155.

Bann, K.L., Fielding, C.R., 2004. An integrated ichnological and sedimentological comparison of non deltaic shoreface and subaqueous delta deposits in Permian reservoir units of Australia. In McIlroy, D. (Ed), The Application of Ichnology to Paleoenvironmental and Stratigraphic Analysis. *Geological Society of London*, Special Publication 228, 273–310.

Baud, A., Richoz, S., Pruss, S., 2007. The Lower Triassic anachronistic carbonate facies in space and time. *Global and Planetary Change* 55, 81–89.

Benson, S., Lennard, C., Maynard, P., Roux, C., 2006. Forensic applications of isotope ratio mass spectrometry–A review. *Forensic Science International* 157, 1–22.

Benton, M.J., Twitchett, R.J., 2003. How to kill (almost) all life: the end-Permian extinction event. *Trends Ecology and Evolution* 18, 358–365.

Benton, M.J., Newell, A. J., 2013. Impacts of global warming on Permo–Triassic terrestrial ecosystems, *Gondwana Research* 25, 1308–1337.

Betzer, P.R., Byrne, R.H., Acker, J.G., Lewis, C.S., Jolley R.R., Feely R.A., 1984. The oceanic carbonate system: A reassessment of biogenic controls. *Science* 226, 1074–1077.

Bigeleisen, J., Mayer, M.G., 1947. Calculation of equilibrium constants for isotopic exchange reactions. *Journal of Chemical Physics* 15, 261–267.

Bigeleisen, J., Wolfsberg, M., 1958. Theoretical and experimental aspects of isotope effects in chemical kinetics. *Advances in Chemical Physics* 1, 15–76.

Bolliger, C., Schroth, M.H., Bernasconi, S.M., Kleikemper, J., Zeyer, J., 2001. Sulfur isotope fractionation during microbial sulfate reduction by toluene-degrading bacteria. *Geochimica et Cosmochimica Acta* 65, 3289.

Bond, D.P.G., Wignall, P.B., 2010. Pyrite framboid study of marine Permian–Triassic Boundary sections: A complex anoxic event and its relationship to contemporaneous mass extinction. *Geological Society of America Bulletin* 122, 1265–1279.

Boreham, C.J., Golding, S.D., Glikson, M., 1998. Factors controlling the origin of gas in Australia Bowen Basin coals. *Organic Geochemistry* 29, 347–362.

Böttcher, M.E., Lepland, A., 2000. Biogeochemistry of sulfur in a sediment core from the west-central Baltic Sea: Evidence from stable isotopes and pyrite textures. *Journal of Marine Systems* 25, 299–312.

Böttcher, M.E., Boetius, A., Rickert, D., 2006. Sulfur isotope fractionation during microbial sulfate reduction associated with anaerobic methane oxidation. *Geophysical Research Abstrac*t 8, 10040.

Bowring, S.A., Erwin, D.H., Isozaki, Y., 1999. The tempo of mass extinction and recovery: The end-Permian example. *Proceedings of the National Academy of Sciences of the United States of America* 96, 8827–8828.

Brayard, A., Bucher, H., Escarguel, G., Fluteau, F., Bourquin, S., Galfetti, T., 2006. The early Triassic ammonoid recovery: Paleoclimatic significance of diversity gradients. *Paleogeography, Paleoclimatology, Paleoecology* 239, 374–395.

Brayard, A., Vennin, E., Olivier, N., Bylund, K.G., Jenks, J., Stephen, D.A., Bucher, H., Hofmann, R., Goudemand, N., Escarguel, G., 2011. Transient metazoan reefs in the aftermath of the end-Permian mass extinction. *Nature Geoscience* 4, 693–697.

Brocks, J., Grice, K., 2011. Biomarker (Organic, Coumpound–Specific Isotopes) in: Reitner, J., Thiel, V. (Eds.), *Encyclopedia of Geobiology*. Springer, Dordrecht Netherlands.

Brookfield, M.E., Twitchett, R.J., Goodings, C., 2003. Paleoenvironments of the Permian–Triassic transition sections in Kashmir, India. *Paleogeography, Paleoclimatology, Paleoecology* 198, 353–371.

Burgoyne, T.W., Hayes, J.M., 1998. Quantitative production of H_2 by pyrolysis of gas chromatographic effluents. *Analytical Chemistry* 70, 5136–5141.

C

Canfield, D. E., Thamdrup, B., 1994. The production of ^{34}S-depleted sulfide during bacterial disproportionation of elemental sulfur. *Science* 266, 1973–1975.

Canfield, D.E., 2001. Biogeochemistry of sulfur isotopes. In Valley, J. W., and Cole, D. R. (eds.), Reviews in Mineralogy and Geochemistry. *The Mineralogical Society of America* 607.

Canfield, D.E., 2004. The evolution of the Earth surface sulfur reservoir. *American Journal of Science* 304, 839–861.

Chambers, L.A., Trudinger, P.A., 1979. Microbiological fractionation of stable sulfur isotopes: a review and critique. *Geomicrobiology Journal* 1, 249.

Chen, Z.Q., Benton, M. J., 2012. The timing and pattern of biotic recovery following the end-Permian mass extinction. *Nature Geoscience* 5, 375–383.

Chung, H.M., Rooney, M.A., Toon, M.B., Claypool, G.E., 1992. Carbon isotope composition of marine crude oils. *The American Association of Petroleum Geologists Bulletin* 76, 1000–1007.

Clark, I.D., Fritz, P., 1997. Environmental Isotopes in Hydrogeology.Boca Raton: Lewis Publishers.

Clarkson, M.O., Richoz, S., Wood, R.A., Maurer, F., Krystyn, L., McGurty, D.J., Astratti, D., 2013. A new high-resolution $\delta^{13}C$ record for the Early Triassic: Insights from the Arabian Platform. *Gondwana Research* 24, 233–242.

Claypool, G.E., Hosler, W.T., Kaplan, I.R., Sakai, H., Zak, I., 1980. The age curves of sulfur and oxygen isotopes in marine sulfate and their mutual interpretation. *Chemical Geology* 28, 199–260.

Clayton, C., 1991. Effect of maturity on carbon isotope ratios of oils and condensates. *Organic Geochemistry* 17, 887–899.

Coplen, T.B., 2011. Guidelines and recommended terms for expression of stable-isotope-ratio and gas-ratio measurement results. *Rapid Communications in Mass Spectrometry* 25, 2538–2560.

Corsetti, F.A., Baud, A., Marenco, P.J., Richoz, S., 2005. Summary of early Triassic carbon isotope records. *Comptes Rendus Palevol* 4, 473–486.

Craig, H., 1957. Isotopic standards for carbon and oxygen and correction factors for mass-spectrometric analysis of carbon dioxide. *Geochimica et Cosmochimica Acta* 12, 133–149.

Craig, H., 1961. Isotopic variations in meteoric waters. *Science* 133, 1702–1703.

D

Dawson, D., Grice, K., Wang, S.X., Alexander, R., Radke, J., 2004. Stable hydrogen isotopic composition of hydrocarbons in torbanites (late Carboniferous to late Permian) deposited under various climatic conditions. *Organic Geochemistry* 35, 189–197.

Dawson, D., Grice, K., Alexander, R., 2005. Effect of maturation on the indigenous δD signatures of individual hydrocarbons in sediments and crude oils from the Perth Basin (Western Australia). *Organic Geochemistry* 36, 95–104.

Dawson, D., Grice, K., Alexander, R., Edwards, D., 2007. The effect of source and maturity on the stable isotopic compositions of individual hydrocarbons in

sediments and crude oils from the Vulcan Sub-basin, Timor Sea, Northern Australia. *Organic Geochemistry* 38, 1015–1038.

Demaison, G.J., Moore, G.T., 1980. Anoxic environments and oil source bed genesis. *Organic Geochemistry* 2, 9–31.

Demaison, G.J., Holck, A.J.J., Jones, R.W., Moore, G.T., 1984. Predictive source bed stratigraphy: A guide to regional petroleum occurrence - North Sea Basin and eastern North American continental margin: *Proceedings of the Eleventh World Petroleum Congress*, London, 1983. New York, John Wiley and Sons, 17–29.

Dickins, J.M., Mctavish, R.A., Balme, B. E.,1961. The Beagle Ridge bore: *Australian Oil and Gas Journal* 1960, 20–21.

Dieckmann, V., Ondrak, R., Cramer, B., Horsfield, B., 2006. Deep basin gas: New insights from kinetic modelling and isotopic fraction in deep-formed gas precursors. *Marine and Petroleum Geology* 23, 183–199.

Dolenec, T., Lojen, S., Ramovs, A., 2001. The Permian–Triassic Boundary in Western Slovenia (Idrijca Valley section): Magnetostratigraphy, stable isotopes, and elemental variations. *Chemical Geology* 175, 175–190.

Durand, B., Espitalié, J., 1973. Evolution de la matiere organique au cours de l'enfouissement des sediments. *Compte Rendu de l'Academie des Sciences* 276, 2253–2256.

Durand, B., 1980. Sedimentary organic matter and kerogen. Definition and quantitative importance of kerogen: insoluble organic matter from sedimentary rocks (ed. B. Durand). Editions Technip, Paris, 13–33.

E

Eglinton, G., Scott, P.M., Besky, T., Burlingame, A.L., Calvin, M., 1964. Hydrocarbons from a one-billion-year-old sediment. *Science* 145, 263–264.

Eglinton, G., Hamilton, R.J., 1967. Leaf Epicuticular Waxes. *Science* 156, 1322–1334.

Epstein, A.G., Epstein, J.B., Harris, L.D., 1977. Conodont colour alteration; an index to organic metamorphism. U.S. *Geological Survey Professional Paper* 995, 27.

Erwin, D.H., 1993. The Great Paleozoic Crisis. Columbia Univ. Press, New York.

Erwin, D.H., 1994. The Permo–Triassic Extinction. *Nature* 367, 231–236.

Espitalié, J., Laporte, J.L., Madec, M., Marquis, F., Leplat, P., Paulet, J., Boutfeu, A., 1977. Méthode rapide de charactérisation des roches méres, de leur potential pétrolier et de leur degré d'évolution. *Revue de l'Institut Français du Pétrole* 32, 23–42.

F

Farquhar, J., Johnston, D.T.,Wing, B.A., Habicht, K.S., Canfield, D.E., Airieau, S., Thiemens, M.H., 2003. Multiple sulfur isotopic interpretations of biosynthetic pathways: implications for biological signatures in the sulfur isotope record. *Geobiology* 1, 27.

Faure, G., Mensing, T.M., 2005. Isotopes, Principles and Applications, Third Edition. John Wiley & Sons, Inc., Hoboken, New Jersey.

Felton, E.A., Miyazaki, S., Dowling, L. Pain, L., Vuckovic V., le Poidevin, S.R., 1993. Carnarvon Basin, W.A., Bureau of Resource Sciences, *Australian Petroleum Accumulations* Report 8.

Fenton, S., Grice, K., Twitchett, R.J., Böttcher, M.E., Looy, C.V., Nabbefeld, B., 2007. Changes in biomarker abundances and sulfur isotopes of pyrite across the Permian–Triassic (P/Tr) Schuchert Dal section (East Greenland). *Earth and Planetary Science Letters* 262, 230–239.

Fossing, H., Jørgensen, B.B., 1989. Measurement of bacterial sulfate reduction in sediments: evaluation of a single-step chromium reduction method. *Biogeochemistry* 8, 205–222

Foster, C.B, Logan, A., Summons, R.E, Gorter, J.D., Edwards, D.S., 1997. Carbon isotopes, kerogen types and the Permian–Triassic Boundary in Australia: implications for exploration. *Australian Petroleum Production and Exploration Association* 37, 472–789.

Freeman, K.H., Hayes, J.M., Trendel, J.M., Albrecht, P., 1990. Evidence from Carbon Isotope Measurements for Diverse Origins of Sedimentary Hydrocarbons. *Nature* 343, 254–256.

Fry, B., Jannasch, H.W., Molyneaux, S.J., Wirsen, C.O., Muramoto, J.A., King, S., 1991. Stable isotope studies of the carbon, nitrogen and sulfur cycles in the Black Sea and the Cariaco Trench. *Deep Sea Research* 38, 1003–1019.

G

Gaffney, J.S., Premuzic, E.T., Manowitz, B., 1980. On the usefulness of sulfur isotope ratios in crude oil correlations. *Geochimica et Cosmochimica Acta* 44, 135–139.

Galfetti, T., Bucher, H., Brayard, A., Hochuli, P.A., Weissert, H., Guodun, K., Atudorei, V., Guex, J., 2007a. Late Early Triassic climate change: insights from carbonate carbon isotopes, sedimentary evolution and ammonoid paleobiogeography. *Paleogeography, Paleoclimatology, Paleoecology* 243, 394–411.

Galfetti, T., Bucher, H., Ovtcharova, M., Schaltegger, U., Brayard, A., Bruhwiler, T., Goudemand, N., Weissert, H., Hochuli, P.A., Cordey, F., Guodun, K., 2007b. Timing of the early Triassic carbon cycle perturbations inferred from new U–Pb ages and ammonoid biochronozones. *Earth and Planetary Science Letters*

258, 593–604.

Galimov, E.M., 1975. Carbon isotopes in oil-gas geology. NASA Technical Translation. NASA TT F–682, Washington DC, 395.

Gat, J.R., 1996. Oxygen and hydrogen isotopes in the hydrologic cycle. *Annual Review of Earth and Planetary Sciences* 24, 225–262.

Gelin, F., Damsté, J.S.S., Harrison, W.N., Reiss, C., Maxwell, J.R., De Leeuw, J.W., 1996. Variations in origin and composition of kerogen constituents as revealed by analytical pyrolysis of immature kerogens before and after desulfurization. *Organic Geochemistry* 24, 705–714.

Gelpi, V., Schneider, H., Mann, J., Oro, J., 1970. Hydrocarbons of geochemical significance in microscopic algae. *Phytochemistry* 9, 603–612.

Gorjan, P., Kaiho, K., Kakegawa, T., Niitsuma, S., Chen, Z.Q., Kajiwara., Nicora, A., 2007. Paleoredox, biotic and sulfur-isotopic changes associated with the end-Permian mass extinction in the western Tethys. *Chemical Geology* 244, 483–492.

Gorter, J.D., Nicoll, R.S., Metcalfe, I., Willink, R.J., Ferdinando, D., 2009. The Permian–Triassic Boundary in Western Australia: evidence from the Bonaparte and Northern Perth basins: exploration implications. *Australian Petroleum Production and Exploration Association Journal* 2009, 311–336.

Grice, K., Gibbison, R., Atkinson, J.E., Schwark, L., Eckardt, C.B., Maxwell, J.R., 1996. Maleimides (1H-pyrrole-2,5-diones) as molecular indicators of anoxygenic photosynthesis in ancient water columns. *Geochimica et Cosmochimica Acta* 60, 3913–3924.

Grice, K., Schouten, S., Nissenbaum, A., Charrach, J., Sinninghe Damsté, J.S., 1998. A remarkable paradox: Sulfurised freshwater algal (*Botryococcus braunii*) lipids in an ancient hypersaline euxinic ecosystem. *Organic Geochemistry* 28, 195–216.

Grice, K., Schouten, S., Blokker, P., Derenne, S., Largeau, C., Nissenbaum, A., Damsté, J.S.S., 2003. Structural and isotopic analysis of kerogens in sediments rich in free sulfurised Botryococcus braunii biomarkers. *Organic Geochemistry* 34, 471–482.

Grice, K., Cao, C., Love, G.D., Böttcher, M.E., Twitchett, R.J., Grosjean, E., Summons, R.E., Turgeon, S.C., Dunning, W., Jin, Y., 2005a. Photic Zone Euxinia During the Permian–Triassic Superanoxic Event. *Science* 307, 706–709.

Grice, K., Backhouse, J., Alexander, R., Marshall, N., Logan, G.A., 2005b. Correlating terrestrial signatures from biomarker distributions, $\delta^{13}C$, and palynology in fluvio-deltaic deposits from NW Australia (Triassic–Jurassic). *Organic Geochemistry* 36, 1347–1358.

Grice, K., Summons, R.E., Grosjean, E., Twitchett, R.J., Dunning, W., Wang, S.X., Böttcher, M.E., 2005c. Depositional conditions of the northern onshore Perth Basin (basal Triassic). *Australian Petroleum Production and Exploration Association Journal* 45, 263–273.

Grice, K., Nabbefeld, B., Maslen, E., 2007. Source and significance of selected polycyclic aromatic hydrocarbons in sediments (Hovea–3 well, Perth Basin, Western Australia) spanning the Permian–Triassic Boundary. *Organic Geochemistry* 38, 1795–1803.

Grice, K., de Mesmay, R., Glucina, A., Wang, S., 2008. An improved and rapid 5A molecular sieve method for gas chromatography isotope ratio mass spectrometry of *n*-alkanes (C8-C30+). *Organic Geochemistry* 39, 284–288.

Grice, K., Brocks, J.J., 2009a. Biomarkers (organic, compound specific isotopes) In: J. Reitner, V. Thiel (Eds.), *Encyclopedia of Geobiology in review*. Springer.

Grice, K., Lu, H., Atahan, P., Asif, M., Hallmann, C., Greenwood, P., Maslen, E., Tulipani, S., Williford, K., Dodson, J., 2009b. New insights into the origin of perylene in geological samples. *Geochimica et Cosmochimica Acta* 73, 6531–6543.

Grice, K., Brocks, J., 2011. Biomarkers (Molecular fossils), in: Reitner, J., Thiel, V. (Eds.), *Encyclopedia of Geobiology*. Springer, Dordrecht Netherlands, 147–167.

H

Habitch, K.S., Canfield, D.E., 1997. Sulfur isotope fractionation during bacterial sulfate reduction in organic-rich sediments. *Geochimica et Cosmochimica Acta* 61, 5351–5361.

Hallmann, C., Grey, K., Webster, L., McKirdy, D., Grice, K., 2010. Molecular signature of the Neoproterozoic Acraman impact event. *Organic Geochemistry* 41, 111–5.

Hartmann, M., Nielsen, H., 2012. $\delta^{34}S$ values in recent sea sediments and their significance using several sediment profiles from the western Baltic Sea. *Isotopes in Environmental and Health Studies* 48, 7–32.

Hassan, K.M., Spalding, R.F., 2001. Hydrogen isotope values in lacustrine kerogen. *Chemical Geology* 175, 713–721.

Hayes, J.M., 1993. Factors controlling ^{13}C contents of sedimentary organic compounds: Principles and evidence. *Marine Geology*, 113, 111–125.

Hays, L., Love, G.D., Foster, C.B., Grice, K., Summons, R.E., 2006. Lipid biomarker records across the Permian–Triassic Boundary from Kap Stosch, Greenland: Eos (*Transactions, American Geophysical Union*) 87, no. 52, PP41B–1203.

Hays, L.E., Beatty, T., Henderson, C.M., Love, G.D., Summons, R.E., 2007. Evidence for photic zone euxinia through the end-Permian mass extinction in the Panthalassic Ocean (Peace River Basin, Western Canada). *Paleoworld* 16, 39–50

Hermann, E., Hochuli, P.A., Méhay, S., Bucher, H., Brühwiler, T., Ware, D., Hautmann, M., Roohi, G., ur-Rehman, K., Yaseen, A., 2011. Organic matter and paleoenvironmental signals during the early Triassic biotic recovery: The

Salt Range and Surghar Range records. *Sedimentary Geology* 234, 19–41.

Hoefs J., 1987. Stable Isotope Geochemistry. Springer Verlag, Berlin.

Hoefs, J., 1997. Stable Isotope Geochemistry. Springer Verlag, New York.

Hoefs, J., 2008. Stable Isotope Geochemistry, 6th edn. Berlin: Springer.

Holman, A.I., Grice, K., Jaraula, C.M.B., Schimmelmann, A., Brocks, J.J., 2012. Efficiency of extraction of polycyclic aromatic hydrocarbons from the Paleoproterozoic Here's Your Chance Pb/Zn/Ag ore deposit and implications for a study of Bitumen II. *Organic Geochemistry* 52, 81–87.

Horacek, M., Brandner, R., Abart, R., 2007. Carbon isotope record of the Permian–Triassic Boundary and the Lower Triassic in the Southern Alps: evidence for rapid changes in storage of organic carbon. *Paleogeography, Paleoclimatology, Paleoecology* 252, 347–354.

Horacek, M., Koike, T., Richoz, S., 2009. Lower Triassic $\delta^{13}C$ isotope curve from shallow-marine carbonates in Japan, Panthalassa realm: Confirmation of the Tethys $\delta^{13}C$ curve. *Journal of Asian Earth Sciences* 36, 481–490.

Horsfield, B., di Primio, R., 2010. Oil and gas generation characteristics of a kerogen concentrate and an oil asphaltene as inferred from Phase Kinetic analysis. GeoS4 Report 20100703.

Horsfield, B., Disko, U., Leistner, F., 1989. The micro-scale simulation of maturation: Outline of a new technique and its potential application. *Geologische Rundschau* 78, 361–374.

Hotinski, R.M., Bice, K.L., Kump, L.R., Najjar, R.G., Arthur, M.A., 2001, Ocean stagnation and end-Permian anoxia. *Geology* 29, 7–10.

Huang, C., Tong, J., Hinnov, L., Chen, Z.Q., 2011. Did the great dying of life take 700 k.y.? Evidence from global astronomical correlation of the Permian–Triassic Boundary interval. *Geology* 39, 779–782.

Huc, A.Y., 1980. Origin and formation of organic matter in recent sediments and its relation to kerogen. In Kerogen insoluble organic matter from sedimentary rocks (ed. B. Durand). Editions Technip, Paris, 475–484.

Hunt, J.M., 1996. Petroleum geochemistry and geology. 2nd Editon. Freeman. 743.

I

Ingram, B.L., Conrad, M.E., Ingle, J.C., 1996. Stable isotope and salinity systematics in estuarine waters and carbonates: San Francisco Bay. *Geochimica Cosmochimica Acta* 60, 455–467.

Isozaki, Y., 1997. Permo–Triassic Boundary superanoxia and stratified superocean: Records from lost deep sea. *Science* 276, 235–238.

Isozaki, Y. 2009. Integrated ''plume winter" scenario for the double-phased extinction during the Paleozoic–Mesozoic transition: The G-LB and P-TB

events from a Panthalassan perspective. *Journal of Asian Earth Sciences* 36, 459–480.

J

Jarvie, D.M., Claxton, B.L., Henk, F., Breyer, J.T., 2001. Oil and shale gas from the Barnett Shale, Fort Worth basin, Texas. *American Association of Petroleum Geologists*, Annual Meeting Program 10, 100.

Jiang, C., Alexander, R., Kagi, R.I., Murray, A.P., 1998. Polycyclic aromatic hydrocarbons in ancient sediments and their relationships to paleoclimate. *Organic Geochemistry* 29, 1721–1735.

Joachimski, M.M., Ostertag-Henning, C., Pancost, R.D., Strauss, H., Freeman, K.H., Littke, R., Sinninghe Damsté, J.S., Racki, G., 2001. Water column anoxia, enhanced productivity and concomitant changes in $\delta^{13}C$ and $\delta^{34}S$ across the Frasnian–Famennian boundary (Kowala–Holy Cross Mountains/Poland). *Chemical Geology* 175, 109–131.

Joachimski, M.M., Lai, X., Shen, S., Jiang, H., Luo, G., Chen, J., Sun, Y., 2012. Climate warming in the latest Permian and the Permian–Triassic mass extinction. *Geology* 40, 195–198.

K

Kajiwara, Y., Ishida, K., Tanikura, Y., Ishiga, H., 1993a. Sulfur isotope data from the Permian–Triassic Boundary at Sasayama in the Tanba Terrane in southwestern Honshu, Japan. *Annual Report of Institut Geoscience.*, University of Tsukuba 19, 67–72.

Kajiwara, Y., Yamakita, S., Kobayashi, D., Imai, A., 1993b. Sulfur isotope data from the Permian–Triassic Boundary at Tenjinmaru in the Chichibu Terrane in eastern Shikoku, Japan. *Annual Report of Institut Geoscience.*, University of Tsukuba 19, 59–66.

Kajiwara, Y., Yamakita, S., Ishida, K., Ishiga, H., Imai, A., 1994. Development of a largely anoxic stratified ocean and its temporary massive mixing at the Permian Triassic Boundary supported by the sulfur isotopic record. *Paleogeography, Paleoclimatology, Paleoecology* 111, 367–379.

Kakuwa, Y., 2008. Evaluation of paleo-oxygenation of the ocean bottom across the Permian–Triassic Boundary. *Global and Planetary Change* 63, 40–56.

Kakuwa, Y., Matsumoto, R., 2006. Cerium negative anomaly just before the Permian and Triassic Boundary event — The upward expansion of anoxia in the water column. *Paleogeography, Paleoclimatology, Paleoecology* 229, 335– 344.

Kamo, S.L., Crowley, J., Bowring, S.A., 2006. The Permian–Triassic Boundary event and eruption of the Siberian flood basalts: An inter-laboratory U-Pb dating study. *Geochimica et Cosmochimica Acta* 70, 303–405.

Kaplan, I.R., Rittenberg, S.C., 1964. Microbiological fractionation of sulfur isotopes. *Journal of General Microbiology* 34, 195.

Kato, Y., Nakao, K., Isozaki, Y., 2002. Geochemistry of late Permian to early Triassic pelagic cherts from southwest Japan: implications for an oceanic redox change. *Chemical Geology* 182, 15–34.

Kehew, A.E., 2001. Applied Chemical Hydrogeology. Prentice Hall, New Jersey.

Kershaw, S., Zhang, T., Lan, G., 1999. A microbialite carbonate crust at the Permian–Triassic Boundary in South China, and its paleoenvironmental significance. *Paleogeography, Paleoclimatology, Paleoecology* 146, 1–18.

Kidder, D.L., Worsley, T.R., 2004. Causes and consequences of extreme Permo–Triassic warming to globally equable climate and relation to the Permo–Triassic extinction and recovery. *Paleogeography, Paleoclimatology, Paleoecology* 203, 207–237.

Killops, S.D., Massoud, M.S., 1992. Polycyclic aromatic hydrocarbons of pyrolytic origin in ancient sediments: evidence for Jurassic vegetation fires. *Organic Geochemistry* 18, 1–7.

Killops, S., Killops, V., 2005. Introduction to Organic Geochemistry. *Blackwell publishing*.

Kling, G.W., 1988. Comparative Transparency, Depth of Mixing, and Stability of Stratification in Lakes of Cameroon, West Africa. *Limnology and Oceanography* 33, 27–40.

Knoll, A.H., Bambach, R.K., Canfield, D.E., Grotzinger, J.P., 1996. Comparative Earth History and late Permian Mass Extinction. *Science* 273, 452–457.

Knoll, A.H., Bambach, R.K., Payne, J.L., Pruss, S., Fischer, W.W., 2007. Paleophysiology and end-Permian mass extinction. *Earth and Planetary Science Letters* 256, 295–313.

Koeberl, C., Farley, K.A., Peucker-Ehrenbrink, B., Sephton, M.A., 2004. Geochemistry of the end-Permian extinction event in Austria and Italy: no evidence for an extraterrestrial component. *Geology* 32, 1053–1056.

Kohnen, M.E.L., Schouten, S., Sinninghe Damsté, J.S., De Leeuw, J.W., Merrit, D.A., Hayes, J.M., 1992. Recognition of paleobiochemicals by a combined molecular sulfur and isotope geochemical approach. *Science* 256, 358–362.

Koopmans, M.P., Rijpstra, W.I.C., Klapwijk, M.M., de Leeuw, J.W., Lewan, M.D., Sinninghe Damsté, J.S., 1999. A thermal and chemical degradation approach to decipher pristane and phytane precursors in sedimentary organic matter. *Organic Geochemistry* 30, 1089–1104.

Korte, C., Kozur, H.W., Joachimski, M.M., Strauss, H., Veizer, J., Schwark, L., 2004. Carbon, sulfur, oxygen and strontium isotope records, organic geochemistry and biostratigraphy across the Permian/Triassic Boundary in Abadeh, Iran. *International Journal of Earth Sciences* 93, 565–581.

Korte, C., Kozur, H.W., 2010. Carbon-isotope stratigraphy across the Permian–Triassic Boundary: A review. *Journal of Asian Earth sciences* 39, 215–235.

Korte, C., Pnade, P., Kalle, P., Kozur, H.W., Joachimski, M.M., and Oberhänsli, H., 2010, Massive volcanism at the Permian–Triassic Boundary and its impact on the isotopic composition of the ocean and atmosphere. *Asian Journal of Earth Sciences* 37, 293–311.

Kozur, H., 1990. The taxonomy of the gondolellid conodonts in the Permian and Triassic. *Courier Forschungs Institut Senckenberg* 117, 409–469.

Krishnamurthy, R.V., Syrup, K.A., Baskaran, M., Long, A., 1995. Late glacial climate record of midwestern United States from the hydrogen isotope ratio of lake organic matter. *Science* 269, 1565–1567.

Krystyn, L., Bhargava, O. N., Richoz, S., 2007. A candidate GSSP for the base of the Olenekian Stage: Mud at Pin Valley; district Lahul and Spiti, Himachal Pradesh (Western Himalaya), India. *Albertiana* 35, 5–29.

Kump, L.R., Pavlov, A., Arthur, M.A., 2005. Massive release of hydrogen sulfide to the surface ocean and atmosphere during intervals of oceanic anoxia. *Geology* 33, 397–400.

L

Lafargue, E., Marquis, F., Pillot, D., 1998. Rock-Eval 6 Applications in Hydrocarbon Exploration, Production, and Soil Contamination Studies. *Revue de l'institut Francais du Petrole* 53, 421–437.

Laflamme, R.E., Hites, R.A., 1978. The global distribution of polycyclic aromatic hydrocarbons in recent sediments. *Geochimica et Cosmochimica Acta* 42, 289–303.

Largeau, C., Derenne, S., 1993. Relative efficiency of the Selective Preservation and Degradation Recondensation pathways in kerogen formation. Source and environment influence on their contributions to type I and II kerogens. *Organic Geochemistry* 20, 611–615.

Laws, E.A., Popp, B.N., Bidigare, R.R., Kennicutt, M.C., Macko, S.A., 1995. Dependence of phytoplankton isotopic composition on growth rate and [CO_2]aq: Theoretical considerations and experimental results. *Geochimica et Cosmochimica Acta* 59, 1131–1138.

Lehrmann, D.J., Ramezani, J., Bowring, S.A., Martin, M.W., Montgomery, P., Enos, P., Payne, J.L., Orchard, M.J., Wang, H., Wei, J.Y., 2006. Timing of recovery from the end-Permian extinction: geochronologic and biostratigraphic constraints from South China. *Geology* 34, 1053–1056.

Lichtfouse, É., Budzinski, H., Garrigues, P., Eglinton, T.I., 1997. Ancient polycyclic aromatic hydrocarbons in modern soils: ^{13}C, ^{14}C and biomarker evidence. *Organic Geochemistry* 26, 353–359.

Lima, A.L., Farrington, J.W., Reddy, C.M., 2005. Combustion-derived polycyclic aromatic hydrocarbons in the environment. *Environmental Forensics* 6, 109–131.

Lis, G.P., Schimmelmann, A., Mastalerz, M., 2006. D/H ratios and hydrogen exchangeability of type-II kerogens with increasing thermal maturity. *Organic Geochemistry* 37, 342–353.

M

Mann, J.L., Vocke, R.D., Kelly, W.R., 2009. Revised $\delta^{34}S$ reference values for IAEA sulfur isotope reference materials S-2 and S-3. *Rapid Communications in Mass Spectrometry* 23, 1116–1124.

Maruoka, T., Koeberl, C., Hancox, P.J., Reimold, W.U., 2003. Sulfur geochemistry across a terrestrial Permian–Triassic Boundary section in the Karoo Basin, South Africa. *Earth and Planetary Science Letters* 206, 101–117.

Maslen, E., Grice, K., Gale, J.D., Hallmann, C., Horsfield, B., 2009. Crocetane: A potential marker of photic zone euxinia in thermally mature sediments and crude oils of Devonian age. *Organic Geochemistry* 40, 1–11.

Maslen, E., Grice, K., Métayer, P.L., Dawson, D., Edwards, D., 2011. Stable carbon isotopic compositions of individual aromatic hydrocarbons as source and age indicators in oils from western Australian basins. *Organic Geochemistry* 42, 387–398.

Matthews, D.E., Hayes, J.M., 1978. Isotope-ratio-monitoring gas chromatography-mass spectrometry. *Analytical Chemistry* 50, 1465–1473.

Maxwell, W.D. 1992. Permian and early Triassic extinction of non-marine tetrapods. *Paleontology* 35, 571–583.

McTavish, R.A., 1965. Completion Report, BMR 10 and 10A, Beagle Ridge, Western Australia: Australia Bureau of Mineral Resources, *Geology and Geophysics*, Report 80

McTavish, R. A., 1973. Triassic conodont faunas from Western Australia. *Neues Jahrbuch fur Geologie und Palaontologie Abhandlungen* 143, 275 – 303.

McTavish, R. A., Dickins, J.M., 1974. The age of the Kockatea Shale (Lower Triassic), Perth Basin—a reassessment. *Journal of the Geological Society of Australia* 21, 195–201.

Metcalfe, I., Nicoll, R.S., Willink, R.J., 2008. Conodonts from the Permian Triassic transition in Australia and position of the Permian–Triassic Boundary. *Australian Journal of Earth Sciences* 55, 349 – 361.

Metcalfe, I., Riley, N.J., 2010. Conodont Colour Alteration pattern in the Carboniferous of the Craven Basin and adjacent areas, northern England. *Proceedings of the Yorkshire Geological Society* 58, 1–9.

Metcalfe, I., Nicoll, R.S., Willink, R., Ladjavadi, M., Grice, K., 2013. early Triassic (Induan–Olenekian) conodont biostratigraphy, global anoxia, carbon isotope excursions and environmental perturbations: New data from Western Australian Gondwana. *Gondwana Research* 23, 1136–1150.

Meyer, K.M., Kump, L.R., Ridgwell, A., 2008. Biogeochemical controls on photic-zone euxinia during the end-Permian mass extinction. *Geology* 36, 747–750.

Michaelson, P., 2002. Mass-extinction of peat-forming plants and the effect on flu vial styles across the Permian–Triassic Boundary, northern Bowen Basin, Australia. *Paleogeography, Paleoclimatology, Paleoecology* 179, 173–188.

Michels, R., Raoult, N.E., Elie, M., Mansuay, L., Faure, P., Oudin, J.L., 2002. Understanding of reservoir gas compositions in a natural case using stepwise semi-open artificial maturation. *Marine and Petroleum Geology* 19, 589–599.

Moodley, L., Middelburg, J.J., Herman, P.M.J., Soetaert, K., de Lange, G.J., 2005. Oxygenation and organic-matter preservation in marine sediments: Direct experimental evidence from ancient organic carbon–rich deposits. *Geology* 33, 889–892.

Morante, R., 1995. Permian–Triassic stable isotope stratigraphy of Australia. PhD thesis, Macquarie University, Sydney.

Morante, R., 1996. Permian and early Triassic isotopic records of carbon and strontium in Australia and a scenario of events about the Permian-Triassic boundary. *Historical Biology* 11, 289–310.

Mory, A. J., Iasky, R. P., 1996. Stratigraphy and structure of the onshore northern Perth Basin, Western Australia. *Western Australia Geological Survey,* Report 46, 101.

Mory, A.J., Haig, D.W., McLoughlin, S., Hocking, R., 2005. Geology of the northern Perth Basin, Western Australia — a field guide. *Western Australia Geological Survey*, Record 2005/9, 71.

Mundil, R., Ludwig, K.R., Metcalfe, I., Renne, P.R., 2004. Age and Timing of the Permian Mass Extinctions: U/Pb Geochronology on Closed-System Zircons. *Science* 305, 1760–1763.

Mundil, R., Palfy, J., Renne, P.R., Brack, P., 2010. The Triassic time scale: new constraints and a review of geochronological data. In: Lucas, S.G. (Ed.), The Triassic Timescale. *Geological Society of London Special Publication* 334, 41–60.

Murchison, D.G., Raymond, A.C., 1989. Igneous activity and organic maturation in the Midland Valley of Scotland. *International Journal of Coal Geology* 14, 47–82.

Musashi, M., Isozaki, Y., Koike, T., Kreulen, R., 2001. Stable carbon isotope signature in mid-Panthalassa shallow-water carbonates across the Permo–Triassic Boundary: evidence for ^{13}C-depleted superocean. *Earth and Planetary Science Letters* 191, 9–20.

N

Nabbefeld, B., Grice, K., Twitchett, R.J., Summons, R.E., Hays, L., Böttcher, M.E., Asif, M., 2010a. An integrated biomarker, isotopic and paleoenvironmental

study through the late Permian event at Lusitaniadalen, Spitsbergen. *Earth and Planetary Science Letters* 291, 84–96.

Nabbefeld, B., Grice, K., Schimmelmann, A., Summons, R.E., Troitzsch, U., Twitchett, R.J., 2010b. A comparison of thermal maturity parameters between freely extracted hydrocarbons (Bitumen I) and a second extract (Bitumen II) from within the kerogen matrix of Permian and Triassic sedimentary rocks. *Organic Geochemistry* 41, 78–87.

Nabbefeld, B., Grice, K., Schimmelmann, A., Sauer, P.E., Böttcher, M.E., Twitchett, R., 2010c. Significance of $\delta D_{kerogen}$, $\delta^{13}C_{kerogen}$ and $\delta^{34}S_{pyrite}$ from several Permian/Triassic (P/Tr) sections. *Earth and Planetary Science Letters* 295, 21–29.

Nabbefeld, B., Grice, K., Summons, R.E., Hays, L.E., Cao, C., 2010d. Significance of polycyclic aromatic hydrocarbons (PAHs) in Permian/Triassic Boundary sections. *Applied Geochemistry* 25, 1374–1382.

Neretin, L., Volkov, I., Böttcher, M.E., Grinenko, V.A., 2001. A sulfur budget for the Black Sea anoxic zone. *Deep-Sea Research* I 48, 2569–2593.

Newton, R., Pevitt, E.L., Wignall, P.B., Bottrell, S.H., 2004. Large shifts in the isotopic composition of seawater sulfate across the Permo–Triassic Boundary in northern Italy. *Earth and Planetary Science Letters* 218, 331–345.

Nielsen, J. K., Shen, Y., 2004. Evidence for sulfidic deep water during the late Permian in the East Greenland Basin. *Geology* 32, 1037–1040.

Nielsen, J.K., Shen, Y., Piasecki, S., Stemmerik, L., 2010. No abrupt change in redox condition caused the end-Permian marine ecosystem collapse in the East Greenland Basin. *Earth and Planetary Science Letters* 291, 32–38.

Nowlan, G.S., Barnes, C.R., 1987. Application of conodont colour alteration indices to regional and economic geology. In: Austin, R.L. (Ed.) Conodonts: Investigative Techniques and Applications. *British Micropaleontological Society Series*, Ellis Horwood Limited, Chichester, 188–202.

O

Orchard, M.J., 2007. Conodont diversity and evolution through the latest Permian and early Triassic upheavals. *Paleogeography, Paleoclimatology, Paleoecology* 252, 93–117.

Orchard, M.J., 2010. Triassic conodonts and their role in stage Boundary definition. In: Lucas, S. G. (Ed.) The Triassic Timescale. *Geological Society of London Special Publication* 334, 139–161.

Orchard, M.J., Tozer, E.T., 1997. Triassic conodont biochronology and intercalibration with the Canadian ammonoid sequence. *Albertiana* 20, 33–44.

Orchard, M.J., Krystyn, L., 2007. Conodonts from the Induan–Olenekian Boundary interval at Mud, Spiti. *Albertiana* 35, 30–34.

Ovtcharova, M., Bucher, H., Schaltegger, U., Galfetti, T., Brayard, A., Guex, J., 2006. New Early to Middle Triassic U–Pb ages from South China: calibration with ammonoid biochronozones and implications for the timing of the Triassic biotic recovery. *Earth and Planetary Science Letters* 243, 463–475.

P

Pancost, R.D., Boot, C.S., 2004. The paleoclimatic utility of terrestrial biomarkers in marine sediments. *Marine Chemistry* 92**,** 239–261.

Payne, J.L., Lehrmann, D.J., Wei, J., Orchard, M.J., Schrag, D.P., Knoll, A.H., 2004. Large perturbations of the carbon cycle during recovery from the end-Permian extinction. *Science* 305, 506–509.

Peters, K.E., 1986. Guidelines of evaluating petroleum source rock using programmed pyrolysis. *Association of Petroleum Geologists Bulletin* 70, 318–329.

Peters, K.E., Moldowan J.M., 1993. The Biomarker Guide. Interpreting Molecular Fossils in Petroleum and Ancient Sediments. Prentice Hall, New Jersey.

Peters, K.E., Walters, C.C., Moldowan, J.M., 2005. The biomarker guide: Interpreting molecular fossils in petroleum and ancient sediments. Prentice-Hall, New Jersey.

Philippi G.T., 1965. On the depth, time and mechanism of petroleum generation, *Geochimica et Cosmochimica Acta* 29, 1021–1049.

Philp, R., 1985. Fossil fuel biomarkers: *Methods in geochemistry and geophysics* 23,. Elsevier, New York.

Playford, P. E., Willmott, S.P., 1958. Stratigraphy and structure of the Perth Basin: West Australian Petroleum Pty Ltd, Report (unpublished), *Western Australia Geological Survey*, S-series report S103.

Popp, B.N., Laws, E.A., Bidigare, R.R., Dore, J.E., Hanson, K.L., Wakeham, S.G., 1998. Effect of phytoplankton cell geometry on carbon isotopic fractionation. *Geochimica et Cosmochimica Acta* 62, 69–79.

Posenato, R., 2008. Global correlations of mid early Triassic events: The Induan/Olenekian Boundary in the Dolomites (Italy). *Earth-Science Reviews* 91, 93–105.

Press, F., Siever, R., 2001. *Understanding Earth, 3rd Edition*. W.H. Freeman and Company, New York.

Prosser, S.J., Scrimgeour, C.M., 1995. High-precision determination of D/H in H_2 and H_2O by continuous-flow isotope ratio mass spectrometry. *Analytical Chemistry* 67, 992–1997.

Pruss, S.B., Böttcher, D.J., 2005. The reorganization of reef communities following the end-Permian mass extinction. *Comptes Rendus Palevol* 4, 553–568.

Purcell, R., 2006. Palynology Report Senecio–1, L1, North Perth Basin, Western

Australia. Report to Arc Energy NL, 7.

Puttmann, W., Villar, H., 1987. Occurrence and geochemical significance of 1,2,5,6-tetramethylnaphthalene. *Geochimica et Cosmochimica Acta* 51, 3023–3029.

Q

R

Racki, G., Wignall, P.B., 2005. late permian double-phased mass extinction and volcanism: an oceanographic perspective, in: D.J. Over, J.R.M., Wignall, P.B. (Eds.), *Developments in Paleontology and Stratigraphy* 263–297.

Radke, M., Welte, D.H., Willsch, H., 1982. Geochemical study on a well in the Western Canada Basin: relation of the aromatic distribution pattern to maturity of organic matter. *Geochimica et Cosmochimica Acta* 46, 1–10.

Radke, M., Hilkert, A., Rullkötter, J., 1998. Molecular stable carbon isotope compositions of alkylphenanthrenes in coals and marine shales related to source and maturity. *Organic Geochemistry* 28, 785–795.

Raiswell, R., 1997. A geochemical framework for the application of stable sulfur isotopes to fossil pyritization. *Journal of the Geological Society* 154, 343–356.

Raup, D.M., Sepkoski, J.J. Jr., 1982. Mass extinctions in the marine fossil record. *Science* 215, 1501–1503.

Readman, J.W., Fillmann, G., Tolosa, I., Bartocci, J., Villeneuve, P., Catinni, C., Mee, L.D., 2002. Petroleum and PAH contamination of Black Sea. *Marine Pollution Bulletin* 44, 48–62.

Rees, C.E., 1973. A steady-state model for sulfur isotope fractionation in bacterial reduction processes. *Geochimica et Cosmochimica Acta* 37, 1141–1162.

Retallack, G.J., Veevers, J.J., Morante, R., 1996. Global coal gap between Permian–Triassic extinction and Middle Triassic recovery of peat-forming plants, *Geological Society for American Bulletin* 108, 195–207.

Retallack, G.J., Krull, E.S., 1999. Landscape ecological shift at the Permian–Triassic Boundary in Antarctica. *Australian Journal of Earth Sciences* 46, 785–812.

Rice, D.D., Claypool, G.E., 1981. Generation, accumulation, and resource potential of biogenic gas. *The American Association of Petroleum Geologists Bulletin* 65, 5–25.

Richoz, S. Krystyn, L., Horacek, M., Spötl, C., 2007. Carbon isotope record of the Induan –Olenekian candididate GSSP Mud and comparison with other sections. *Albertiana* 35, 35–39.

Rontani, J.F., Bonin, P., 2011. Production of pristane and phytane in the marine environment: role of prokaryotes. *Research in Microbiology* 162, 923–933.

S

Sachse, D., Radke, J., Gleixner, G., 2006. δD values of individual *n*-alkanes from terrestrial plants along a climatic gradient – Implications for the sedimentary biomarker record. *Organic Geochemistry* 37, 469–483.

Sauer, P.E., Eglinton, T.I., Hayes, J.M., Schimmelmann, A., Sessions, A.L., 2001. Compound specific D/H ratios of lipid biomarkers from sediments as a proxy for environmental and climatic conditions. *Geochimica et Cosmochimica Acta* 65, 213–222.

Sauer, P.E., Schimmelmann, A., Sessions, A.L., Topalov, K., 2009. Simplified batch equilibration for D/H determination of non-exchangeable hydrogen in solid organic material. *Rapid Communications in Mass Spectrometry* 23, 949–956.

Schimmelmann, A., Lewan, M.D., Wintsch, R.P., 1999. D/H isotope ratios of kerogen, bitumen, oil, and water in hydrous pyrolysis of source rocks containing kerogen types I, II, IIS, and III. *Geochimica et Cosmochimica Acta* 63, 3751–3766.

Schimmelmann, A., Boudou, J.P., Lewan, M.D., Wintsch, R.P., 2001. Experimental controls on D/H and $^{13}C/^{12}C$ ratios of kerogen, bitumen and oil during hydrous pyrolysis. *Organic Geochemistry* 32, 1009–1018.

Schimmelmann, A., Sessions, A.L., Boreham, C.J., Edwards, D.S., Logan, G.A., Summons, R.E., 2004. D/H ratios in terrestrially sourced petroleum systems. *Organic Geochemistry* 35, 1169–1195.

Schimmelmann, A., Sessions, A.L., Mastalerz, M., 2006. Hydrogen isotopic (D/H) composition of organic matter during diagenesis and thermal maturation. *Annual Review of Earth and Planetary Science* 34, 501–533.

Schmidt, T., Zwank, L., Elsner, M., Berg, M., Meckenstock, R., Haderlein, S., 2004. Compound-specific stable isotope analysis of organic contaminants in natural environments: a critical review of the state of the art, prospects, and future challenges. *Analytical and Bioanalytical Chemistry* 378, 283–300.

Schoell, M., 1988. Multiple origin of methane in the Earth. *Chemical Geology* 71, 1–10.

Schouten, S., Klein Breteler, W.C.M., Blokker, P., Schogt, N., Rijpstra, W.I.C., Grice, K., Baas, M., Sinninghe Damsté, J.S., 1998. Biosynthetic effects on the stable carbon isotopic compositions of algal lipids: implications for deciphering the carbon isotopic biomarker record. *Geochimica et Cosmochimica Acta* 62, 1397–1406.

Schouten, S., Woltering, M., Rijpstra, W.I.C., Sluijs, A., Brinkhuis, H., Sinninghe Damste, J.S., 2007. The Paleocene-Eocene carbon isotope excursion in higher plant organic matter: Differential fractionation of angiosperms and conifers in the Arctic. *Earth and Planetary Science Letters* 258**,** 581–92.

Schubert, J.K., Bottjer, D.J., 1995. Aftermath of the Permian-Triassic mass extinction event: Paleoecology of Lower Triassic carbonates in the western USA. *Paleogeography, Paleoclimatology, Paleoecology* 116, 1–39.

Schwartzkopf, T. A., 1990. Relationship between petroleum generation, migration and sandstone diagenesis, Middle Jurassic, Gifhorn Trough, N Germany. *Marine Petroleum Geology* 7, 153–170.

Sephton, M.A., Looy, C.V., Brinkhuis, H., Wignall, P.B., de Leeuw, J.W., Visscher, H., 2005. Catastrophic soil erosion during the end– Permian biotic crisis. *Geology* 33, 941–944.

Sepkoski, J.J., 1986. Phanerozoic overview of mass extinction, in: Raup, D.M., Jablonski, D. (Eds.), Patterns and Processes in the History of Life. Springer Verlag, Berlin, 277–295.

Sepkoski, J.J., Jr., 1993. Ten Years in the Library: New Data Confirm Paleontological Patterns. *Paleobiology* 19, 43–51.

Sessions, A.L., Burgoyne, T.W., Schimmelmann, A., Hayes, J.M., 1999. Fractionation of hydrogen isotopes in lipid biosynthesis. *Organic Geochemistry* 30, 1193–1200.

Sheldon, N.D., 2006. Abrupt chemical weathering increase across the Permian–Triassic Boundary. *Paleogeography, Paleoclimatology, Paleoecology* 231, 315– 321.

Shen, S.Z., Henderson, C.M., Bowring, S.A., Cao, C.Q., Wang, Y., Wang, W., Zhang, H., Zhang, Y.C., Mu, L., 2010. High–resolution Lopingian (late Permian) timescale of South China. *Geological Journal* 45, 122–134.

Shen, S. Z., Crowley, J.L., Wang, Y., Bowring, S.A., Erwin, D.H., Sadler, P.M., Cao, C.Q., Rothman, D.H., Henderson, C.M., Ramezani, J., Zhang, H., Shen, Y., Wang, X.d., Wang, W., Mu, L., Li, W.z., Tang, Y.g., Liu, X.l., Liu, L.j., Jiang, Y.f., Jin, Y.g., 2011. Calibrating the end-Permian mass extinction. *Science* 334, 1367–1372.

Shigeta, Y., Zakharov, Y.D., Maeda, H., Popov, A.M., (Eds) 2009. The Lower Triassic System in the Abrek Bay area, South Primorye, Russia. Tokyo, *National Museum of Nature and Science Monographs* 38, 218.

Sim, M.S., Bosak, T., Ono, S., 2011. Large Sulfur Isotope Fractionation Does Not Require Disproportionation. *Science* 333, 74–77.

Smith, J.W., George, S.C., Batts, B.D., 1995. The geosynthesis of alkylaromatics. *Organic Geochemistry* 23, 71–80.

Stanley, S.M., 1988. Paleozoic mass extinctions: shared patterns suggest global cooling as a common cause. *American Journal of Science* 288, 334–352.

Stanley, S.M., 2010. Relation of Phanerozoic stable isotope excursions to climate, bacterial metabolism, and major extinctions. *Geology, Evolution* 107, 19185–19189.

Stein, S.E., 1978. High temperature chemical equilibria of polycyclic aromatic hydraocarbons. *Journal of Physical Chemistry* 82, 566–571.

Stevenson, D.P., Wagner, C.D., Beeck, O., Otvos, J.W., 1948. Isotope Effect in the Thermal Cracking of Propane–1–C^{13}. *Journal of Chemical Physics* 16, 993–994.

Stein, S.E., Fahr, A., 1985. High temperature stability of hydrocarbons. *Journal of Physical Chemistry* 89, 3714–3725.

Suess E., 1980. Particulate organic carbon flux in the oceans: surface productivity and oxygen utilization. *Nature* 288, 260–263.

Summons, R.E., Powell, T.G., 1986. *Chlorobiaceae* in Paleozoic seas revealed by biological markers, isotopes and geology. *Nature* 319, 763–765.

Summons, R.E., Powell, T.G., 1987. Identification of aryl isoprenoids in source rocks and crude oils: Biological markers for the green sulfur bacteria. *Geochimica et Cosmochimica Acta* 51, 557–566.

Summons, R. E., Boreham C. J., Foster C. B., Murray A. P., Gorter, J. D., 1995. Chemostratigraphy and the composition of oils in the Perth Basin, Western Australia. *Australian Petroleum and Production Association Journal* 35, 613–631.

Suzuki, N., Yessalina, S., Kikuchi, T., 2010. Probable fungal origin of perylene in Late Cretaceous to Paleogene terrestrial sedimentary rocks of northeastern Japan as indicated from stable carbon isotopes. *Organic Geochemistry* 41, 234–241.

Svensen, H., Planke, S., Polozov, A.G., Schmidbauer, N., Corfu, F., Podladchikov, Y.Y., Jamtveit, B., 2009. Siberian gas venting and the endPermian environmental crisis. *Earth and Planetary Science Letters* 277, 490–500.

T

Takahashi, S., Yamakita, S., Suzuki, N., Kaiho, K., Ehiro, M., 2009. High organic carbon content and a decrease in radiolarians at the end of the Permian in a newly discovered continuous pelagic section: A coincidence? *Paleogeography, Paleoclimatology, Paleoecology* 271, 1–12.

Takahashi, S., Kaiho, K., Hori, R.S., Gorjan, P., Watanabe, T., Yamakita, S., Aita, Y., Takemura, A., Spörli, K.B., Kakegawa, T., Oba, M., 2013. Sulfur isotope profiles in the pelagic Panthalassic deep sea during the Permian–Triassic transition. *Global and Planetary Change* 105, 68–78.

Tan, Y.L., Kong, A., Monetti, M., 1996. Biogenic polycyclic aromatic hydrocarbons in an Alaskan arctic lake sediment. *Polycyclic Aromatic Compounds* 9, 185–192.

Tang, Y., Perry, J.K., Jenden, P.D., Schoell, M., 2000. Mathematical modelling of stable carbon isotope ratios in natural gases. *Geochimica et Cosmochimica Acta* 64 (15), 2673–2687.

Tegelaar, E.W., de Leeuw, J.W., Derenne, S., Largeau, C., 1989. A reappraisal of kerogen formation. *Geochimica et Cosmochimica Acta* 53, 3103–3106.

Thomas, B.M., Barber, C.J., 2004. A reevaluation of the hydrocarbon habitat of the northern Perth Basin. *Australian Petroleum Production and Exploration Association Journal* 44, 59–92.

Thomas, B.M., Willink, R.J., Grice, K., Twitchett, R.J., Purcell, R.R., Archbold, N.W., George, A.D., Tye, S., Alexander, R., Foster, C.B., Barber, C.J., 2004. Unique marine Permian–Triassic Boundary section from Western Australia. *Australian Journal of Earth Sciences* 51, 423–430.

Tissot, B.P., Welte, D.H., 1978. Petroleum formation and occurrence: a new approach to oil and gas exploration. SpringerVerlag, New York.

Tissot, B., Welte, D.H., 1984. Petroleum Formation and Occurrence, in: Tissot, B., Welte, D.H. (Eds.). Springer, Berlin, 699.

Tong, J., Yin, Y., 2002. The Lower Triassic of South China. *Journal of Asian Earth Sciences* 20, 803–815.

Tong, J., Zhao, L., 2011. Lower Triassic and Induan–Olenekian Boundary in Chaohu, Anhui Province, South China. *Acta Geologica Sinica* 85, 399–407.

Tong, J., Zakharov, Y.D., Orchard, M.J., Yin, H., Hansen, H.J., 2004. Proposal of Chaohu section as the GSSP candidate of the Induan/Olenekian Boundary. *Albertiana* 29, 13–28.

Trull, T., Gibson, J.E., Beaumont, K.L., Bowman, J., Burton, H.R., Davidson, A.T., Summons, R.E., Swadling, K.M., Volkman, J.K., 2001. Site Holds Promise for Ecosystem and Biogeochemical Investigations. Eos Transactions, *American Geophysical Union* 82, 306–311.

Twitchett, R.J., 1999. Paleoenvironments and faunal recovery after the end-Permian mass extinction. *Paleogeography, Paleoclimatology, Paleoecology* 154, 27–37.

Twitchett, R.J., 2007. The Lilliput effect in the aftermath of the end-Permian extinction event. *Paleogeography, Paleoclimatology, Paleoecology* 252, 132–144.

Twitchett, R.J., Wignall, P.B., 1996. Trace fossils and the aftermath of the Permo–Triassic mass extinction: evidence from northern Italy. *Paleogeography, Paleoclimatology, Paleoecology* 124, 137–151.

U

Urey, H.C., 1947. The thermodynamic properties of isotopic substances. *Journal of the Chemical Society (Resumed)* 562–581.

V

Vandenbroucke, M., Largeau, C., 2007. Kerogen origin, evolution and structure. *Organic Geochemistry* 38, 719–833.

Van Krevelen, D.W., 1961. Coal. Elsevier Editions, Amsterdam.

W

Wakeham, S.G., Schaffner, C., Giger, W., 1980. Polycyclic aromatic hydrocarbons in Recent lake sediments–II. Compounds derived from biogenic precursors during early diagenesis. *Geochimica Cosmochimica Acta* 44, 415–429.

Waples, D., 1981. Organic geochemistry for exploration geologists. Burgess Pub.Co., Minneapolis, US, 151.

Ward, P.D., Garrison, G., Botha, J., Buick, R., Erwin, D.H., Kirschvink, J.L., De Kock, M.O., Smith, R., 2005. Abrupt and gradual extinction among land vertebrates in the Karoo Basin, South Africa. *Science* 307, 709–714.

Werner, R.A., Brand, W.A., 2001. Referencing strategies and techniques in stable isotope ratio analysis. *Rapid Communications in Mass Spectrometry* 15, 501–519.

Whiticar, M.J., 1994. Correlation of natural gases with their sources. In: The Petroleum system – from source to trap, Magoon, L.B., Dow, W.G. (Eds.). *American Association of Petroleum Geologists Memoir* 60, 261–283.

Wignall, P.B., 2001. Large igneous provinces and mass extinctions. *EarthScience Reviews* 53, 1–33.

Wignall, P.B., Hallam, A., 1992. Anoxia as a cause of the Permian/Triassic extinction: Facies evidence from northern Italy and the western United States. *Paleogeography, Paleoclimatology, Paleoecology* 93, 21–46.

Wignall, P.B., Hallam, A., 1993. Griesbachian (Earliest Triassic) paleoenvironmental changes in the Salt Range, Pakistan and southeast China and their bearing on the Permo–Triassic mass extinction. *Paleogeography, Paleoclimatology, Paleoecology* 102, 215–237.

Wignall, P.B., Twitchett, R.J., 1996. Oceanic anoxia and the end-Permian mass extinction. *Science* 272, 1155–1158.

Wignall, P.B., Twitchett, R.J., 2002. Extent, duration and nature of the Permian–Triassic superanoxic event. In: Koeberl, C., MacLeod, K.C. (Eds.), Catastrophic events and mass extinctions: impacts and beyond: Boulder, Colorado. *Geological Society of America Special Paper* 356, 395–413.

Wignall, P.B., Newton, R., 2003. Contrasting Deepwater Records from the Upper Permian and Lower Triassic of South Tibet and British Columbia: Evidence for a Diachronous Mass Extinction. *Palaios* 18, 153–167.

Wignall, P.B., Newton, R., Brookfield, M.E., 2005. Pyrite framboid evidence for oxygenpoor deposition during the Permian–Triassic crisis in Kashmir. *Paleogeography, Paleoclimatology, Paleoecology* 216, 183–188.

Wignall, P.B., Bond, D.P.G., Kuwahara, K., Kakuwa, Y., Newton, R.J., Poulton, S.W., 2010. An 80 million year oceanic redox history from Permian to Jurassic pelagic sediments of the MinoTamba terrane, SW Japan, and the origin of four mass extinctions. *Global and Planetary Change* 71, 109–123.

Winguth, A.M.E, MaierReimer, E., 2005. Causes of the marine productivity and oxygen changes associated with the Permian–Triassic Boundary: A reevaluation with ocean general circulation models. *Marine Geology* 217, 283–

304.

Wignuth, C., Winguth, A.M.E, 2012. Simulating Permian–Triassic oceanic anoxia distribution: Implications for species extinction and recovery. *Geology* 40, 127–130.

Williford, K.H., Grice, K., Logan, G.A., Chen, J., Huston, D., 2011. New insights into the hydrothermal alteration of organic matter from the Paleoproterozoic McArthur River Pb/Zn/Ag ore deposit of northern Australia based on compound specific hydrogen and carbon isotopes. *Earth and Planetary Science Letters* 301, 382–392.

X

Xie, S., Pancost, R.D., Huang, X., Jiao, D., Lu, L., Huang, J., Yang, F., Evershed, R.P., 2007. Molecular and isotopic evidence for episodic environmental change across the Permo/Triassic Boundary at Meishan in South China. *Global and Planetary Change* 55, 56–65.

Y

Youngblood, W.W., Blumer, M., 1975. Polycyclic aromatic hydrocarbons in the environment: Homologous series in soils and recent sediments. *Geochimica et Cosmochimica Acta* 39, 1303−1314.

Z

Zhang, X., Gillespie, A.L., Sessions, A.L., 2009. LargeD/H variations in bacterial lipids reflect central metabolic pathways. *Proceedings of the National Academy of Sciences* 106, 12580–12586.

Zhao, L., Orchard, M.J., Tong, J., Sun, Z., Zuo, J., Zhang, S., Yun, A., 2007. Lower Triassic conodont sequence in Chaohu, Anhui Province, China and its global correlation. *Paleogeography, Paleoclimatology, Paleoecology* 252, 24–38.

Zhao, L., Tong, J., Sun, Z., Orchard, M.J., 2008. A detailed Lower Triassic conodont biostratigraphy and its implications for the GSSP candidate of the Induan–Olenekian Boundary in Chaohu, Anhui Province. *Progress in Natural Science* 18, 79–90.

Appendix

Following pages contain documents stating:

The rights, granted by Elsevier to the first author of the publication that forms **Chapter 3, Chapter 5 of** this thesis, to reproduce the contribution in any printed volume (book or thesis). Also permission from the 1st author to include the full paper in **Chapter 2** has been granted.

ELSEVIER Type here to search on Elsevier.com Advanced search Follow us Help & Cc

Journals & books Online tools Authors, editors & reviewers About Elsevier Store

For Authors

- Journal authors' home
- **Rights & responsibilities**
- Ethics
- Funding body agreements
- Open access
- Author services
- Journal performance
- Early career researchers
- Authors' update
- Book authors' home

Rights & responsibilities

At Elsevier, we request transfers of copyright, or in some cases exclusive rights, from our journal authors in order to ensure that we have the r necessary for the proper administration of electronic rights and online dissemination of journal articles. Authors and their employers retain (or granted/transferred back) significant scholarly rights in their work. We take seriously our responsibility as the steward of the online record to e the integrity of scholarly works and the sustainability of journal business models, and we actively monitor and pursue unauthorized and unsubscribed uses and re-distribution (for subscription models).

In addition to authors' scholarly rights, authors have certain responsibilities for their work, particularly in connection with publishing ethics issu View our webinar on Ethics for Authors for a useful resource of information.

Rights | FAQ | Responsibilities | Permissions

As a journal author, you have rights for a large range of uses of your article, including use by your employing institute or company These rights can be exercised without the need to obtain specific permission.

How authors can use their own journal articles

Authors publishing in Elsevier journals have wide rights to use their works for teaching and scholarly purposes without needing to seek permission.

Table of Authors' Rights

	Preprint version (with a few exceptions- see below *)	Accepted Author Manuscript	Published Journal Articles
Use for classroom teaching by author or author's institution and presentation at a meeting or conference and distributing copies to attendees	Yes	Yes with full acknowledgement of final article	Yes with full acknowledgement of final article
Use for internal training by author's company	Yes	Yes with full acknowledgement of final article	Yes with full acknowledgement of final article
Distribution to colleagues for their research use	Yes	Yes	Yes
Use in a subsequent compilation of the author's works	Yes	Yes with full acknowledgement of final article	Yes with full acknowledgement of final article
Inclusion in a thesis or dissertation	Yes	Yes with full acknowledgement of final article	Yes with full acknowledgement of final article
Reuse of portions or extracts from the article in other works	Yes	Yes with full acknowledgement of final article	Yes with full acknowledgement of final article
Preparation of derivative works (other than for commercial purposes)	Yes	Yes with full acknowledgement of final article	Yes with full acknowledgement of final article
Preprint servers	Yes	Yes with the specific written permission of Elsevier	No
Voluntary posting on open web sites operated by author or author's institution for scholarly purposes	Yes (author may later add an appropriate bibliographic citation, indicating subsequent publication by Elsevier and journal title)	Yes, with appropriate bibliographic citation and a link to the article once published	Only with the specific written permission of Elsevier

Mandated deposit or deposit in or posting to subject-oriented or centralized repositories	Yes under specific agreement between Elsevier and the repository	Yes under specific agreement between Elsevier and the repository**	Yes under specific agreement between Elsevier and the repository
Use or posting for commercial gain or to substitute for services provided directly by journal	Only with the specific written permission of Elsevier	Only with the specific written permission of Elsevier	Only with the specific written permission of Elsevier

**Voluntary posting of Accepted Author Manuscripts in the arXiv subject repository is permitted.

Examples of use or posting for commercial gain:

- Posting by companies of employee-authored works for use by customers of those companies (e.g. pharmaceutical companies and physician prescribers)
- Commercial exploitation such as directly associating advertising with posting or charging fees for document delivery or access

*Which journals have different preprint policies?

If an electronic preprint of an article is placed on a public server prior to its submission to an Elsevier journal, this is not generally viewed by Elsevier as 'prior publication' and will not disqualify the article from further consideration by Elsevier, nor will Elsevier require the removal of that preprint version.

However Cell Press and The Lancet have different preprint policies and will not consider for publication articles that have already been posted publicly. This is a rule agreed upon by The International Committee of Medical Journal Editors. Information on Cell Press policy on preprints is available, as is *The Lancet* preprint policy . There are a number of other journals published by Elsevier (principally journals published on behalf of third party owners) that also have their own preprint policies which will be set out in the Guide for Authors for the relevant journal.

Does Elsevier request a transfer of copyright?

Elsevier requests a transfer of copyright for articles published under subscription-based business models but we generally use different licensing approaches for other publishing models where we offer authors a variety of Creative Commons licenses for some of our author-pays journals and are piloting a range of options. Learn more about Creative Commons licenses.

For subscription-based publishing, we ask for a transfer of copyright for a number of reasons, mainly because:

1. By having the ability to exercise all rights under copyright, Elsevier is able to quickly launch new products and services, and to make agreements with other platforms and services to enrich published content and to make it more accessible and usable. Authors may b based in a number of different countries, which will have their own copyright regimes. Copyright assignments give more legal certaint particularly in relation to future rights in new technologies.
2. Elsevier uses copyright to protect the integrity of the journal articles in cases of plagiarism, copyright infringement and other third part infringements. The journal subscription business model depends on a substantial body of subscribing customers providing financial support to a particular journal, and "free-riding" infringements diminish this model.
3. An assignment of rights under copyright means that we can more easily show that we own the rights and do not have to seek the participation of the author or obtain power of attorney from the author in order to bring an enforcement action.

Remember, even though we ask for a transfer of copyright, our journal authors retain (or are granted back) significant scholarly rights, as outlined above.

For a more detailed discussion, see the STM Position Paper on the benefits of copyright assignments.

Does Elsevier claim rights in an author's supporting data?

Elsevier supports the general principle that raw research data should be made freely available to all researchers and encourages the public posting of the raw data outputs of research. (Note that this is distinct from charts, tables, etc. which may be included within an article and in which rights would be transferred or licensed to Elsevier as part of the article, in the same way as text, illustrations or photographs). Elsevier therefore does not claim rights in the raw datasets that may be submitted with an article and the author can make these datasets freely available from other (web) locations.

If supported by the author and journal editor, and when a dataset is hosted in a repository that ensures data integrity and supports long-term preservation and inward linking, Elsevier can further support the discoverability of that dataset by connecting it with the published journal article on ScienceDirect through linking from an article or entity or through article interoperability. Click here tc review examples of how this could work in practice.

For more information on industry positions on this issue supported by Elsevier, view the:

Joint Statement from STM and DataCite on the Linkability and Citability of Research Data, June 2012

Brussels Declaration on STM Publishing , November 2007

STM/ALPSP Statement , June 2006

Can I post my published journal article on open websites?

A published journal article is the definitive final record of published research that appears in the journal and embodies all value-adding publisher activities, including copy editing, formatting and, if relevant, pagination, along with the stewardship of the scholarly record.

You can use your branded and formatted published article for all of the personal and institutional purposes described above. However, in order to safeguard the correct scientific record, Elsevier does not permit the posting of published journal articles (either the pdf provided by Elsevier or HTML files) on any open websites.

As part of its contribution to the stewardship of the scientific literature, Elsevier works with third parties (e.g. national libraries) to preserve its journal articles for posterity and in perpetuity, and invests to drive their usage. Elsevier strictly enforces an absolute guideline on the location of its published journal articles: each branded and formatted published journal article will reside only on a completely controlled site because this is the only way that we as the publisher can guarantee that each published journal article i permanent, authentic and unaltered as part of the 'minutes of science'.

Since Elsevier adds significant value to the final published journal article, we need to take these steps to ensure that this value is maintained, both for Elsevier and for our authors. However, we view preprints and accepted author manuscripts as less formal versions of the article and we therefore take a more liberal approach towards these, as described in more detail on our Article Posting Policies information page.

From: Hunt, Sarah (ELS-OXF) [s.hunt.1@elsevier.com]
Sent: Thursday, 25 April 2013 7:02 PM
To: M. Santosh; Ian Metcalfe
Cc: Mojgan Ladjavardi
Subject: RE: Copyright Issue

Dear Ian and Mojgan,

Thanks for your query. Santosh is correct in thinking that Elsevier do allow for the inclusion of articles in theses provided they are fully cited.

Best of luck with your work and I hope you will both continue to submit work to GR in the future.

Best wishes,

Sarah Hunt
Publisher- STM journals
Atmospheric, Energy, Geology and Planetary
Elsevier, The Boulevard, Langford Lane, Kidlington, Oxford, OX5 1GB
+44 (0)1865 843242
+44 (0)7833 045769
s.hunt.1@elsevier.com

From: M. Santosh [mailto:msantosh.gr@gmail.com]
Sent: Thursday, April 25, 2013 5:04 AM
To: Ian Metcalfe; Hunt, Sarah (ELS-OXF)
Cc: Mojgan Ladjavardi
Subject: Re: Copyright Issue

Dear Ian,
Thank you for your mail. I am sure there should be no problem with copyright issues for your student including a paper from GR as a chapter her Ph.D. thesis. Ph.D. thesis is an unpublished report.
Nevertheless, I am copying this mail to our Publisher at Elsevier, Sarah Hunt. She will reply to you soon with the required advise.
Thank you for all your patronage to GR, and we remember with pride that you are the GR Best Paper Award winner last year!

Best regards,
Santosh